Graphene organic hybrid materials

Andrea Schlierf

UNIVERSITÉ DE STRASBOURG

ÉCOLE DOCTORALE DES SCIENCES CHIMIQUES

Institut De Science Et D'ingénierie Supramoléculaires

THÈSE

présentée par :

Andrea SCHLIERF

soutenue le :
04 septembre 2014

pour obtenir le grade de : **Docteur de l'université de Strasbourg**

Discipline/ Spécialité : Chimie

Matériaux hybrides organiques à base de graphène

THÈSE dirigée par :

M. Paolo Samori	Prof., Université de Strasbourg

RAPPORTEURS :

M. Jérôme Cornil	Prof., Université de Mons, Belgium
M. Pascal Ruffieux	Dr., Swiss Federal Laboratories for Materials Science and Technology (EMPA), Switzerland

---

AUTRES MEMBRES DU JURY :

M. Vincenzo Palermo	Dr., Institute of Synthesis and Photoreactivity (ISOF), Italy
M. Alberto Bianco	Prof., Université de Strasbourg, France

Andrea SCHLIERF

Matériaux hybrides organiques à base de graphène

Résumé

En 2004, le carbone, la base de toute vie connue sur Terre, a marqué les esprits une fois de plus: Les scientifiques de l'Université de Manchester au Royaume Uni ont pu extraire une matière carbonée complètement nouvelle, le graphène à partir d'un morceau de graphite comme celui qui compose les crayons. À l'aide d'un ruban adhésif, ils ont obtenu une paillette de carbone de l'épaisseur d'un atome seulement, à une époque où beaucoup pensaient qu'un matériaux cristallin aussi fin ne pouvait pas être stable. Le graphène parfait est une couche monoatomique composée d'atomes de carbone hybridés sp2, arrangés en structure alvéolaire; sa structure chimique particulière lui donne des propriétés physiques et chimique remarquable. Le graphène est devenu rapidement la matière carbonée la plus intensivement étudiée parmi celles «possiblement révolutionnaires», avec ses applications potentielles s'étendant de la microélectronique aux composites, des énergies renouvelables à la médecine. En 2010, Geim et Novoselov ont été récompensés par le prix Nobel de physique pour leurs «expériences révolutionnaires sur les matériaux bi-dimensionnels en graphène» qui a ouvert une nouvelle ère dans la science des matières carbonées.

La chimie non-covalente du graphène est exploitée et étudiée dans cette thèse dans le but de concevoir, produire, transformer et caractériser les nouveaux matériaux hybrides graphène-organique. L'étendue de ce travail couvre les aspects mécanistiques de l'exfoliation en phase liquide du graphène avec des colorants, les aspects fondamentaux des interactions entre le graphène et le chromophore, en phase liquide et solide, ainsi que l'élaboration de suspensions hybrides de graphène dans le but d'applications en électronique organique et dans les matériaux composites polymères fonctionnels.

graphène; matériaux hybrides ; semi-conducteur ; exfoliation

Résumé en anglais

In 2004, carbon, the basis of all known life on earth, has surprised once again: Researchers from University of Manchester, UK, extracted a completely new carbon material, graphene, from a piece of graphite such as is found in pencils.
Using adhesive tape, they obtained a flake of carbon with a thickness of just one single atom, at a time when many believed it impossible for such thin crystalline materials to be stable. Pristine graphene is a mono□atomic sheet of, sp2 hybridized carbon atoms arranged in a honeycomb network; this particular chemical structure gives rise to its outstanding physical and chemical properties. Graphene rapidly became the most intensively studied among the 'possibly revolutionary' carbon materials, with its potential applications reaching from microelectronics to composites,
from renewable energy to medicine. In 2010, Geim and Novoselov were honored with the Nobel Prize in Physics for their "ground breaking experiments regarding the two-dimensional material graphene" that started a new era in the science of carbon materials.

In this thesis we exploit and study the non-covalent chemistry of graphene to design, produce, process and characterize novel graphene organic hybrid materials. The scope of this work covers mechanistic aspects of graphene liquid phase exfoliation with dyes, fundamental aspects of graphene chromophore interactions in liquid and solid phase and the formulation of graphene hybrid suspensions towards application in organic electronics and functional polymer composite materials.

Graphene; hybrid materials; semiconductor; exfoliation

Table of contents

I. Abbreviations

AFM	Atomic Force Microscopy
CHCl3	Chloroform
CNT	Carbon nanotube
DMF	Dimethylformamide
EMI	Electromagnetic interference
EtOH	Ethanol
GNP	Graphene nano platelets
HOPG	Highly oriented pyrolytic graphite
IBS	Indanthrone bisulphonate
IPA	Isopropanol
IS	Integrating sphere
LPE	Liquid phase exfoliation
NMP	N-Methyl-2-pyrrolidone
oDCB	ortho Dichloro-benzene
OSC	Organic semiconductor
PDI	Perylene-diimide
PDI-CN	butyl dicyano-perylenecarboxy diimide
PDIF-CN	N,N'-1H,1H-perfluorobutyl dicyano perylenecarboxy diimide
PL	Photoluminescence
PS1	1-Pyrenesulfonic acid sodium salt
PS2	6,8-Dihydroxy-1,3-pyrenedisulfonic acid disodium salt
PS3	8-hydroxypyrene-1,3,6-trisulfonic acid
PS4	1,3,6,8-Pyrenetetrasulfonic acid tetra sodium salt
PVA	Polyvinyl alcohol
SAED	Selected area electron diffraction
SEM	Scanning electron microscope
TA1	N',N'-bis(2-methy, 6-ethyl-sulfonic acid) perylene-3,4,9,10-tetracarboxylic diimide
TA2	N',N'-bis(2,6 dimethyl) disulfonic perylene-3,4,9,10-tetracarboxylic diimide
TEM	Transmission electron microscope
UV	Ultraviolet/visible absorption
α	Absorption coefficient

II. Abstract

Carbon materials have evoked tremendous interest both in fundamental research and materials' innovation, and graphite, carbon black and new, sophisticated carbon allotropes such as fullerenes or carbon nanotubes expanded into many aspects of daily life.

Historically, the great potential of carbon materials remained unexploited until the discovery of pure graphite in the mid-16th century, when the shepherds of Borrowdale, a village in Cumbria, England, discovered a new material - native, high quality graphite. Shortly after, the Borrowdale graphite mine was in full operation, allowing exploitation of graphite's excellent lubricant properties that found application in cannon ball molding, a military craft of strategic relevance at that time. [1] Nearly 300 years later, in the 18th century, graphite was gaining popularity particularly as an artist's medium for drawing: Simultaneously with the increasing difficulty of obtaining good-quality natural chalks at this time, graphite processing and production became more and more sophisticated and made a fine range of graphite pencils accessible for artworks. [2]

In 2004, carbon, the basis of all known life on earth, has surprised once again: Researchers from University of Manchester, UK, extracted a completely new carbon material, graphene, from a piece of graphite such as is found in pencils. Using adhesive tape, they obtained a flake of carbon with a thickness of just one single atom, at a time when many believed it impossible for such thin crystalline materials to be stable.[3] Pristine graphene is a mono-atomic sheet of, sp2 hybridized carbon atoms arranged in a honeycomb network; this particular chemical structure gives rise to its outstanding physical and chemical properties. Graphene rapidly became the most intensively studied among the 'possibly revolutionary' carbon materials, with its potential applications reaching from microelectronics to composites, from renewable energy to medicine.[4] In 2010, Geim and Novoselov were honoured with the Nobel Prize in Physics for their *"ground breaking experiments regarding the two-dimensional material graphene" that* started a new era in the science of carbon materials.

II. Abstract

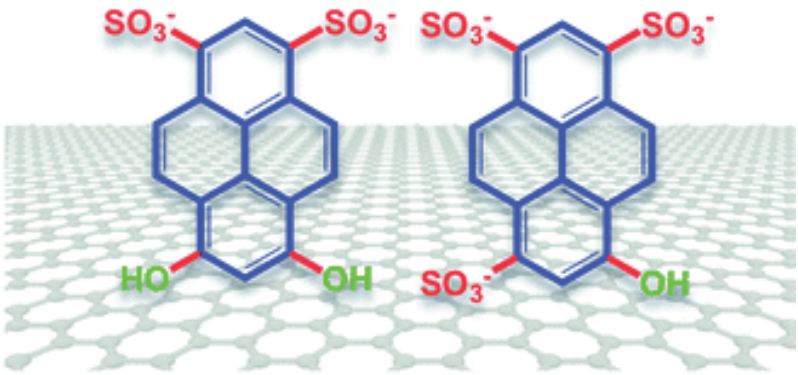

Fig. 1 Illustration of graphene organic hybrid materials based on amphiphilic chromophores, here pyrene derivatives functionalized with sulphonic and hydroxyl groups.

In this thesis we focus our attention on the non-covalent chemistry of graphene: We create and study all-organic graphene hybrid materials based on small aromatic dyes and organic semiconductor molecules, and address the design and processing of such novel graphene organic hybrid structures. This work further investigates properties of such novel graphene-based hybrid materials starting from fundamental physico-chemical aspects towards an application oriented point of view.

The graphene-organic hybrid materials developed here are not only valuable model systems to investigate the non-covalent chemistry of graphene, but they have great potential for application particularly related to nanotechnologies and organic electronics. With our approach, we focus on a new and versatile route of graphene production which allows accessing graphene's outstanding properties, namely the implementation of graphene into all-organic graphene hybrid materials based on small aromatic dyes or organic semiconductor molecules:[5]

Through careful design and manipulation of small, aromatic carbon-based molecules, hybrid structures with graphene are accessible through non-covalent interactions. The controlled interaction of graphene with, for instance, organic semiconductors (OSC) can offer an in-situ solution to improve graphene's processibility [5-7] and to tailor graphene properties for application, enabling an optimal control over the molecular self-assembly process with graphene to form low-dimensional graphene-organic architectures. [8-10]

II. Abstract

To explore some of the most relevant aspects of the non-covalent chemistry of graphene and OSCs, and the potential of such graphene-organic hybrid materials towards application, we have selected to study:

- Aqueous graphene-hybrid suspensions obtained by direct exfoliation of graphite with pyrene sulphonic acid sodium salt, suggesting an innovative exfoliation and purification technique.

- Graphene suspensions based on pyrene derivatives with systematically varying polar functionalization, a mechanistic study unravelling the role of charge, dipole and functionalization in chromophore assisted graphite liquid phase exfoliation.

- Steady state optical and Raman spectroscopy on graphene directly exfoliated with a water soluble perylene diimide derivative.

- Solvent effects on the dispersion of graphene hybrids with high performance n-type organic semiconductors investigated as well as fundamental aspects and technical challenges of optical spectroscopy on such materials.

- Indanthrone bisulphate based graphene hybrid material, as functional polymer filler for its anti-static applications.

In more detail, we have first developed a simple method to produce graphene suspensions by using non-covalent interaction with Py–1SO3 (pyrenes sulfonic acid sodium salt), using only water as solvent. We found that by using our method, based on ultra-sonication with Py–1SO3, it is possible to achieve stable graphene suspensions directly in water. With a washing procedure based on centrifugation and solvent exchange, the suspensions could be purified, yielding hydrophobic graphene flakes stabilized with Py-SO3 in aqueous solution. This project was realized in close collaboration with university of Manchester, UK.

II. Abstract

As our results of this first project indicated that functionalization of pyrene with one sulfonic group has a major impact on the eligibility as graphite exfoliation agent, we extended our study comparing the results on Py-1SO3 with further -SO3 functionalized pyrene derivatives to achieve a better understanding of the exfoliation mechanism. In an interdisciplinary study correlating experimental data with DFT simulations (performed at University of Mons, Belgium), we found an unambiguous correlation between the graphene-dye interaction energy, the dye's molecular structure and the amount of graphene obtained with liquid phase exfoliation.

We then extend our approach to perylene diimide (PDI) derivatives with polar moieties, as a model system for perylene diimide based organic semiconductor materials commonly applied in organic electronics.
These molecules are based on an extended π-system which can be expected to favour non-covalent functionalization of the graphene lattice through π-π interaction, similar to what has been found for sulphonated pyrene derivatives. In close collaboration with NMS at University of Cambridge, and University College of London, UK, we first investigated the direct production of graphene-PDI hybrids in polar solvents such as water, EtOH or isopropanol. Raman, steady state and time resolved spectroscopy was applied on in-situ exfoliated graphene organic hybrids, obtaining information on graphene quality, graphene-perylene diimide interaction and the fingerprint of the dye itself.

In a next step towards application of graphene-organic hybrids in organic electronics, we studied the direct exfoliation with high performance n-type semiconductors in organic solvents. N-type PDI derivatives (butyl dicyano perylene carboxydiimide PDI-CN2 and fluoroalkyl chains, N,N'-1H,1H-perfluorobutyl dicyano perylene carboxydiimide PDIF-CN2), have been employed as exfoliation agents and studied for their steady state optical properties in liquid phase. We compare OSC assisted exfoliation in an aromatic with an aliphatic chlorinated solvent to better unravel the complex interplay of graphene, OSC and solvent interaction in suspension.

Another important research line towards application are polymer composite materials: Graphitic nanostructures attract increasing attention as filler in polymer composites, owing to their unique electrical, optical and mechanical properties [11]. In particular, the properties of graphene, such as its large specific surface area, high electrical conductivity, well-defined thermal conductivity and

thermal stability make it an ideal choice as nanofiller for the preparation polymer composites [12]. The dye studied here is indanthrone sulphonic acid sodium salt (IBS), a commercial chromophore applied on large scale in industrial pigment formulations.[13] In collaboration with BASF, Germany, direct exfoliation of graphite with IBS was used to achieve aqueous suspensions of graphene hybrids, readily dispersible in a polyvinyl-alcohol matrix for prospective application in anti-statics.

Overall, in this thesis we exploit and study the non-covalent chemistry of graphene to design, produce, process and characterize novel graphene organic hybrid materials. The scope of this work covers mechanistic aspects of graphene liquid phase exfoliation with dyes, fundamental aspects of graphene-chromophore interactions in liquid and solid phase and the formulation of graphene hybrid suspensions towards application in organic electronics and functional polymer composite materials.

II. Abstract

(1) Palermo, V. *Chemical Communications* 2013, *49*, 2848.

(2) Millidge, S. *Oxford Press and New York Museum of Modern Arts* 2014.

(3) Peierls, R. E. *Ann. I. H. Poincare* 1935, *5*, 177.

(4) Novoselov, K. S.; Fal'ko, V. I.; Colombo, L.; Gellert, P. R.; Schwab, M. G.; Kim, K. *Nature* 2012, *490*, 192.

(5) Schlierf, A.; Samori, P.; Palermo, V. *Journal of Materials Chemistry C* 2014.

(6) Ciesielski, A.; Samori, P. *Chemical Society Reviews* 2013.

(7) Yang, J.; Bai, L.; Feng, G.; Yang, X.; Lv, M.; Zhang, C. a.; Hu, H.; Wang, X. *Industrial & Engineering Chemistry Research* 2013, *52*, 16745.

(8) Pathipati, S. R.; Pavlica, E.; Treossi, E.; Rizzoli, R.; Veronese, G. P.; Palermo, V.; Chen, L.; Beljonne, D.; Cai, J.; Fasel, R.; Ruffieux, P.; Bratina, G. *Organic Electronics* 2013, *14*, 1787.

(9) Xiao, K.; Deng, W.; Keum, J. K.; Yoon, M.; Vlassiouk, I. V.; Clark, K. W.; Li, A.-P.; Kravchenko, I. I.; Gu, G.; Payzant, E. A.; Sumpter, B. G.; Smith, S. C.; Browning, J. F.; Geohegan, D. B. *Journal of the American Chemical Society* 2013, *135*, 3680.

(10) Järvinen, P.; Hämäläinen, S. K.; Banerjee, K.; Häkkinen, P.; Ijäs, M.; Harju, A.; Liljeroth, P. *Nano Letters* 2013, *13*, 3199.

(11) Yu, D. S.; Kuila, T.; Kim, N. H.; Lee, J. H. *Chemical Engineering Journal* 2014.

(12) Stankovich, S.; Piner, R. D.; Nguyen, S. T.; Ruoff, R. S. *Carbon* 2006, *44*, 3342.

(13) Baebler Fridolin, J. E. E., Medinger Bernhard In *CIBA Patent* 1987; Vol. 4692189.

III. Résumé

Les matières carbonées suscitent un formidable intérêt dans la recherche fondamentale et l'innovation de matériaux. Depuis, le graphite, le noir de carbone, ainsi que les allotropes nouveaux et complexes du carbone, tels que les fullerènes ou les nanotubes de carbone, se sont développés dans beaucoup d'aspect de la vie quotidienne.

Historiquement, le potentiel des matières carbonées est resté inexploité jusqu'à la découverte dans le milieu du 16éme siècle du graphite pur, un nouveau matériau, par les bergers de Borrowdale, un village dans le comté de Cumbrie en Angleterre. Peu de temps après, la mine de graphite de Borrowdale se mit à fonctionner à plein régime permettant l'exploitation des excellentes propriétés lubrifiantes du graphite, notamment pour le moulage des boulets de canon, un savoir-faire militaire stratégique à cette époque. [1] Presque 300 ans plus tard, au 18éme siècle, le graphite a gagné en popularité, particulièrement en tant qu'outil pour le dessin. La difficulté croissante à obtenir de la craie naturelle de bonne qualité à cette époque, ainsi qu'une production et un traitement du graphite de plus en plus élaboré, permirent la production nouvelle d'une gamme raffinée de crayons graphites pour le dessin. [2]

En 2004, le carbone, la base de toute vie connue sur Terre, a marqué les esprits une fois de plus : Les scientifiques de l'Université de Manchester au Royaume Uni ont pu extraire une matière carbonée complètement nouvelle, le graphène à partir d'un morceau de graphite comme celui qui compose les crayons. À l'aide d'un ruban adhésif, ils ont obtenu une paillette de carbone de l'épaisseur d'un atome seulement, à une époque où beaucoup pensaient qu'un matériau cristallin aussi fin ne pouvait pas être stable. [3]

Le graphène parfait est une couche monoatomique composée d'atomes de carbone hybridés sp2, arrangés en structure alvéolaire ; sa structure chimique particulière lui donne des propriétés physiques et chimique remarquable. Le graphène est devenu rapidement la matière carbonée la plus intensivement étudiée parmi celles «possiblement révolutionnaires », avec ses applications potentielles s'étendant de la microélectronique aux composites, des énergies renouvelables à la médecine. [4] En 2010, Geim et Novoselov ont été récompensés par le prix Nobel de physique pour leurs «expériences révolutionnaires sur les matériaux bi-dimensionnels en graphène» qui a ouvert une nouvelle ère dans la science des matières carbonées.

III. Résumé

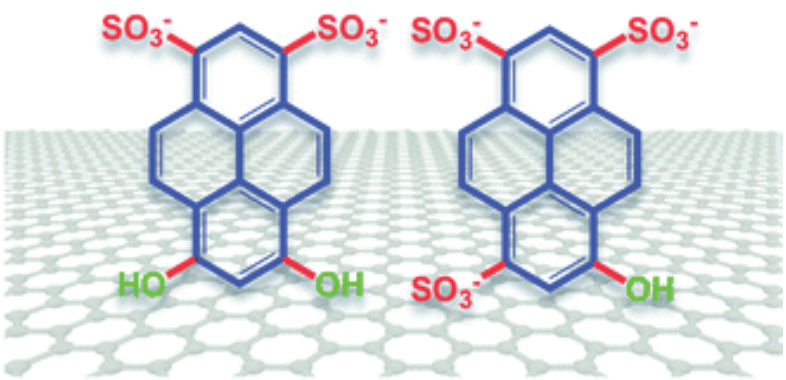

Fig. 1 Illustration de matériaux hybrides organiques de graphène basés sur des chromophores amphiphiliques, ici des dérivés de pyrène fonctionnalisés avec des groupes sulphoniques et hydroxyles.

Cette thèse porte sur la chimie non-covalente du graphène : Nous créons et étudions des matériaux graphène tout organiques hybrides basés sur des petits colorants aromatiques et des molécules organiques semi-conductrices et nous abordons la conception et le traitement de ces structures hybrides novatrices de graphène organique. Ce travail examine plus en détails les propriétés de ces nouveaux matériaux hybrides de graphène, commençant par les aspects physico-chimiques fondamentaux jusqu'aux domaines d'applications.

Les matériaux hybrides de graphène organique développés ici ne sont pas seulement des systèmes modèles précieux pour étudier la chimie non-covalente du graphène, mais ils ont aussi un grand potentiel, particulièrement pour les applications apparentées aux nanotechnologies et à l'électronique organique. Avec notre approche, nous nous concentrons sur une voie de production de graphène nouvelle et polyvalente qui nous permet d'accéder aux propriétés exceptionnelles du graphène par l'implémentation du graphène dans des matériaux hybrides tout organiques du graphène, basés sur des petits colorants aromatiques et sur des molécules organiques semi-conductrices. [5] Grâce à une conception et une manipulation minutieuse de petites molécules aromatiques, des structures hybrides de graphène sont accessibles par des interactions non-covalentes.

L'interaction contrôlée du graphène avec, par exemple, des semi-conducteurs organiques (SCO) peut offrir une solution in-situ pour améliorer le traitement du graphène, [5-7] ainsi que pour adapter les propriétés du graphène pour ses applications, rendant possible un contrôle optimal des procédés moléculaires auto-assemblant avec le graphène pour former des architectures graphène-organique de faibles dimensions. [8-10]

III. Résumé

Pour explorer quelques un des aspects les plus pertinents de la chimie non-covalente du graphène et des SCOs, ainsi que le potentiel de tels matériaux hybrides graphène-organique pour les applications, nous avons étudié

- Des suspensions en phase aqueuse d'hybride de graphène obtenues à partir de l'exfoliation directe du graphite avec du pyrène-1-sulfonate de sodium, suggérant une méthode d'exfoliation et de purification innovatrice.
- Des suspensions de graphène basées sur les dérivés de pyrène, avec une fonctionnalisation polaire variée de façon systématique, une étude mécanistique dissociant le rôle de la charge, du dipôle et de la fonctionnalisation dans l'exfoliation en phase liquide du graphène assistée par chromophore.
- Spectroscopie optique et de Raman du graphène directement exfolié avec un dérivé de perylène diimide soluble dans l'eau.
- L'investigation des effets du solvant sur la dispersion des hybrides de graphène avec un composé semi-conducteur organique de type n de haute performance, ainsi que les aspects fondamentaux et les défis technique de la spectroscopie optique sur ces matériaux.
- Du matériel hybride graphène basé sur le bisulfate d'indanthrone, en tant que charge fonctionnelle de polymère pour ses applications antistatiques.

De façon plus détaillée, nous avons premièrement développé une méthode simple de production des suspensions de graphène en utilisant l'interaction non-covalente avec le PS1 (pyrène-1-sulfonate de sodium) en utilisant seulement de l'eau comme solvant. Nous avons découvert qu'en utilisant notre méthode, basée sur la sonication avec du PS1, il est possible d'obtenir une suspension stable de graphène directement dans l'eau. Puis, avec une procédure de purification basée sur la centrifugation et l'échange de solvant, la suspension a pu être purifiée, laissant des flocons de graphène hydrophobe, stabilisés par le PS1 en solution aqueuse. Ce projet a été réalisé en collaboration étroite avec l'Université de Manchester au Royaume-Uni.

III. Résumé

Comme les résultats de ce premier projet montrent que la fonctionnalisation du pyrène avec un groupe sulfonique a un impact majeur sur la capacité en tant qu'agent exfoliant du graphite, nous avons poursuivi notre étude en comparant nos résultats PS1 avec d'autres dérivés du pyrène contenant des groupes fonctionnels -SO3, pour améliorer la compréhension du mécanisme d'exfoliation. Dans une étude interdisciplinaire comparant les résultats expérimentaux et des simulations DFT (effectuées à l'Université de Mons en Belgique), nous avons trouvé une corrélation sans équivoque entre l'énergie d'interaction graphène-colorant, la structure moléculaire du colorant et la quantité de graphène obtenue par exfoliation en phase liquide.

Nous avons étendu cette approche aux dérivés du pérylène diimide (PDI) avec des groupements polaires, comme système modèle pour des matériaux organiques semi-conducteur basés sur le pérylène diimide et couramment utilisés en électronique organique. Ces molécules sont basées sur un système conjugué étendu, qui pourrait favoriser la fonctionnalisation non-covalente du réseau du graphène à travers une interaction π-π, identique à celle découverte pour les dérivés sulfonés du pyrène.

En collaboration étroite avec le NMS de l'Université de Cambridge ainsi que l'University College de Londres au Royaume-Uni, nous avons étudié la production dirècte d'hybrides graphène-PDI, dans un solvant polaire tel que l'eau, l'éthanol ou l'isopropanol. La spectroscopie de Raman en état stationnaire et à résolution dans le temps a été réalisé sur des hybrides organiques de graphène exfolié in-situ, révélant des informations sur la qualité du graphène, sur l'interaction entre le graphène et le pérylène diimide et sur l'empreinte du colorant lui-même.

Dans une prochaine étape vers l'application des hybrides organiques de graphène en électronique organique, nous avons étudiés l'exfoliation directe avec des semi-conducteurs de type n de haute performance dans des solvants organiques. Des dérivés PDI de type n (butyle dicyano- perylenecarboxydiimide PDI-CN2 et les chaînes fluoro-alkyle, N,N'-1H,1H-perfluorobutyle dicyanoperylenecarboxydiimide PDIF-CN2), ont été utilisés comme des agents d'exfoliation et étudiés pour leurs propriétés optiques en phase liquide. Nous comparons les exfoliations assistées par SCO dans un aromatique avec un solvant aliphatique chloré pour élucider les interactions complexes dans la suspension entre le graphène, le SCO et le solvant.

III. Résumé

Les matériaux polymères composites représentent un autre domaine d'application pour la recherche: Les nanostructures graphitiques retiennent de plus en plus l'attention comme charge dans les composites polymères, en raison de leurs propriétés électriques, optiques et mécaniques uniques.[11] En particulier, les propriétés du graphène, tels que sa grande surface spécifiques, sa haute conductivité électrique, sa conductivité thermique et sa stabilité thermique en font un choix idéal en tant que nano-charge pour la préparation de composites polymères.[12] Le colorant étudié ici est le sel d'indanthrone bisulfate de sodium (IBS), un chromophore commercial utilisé à grande échelle pour les formulations industrielles de pigmentation.[13] En collaboration avec BASF en Allemagne, l'exfoliation directe du graphite avec de l'IBS a été utilisée pour produire un graphène pur, soluble dans l'eau, facilement dispersable dans une matrice d'alcool polyvinylique, pour de potentielles applications antistatiques.

Globalement, la chimie non-covalente du graphène est exploitée et étudiée dans cette thèse dans le but de concevoir, produire, transformer et caractériser les nouveaux matériaux hybrides graphène-organique. L'étendue de ce travail couvre les aspects mécanistiques de l'exfoliation en phase liquide du graphène avec des colorants, les aspects fondamentaux des interactions entre le graphène et le chromophore, en phase liquide et solide, ainsi que l'élaboration de suspensions hybrides de graphène dans le but d'applications en électronique organique et dans les matériaux composites polymères fonctionnels.

(1) Palermo, V. Chemical Communications 2013, 49, 2848.
(2) Millidge, S. Oxford Press and New York Museum of Modern Arts 2014.
(3) Peierls, R. E. Ann. I. H. Poincare 1935, 5, 177.
(4) Novoselov, K. S.; Falko, V. I.; Colombo, L.; Gellert, P. R.; Schwab, M. G.; Kim, K. Nature 2012, 490, 192.
(5) Schlierf, A.; Samori, P.; Palermo, V. Journal of Materials Chemistry C 2014.
(6) Ciesielski, A.; Samori, P. Chemical Society Reviews 2013.
(7) Yang, J.; Bai, L.; Feng, G.; Yang, X.; Lv, M.; Zhang, C. a.; Hu, H.; Wang, X. Industrial & Engineering Chemistry Research 2013, 52, 16745.
(8) Pathipati, S. R.; Pavlica, E.; Treossi, E.; Rizzoli, R.; Veronese, G. P.; Palermo, V.; Chen, L.; Beljonne, D.; Cai, J.; Fasel, R.; Ruffieux, P.; Bratina, G. Organic Electronics 2013, 14, 1787.
(9) Xiao, K.; Deng, W.; Keum, J. K.; Yoon, M.; Vlassiouk, I. V.; Clark, K. W.; Li, A.-P.; Kravchenko, I. I.; Gu, G.; Payzant, E. A.; Sumpter, B. G.; Smith, S. C.; Browning, J. F.; Geohegan, D. B. Journal of the American Chemical Society 2013, 135, 3680.
(10) Järvinen, P.; Hämäläinen, S. K.; Banerjee, K.; Häkkinen, P.; Ijäs, M.; Harju, A.; Liljeroth, P. Nano Letters 2013, 13, 3199.
(11) Yu, D. S.; Kuila, T.; Kim, N. H.; Lee, J. H. Chemical Engineering Journal 2014.
(12) Stankovich, S.; Piner, R. D.; Nguyen, S. T.; Ruoff, R. S. Carbon 2006, 44, 3342.
(13) Baebler Fridolin, J. E. E., Medinger Bernhard. CIBA Patent 1987; Vol. 4692189.

Chapter 1

Carbon materials and graphene

1.1. Carbon allotropes - from graphite to graphene hybrid materials

Carbon is the basis of organic chemistry and therefore of life on earth: the reason of this extraordinary role is carbon's chemical versatility, resulting in a great variety of physical and chemical properties. Atomic carbon exists in three bonding states with different geometry, shape and dimension, corresponding to sp3, sp2 and sp hybridization of the atomic orbital. These different bonds lead to diverse carbon allotrope structures such are diamond, graphite, carbyne, fullerenes, nanotubes, polyaromatic hydrocarbons, graphene, and amorphous carbon to mention some of the most prominent forms of carbon.

Diamond for instance exhibits a typical cubic crystal structure with a repeating pattern of 8 atoms; the strong bonding leads to the highest hardness and thermal conductivity of any bulk material, determining the major industrial application of diamond in cutting and polishing tools. Graphite, in contrary, is based on sp2 hybridized carbons and has a layered, planar structure. In each layer, the carbon atoms are arranged in a honeycomb lattice with separation of 0.142 nm, and the distance between planes is 0.335 nm.[1] The two known forms of graphite, alpha (hexagonal) and beta (rhombohedral), have very similar physical properties, except that the single carbon layers stack slightly differently.[2] The layered structure of graphite and the weak forces between single carbon layers allow for application for refractories, batteries, steelmaking, brake linings, foundry facings and lubricants.

The newest and most exiting carbon allotrope, graphene, can be considered as a border case of an extended aromatic system, being a mono-atomic layer of sp2 carbon reaching macroscopic lateral extension. As demonstrated in 2004, layers of graphene can be extracted from a graphite crystal by peeling of the sheets with simple adhesive tape.

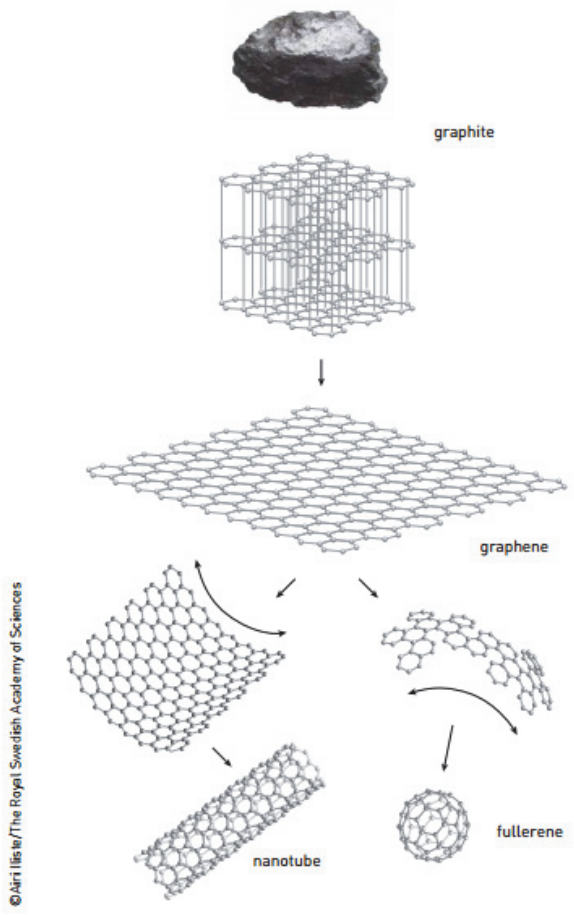

Fig. 1. Illustration of carbon allotropes derived from graphite; layered structure of graphite, single layer of graphene, carbon nanotubes and fullerenes. Reprinted with permission from the Royal Swedish Academy of Science.

On the very extreme of sp2 hybridized carbon systems are polyaromatic hydrocarbons (PAHs). These systems are based on a sp2 hybridized carbon backbone based on a defined number of aromatic rings, organized in a – usually planar - honeycomb network. Synthetic PAHs find application as photo-sensitizer, fluorescence markers and dyestuff, but they also appear naturally and are suspected to play a crucial role in the formation of life on our planet: According to NASA experts, more than 20% of the carbon in the universe may be associated with PAHs being possible starting materials for the formation of life. PAHs seem to have been formed shortly after the Big Bang, and are widespread throughout the universe. (see Ref. [3]). Carbon science, especially related to nanotechnologies, has great potential and in the next years can offer more interesting discoveries and new solution, from a fundamental understanding of such new materials towards application in industry and everyday life.

1.2. Challenges in graphene production

Emerging technologies, no matter how revolutionary they are, initially face significant cost barriers to compete with established technologies. Thus, cheap production of large amounts of graphene with controlled electrical, chemical and structural properties is fundamental for graphene to have a significant impact on society. While high-end electronic devices need highest quality material in terms of electronic and crystalline properties, applications like transparent electrodes or functional polymer composites demand cost efficient solutions. A major advantage of graphene is that, despite its young age, it can be already produced with many different techniques; the production techniques yield graphene of varying quality and quantity, often facing a trade off in quality and production volume and cost.

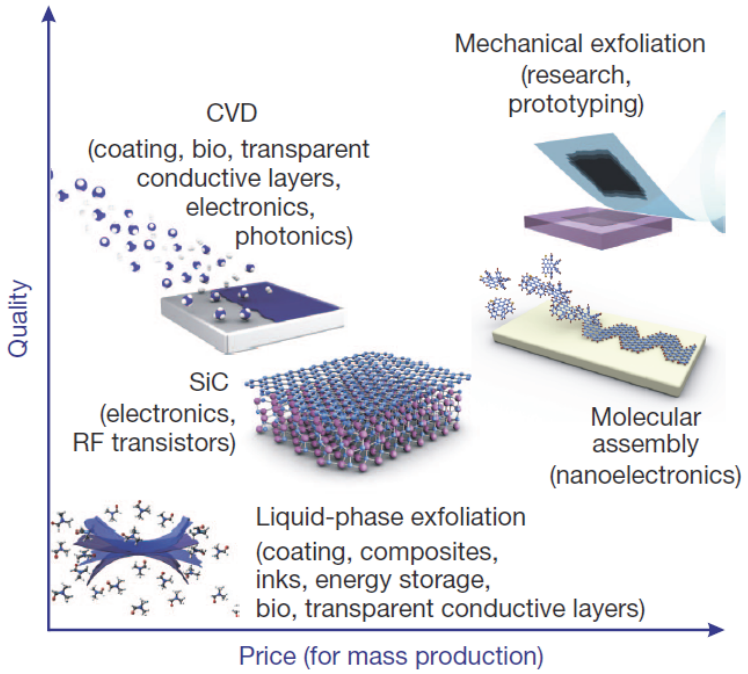

Fig. 2. There are several methods suggested for mass-production of graphene, which allow a wide choice of graphene-type materials in terms of size, quality and price for any particular application. [4]

Graphene production remains a challenging and active field of research. Different approaches are followed to produce graphene; for instance, very high quality graphene sheets can be obtained in low quantities by the so-called bottom-up approach, including processes such as chemical vapour growth, [5,6] annealing SiC substrates,[7] and chemically building up graphene from molecular building blocks [8,9]. Alternatively, defect-free sheets

can be produced with a top-down approach; here, graphene sheets are obtained from bulk graphite by micromechanical cleavage [10] or ball-milling [11] and ultrasound based exfoliation of graphite [12,13]: The latter particularly raised interests, as graphite can be exfoliated directly into liquid environments prospectively opening ways for up-scaling and processing of this new material with industrially relevant techniques such as ink jet printing, coating etc..

Micromechanical cleavage. This simple technique was presented first by Geim and Novosolov who used conventional adhesive tape to repeatedly divide graphite into increasingly thinner pieces. The graphene layers are then transferred on silicon oxide. An extraordinarily high quality of graphene can be produced in this way, and no special equipment needed. However, this technique is obviously not applicable in large-scale production; it often yields uneven films with the single sheets difficult to localize upon transfer on a substrate. The scotch tape approach is mainly of importance for fundamental research.

Chemical method: Here, reduced graphene oxide, a graphene allotrope typically exhibiting heavy doping due to oxidative and structural defects, is produced by reducing graphene oxide (GO) via thermal, chemical or electrical methods. Advantages: reduced graphene oxide is suitable for large area and up-scaling production and can be chemically functionalized. Disadvantages of that method are the poor quality of reduced graphene oxide which does not achieve the performance of pristine graphene layers. Covalently modified reduced graphene oxide finds targeted applications, such as biological sensors, composites or as gas barrier.

Thermal decomposition of SiC: Another approach to the production of graphene is thermal treatment of silicon carbide under vacuum or an inert ambient, causing sublimation of the silicon atoms while carbon reorganizes from graphenic domains to continuous film. Advantages: The decomposition can be applied even on insulating substrates, thus no transfer necessary. The wafers are available on varying scales scale and the graphene obtained is of good quality. However, it is a high temperature process and it is difficult control of the final morphology of the graphene film. Thermal decomposition finds applications mainly in high frequency transistors, sensor and electronics.

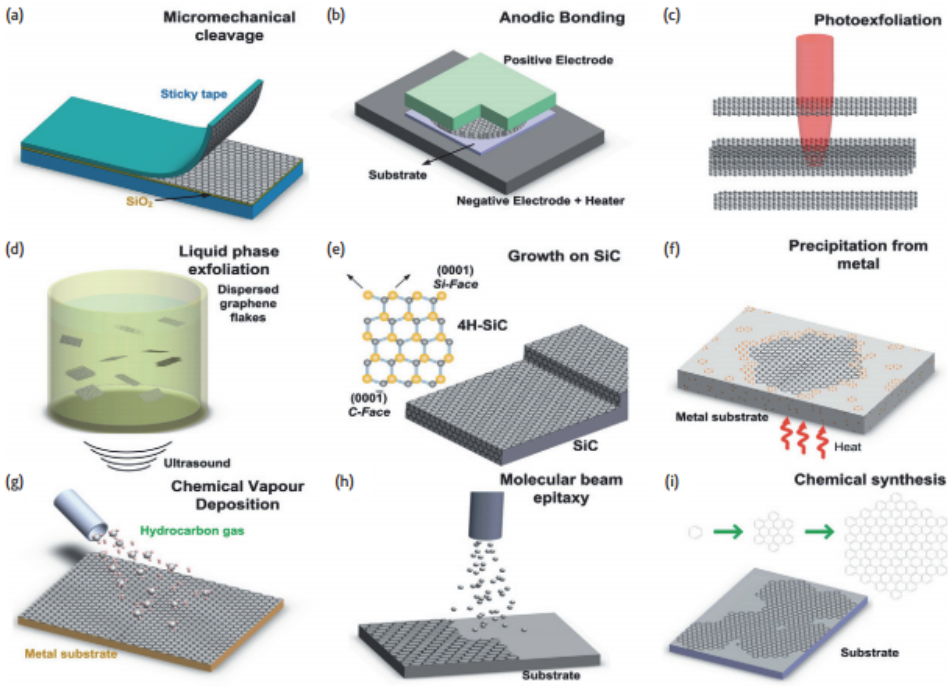

Fig. 3. Schematic illustration of the main graphene production techniques. (a) Micromechanical cleavage. (b) Anodic bonding. (c) Photo-exfoliation. (d) Liquid phase exfoliation. (e) Growth on SiC. Gold and grey spheres represent Si and C atoms, respectively. At elevated T, Si atoms evaporate (arrows), leaving a carbon-rich surface that forms graphene sheets. (f) Segregation/precipitation from carbon containing metal substrate. (g) Chemical vapour deposition. (h) Molecular Beam epitaxy. (i) Chemical synthesis using benzene as building block. (reprinted with permission from Ref. [14])

Chemical vapour deposition (CVD): In this method graphene is grown on a metal catalyst, typically a copper substrate, from a gaseous carbon source (i.e. methane, ethylene) at high temperature and an inert ambient. The carbon precursor dissociates at high temperature on the catalyst surface, the remaining carbon dissolves in the catalyst and then precipitates out during the cooling process. Good quality of graphene can be produced even on large substrates. However, as it is a high temperature process, the resulting film morphology is difficult to control and a transfer from the conducting substrate is necessary after synthesis. Prospective applications are flexible display or transparent conductors, sensor, solar cells or OFETs.

Solution-based exfoliation: it is possible to produce graphene from sonication of graphite in special solvents (i.e. dimethylformamide) or with particular molecules (i.e. pyrene

derivatives). These molecules, under sonication, have ability to interact strongly with graphite, possibly infiltrating between the planes and making possible the exfoliate graphite in graphene. Newer approaches include the application of a solvent /surfactant system that allows for graphene exfoliation and subsequent stabilization in suspension. Advantages of that method are up-scalability and simple processing of suspensions. Disadvantages are that the liquid medium required for exfoliation includes poisonous or high boiling solvents. Applications: transparent conductors, sensors, composites, coating and gas barrier.

Production-wise, in the focus of this thesis are new approaches in liquid-phase exfoliation of ‘‘pristine’’ graphite by exploiting a method based on ultra sonication: As described above, graphite can be successfully exfoliated in liquid environments by exploiting ultrasound to extract individual layers. The liquid-phase exfoliation (LPE) process (shown in Fig. 4) typically involves three steps:

(1) Graphite dispersion in a solvent
(2) Exfoliation of graphene from bulk graphite
(3) Purification of the dispersed material

Graphene flakes can be produced by surfactant-free exfoliation of graphite via chemical wet dispersion, followed by ultrasonication in selected organic solvents such as NMP, DMF or oDCB.[13,15,16] During ultrasonication, shear forces and cavitation,[17] such as the growth and collapse of the micrometer-sized bubbles or voids in liquids due to pressure fluctuations, act on the bulk graphite material and induce exfoliation.

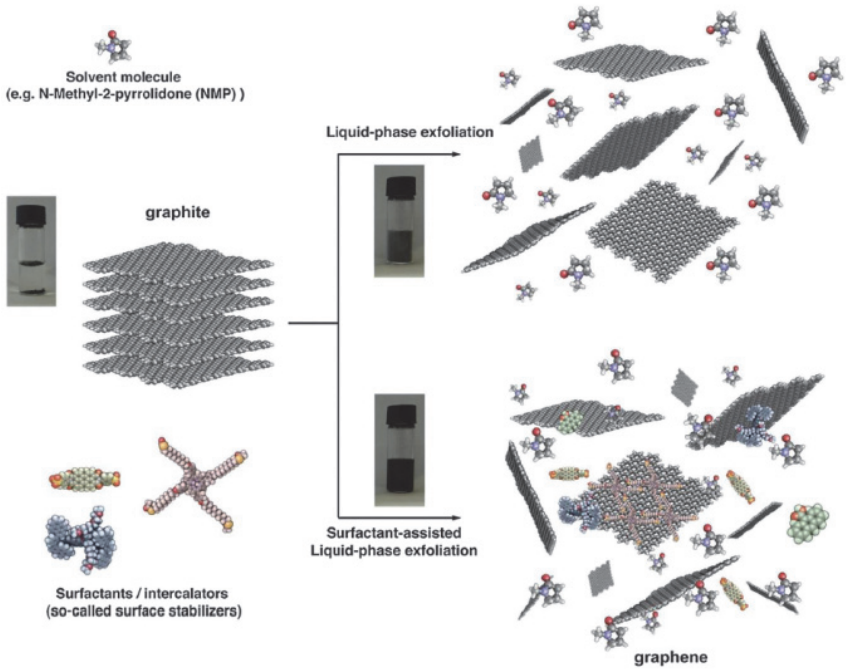

Fig. 4. Schematic representation of the liquid-phase exfoliation process of graphite in the absence (top-right) and presence (bottom-right) of surfactant molecules. Reprinted with permission from Ref. [18]

Following the exfoliation step, solvent–graphene interactions need to avoid attractive forces between the sheets destabilizing the suspension. Solvents being ideal to disperse graphene are those that minimize the interfacial tension between the liquid and graphene flakes, i.e. the force that minimizes the area of the surfaces in contact. [19] In other solvent systems, using a surfactant can help to overcome inter-sheet attractive forces that destabilize the dispersion and induce re-aggregation and even precipitation of graphene from the liquid phase.

A new versatile route to exploit graphene's outstanding properties is the implementation into all-organic graphene hybrid materials based on small aromatic dyes and organic semiconductor molecules. Through careful design and manipulation of such small, carbon-based molecules, graphene hybrid structures with tuneable, tailored properties are accessible through non-covalent interactions and are discussed in detail in the next chapter.

References.

(1) Delhaes, P. *Graphite and Precursors*; CRC Press, 2001.

(2) Lipson, H. S. A. R. *Nature* 1942, *149*, 328.

(3) Rachel, H. *NASA* 2014.

(4) Novoselov, K. S.; Falko, V. I.; Colombo, L.; Gellert, P. R.; Schwab, M. G.; Kim, K. *Nature* 2012, *490*, 192.

(5) Kim, K. S.; Zhao, Y.; Jang, H.; Lee, S. Y.; Kim, J. M.; Kim, K. S.; Ahn, J. H.; Kim, P.; Choi, J. Y.; Hong, B. H. *Nature* 2009, *457*, 706.

(6) Li, X.; Cai, W.; An, J.; Kim, S.; Nah, J.; Yang, D.; Piner, R.; Velamakanni, A.; Jung, I.; Tutuc, E.; Banerjee, S. K.; Colombo, L.; Ruoff, R. S. *Science* 2009, *324*, 1312.

(7) Berger, C.; Song, Z.; Li, X.; Wu, X.; Brown, N.; Naud, C.; Mayou, D.; Li, T.; Hass, J.; Marchenkov, A. N.; Conrad, E. H.; First, P. N.; de Heer, W. A. *Science* 2006, *312*, 1191.

(8) Chen, L.; Hernandez, Y.; Feng, X.; Müllen, K. *Angewandte Chemie International Edition* 2012, *51*, 7640.

(9) Palma, C. A.; Samorì, P. *Nat. Chem.* 2011, *3*, 431.

(10) Novoselov, K. S.; Jiang, D.; Schedin, F.; Booth, T. J.; Khotkevich, V. V.; Morozov, S. V.; Geim, A. K. *PNAS* 2005, *102*, 10451.

(11) Leon, V.; Quintana, M.; Antonia Herrero, M.; Fierro, J. L. G.; de la Hoz, A.; Prato, M.; Vazquez, E. *Chemical Communications* 2011, *47*, 10936.

(12) Coleman, J. N. *Advanced Functional Materials* 2009, *19*, 3680.

(13) Hernandez, Y.; Nicolosi, V.; Lotya, M.; Blighe, F. M.; Sun, Z. Y.; De, S.; McGovern, I. T.; Holland, B.; Byrne, M.; Gun'ko, Y. K.; Boland, J. J.; Niraj, P.; Duesberg, G.; Krishnamurthy, S.; Goodhue, R.; Hutchison, J.; Scardaci, V.; Ferrari, A. C.; Coleman, J. N. *Nature Nanotechnology* 2008, *3*, 563.

(14) Bonaccorso, F.; Sun, Z.; Hasan, T.; Ferrari, A. C. *Nat. Photonics* 2010, *4*, 611.

(15) Hamilton, C. E.; Lomeda, J. R.; Sun, Z.; Tour, J. M.; Barron, A. R. *Nano Letters* 2009, *9*, 3460.

(16) Khan, U.; O'Neill, A.; Lotya, M.; De, S.; Coleman, J. N. *Small* 2010, *6*, 864.

(17) Mason, T. J.; Lorimer, J. P. In *Applied Sonochemistry*; Wiley-VCH Verlag GmbH & Co. KGaA: 2003, p 25.

(18) Ciesielski, A.; Samori, P. *Chemical Society Reviews* 2013.

(19) Israelachvili, J. N. *Intermolecular and Surface Forces, 3rd Edition*; Elsevier Academic Press Inc: San Diego, 2011.

Chapter 2

Graphene-organic hybrid materials

2. Graphene-organic hybrid materials

2.1. Introduction

Carbon-based systems such as small molecules, polymers, nanotubes and graphenes are active components for many materials for opto-electronics applications. Their physical and chemical properties are tunable and strictly depend on their precise chemical structure and size. All these carbon-based systems possess an extended π-conjugated scaffold that can be decorated with functional groups. Their functionalization can be optimized in order to programme their self-assembly into highly ordered supramolecular architectures, as driven by non-covalent interactions such as π-π stacking, hydrogen-bonding, etc. Small π-conjugated molecules (pyrenes, pentacenes, coronenes, polythiophenes, etc.), possess a well-defined electronic bandgap and a mono-dispersed nanometric size, the latter enabling a molecular self-assembly into highly ordered low-dimensional architectures such as fibers, nano-crystals or uniform monolayers (Fig. 1a ,b).

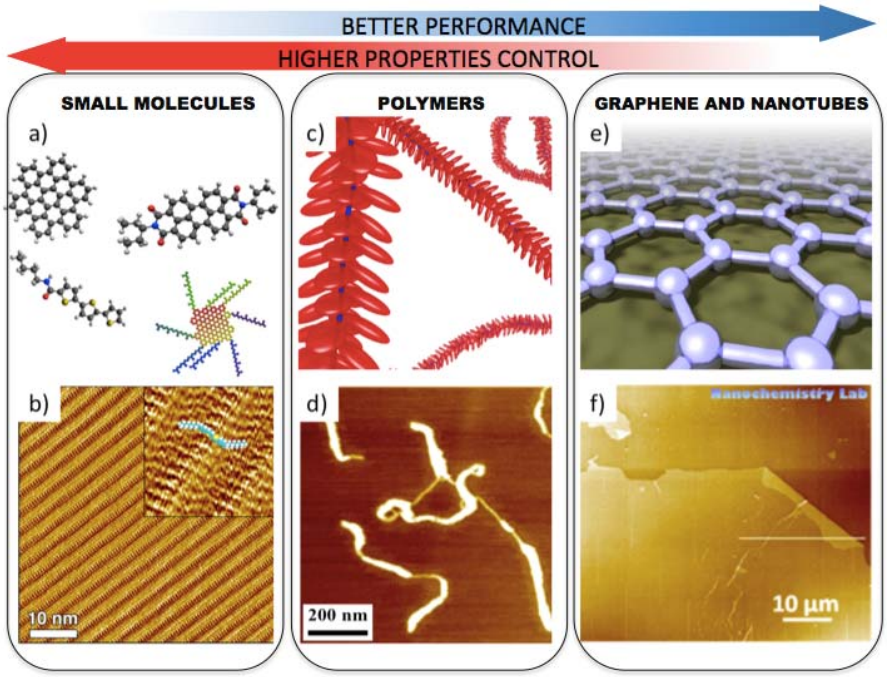

Fig. 1. Schematic representation and scanning probe microscopy images of different classes of carbon-based materials for (opto)electronics: a,b) Small molecules,[1] c,d) Polymers, [2] e,f) Graphenes.[3,4] Adapted with permission from Ref. 42, Copyright American Chemical Society. Adapted from Ref. 83 and Ref. 84 with permission from Wiley VCH.

Polymers, conversely, feature a larger linear backbone of sp2 carbons, ranging between a few to hundreds of nm in length; unlike small aromatic molecules, they tend to form more disordered assemblies (Fig. 1c,d), but can have an elongated and highly flexible shape that allows high solubility and efficient transport of electric charges.

Carbon nanotubes (CNT) and graphene are based on an aromatic honeycomb network reaching sizes up to a few tens of microns (Fig. 1 e, f). This exceptional molecular structure leads to extraordinary optical, electronic and mechanical properties that triggered research activities in various fields and resulted in the Nobel Prize in physics awarded to graphene. However, two are the greatest challenges that nowadays remain to be addressed in the research of carbon nanotubes and graphene: (1) process them using up-scalable approaches, and (2) obtain an ad-hoc chemical functionalization to control their physical and chemical properties. CNT samples are usually a mixture of semiconducting and metallic tubes; graphene, while having very high charge mobility, is a semi-metal, a zero-bandgap semiconductor, thus giving electrical devices with very poor Ion/Ioff ratio.

While many OS, thanks to their small size and flexible side chains, are easily sublimed in vacuum or processed from solution, pristine graphene sheets have a strong tendency to undergo aggregation, in solvents or in polymer matrices, to give graphitic clusters. Composites merging together the excellent properties of graphene with the high tunability and processability of organic molecules are highly requested in different research fields. As example, graphene could improve the mechanical and electrical properties of commercial polymers, but the interaction between graphene and the polymer matrix is often poor, and the graphene sheets tend to aggregate when processed with polymer. Graphene is also an interesting substrate for biomedical applications, but its interaction with biomolecules, as well as its biological activity, are still controversial.[5]

In particular, many of the possible applications of graphene are in electronics, but its zero-bandgap and poor processability on insulating substrates are major issues hindering this potential technological development. Many groups are trying to open a bandgap in graphene, for example by using graphene nanoribbons [6,7] or stacked bilayers [8] to combine high charge carrier mobility with high Ion/Ioff ratios in transistors.

Organic semiconductors (OS) already have a well-defined and tunable bandgap. By merging together their properties with those of graphene one may obtain an "ideal material" for semiconductor industry, optimal for flexible electronics applications. However, even if small polyaromatics, conjugated polymers and graphene or nanotubes exhibit a sp2 carbon based backbone, these different classes of materials cannot always be blended together effectively enough to yield beneficial effects on the materials' properties:

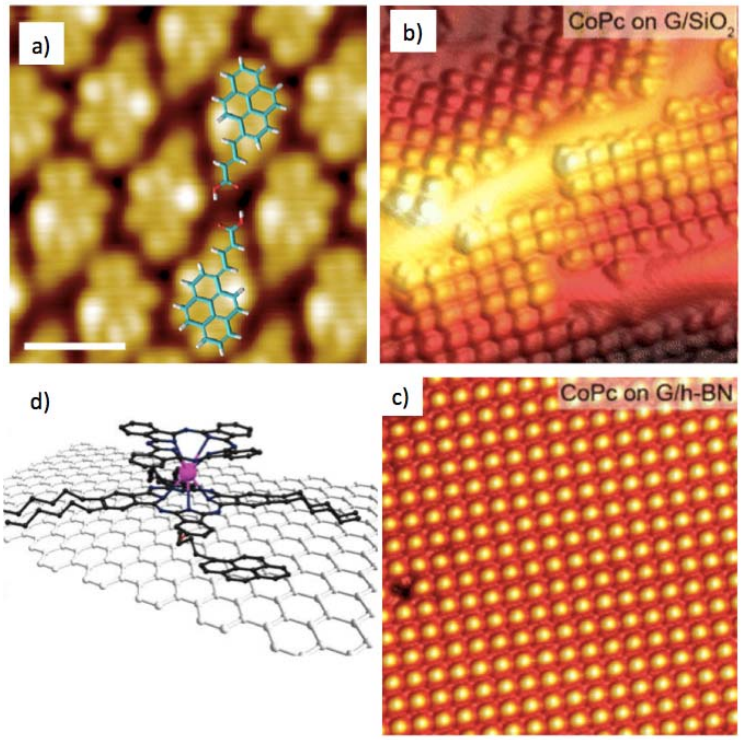

Fig. 2. a) STM images of 1-pyrene butyric acid deposited on graphene/Pt (111) with superimposed molecular structure.[9] b,c) STM images of a single domain of CoPc molecules on (b) G/SiO2 and (c) G/h-BN [10] d) Schematic representation of a TbPc2 single molecule magnet (SMM) on graphene. [11] Reprinted from Ref. 7 with permission from Elsevier, others adapted with permission from Ref.13 and Ref.57, Copyright American Chemical Society.

The co-processing of graphene and organic semiconductor molecules remains a challenge and a very active field of research, with a particular focus on controlling and optimizing the process of intermolecular charge transport, and exploitation of tailored transport properties in high-performance devices. This requires the structural and energetic tuning of the interfaces between the two components to ensure efficient fundamental processes such as charge exchange or exciton splitting in the final material.

A high number of published results is available, giving in some cases conflicting outcomes. In this chapter, an extensive overview is provided of possible ways that graphene and organic semiconductors can interact. To obtain a clear and useful picture of the state-of-the-art, we will use a "bottom up" approach describing the interaction of graphene with organic molecules starting from the simplest systems at molecular scale, i.e. single molecules on single layer graphene in UHV, to the mesoscopic, most complex materials, i.e. thick layers of graphene-organic composites embedded in working electronic devices.

2.2. Graphene-organic interactions in vacuum: single molecules on single sheets

The simplest model for graphene-organic interaction is that of a single molecule adsorbed on a graphene sheet, in vacuum, i.e. not surrounded by neither gas nor solvent molecules. Such model systems are routinely obtained in ultra-high-vacuum (UHV) chambers, by thermal evaporation of different small molecules on graphene produced by chemical vapour deposition (CVD)[12] or by epitaxial growth on silicon carbide [13]. A main advantage of molecules deposited from vapour on graphene is that the spatial arrangement and electronic properties of the molecule-graphene interaction are accessible simultaneously; the interactions can be studied with a high resolution by means of Scanning Tunneling Microscopy (STM, Fig. 2a).

It is well known that small conjugated molecules undergo adsorption on solid and flat sp^2-carbon surfaces forming highly ordered nanostructures, similar to 2-dimensional crystals. This approach is thus very useful to create a periodic electronic modulation of the graphene surface through self-assembly of aromatic molecules. Many different classes of molecules are known to form robust, stable physisorbed self-assembled monolayers on graphite or graphene, from simple alkanes to phthalocyanine, benzenes, anthracene, pyrenes and perylenes, to larger polycyclic aromatic hydrocarbons such as coronene derivatives. [9]
Generally, the morphology of such self-assembled architectures is driven by a complex interplay between non-covalent intermolecular and molecule-substrate interactions.[14] In the case of polyaromatic molecules such as most organic semiconductors, π-π interactions play of course a paramount role in governing the molecular orientation and packing. Polyaromatic molecules are also considered as "nanographenes",[15] given that their

aromatic core is like a small 2D fragment of graphene, and thus have a strong tendency to stack over each other and over graphene with a stacking distance of ca. 3.3 Å, i.e. similar to the interlayer distance in graphite.

Overall, several results indicate that nucleation, orientation, and packing of OS on graphene are different compared to those grown on conventional substrates such as silicon or even graphite.[10,16-19]

A detailed theoretical analysis of the adsorption of neutral molecules on graphene was performed by Mat Persson's group applying density functional theory. [20] It revealed that for neutral (poly)-aromatic, anti-aromatic, and more generally for π-conjugated systems, purely dispersive forces drive the docking of adsorbates on graphene, whereas short-range electrostatic interactions ultimately stabilize the complex.

However, if the aromatic backbone of the molecule is decorated by side groups exposing well defined functionalities, the latter can work in synergy or in opposition to the π-π interactions between the adsorbed molecules and graphene, leading to more complex self-assembly pathways. Functionalization of the aromatic core gives rise to strong medium-range interactions involving the substituents: e.g., ab initio simulations revealed that derivatives of benzoic acids serve as sub-units for the controlled formation of ordered nanopatterns on graphitic surfaces. Three types of molecule-molecule or molecule-substrate interactions control the nature of the ultimate assembly: (1) long-range repulsive π-π interactions (0.10-0.30 eV), (2) medium-range attractive π-π* interactions (0.30-0.60 eV), and (3) short-range hydrogen bonding (0.60-0.80 eV) the latter giving strong directional intermolecular interactions that position adjacent molecules in predictable ways. [21]

These strong intermolecular interactions on graphene have been observed experimentally in continuous uniform layers of perylenes bearing carboxyl groups (perylene-3,4,9,10-tetracarboxylic dianhydride).[19,22,23] An extensive study by STM, X-rays reflectivity and modelling indicates that such molecules form an highly uniform and coherent layer of molecules, parallel to graphene surface but weakly interacting with it, held together by hydrogen bonds. Perylene layers adsorb on the graphene surface with characteristic π–π stacking bond lengths, thus indicating weak interaction with the graphene.

One can expect molecules with a greater electron acceptor or donor character to interact more effectively with graphene; in fact, another example of directed, self-assembled layers

on graphene describes the epitaxial growth of perfluoro-pentacene yielding a π-stacked arrangement of coplanar molecules with an exceedingly low π-stacking distance of 3.07 Å, among the lowest π-stacking distance ever reported for organic semiconductor crystal lattices, likely due to the effect of fluorine side-groups. This low stacking distance gives rise to significant electronic band dispersion along the π-stacking direction.[24]

Interfacial dipole interactions induced by charge transfer between copper phtalocyanine (CuPc) molecules and graphene are shown to epitaxially align the CuPc molecules in a face-on orientation in a series of ordered superstructures on CVD graphene. [16] Further, the assembled structure can be used as a molecular probe to visualize the graphene's domain boundaries as Ogawa et al. demonstrated for chloro-aluminum phthalocyanine on CVD graphene.[17] In another example, Gao's group demonstrated that monolayer graphene can act as a template for fabrication of unique nanoarchitectures.

A molecular layer of magnetic iron(II)-phthalocyanine was deposited on single crystal, monolayer graphene grown via chemical vapour deposition. The iron(II)phthalocyanine arranged in regular Kagome lattices on the surface, following the lattice of the graphene moiré pattern. A monolayer of graphene is thus sufficient to direct the molecules' self-assembly and to decouple the adsorption process of the phthalocyanine derivative from the underlying metal surface[18].

Slightly different results have been obtained on graphene and graphite[19] indicating that, while graphene templates effectively the molecules´ adsorption, it does not shield the molecules entirely from the underlying substrate, which was anyhow found to influence the final structure of the adsorption layer.

The influence of the substrate underlying graphene was in fact demonstrated for cobalt phthalocyanine (CoPc) on graphene[10] (Fig. 2 b,c) transferred on silicon dioxide (SiO_2) or hexagonal boron nitride (BN). With both underlying substrates, CoPc molecules formed a square lattice on the graphene layer. However, with graphene on SiO_2, the domain size was limited by the surface corrugation due to SiO_2 atomic roughness and chemical inhomogeneity, and there was a degree of disorder in the molecular ordering within the domains which was not observed for graphene on BN. Additionally, Scanning Tunnelling Spectroscopy (STS) measurements revealed that

the energy of the orbitals shifted from one molecule to another, and that this effect was stronger on graphene/SiO_2 compared to graphene/BN hybrids. In graphene/SiO_2 the substrate underlying the graphene layer does not only govern disorder in the self-assembled cobalt centred phthalocyanine layer, but it influences as well the system's electronic properties. Interestingly, the molecule/graphene interaction could be dramatically enhanced by introducing metal atoms obtaining molecule/metal/graphene sandwich structures.[25].

2.3. Graphene organic interactions in liquids: Supramolecular self-assembly, stabilization and processing

Graphene processability is key for large-scale exploitation of graphene's unique properties. To this end, soluble graphene-organic hybrid systems have a clear advantage over CVD or epitaxial graphene because of their properties´ tunability and low cost.[26] Graphene-organic suspensions can be processed with large area deposition techniques in coatings, screen or ink-jet printed electronic devices [27],[28] allowing to embed graphene into functional composite materials[29].

Graphene suspensions are typically obtained by liquid-phase exfoliation in a suitable organic solvent, frequently assisted by ultrasonicating treatments.[30-32]. Aromatic cores based on anthracene[33], pyrene[34-36], perylene[37,38] and coronene[39] with side functionalization to tailor solubility and electronic properties, have also been employed as agents to promote graphene liquid phase exfoliation and stabilize the exfoliated sheets. The surfactant effect of aromatics has been at first demonstrated for aqueous dispersions of reduced graphene oxide (RGO); by means of non-covalent interaction a water soluble, sulphonated derivatives of pyrene and perylenediimide respectively can efficiently stabilize the RGO sheets in aqueous suspension, while aqueous suspensions of RGO undergo heavy agglomeration and precipitation.[37]

More interestingly, the approach of non-covalent functionalization works also for pristine, non-oxidized graphene; graphite is directly transferred into a solution of a small aromatic exfoliation agent in a process assisted by ultra-sonication (Fig. 3):

Dong et al. show that the aromatic molecule tetrasodium 1,3,6,8-pyrenetetrasulfonic acid (PS4) can effectively exfoliate graphite into graphene monolayers with sonication in aqueous solutions, yielding up to 90% of graphene single layers[40]. Besides sulphonated pyrene and perylenediimide derivatives, stabilization of graphene in aqueous suspension was successfully demonstrated with carboxyl functionalized coronene[39] and a cationic aza-pyrene and aza-perylene derivative[41].

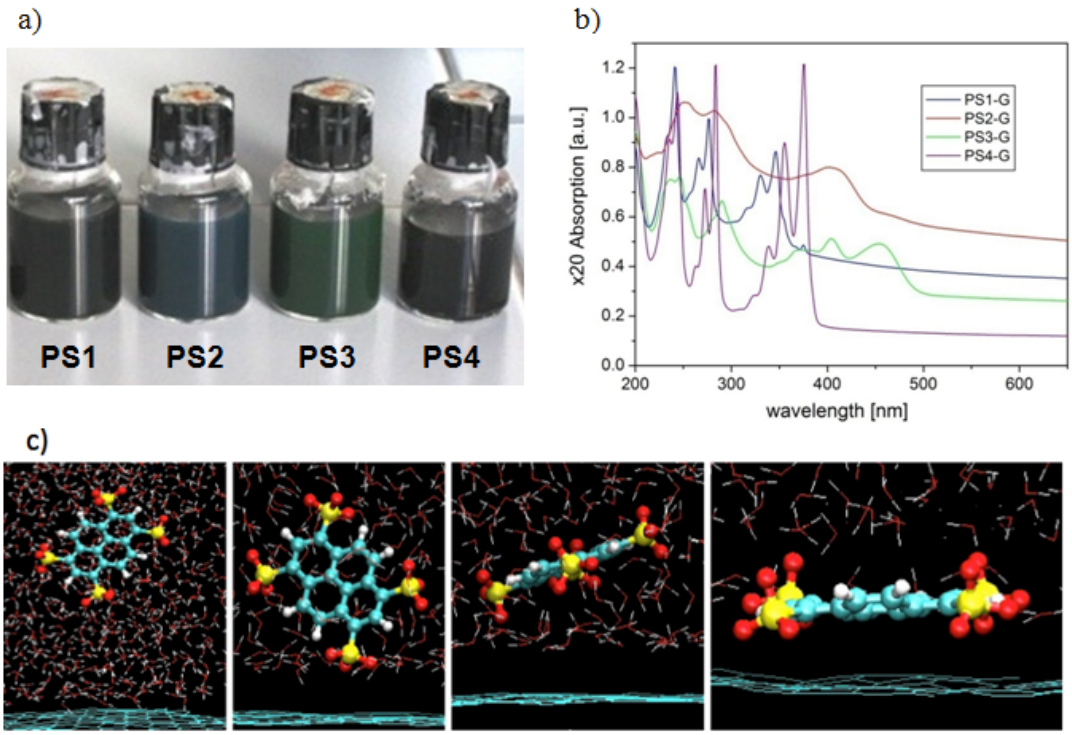

Fig. 3. Picture of different pyrene-graphene solutions in water after sonication with graphite. b) UV/VIS absorption spectra of the suspensions (samples diluted 1:20 for measurement). c) Snapshots of molecular dynamic simulations of pyrene sulphonate molecule adsorbing in water on graphene. Reproduced from Ref. 36 with permission from The Royal Society of Chemistry.

Direct exfoliation of graphite to graphene in aqueous media with organic dyes involves a complex process that requires not only a strong graphene-molecule interaction, but also well-defined kinetics of the adsorption process and solvent choice (see Fig. 3). We address these aspects in detail in the following experimental chapters of this thesis, combining experimental exfoliation data with modelling (also see our works [36,42] and references therein).

The choice of suitable aromatic systems non-covalently interacting with graphene has a triple bonus: (i) improve yield of exfoliation in liquid-phase exfoliated graphene, (ii) stabilize the graphene suspension, and (iii) confer new physical and chemical properties to the graphene. Specific interactions between graphene and an aromatic core do come into play not only in the case of small polyaromatic molecules, but also if the aromatic system is incorporated into a polymer chain. In this regard, pyrene-functionalized amphiphilic block copolymers can drive exfoliation of graphene in either aqueous or organic media to give composite films with improved tensile strength and tunable conductivity.[43].

The non-covalent interaction with graphene and organic dyes involving a conjugated π-system can be controlled by varying the aromatic core and functionalization; this allows a systematic fine-tuning of the electronic properties of graphene. As an additional advantage, the exceptional optical properties of these organic molecules (strong and well-defined absorption spectra in the visible spectrum, efficient light-emission, etc.) allows for application of optical spectroscopy as valuable methods to investigate the interactions between aromatic molecules and graphene, as will be demonstrated in the following experimental chapters of this thesis.

2.4. Effect of Graphene-organic interactions on electronic properties

Prior describing the most complex systems of interaction in devices, we detail on the different physico-chemical effects that appear when combining OS and graphene. As mentioned in the introduction, organic molecules may be used to modify, in certain cases significantly, the properties of graphene, and *vice versa.*

Doping

The adsorption of molecules such as anthracene, naphtalene and pyrene on graphene has a noteworthy effect on graphene electronic properties, inducing p- or n- type doping as demonstrated indirectly by Raman spectroscopy.[44] G-band splitting was observed in these systems, and explained by a lifting of the two-fold degeneracy of the optical phonons at the Γ point.[40] Larger aromatic rings such as anthracene and pyrene produce a wider G-band splitting (≈23 cm^{-1}) than smaller rings such as

naphthalene (≈20 cm^{-1}). This kind of doping was observed also monitoring charge transport in transistors[9,44] as will be detailed in the following section.

From a theoretical point of view, Yong Peng's group addressed the binding of organic donor, acceptor and metal atoms on graphene sheets, and revealed the effects of different non-covalent functionalizations on electronic structure and transport properties of graphene[25]. Their simulations suggest that a strong hybridization between the molecular levels and the graphene valence bands can be achieved through adsorptions of particular OS such as 2,3-dichloro-5,6-dicyano-1,4-benzoquinone (DDQ) and tetrathiafulvalene (TTF). P-doping and n-doping was monitored by combined Raman and X-ray photoelectron spectroscopy (XPS) on an oxidized few layer thick graphene combined with tetracyanoethylene (TCNE) and tetrathiafulvalene (TTF) molecules, observing shifts in S *2p* and N *1s* XPS peaks for the two molecules.[45] This kind of dopant layers was demonstrated be very stable, and is preserved in air up to 200° C.[46]

Fluorescence quenching by charge or energy transfer

The interaction between a light-emitting dye and graphene is interesting from a fundamental point of view (because it can be considered as the interaction between a 0D small emitter and a 2D, semi-infinite quencher), and from a technological point of view (for applications in LEDs, photovoltaics, sensors, etc.). Fluorescence quenching and excited energy transfer from dyes to graphene have been demonstrated with reduced graphene oxide, carbon nanotubes, and pristine graphene[4,38,47,48] (Fig. 4).

The interaction between fluorescent emitters and graphene is associated with local dipole-induced electromagnetic fields that are strongly enhanced due to the unique properties of graphene: graphene is an extraordinary energy sink with great potential for prospective application in photo-detection, nano-photonic and photovoltaic devices.

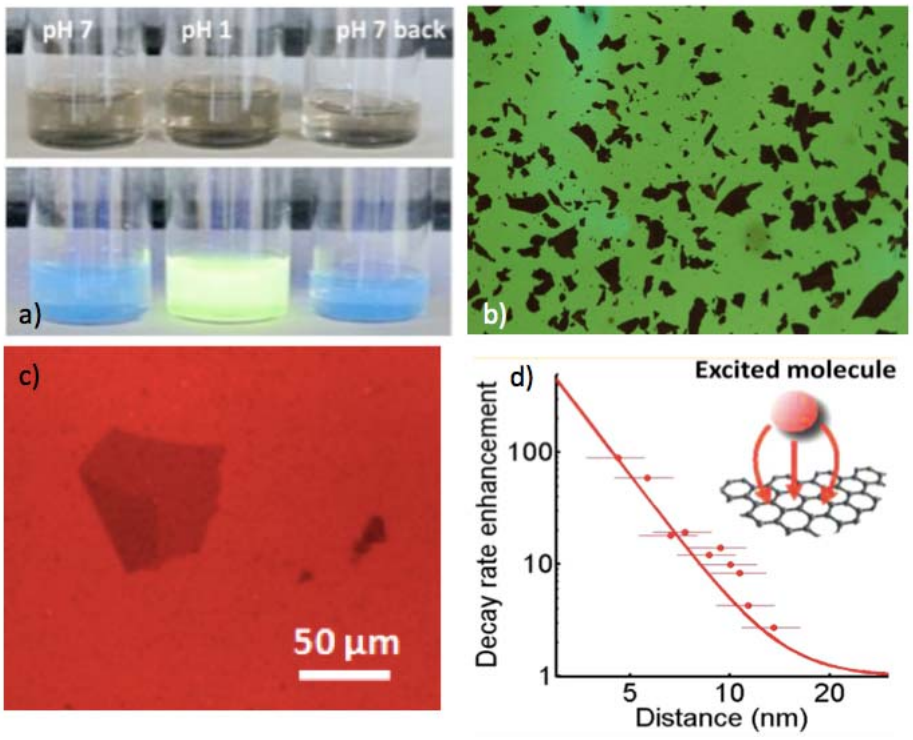

Fig. 4. Images of GO-oligothiophene covalent composites in EtOH at neutral pH, upon acidification with HCl and re-neutralization by triethanolamine (TEA) (from left to right) under normal light (top) and UV irradiation (bottom) showing the reversible emission switch. [49] b,c) Optical fluorescence image of GO monolayers deposited b) over and c) below fluorescent OS layer, showing strong fluorescence quenching.[4 50] d) Decay rate enhancement in graphene/rhodamine system, obtained from the lifetime measurements as a function of graphene/rhodamine distance.[51] Reproduced from Ref. 54 and Ref. 64 with permission from The Royal Society of Chemistry. Adapted with permission from Ref. 42 and Ref. 47, copyright 2009 and 2013, American Chemical Society.

Quenching of pyrene emission through energy transfer to graphene is proportional to graphene-pyrene distance *d*. A rate of energy transfer proportional to d^{-4} has been calculated, suggesting that quenching should be observable for distances up to 30 nm, much larger than what observed for any other surface[52,53]. A d^{-4} distance dependence in the quenching of emitters with monolayer graphene was confirmed experimentally with rhodamine molecules by Koppens et al.[51] (Fig. 4d). In this work the emitter lifetimes were also measured as a function of emitter-graphene distance *d*, revealing an agreement with a universal scaling law governed by the fine-structure constant. On graphene, the emitter decay rate exhibited a 90-fold enhancement

(corresponding to an energy transfer efficiency of 99%) with respect to the decay in vacuum at distances *d* = 5 nm. The high energy transfer rate was associated mainly to the two-dimensionality and gapless character of monolayer graphene.[51] Thin layers of reduced graphene oxide and porphyrin showed fluorescent quenching and superior optical limiting effect, better than the benchmark optical limiting material C_{60} and the control sample.[54]

Hirsch and co-workers demonstrated the binding and electronic interactions of pristine single- and few-layer thick graphene with an organic dye molecule in homogeneous solutions. [48] Electronic cross-talk with dendronized perylenebisimides and graphene suspended in NMP was confirmed spectroscopically by photoluminescence and Raman measurements, confirming experimentally an efficient fluorescence quenching with graphene. The emission quenching by energy or electron-transfer mechanisms provides clear evidence for the non-covalent binding of the two π–systems.

Quenching with graphene in liquid phase has been explained with the occurrence of both energy and electron transfer, according to the system under study. Investigations on the fluorescence quenching of graphene with two organic donor molecules, pyrene butanoic acid succinimidyl ester (PyBS) and oligo(p-phenylenevinylene) methylester (OPV-ester) have been carried out by Matte and co-workers[55]. They did not use pristine graphene, but amide-functionalized graphene soluble in chloroform ($CHCl_3$) and dimethylformamide (DMF). For the two molecules selected, the absorption and photoluminescence spectra were recorded in mixtures with graphene at increasing concentration of the latter component. The emission spectra of the molecules in a solution with graphene did not show any additional bands that could be ascribed to a charge-transfer complex. Unlike the absorption spectra, the emission markedly changes with the increasing graphene concentration, resulting in a dramatic loss in emission intensity. Given that no change was observed in absorption, Matte et al. attributed the strong emission quenching to photo-induced electron transfer, an excited state phenomenon. The ability of graphene to quench fluorescence of these aromatic molecules was attributed to photo-induced electron transfer on the basis of fluorescence decay and time-resolved transient absorption spectroscopic measurements. The occurrence of energy transfer could

not be entirely excluded, but the main effect is attributed to photo-generated, charge-separated species in which graphene acts as an acceptor. These charge-separated species are long-lived and thus interesting for the design of photovoltaics. Photo-induced interaction of graphene-organic hybrids can proceed as well through the transfer of phonon energy: Since a phonon is a quantum mechanical description of a specific type of vibrational motion, the enhancement of the phonon energy transfer will increase the vibrational energy of a phonon acceptor. Pan and co-workers demonstrated phonon energy transfer to reduced graphene oxide with water-soluble, sulphonated pyrene derivatives in solution. Phonon transfer with water soluble systems is of particular interest as it allows for prospective medical application in photo-thermal therapy[56].

2.5. Graphene-organic interactions in solid: thin films and electronic devices

Besides fundamental studies in vacuum or solutions, graphene interaction with organic semiconductors can be exploited in bulk systems consisting of OS/graphene blends. These bulk composite systems are particularly relevant for applications in organic field-effect transistors (FETs), photovoltaics and sensing devices (Fig. 5).

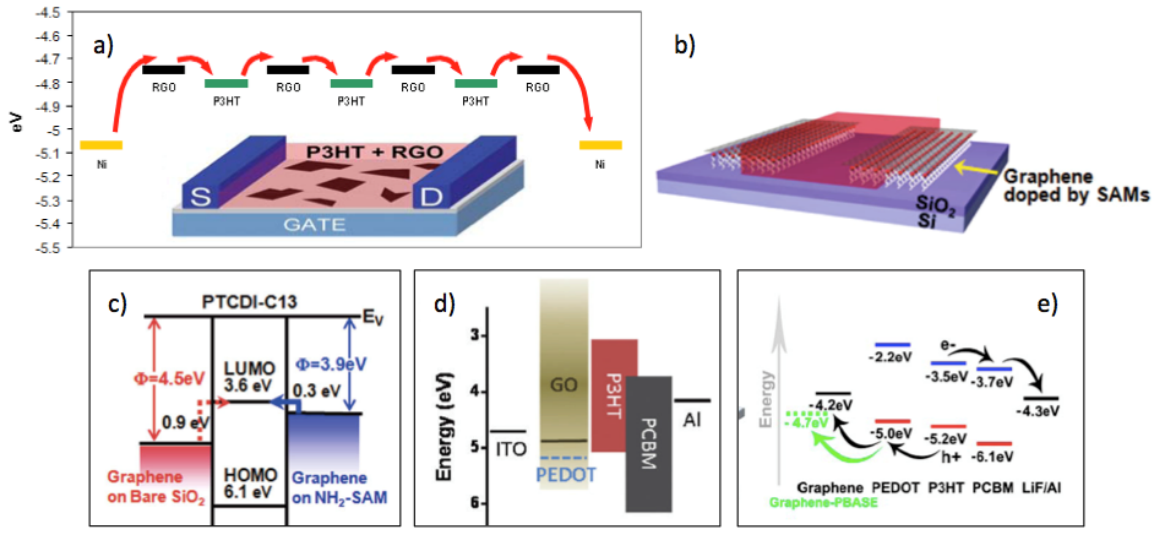

Fig. 5. a) Work function of Nickel, RGO and P3HT into an RGO-P3HT transistor. Arrows schematize the charge transport across the device, form source to drain, passing across different RGO sheets and P3HT domains. The image is not a cartoon, but shows the experimental WF values as measured by KPFM. In the inset, a schematic representation of the device.[50] b) schematic structure of a transistor

using a modified perylene (PTCDI-13) as active layer and graphene as source/drain [57] c,d,e) Examples of energy diagrams of graphene interacting with metal, conductive oxides and OS, from ref [57-59] respectively. Reproduced from Ref. 64 with permission from The Royal Society of Chemistry. Adapted with permission from Ref. 73 and Ref.74, Copyright American Chemical Society.

To better evaluate the possibilities offered by graphene-organic FETs, we should also mention briefly the numerous interesting results obtained with carbon nanotubes. Nanotube bundles can be effectively employed to template the growth of organic crystals under certain experimental conditions, resulting in the formation of organic nucleates with preferred orientations. Incorporation of an appropriate amount of random bundles of single-walled nanotubes in pentacene or sexithiophene films was observed to give 20-fold enhancement in field-effect mobility without reduction of the I_{on}/I_{off} ratio. [60] The use of carbon nanotubes as all-carbon electrodes integrated in both nanoscale and thin-film pentacene transistors made it possible to improve the charge injection at the electrode-semiconductor interfaces, leading to increased device performances when compared to devices based on traditional noble metals as electrodes [61].

However, studies on CNT showed that they do not act just as preferential, highly conductive additives to enhance mobility of OS; the electronic processes within such devices are more complex, with a key effect on charge transport characteristics of the interfaces present in the devices. Charge trapping at the dielectric/polymer (e.g. polythiophene) interfaces have been used in transistors based on carbon nanotubes for sensing applications.[62] Sufficient power and selection of an eligible wavelength induces a change in conductance upon illumination, up to four orders of magnitude.[63] All these approaches based on CNTs have anyhow to deal with the well-known negative aspects of CNT such as the mixture of properties (semiconducting & metallic) typical in CNT batches.

The lessons learned from CNT are now transferred to graphene that can be expected to exhibit better processability and lower dimensionality as compared to 1D nanotubes. FETs based on pristine graphene typically show very high charge mobility (>10^5 cm^2/ V s), but a very poor I_{on}/I_{off} ratio. Achieving high mobility while maintaining high I_{on}/I_{off} ratio is the greatest challenge to allow development of

graphene-based (flexible) electronics; a viable approach intensively explored relies on the incorporation of graphene into solution processed organic field-effect transistors (OFET). The addition of an organic semiconductor can bring into play new physical processes like the controlled doping of the graphene.

The effect of adsorbed molecules on graphene doping and related charge transport was explored by drop casting on a "scotch tape" graphene layer a solution of either pyrene, naphthalene or antracene derivatives (as mentioned above). Shifts in threshold voltage from -108 V to + 62 V could be observed in this way, together with significant changes in Raman spectra indicating significant doping [44]

Transistors based on CVD graphene were realized in a recent study with self-assembly of solution processed triethylsilylethynyl-anthradithiophene (TES-ADT). TES-ADT displayed a standing-up molecular assembly, which facilitates lateral charge transport on graphene.[64]

Blends of reduced graphene oxide microsheets and OS polymers such as poly-3-hexyl thiophene (P3HT) and poly(*p*-phenylene vinylene) (PPV) have shown significant fluorescent quenching as compared to the pure OS, providing evidence for a good interaction between the two materials in the solid state.[22,50] In particular, efficient charge transport across graphene and polymers has been demonstrated for simple bilayer systems composed by reduced graphene oxide (RGO) and P3HT, with a 20-fold increase of the effective mobility and I_{on}/I_{off} ratios $>10^3$.[50]. The use of bi-component system as active layers of FET has a major disadvantage: charges will have to face several injection barriers, hopping continuously from P3HT to RGO and *vice versa*. However, the WF values measured by Kelvin Probe Force Microscopy[65,66] (KPFM) on RGO monolayers and P3HT amounted to 4.75 ± 0.02 and 4.80 ± 0.03 eV, respectively. The low WF difference favors charge transport from one material to the other.

It should be noted that the WF of organic semiconductors like P3HT depends significantly on molecular packing, which in turn depends on other parameters such as deposition conditions and molecular weight. The value obtained by KPFM measurements for the P3HT is in fairly good agreement with the HOMO of P3HT

estimated by cyclic voltammetry measurements, i.e. 4.9 eV. The WF of P3HT is close to the RGO value thus allowing efficient charge transport across the two materials, as shown in fig. 5a that is a schematic representation of charge transport across the RGO-P3HT blend reporting the experimental WF values as measured by KPFM.
Huang et al. show that, when compared to pure organic semiconductor layers, graphene-organic hybrid FETs exhibit up to 20-fold increase in effective field-effect mobilities maintaining an I_{on}/I_{off} ratio comparable or better than what observed without graphene. The mobilities determined in P3HT/graphene PQT-12/graphene hybrid FETs resulted in values as high as 0.17 $cm^2\ V^{-1}\ s^{-1}$ and 0.6 $cm^2\ V^{-1}\ s^{-1}$, respectively [67]. In addition, non-covalent interactions in bulk GO-P3HT hybrid assemblies were found to enhance optical absorption, charge transfer, and photo-catalytic properties. With their broad absorption, excited states can be generated with sunlight, rendering GO-P3HT hybrids highly promising for potential application as an efficient, green photo-catalyst in organic synthesis [68].

Organo- and water- dispersible GO-polymer nanosheets were used also for organic electronic memory devices. Thin films of poly(tert-butyl acrylate), covalently bound to GO sheets, showed bistable electrical conductivity switching behaviour and a non-volatile, rewritable memory effect in an Al/GO-g-PtBA+P3HT/ITO sandwich device [69]. Non-volatile rewritable memory effect has been also demonstrated with a nanocomposite of hexadecylamine-functionalized graphene oxide (HDAGO) and poly(3-hexylthiophene) (P3HT). The device had an ITO/P3HT-HDAGO/Al sandwich structure, in which the composite film of P3HT-HDAGO was prepared by simple solution phase mixing and spincoating. This memory device exhibited typical bistable electrical switching behavior and a non-volatile rewritable memory effect, with a turn-on voltage of about 1.5 V and an I_{on}/I_{off} ratio of 10^5. The electrical switching behavior was attributed to the electric-field-induced charge transfer between P3HT and HDAGO nanosheets.[70]

The full potential of graphene in integrated circuits can be accessed only with a reliable ultrathin high-κ top-gate dielectric. In top-gated graphene devices an oxide layer, typically Al_2O_3 and HfO_2, is grown on graphene with atomic layer deposition.

Even in this case, OS shall have a beneficial effect; a molecularly thin organic seeding layer of perylene-3,4,9,10-tetracarboxylic-3,4,9,10-dianhydride (PTCDA) has been found to beneficially direct oxide deposition, with significant improvements in dielectric performance limits for ALD-grown oxides on graphene [71].

A main potential application of graphene, intensively studied worldwide, is to use it as transparent conductor, and this application has been studied also for organic electronic devices.

Although GO is known to be insulating, when deposited as a thin coating layer it shall have a beneficial effect on charge transport in organic photovoltaic devices. The incorporation of GO deposited from neutral solutions between the photoactive poly(3-hexylthiophene) (P3HT):phenyl-C61-butyric acid methyl ester (PCBM) layer and the transparent and conducting indium tin oxide (ITO) gives a decrease in recombination of electrons and holes and leakage currents, and a dramatic increase in the photovoltaic efficiencies to values that are comparable to devices fabricated with PEDOT:PSS as the hole transport layer (fig. 5d).[58] Large-area, continuous anodes composed of pristine few-layered graphene were also realized by CVD and tested in organic photovoltaic devices: non-covalent functionalization of graphene with pyrene butanoic acid succidymidyl ester (PBASE) allows for alignment of the Fermi level of graphene very close to the highest occupied molecular orbital of PEDOT:PSS for efficient hole collection. Graphene anodes modified by self-assembled PBASE exhibit excellent performance characteristics [59] (fig. 5e).

Also the work function of graphene electrodes in OFETs can be engineered by functionalizing the surface of SiO_2 substrates with self-assembled monolayers (SAMs). In general, the measured WF of graphene shall vary significantly, as shown as well in the band diagrams of fig. 5; graphene WF depends on production method and the on underlying substrate that shall induce relevant doping. The electron-donating NH_2-terminated SAMs with aminotriethoxy-silane induce strong n-doping in graphene, whereas the CH_3-terminated SAMs neutralize the p-doping induced by SiO_2 substrates. Graphene doped by SAMs displays a Dirac voltage shift over 150 V in transistor application and enables graphene to have a tunable work function. The work function of graphene shifts down to 3.9 eV for NH_2-SAM-modified SiO_2,

facilitating electron injection at this low work function graphene electrode [57] (fig. 5b,c). Should be noted that the quality of the underlying CVD graphene is critical for interaction with OS in devices; Sun et al. studied the assembly of oligothiophene derivatives on graphene and found that defect-like ripples and wrinkles significantly weaken the molecule–graphene interaction. By using two different quaterthiophene derivatives they showed that such structural irregularities in graphene hinder a stable molecular adsorption.[72]

An original approach was also reported by Eda and Chhowalla, who managed to obtain working transistors even via blending RGO with an *insulating* polymer. By preparing a well dispersed mixture of RGO with polystyrene (PS), they obtained working ambipolar transistors with electron and hole mobilities of 0.2 $cm^2 V^{-1} s^{-1}$ and 0.7 $cm^2 V^{-1} s^{-1}$, respectively, although accompanied with a very low I_{on}/I_{off} ratios ranging between 3 and 6. In this last case, of course, the polymer was not actively contributing to the charge transport process, the latter taking place via percolation among RGO sheets dispersed in the insulating PS matrix.[73] Blending an insulating polymer in the active layer of microelectronic devices is not meant to have high performance, but this result is interesting as it lies at the edge between organic electronics and research on bulk composites: nowadays, many groups are trying to use graphene in commercial polymers to increase electrical conductivity and give "functional" properties to structural materials already used in automotive and aerospace technologies.

References.

(1) Liscio, A.; Bonini, M.; Treossi, E.; Orgiu, E.; Kastler, M.; Dotz, F.; Palermo, V.; Samori, P. *Journal of Polymer Science Part B-Polymer Physics* 2012, *50*, 642.
(2) Palermo, V.; Schwartz, E.; Finlayson, C. E.; Liscio, A.; Otten, M. B. J.; Trapani, S.; Mullen, K.; Beljonne, D.; Friend, R. H.; Nolte, R. J. M.; Rowan, A. E.; Samori, P. *Advanced Materials* 2010, *22*, E81.
(3) Schlierf, A.; Yang, H.; Gebremedhn, E.; Treossi, E.; Ortolani, L.; Chen, L.; Minoia, A.; Morandi, V.; Samori, P.; Casiraghi, C.; Beljonne, D.; Palermo, V. *Nanoscale* 2013, *5*, 4205.
(4) Treossi, E.; Melucci, M.; Liscio, A.; Gazzano, M.; Samorì, P.; Palermo, V. *Journal of the American Chemical Society* 2009, *131*, 15576.

(5) Bianco, A. *Angewandte Chemie International Edition* 2013, *52*, 4986.
(6) Cai, J.; Ruffieux, P.; Jaafar, R.; Bieri, M.; Braun, T.; Blankenburg, S.; Muoth, M.; Seitsonen, A. P.; Saleh, M.; Feng, X.; Mullen, K.; Fasel, R. *Nature* 2010, *466*, 470.
(7) Palma, C. A.; Samorì, P. *Nat. Chem.* 2011, *3*, 431.
(8) Ohta, T.; Bostwick, A.; Seyller, T.; Horn, K.; Rotenberg, E. *Science* 2006, *313*, 951.
(9) Pathipati, S. R.; Pavlica, E.; Treossi, E.; Rizzoli, R.; Veronese, G. P.; Palermo, V.; Chen, L.; Beljonne, D.; Cai, J.; Fasel, R.; Ruffieux, P.; Bratina, G. *Organic Electronics* 2013, *14*, 1787.
(10) Järvinen, P.; Hämäläinen, S. K.; Banerjee, K.; Häkkinen, P.; Ijäs, M.; Harju, A.; Liljeroth, P. *Nano Letters* 2013, *13*, 3199.
(11) Candini, A.; Klyatskaya, S.; Ruben, M.; Wernsdorfer, W.; Affronte, M. *Nano Letters* 2011, *11*, 2634.
(12) Li, X. S.; Cai, W. W.; Colombo, L.; Ruoff, R. S. *Nano Letters* 2009, *9*, 4268.
(13) Berger, C.; Song, Z. M.; Li, X. B.; Wu, X. S.; Brown, N.; Naud, C.; Mayou, D.; Li, T. B.; Hass, J.; Marchenkov, A. N.; Conrad, E. H.; First, P. N.; de Heer, W. A. *Science* 2006, *312*, 1191.
(14) Palermo, V.; Samorì, P. *Angew. Chem.-Int. Edit.* 2007, *46*, 4428.
(15) Samorì, P.; Severin, N.; Simpson, C. D.; Müllen, K.; Rabe, J. P. *J. Am. Chem. Soc.* 2002, *124*, 9454.
(16) Xiao, K.; Deng, W.; Keum, J. K.; Yoon, M.; Vlassiouk, I. V.; Clark, K. W.; Li, A.-P.; Kravchenko, I. I.; Gu, G.; Payzant, E. A.; Sumpter, B. G.; Smith, S. C.; Browning, J. F.; Geohegan, D. B. *Journal of the American Chemical Society* 2013, *135*, 3680.
(17) Ogawa, Y.; Niu, T.; Wong, S. L.; Tsuji, M.; Wee, A. T. S.; Chen, W.; Ago, H. *The Journal of Physical Chemistry C* 2013.
(18) Mao, J. H.; Zhang, H. G.; Jiang, Y. H.; Pan, Y.; Gao, M.; Xiao, W. D.; Gao, H. J. *Journal of the American Chemical Society* 2009, *131*, 14136.
(19) Wang, Q. H.; Hersam, M. C. *Nature Chemistry* 2009, *1*, 206.
(20) Bjork, J.; Hanke, F.; Palma, C. A.; Samori, P.; Cecchini, M.; Persson, M. *Journal of Physical Chemistry Letters* 2010, *1*, 3407.
(21) Rochefort, A.; Wuest, J. D. *Langmuir* 2009, *25*, 210.
(22) Smith, R. J.; Lotya, M.; Coleman, J. N. *New J. Phys.* 2010, *12*.
(23) Emery, J. D.; Wang, Q. H.; Zarrouati, M.; Fenter, P.; Hersam, M. C.; Bedzyk, M. J. *Surface Science* 2011, *605*, 1685.
(24) Salzmann, I.; Moser, A.; Oehzelt, M.; Breuer, T.; Feng, X.; Juang, Z.-Y.; Nabok, D.; Della Valle, R. G.; Duhm, S.; Heimel, G.; Brillante, A.; Venuti, E.; Bilotti, I.; Christodoulou, C.; Frisch, J.; Puschnig, P.; Draxl, C.; Witte, G.; Müllen, K.; Koch, N. *Acs Nano* 2012, *6*, 10874.

(25) Zhang, Y. H.; Zhou, K. G.; Xie, K. F.; Zeng, J.; Zhang, H. L.; Peng, Y. *Nanotechnology* 2010, *21*.
(26) Novoselov, K. S.; Fal'ko, V. I.; Colombo, L.; Gellert, P. R.; Schwab, M. G.; Kim, K. *Nature* 2012, *490*, 192.
(27) Torrisi, F.; Hasan, T.; Wu, W.; Sun, Z.; Lombardo, A.; Kulmala, T. S.; Hsieh, G.-W.; Jung, S.; Bonaccorso, F.; Paul, P. J.; Chu, D.; Ferrari, A. C. *Acs Nano* 2012, *6*, 2992.
(28) Secor, E. B.; Prabhumirashi, P. L.; Puntambekar, K.; Geier, M. L.; Hersam, M. C. *Journal of Physical Chemistry Letters* 2013, *4*, 1347.
(29) Xu, Y.; Schwab, M. G.; Strudwick, A. J.; Hennig, I.; Feng, X.; Wu, Z.; Müllen, K. *Advanced Energy Materials* 2013, *3*, 1035.
(30) Hernandez, Y.; Nicolosi, V.; Lotya, M.; Blighe, F. M.; Sun, Z. Y.; De, S.; McGovern, I. T.; Holland, B.; Byrne, M.; Gun'ko, Y. K.; Boland, J. J.; Niraj, P.; Duesberg, G.; Krishnamurthy, S.; Goodhue, R.; Hutchison, J.; Scardaci, V.; Ferrari, A. C.; Coleman, J. N. *Nature Nanotechnology* 2008, *3*, 563.
(31) Lotya, M.; Hernandez, Y.; King, P. J.; Smith, R. J.; Nicolosi, V.; Karlsson, L. S.; Blighe, F. M.; De, S.; Wang, Z. M.; McGovern, I. T.; Duesberg, G. S.; Coleman, J. N. *Journal of the American Chemical Society* 2009, *131*, 3611.
(32) Ciesielski, A.; Samori, P. *Chemical Society Reviews* 2013.
(33) Saswata, B.; Tapas, K.; Ananta Kumar, M.; Nam Hoon, K.; Joong Hee, L. *Nanotechnology* 2011, *22*, 405603.
(34) An, X. H.; Simmons, T. J.; Shah, R.; Wolfe, C.; Lewis, K. M.; Washington, M.; Nayak, S. K.; Talapatra, S.; Kar, S. *Nano Letters* 2010, *10*, 4295.
(35) Parviz, D.; Das, S.; Ahmed, H. S. T.; Irin, F.; Bhattacharia, S.; Green, M. J. *Acs Nano* 2012, *6*, 8857.
(36) Schlierf, A.; Yang, H.; Gebremedhn, E.; Treossi, E.; Ortolani, L.; Chen, L.; Minoia, A.; Morandi, V.; Samori, P.; Casiraghi, C.; Beljonne, D.; Palermo, V. *Nanoscale* 2013.
(37) Su, Q.; Pang, S.; Alijani, V.; Li, C.; Feng, X.; Müllen, K. *Advanced Materials* 2009, *21*, 3191.
(38) Backes, C.; Schmidt, C. D.; Rosenlehner, K.; Hauke, F.; Coleman, J. N.; Hirsch, A. *Advanced Materials* 2010, *22*, 788.
(39) Ghosh, A.; Rao, K. V.; George, S. J.; Rao, C. N. R. *Chemistry – A European Journal* 2010, *16*, 2700.
(40) Dong, X. C.; Shi, Y. M.; Zhao, Y.; Chen, D. M.; Ye, J.; Yao, Y. G.; Gao, F.; Ni, Z. H.; Yu, T.; Shen, Z. X.; Huang, Y. X.; Chen, P.; Li, L. J. *Physical Review Letters* 2009, *102*, 135501.
(41) Sampath, S.; Basuray, A. N.; Hartlieb, K. J.; Aytun, T.; Stupp, S. I.; Stoddart, J. F. *Advanced Materials* 2013, *25*, 2740.

(42) Yang, H.; Hernandez, Y.; Schlierf, A.; Felten, A.; Eckmann, A.; Johal, S.; Louette, P.; Pireaux, J. J.; Feng, X.; Mullen, K.; Palermo, V.; Casiraghi, C. *Carbon* 2013, *53*, 357.

(43) Liu, Z.; Liu, J.; Cui, L.; Wang, R.; Luo, X.; Barrow, C. J.; Yang, W. *Carbon* 2013, *51*, 148.

(44) Dong, X. C.; Fu, D. L.; Fang, W. J.; Shi, Y. M.; Chen, P.; Li, L. J. *Small* 2009, *5*, 1422.

(45) Choudhury, D.; Das, B.; Sarma, D. D.; Rao, C. N. R. *Chemical Physics Letters* 2010, *497*, 66.

(46) Coletti, C.; Riedl, C.; Lee, D. S.; Krauss, B.; Patthey, L.; von Klitzing, K.; Smet, J. H.; Starke, U. *Physical Review B* 2010, *81*, 235401.

(47) Kim, J.; Cote, L. J.; Kim, F.; Huang, J. X. *Journal of the American Chemical Society* 2010, *132*, 260.

(48) Kozhemyakina, N. V.; Englert, J. M.; Yang, G. A.; Spiecker, E.; Schmidt, C. D.; Hauke, F.; Hirsch, A. *Advanced Materials* 2010, *22*, 5483.

(49) Melucci, M.; Durso, M.; Zambianchi, M.; Treossi, E.; Xia, Z. Y.; Manet, I.; Giambastiani, G.; Ortolani, L.; Morandi, V.; De Angelis, F.; Palermo, V. *Journal of Materials Chemistry* 2012, *22*, 18237.

(50) Liscio, A.; Veronese, G. P.; Treossi, E.; Suriano, F.; Rossella, F.; Bellani, V.; Rizzoli, R.; Samori, P.; Palermo, V. *Journal of Materials Chemistry* 2011, *21*, 2924.

(51) Gaudreau, L.; Tielrooij, K. J.; Prawiroatmodjo, G. E. D. K.; Osmond, J.; de Abajo, F. J. G.; Koppens, F. H. L. *Nano Letters* 2013, *13*, 2030.

(52) Swathi, R. S.; Sebastian, K. L. *Journal of Chemical Physics* 2009, *130*.

(53) Swathi, R. S.; Sebastian, K. L. *J. Chem. Phys.* 2008, *129*, 054703.

(54) Xu, Y. F.; Liu, Z. B.; Zhang, X. L.; Wang, Y.; Tian, J. G.; Huang, Y.; Ma, Y. F.; Zhang, X. Y.; Chen, Y. S. *Adv. Mater.* 2009, *21*, 1275.

(55) Matte, H.; Subrahmanyam, K. S.; Rao, K. V.; George, S. J.; Rao, C. N. R. *Chemical Physics Letters* 2011, *506*, 260.

(56) Pan, X. Y.; Li, H.; Nguyen, K. T.; Gruner, G.; Zhao, Y. L. *Journal of Physical Chemistry C* 2012, *116*, 4175.

(57) Park, J.; Lee, W. H.; Huh, S.; Sim, S. H.; Kim, S. B.; Cho, K.; Hong, B. H.; Kim, K. S. *Journal of Physical Chemistry Letters* 2011, *2*, 841.

(58) Li, S. S.; Tu, K. H.; Lin, C. C.; Chen, C. W.; Chhowalla, M. *ACS Nano* 2010, *4*, 3169.

(59) Wang, Y.; Chen, X. H.; Zhong, Y. L.; Zhu, F. R.; Loh, K. P. *Applied Physics Letters* 2009, *95*, #063302.

(60) Liu, S.; Mannsfeld, S. C. B.; LeMieux, M. C.; Lee, H. W.; Bao, Z. *Applied Physics Letters* 2008, *92*, 053306.

(61) Aguirre, C. M.; Ternon, C.; Paillet, M.; Desjardins, P.; Martel, R. *Nano Letters* 2009, *9*, 1457.

(62) Anghel, C.; Derycke, V.; Filoramo, A.; Lenfant, S.; Giffard, B.; Vuillaume, D.; Bourgoin, J. P. *Nano Lett.* 2008, *8*, 3619.

(63) Borghetti, J.; Derycke, V.; Lenfant, S.; Chenevier, P.; Filoramo, A.; Goffman, M.; Vuillaume, D.; Bourgoin, J. P. *Adv. Mater.* 2006, *18*, 2535.

(64) Jang, J.; Park, J.; Nam, S.; Anthony, J. E.; Kim, Y.; Kim, K. S.; Kim, K. S.; Hong, B. H.; Park, C. E. *Nanoscale* 2013, *5*, 11094.

(65) Palermo, V.; Palma, M.; Samorì, P. *Advanced Materials* 2006, *18*, 145.

(66) Liscio, A.; Palermo, V.; Samori, P. *Accounts of Chemical Research* 2010, *43*, 541.

(67) Huang, J.; Hines, D. R.; Jung, B. J.; Bronsgeest, M. S.; Tunnell, A.; Ballarotto, V.; Katz, H. E.; Fuhrer, M. S.; Williams, E. D.; Cumings, J. *Organic Electronics* 2011, *12*, 1471.

(68) Wang, S.; Nai, C. T.; Jiang, X.-F.; Pan, Y.; Tan, C.-H.; Nesladek, M.; Xu, Q.-H.; Loh, K. P. *The Journal of Physical Chemistry Letters* 2012, *3*, 2332.

(69) Li, G. L.; Liu, G.; Li, M.; Wan, D.; Neoh, K. G.; Kang, E. T. *The Journal of Physical Chemistry C* 2010, *114*, 12742.

(70) Zhang, L.; Li, Y.; Shi, J.; Shi, G.; Cao, S. *Materials Chemistry and Physics* 2013, *142*, 626.

(71) Sangwan, V. K.; Jariwala, D.; Filippone, S. A.; Karmel, H. J.; Johns, J. E.; Alaboson, J. M. P.; Marks, T. J.; Lauhon, L. J.; Hersam, M. C. *Nano Letters* 2013, *13*, 1162.

(72) Sun, X.; Zhang, J.; Wang, X.; Zhang, C.; Hu, P.; Mu, Y.; Wan, X.; Guo, Z.; Lei, S. *Chemical Communications* 2013, *49*, 10317.

(73) Eda, G.; Chhowalla, M. *Nano Lett.* 2009, *9*, 814.

Chapter 3

Exfoliating graphene with organic dyes:

An innovative exfoliation and purification technique

3. Exfoliating graphene with organic dyes

3.1. Introduction

Graphene, a single-layer of graphite, has become one of the most exciting topics of research because of its outstanding optical, electronic and mechanical properties [1,2].

Few-layers thick graphene (less than ten layers) are being investigated with equal interest to monolayer graphene[3-6]. Liquid-phase exfoliation is a mass-scalable approach for the production of graphene [7-10], and graphene can be produced in aqueous surfactant solutions – even yields are as low as 10% (Ref.[10]). A few recent works[11,12] report on the exfoliation of graphite through noncovalent interactions between graphene and pyrene derivatives that can be seen as ''nano-graphene units''. The aromatic core of the molecule allows its intercalation and physisorption on the hydrophobic surface of graphene through π-π interactions, while appropriate functional groups attached to the molecule allows the electrostatic stabilization of graphene in the solvent. Pyrene, as it is, is not soluble in water. Different groups can be attached to pyrene to tune its solubility such as sulphonic groups ($-SO3^-$)[11,13,14], carboxylic acid groups (-COOH) [12] or more complex groups generating aromatic amphiphiles [14]. The nature and number of the functional groups is very important because the molecule must have a good affinity with the solvent, i.e. it needs to get sufficiently dissolved, but at the same time, the solvent has to allow hydrophobic interactions between graphene and the molecule's core [12]. An overview of recent works is reported in Fig. 1.

Ref.	Molecule	Exfoliation process and yield
[13]	Py–1SO_3	– Bath sonicator, mixed solvent – Mono and double layers (60%)
[14]	Py–COOH	– Bath sonicator; mixed solvent – Single (<10%) and few-layers
[15]	Py–4SO_3	– Tip sonicator; deuterium oxide – Mostly single-layers
[16]	Py–NH_2 Py–4SO_3	– Bath sonicator; water – Single-layers and bilayers
[17]	Amophiphilic–Py	– Bath sonicator; mixed solvent – Single layers and bilayers
This work	Py–1SO_3	– Bath sonicator; water – Single (~20%) and few-layers

Fig. 1. List of the works reporting production of graphene by chemical exfoliation of graphite with pyrene, as compared with our work. Details of the exfoliation process and the yield obtained.

3. Exfoliating graphene with organic dyes

This chapter discusses the use of 1-pyrenesulphonic acid sodium salt (PS1 or Py–1SO3) to achieve exfoliation of graphite by using water. The sulphonic group of this molecule improves the affinity of the molecule in the solvent, while at the same time hydrophobic interactions between graphene and the molecule are allowed. Aim is to investigate the direct exfoliation of graphite in water using PS1 by using a combination of microscopic and spectroscopic techniques.

3.2. Results

3.2.1. Material Preparation

Graphene suspensions were prepared in sonicating graphite flakes in 0.1mg/mL pyrene-SO3 aqueous solution. Then, a solvent exchange procedure based on centrifugation of applied to remove excess dye from solution for further analysis. The schematic of the exfoliation and subsequent purification process are shown in Fig. 2.

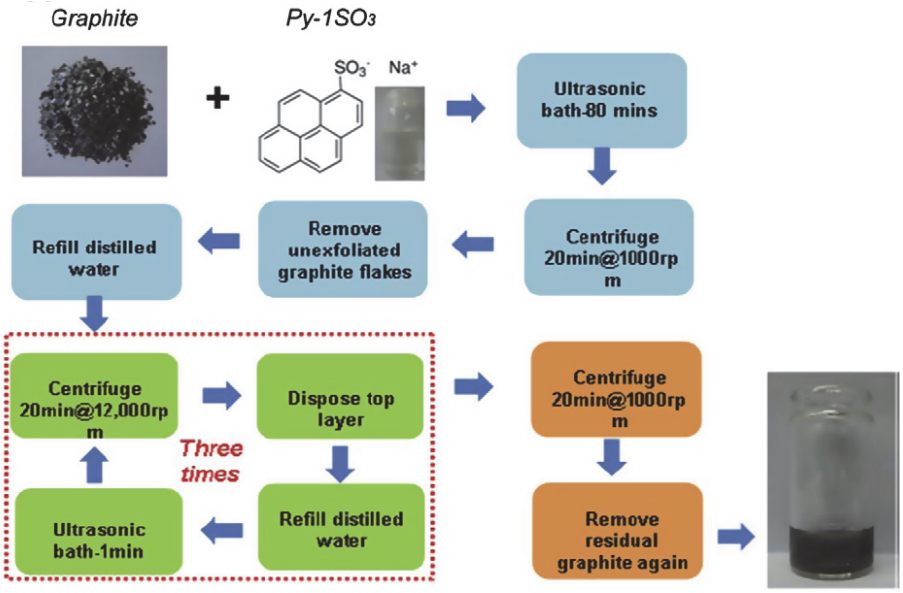

Fig. 2. Schematic of the exfoliation of graphite flakes using 1-pyrenesulphonic acid sodium salt (Py–1SO3). The process includes different steps (mixing, exfoliation, and washing). The washing step is repeated for three times in order to remove the excess Py–1SO3.

After 80 min sonication, the large cluster of non-exfoliated graphite can be removed by mild centrifugation at 1000 rpm for 20 min. The dispersion was then refilled with water and centrifuged

at 12,000 rpm for 20 min for three times in order to wash the excess Py–1SO3. The resulting dispersion is gray and stable over months.

The concentration of dispersion remaining after centrifugation is 0.074 mg/mL, calculated using an extinction coefficient α(660nm) = 2460 L g^{-1} m^{-1}.

3.2.2. Flakes in suspension

The spectrum of PS1 solution shows the characteristic peaks between 200nm and 400nm [15].

Fig. 3 shows the absorption spectra of the PS1 solution (bottom) and the Py–1SO3/graphene dispersion (top). Compared to the absorption spectrum of a PS1 blank solution, the baseline of the absorption of the graphene-based dispersion absorbs over the whole frequency range, as it is expected for graphene dispersions [12]. The original peaks of the PS1 solution are still visible, but they are broadened: this is fingerprint of the π-π interaction between PS1 and graphene, as observed when single-walled carbon nanotubes were dispersed by pyrene molecules [15] .

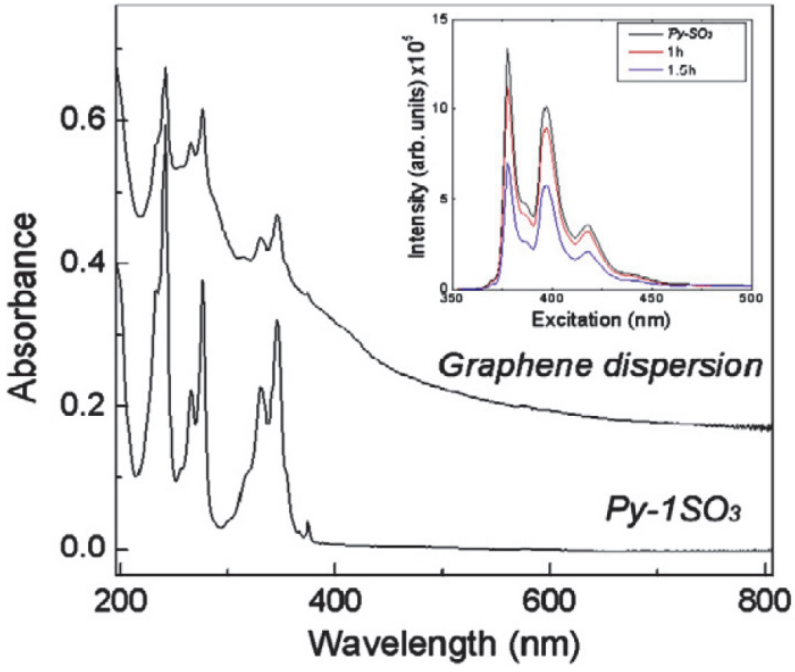

Fig. 3. Absorption spectra of the PS1based graphene dispersion (top) and the PS1solution (bottom). Inset: Fluorescence measurements of Py–1SO3/graphene hybrids obtained with different sonication time.

Collectively, these observations confirm the presence of both pyrene and graphene after exfoliation and washing; there is indication that the molecules interact with the graphene sheets,

thus exfoliating and stabilizing graphene in water. Fluorescence measurements further confirm this result: the inset in Fig. 3 shows a strong decrease of the fluorescence after 1.5 h sonication. This can be fingerprint of interaction between the molecules and graphene [16,17]. Such charge transfer interaction is of great importance for the design of optoelectronic composite materials. In the case of composite materials based on graphene oxide, the nano-graphene molecules anchor on the functional groups on the basal plane causing the fluorescence to be fully quenched [18]. Note that in the case of the here discussed suspensions, the fluorescence is not completely quenched. This means that there is still an excess of molecules in solution, even a significant amount of dye was removed from suspension with solvent exchange. Indeed, we did try to perform Raman spectroscopy directly on the dispersion, but the Raman signal was completely hidden by a strong fluorescence background.

3.2.3. Flakes morphology – microscopy approach

TEM analysis was performed to characterize the graphene flakes in dispersion (Fig. 4). TEM shows a large quantity of flakes with lateral size of 200–400 nm, in agreement with AFM (Fig. 5). Most of the flakes are characterized by folded and wrinkled area, such as in Fig. 4A and C.

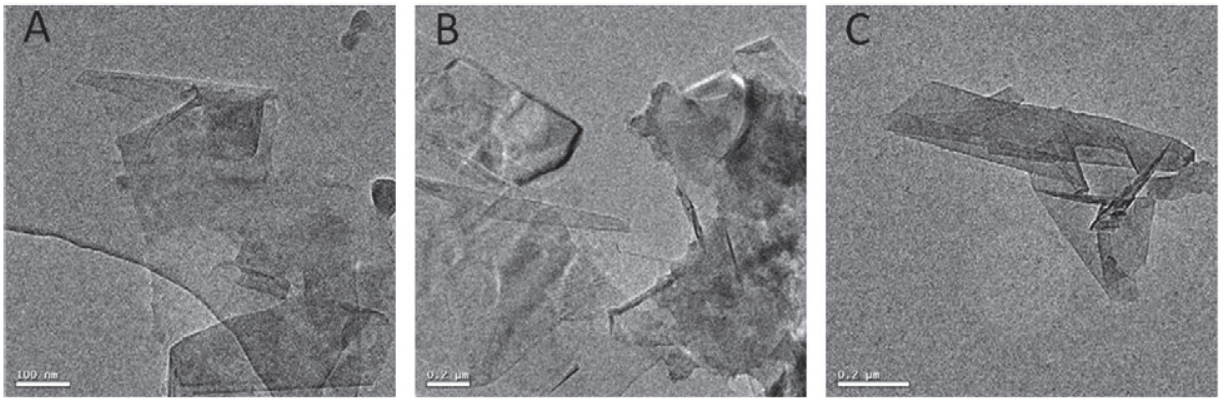

Fig. 4. Selected TEM images of flakes prepared by PS1assisted exfoliation of graphite. (A) A few-graphene layers flake (probably a folded bilayers); (B) A thin (on the left) and thick (on the right) flake. (C) A folded and wrinkled flake: most of our flakes have folded and wrinkled area.

This can further affect the thickness measured by AFM and contribute to the D peak intensity. In particular, by looking at the folded edges, the flake in Fig. 4A seems to be a large bilayer graphene folded on itself. The colour contrast of the suspended part of this flake corresponds indeed to 3–4 layers. Some of the flakes are composed by many and disordered layers, which may indicate that

these flakes are formed by re-aggregation during deposition on the TEM grid. Note that the TEM analysis is usually based on the colour contrast of graphene.

However, our flakes are covered with a large amount of molecules and this may cause a change in the contrast. This is for example visible in the thick layer in Fig. 4B, which is characterized by a non-uniform colour, probably related to an inhomogeneous film of molecules.

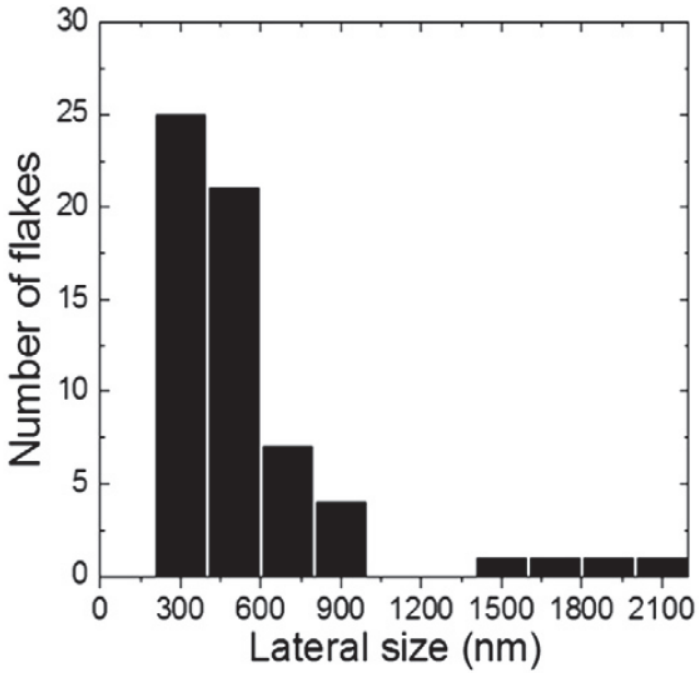

Fig. 5. Lateral size distribution of the flakes obtained from AFM analysis, on flakes deposit on SiO2 substrates.

To further confirm the results obtained from TEM, AFM analysis is shown in Fig. 5.

AFM is a commonly used tool for morphological characterization of pristine graphene that gives information on flake quality in terms of layer thickness and lateral dimensions. However, in because of the molecules residual on the flakes, AFM is not able to provide reliable information on the thickness distribution with our system. A large amount of flakes (62) were measured, but the smallest thickness was 5 nm, well above 0.33 nm (theoretical thickness of a supported single-layer graphene), as expected. AFM also shows that the average lateral size of the flakes is 200–400 nm (Fig. 5). A few large flakes with lateral size around 2 μm can also be found in the dispersion. These larger flakes can be used to perform both Raman mapping and AFM on the same sample and thus compare the results obtained by the two techniques (see following section).

3.2.4. Flakes morphology – spectroscopic approach

Raman spectroscopy is a powerful probe for characterizing graphene [19]. A typical Raman spectrum of monolayer graphene shows two main features [19]: the G peak, corresponding to the E2g phonon mode at the Brillouin zone center, at 1580 cm^{-1} and 2D peak, which is activated by two-phonons intervalley assisted Raman scattering, at 2700 cm^{-1}.

The 2D peak can be used to identify graphene [20]: the 2D peak is a single and sharp peak in the case of monolayer graphene, while in AB-stacked bilayer the 2D peak is composed by four bands. Graphite shows a broad and up-shifted 2D peak, which in first approximation can be fitted with two peaks. The 2D peak shape quickly evolves with the number of layers, so that the 2D band of a sample containing more than 8–10 layers is hardly distinguishable from that of bulk graphite [20]. In case of disorder, defect-activated features appear in the Raman spectrum: the D peak, first order of the 2D peak, which lies at 1350 cm^{-1}, and the D' peak, which appears at 1620 cm^{-1} [21]. It is common for pristine graphene not to have enough structural defects for the D and D' peaks to be Raman active so that they can only be seen at the edges[20,22].

Fig. 6 shows typical Raman spectra of our flakes deposited on SiO2, taken at 2.41 eV. In order to have a good statistics of the composition of the material obtained, Raman spectroscopy was performed on a large amount of flakes (130) deposited on a silicon substrate. We selected only flakes large enough to be observed under the optical microscope.

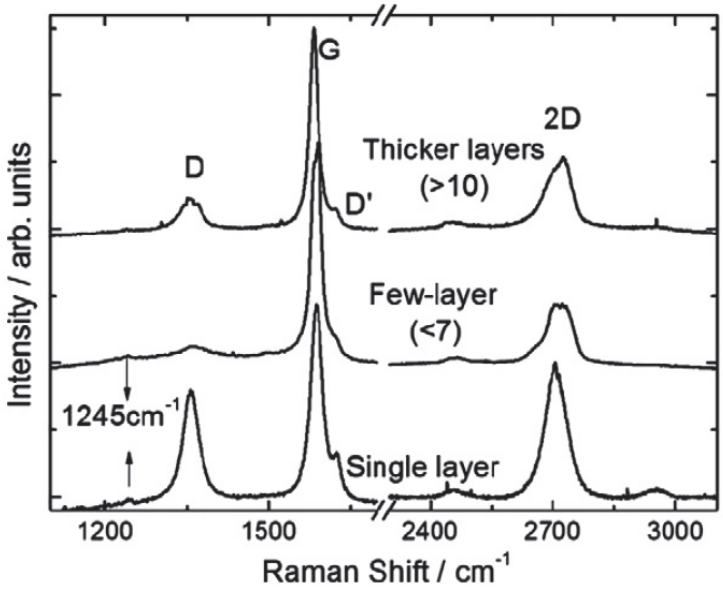

Fig. 6. Representative Raman spectra taken at 2.41 eV of the different flakes obtained by exfoliation of graphite in PS1 aqueous solutions, deposited by dropcasting on silicon.

In our sample, the shape of the 2D peak strongly changes with the flake analyzed (Fig. 6), reflecting the different thickness composition of the flakes. Based on the shape of the 2D peak, we attempt to derive the composition in flake thickness of graphene in solution. We found 18% of the flakes being single-layers, 68% are few-layer graphene flakes (<7 layers) and 14% are thick flakes.
The same method was applied to test flake stability against reaggregation in dispersion over longer time: We repeated the statistics on the same dispersions which stand undisturbed for 8 months, analysing about 130 flakes. The aged graphene dispersion is composed by 22% single-layers, 61% few graphene layers (<7) and 17% thicker flakes. Thus, no significant difference is observed in the composition of the flakes after 8 months, suggesting a good degree of stability for this system.
However it has to be mentioned that these numbers need to be treated with care since the composition of the flakes on the substrate may not correspond exactly to the composition of the flakes in suspension. Still, this quantification offers a rough idea on the exfoliation efficiency and give first indication on the distribution in flake thickness obtained with our method.

3.2.5. XPS measurements on graphene films

We then performed X-Ray photoelectron spectroscopy (XPS) on the flakes to verify that no graphene oxide or a similar derivatised graphene is present in our dispersion, and in order to obtain the percentage of residual PS1 after washing. Graphene films were obtained by filter deposition from the as-prepared graphene suspension. Fig. 7 shows the survey spectrum taken on the PS1-based graphene films, revealing the presence of oxygen, nitrogen and sulfur with respective concentrations of 4.9%, 0.7% and 0.8%. Using the value for sulfur, we estimate that 13% of the carbon signal is not graphene correlated and originating the PS1 molecule. The relatively high oxygen content is explained by the presence of sulphonic groups attached at the PS1 core, with a possible contribution from atmospheric adsorbates. These atmospheric adsorbates are also probably contributing to the nitrogen peak.
The carbon 1s spectrum of the PS1 exfoliated graphene film is presented in Fig. 7b. No large peak between 286 and 288 eV (corresponding to C–O and C=O groups [23]), is observed showing that our material does not contain graphene oxide. The C1s line is, on the contrary, very similar to the graphite signal with a slightly larger full width at half maximum (0.77 eV instead of 0.65 eV in graphite), a further evidence for the presence of the PS1 molecules.

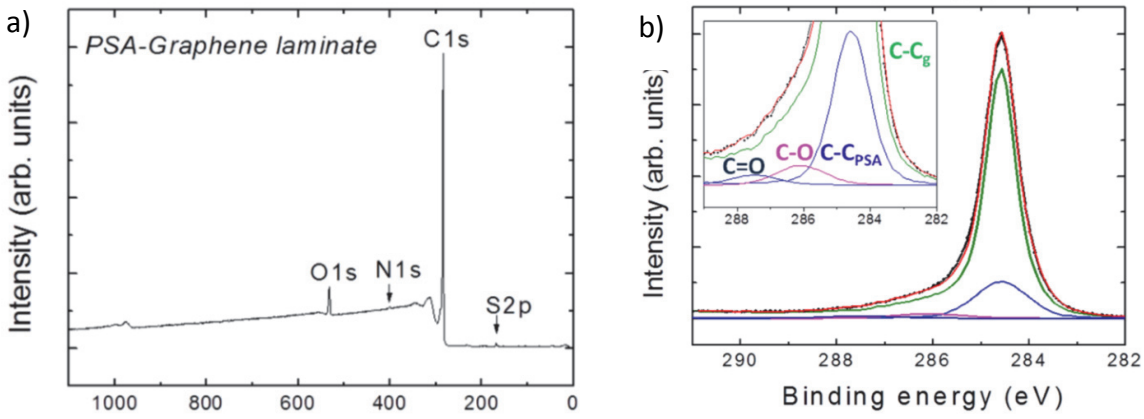

Fig. 7. Survey (a) and carbon 1s (b) spectra of the PSA-based graphene films. The C1s spectrum is fitted using the graphite signal (C-Cg), the PS1 powder signal (C-CPSA), and C-O and C=O bonds.

The carbon 1s peak of the PS1 based graphene film was fitted using the pristine graphite signal, and both graphite and PS1 powder spectrum used here were recorded under the same conditions. We observed a very good match using a PS1 powder peak area of 14% of the total area which is in accordance with the PS1 concentration calculated using the survey spectrum. XPS measurements indicate that the method suggested in this chapter produces graphene films free from graphene oxide. A carbon content of roughly 13 – 14% in the graphene-PS1 film is resulting from PS1 molecules.

3.3. Discussion

We have developed a simple method to produce graphene suspensions by using non-covalent interaction with PS1 using only water as solvent. We found that by using our method, based on ultra-sonication with PS1, it is possible to achieve stable graphene suspensions directly in water. With a washing procedure based on centrifugation and solvent exchange, most of the excess dye could be remove from suspension; still the strong fluorescence background observed indicate that there is still a significant amount of Py-1SO3 left, stabilizing hydrophobic graphene flakes in aqueous solution. We observe a strong decrease of the fluorescence after 1.5 h sonication, which can be fingerprint of interaction between the molecules and graphene [17,24].

Such charge transfer interaction is of great importance for the design of optoelectronic composite materials. In the case of composite materials based on graphene oxide, the nano-graphene molecules anchor on the functional groups on the basal plane causing the fluorescence to be fully quenched [18]. However, ground state charge transfer interaction usually comes with a distortion of the electronic transition in the dye, often causing a shift of the absorption peak to lower energies (red shift), which was not observed in our system.

The flakes obtained with our method characteristically have lateral dimensions of 200nm to 400nm, with few flakes having lateral size of around 2 μm. The flakes are mainly multilayered as expected for direct exfoliation of graphite in water. XPS measurements indicate that the method suggested in this chapter produces graphene films free from graphene oxide. A carbon content of roughly 13 – 14% in the graphene-PS1 film is resulting from PS1 molecules.

Our results indicate that, in agreement with previous works, functionlization of pyrene with a polar moiety is a valuable approach to achieve graphene stabilization in water in a one-step exfoliation procedure. As we found that functionalization of pyrene with one sulphonic group has a major impact on the molecules solubility and eligibility as exfoliation agent, it is interesting to compare the results on Py-1SO3 with further -SO3 functionalized pyrene derivatives in order to achieve a further understanding of the exfoliation mechanism, as will be detailed in the next chapter.

3. Exfoliating graphene with organic dyes

3.4. Experimental

Graphene liquid phase exfoliation. The schematic of the exfoliation process is shown in Fig. 1. The yellowish of PS1 solution was prepared by dissolving 1 mg of PS1 powder (Sigma–Aldrich, P97.0% (HPLC)) in 10 mL of distilled water. The dispersion was produced by sonicating (Bandelin DK 102P bath sonicator) 30 mg of graphite flakes (Bran Well UK, Grade: 99.5) with 10 mL of as-prepared PS1 solution. After 80 min sonication, the large cluster of non-exfoliated graphite can be removed by mild centrifugation at 1000 rpm for 20 min. The dispersion was then refilled with water and centrifuged at 12,000 rpm for 20 min for three times in order to wash the excess PS1. Graphene films for XPS measurement were obtained by filter deposition from a graphene suspension that was prepared as described above.

Characterization. A Perkin-Elmer k-900 UV–vis-NIR spectrophotometer was used to perform UV–vis spectroscopy of the dispersion. Fluorescence measurements were obtained by using a Spex Fluorolog II, equipped with a 450Watt Xenon lamp.
The Raman peaks were fitted with Lorentzian lines. The laser power on the sample was below 1mW in order to avoid damage of graphene and desorption of the molecules. The prepared dispersion was drop casted on a SiO2/Si substrate for Atomic Force Microscopy (AFM) and Raman Spectroscopy characterization. A Nanoscope (R) III a, operating in tapping mode was used. A Witec alpha300 Raman spectrometer, equipped with 488, 514.5 and 633 nm excitation lines and a piezoelectric stage for Raman mapping, was used. For Transmission Electron Microscopy (TEM) analysis, the flakes were deposited by pipetting a few millilitres of the dispersion onto holey carbon mesh grid, a FEI Tecnai F20 with 200 kV accelerating voltage was used was measurement.

Extensive Raman analysis of the material has been performed in collaboration with Dr. Huafeng Yang, University of Manchester (UK), and this work has been published in Carbon 53 (2013) 357–365.

References.

(1) Novoselov, K. S. Reviews of Modern Physics 2011, 83, 837.
(2) Geim, A. K. Angewandte Chemie International Edition 2011, 50, 6966.
(3) Geim, A. K. Science 2009, 324, 1530.
(4) Cai, W.; Zhu, Y.; Li, X.; Piner, R. D.; Ruoff, R. S. Applied Physics Letters 2009, 95.
(5) Kim, K. S.; Zhao, Y.; Jang, H.; Lee, S. Y.; Kim, J. M.; Kim, K. S.; Ahn, J. H.; Kim, P.; Choi, J. Y.; Hong, B. H. Nature 2009, 457, 706.
(6) Ohta, T.; Bostwick, A.; Seyller, T.; Horn, K.; Rotenberg, E. Science 2006, 313, 951.
(7) Blake, P.; Brimicombe, P. D.; Nair, R. R.; Booth, T. J.; Jiang, D.; Schedin, F.; Ponomarenko, L. A.; Morozov, S. V.; Gleeson, H. F.; Hill, E. W.; Geim, A. K.; Novoselov, K. S. Nano Letters 2008, 8, 1704.
(8) Hernandez, Y.; Nicolosi, V.; Lotya, M.; Blighe, F. M.; Sun, Z. Y.; De, S.; McGovern, I. T.; Holland, B.; Byrne, M.; Gun'ko, Y. K.; Boland, J. J.; Niraj, P.; Duesberg, G.; Krishnamurthy, S.; Goodhue, R.; Hutchison, J.; Scardaci, V.; Ferrari, A. C.; Coleman, J. N. Nature Nanotechnology 2008, 3, 563.
(9) Shih, C. J.; Lin, S. C.; Strano, M. S.; Blankschtein, D. Journal of the American Chemical Society 2010, 132, 14638.
(10) Lotya, M.; Hernandez, Y.; King, P. J.; Smith, R. J.; Nicolosi, V.; Karlsson, L. S.; Blighe, F. M.; De, S.; Wang, Z. M.; McGovern, I. T.; Duesberg, G. S.; Coleman, J. N. Journal of the American Chemical Society 2009, 131, 3611.
(11) Jang, J. H.; Rangappa, D.; Kwon, Y. U.; Honma, I. Journal of Materials Chemistry 2011, 21, 3462.
(12) An, X. H.; Simmons, T. J.; Shah, R.; Wolfe, C.; Lewis, K. M.; Washington, M.; Nayak, S. K.; Talapatra, S.; Kar, S. Nano Letters 2010, 10, 4295.
(13) Dong, X. C.; Shi, Y. M.; Zhao, Y.; Chen, D. M.; Ye, J.; Yao, Y. G.; Gao, F.; Ni, Z. H.; Yu, T.; Shen, Z. X.; Huang, Y. X.; Chen, P.; Li, L. J. Physical Review Letters 2009, 102, #135501.
(14) Zhang, M.; Parajuli, R. R.; Mastrogiovanni, D.; Dai, B.; Lo, P.; Cheung, W.; Brukh, R.; Chiu, P. L.; Zhou, T.; Liu, Z.; Garfunkel, E.; He, H. Small 2010, 6, 1100.
(15) Ehli, C.; Rahman, G. M. A.; Jux, N.; Balbinot, D.; Guldi, D. M.; Paolucci, F.; Marcaccio, M.; Paolucci, D.; Melle-Franco, M.; Zerbetto, F.; Campidelli, S.; Prato, M. Journal of the American Chemical Society 2006, 128, 11222.
(16) Treossi, E.; Melucci, M.; Liscio, A.; Gazzano, M.; Samorì, P.; Palermo, V. Journal of the American Chemical Society 2009, 131, 15576.
(17) Melucci, M.; Treossi, E.; Ortolani, L.; Giambastiani, G.; Morandi, V.; Klar, P.; Casiraghi, C.; Samori, P.; Palermo, V. Journal of Materials Chemistry 2010, 20, 9052.
(18) Su, Q.; Pang, S.; Alijani, V.; Li, C.; Feng, X.; Müllen, K. Advanced Materials 2009, 21, 3191.

(19) Ferrari, A. C. Solid State Communications 2007, 143, 47.
(20) Ferrari, A. C.; Meyer, J. C.; Scardaci, V.; Casiraghi, C.; Lazzeri, M.; Mauri, F.; Piscanec, S.; Jiang, D.; Novoselov, K. S.; Roth, S.; Geim, A. K. Physical Review Letters 2006, 97, 187401.
(21) Casiraghi, C. physica status solidi (RRL) – Rapid Research Letters 2009, 3, 175.
(22) Casiraghi, C.; Hartschuh, A.; Qian, H.; Piscanec, S.; Georgi, C.; Fasoli, A.; Novoselov, K. S.; Basko, D. M.; Ferrari, A. C. Nano Letters 2009, 9, 1433.
(23) Dreyer, D. R.; Park, S.; Bielawski, C. W.; Ruoff, R. S. Chem. Soc. Rev., 39, 228.
(24) Treossi, E.; Melucci, M.; Liscio, A.; Gazzano, M.; Samorì, P.; Palermo, V. Journal of the American Chemical Society 2009, 131, 15576.

Chapter 4

Nanoscale insight into the exfoliation mechanism of graphene with pyrene based dyes: Effect of charge, dipole and molecular structure

4. Nanoscale insight into the exfoliation mechanism

4.1. Introduction

Suitable moieties that can successfully exfoliate graphene include organic solvents, [1] surfactants,[2,3] block copolymers, [4] superacids [5] or even metal atoms. [6] As we suggested in the previous chapter, a natural approach to exfoliate graphene is to use surfactants based on nano-graphenes (NGs), i.e., small polyaromatic hydrocarbons such as pyrenes, perylenes, coronenes, tetracenes, etc. These conjugated moieties exhibit a polyaromatic structure similar, yet smaller, to that of graphene, and are able to self-assemble on its surface forming ordered layers, at least in ultra-high vacuum conditions. [7] NG molecules feature unique physico-chemical properties making them interesting for applications as dyes or as organic semiconductors for the fabrication of opto-electronic devices such as organic light emitting diodes (OLEDs), [8] organic photovoltaics, [9-11] flexible electronics and sensors. [12-14] The optical and electronic properties of these NGs can be tuned by functionalizing their peripheries with electron accepting or electron withdrawing groups. [12,15] The side-groups can also improve their solubility not only in organic solvents but also in water, being the best solvent possible for large scale, environmentally friendly and cheap technological applications. In particular, several works have demonstrated the efficiency of water-soluble pyrenes to solubilize graphene sheets in water. The single or multiple functional moieties attached to the pyrene's periphery include negatively charged sulphonic groups, [16,17] amines, [18] carboxylic, [19] butyric [20] or butylphenyl groups.

While the efficiency of pyrene derivatives in exfoliating graphene is well known, the exact details of pyrene–graphene interactions, and more generally of NG–graphene interactions, are still unclear. By using a rather simplistic description of the exfoliation process, organic molecules such as these are often described as aromatic surfactants, “molecular wedges” [19] with the apolar, aromatic part interacting with graphene through π-π stacking and the negatively charged part favouring sheet stabilization in solvents and hindering re-aggregation.

We already discussed the efficiency of amphiphilic pyrenes in graphite liquid phase exfoliation in the previous chapter. Their potential to interact non-covalently with graphene has been attributed to their aromatic nature and to their electron donating/withdrawing [21] character due to the difference in the dyes’ electronegativity with respect to graphene. Yet, unexpectedly, a recent work by Green and co-workers found that an increase in the number of electron-withdrawing sulphonic groups yields a more modest graphene exfoliation in solution and that the adsorption efficiency of the stabilizer on graphene is not related to the protonation/deprotonation of pyrenes. These results indicate that, while the amphiphilic nature of these organic molecules is

fundamental to stabilize graphene in polar solvents, the simple “molecular wedge” model is not sufficient to describe both the interaction of aromatic molecules with graphene and their ability to exfoliate and solubilise graphite. The final efficiency of graphite exfoliation with small aromatic dyes ultimately depends not only on the thermodynamics of exfoliation, but also on the presence of local energy minima which will influence kinetics, and on the solvent– molecule, graphene–molecule and graphene–solvent competitive interactions. [22]

To gain a thorough molecular scale understanding on the interaction process between graphene and the dye it is key to perform and compare nano-scale and multiscale experimental studies. In this work, we exfoliate graphene using a series of pyrene molecules functionalized in the peripheral positions with an increasing number of sulphonic groups. Our study contributes to derive the most important factors driving small molecule assisted graphene exfoliation and stabilization in suspension. We compare two complementary processes that take place during graphene liquid phase exfoliation, namely:

(a) the adsorption of the molecules from a water solution to the surface of the bulk graphite.
(b) the exfoliation, induced by the molecules, of graphene sheets from the bulk graphite to a water solution.

Both processes are caused by the affinity between the molecule and graphene, and depend strongly on the molecular structure and processing conditions. In this chapter, our comparative study on four different pyrene sulphonic acid sodium salt derivatives (Fig. 1) is presented. All these pyrenes are functionalized with side-groups featuring different steric hindrance, electronegativity and pH response to the respective molecule.

The molecules studied are: 1-pyrenesulphonic acid sodium salt (PS1), 6,8-dihydroxy-1,3-pyrenedisulphonic acid disodium salt (PS2), 8-hydroxypyrene-1,3,6-trisulphonic acid trisodium salt (PS3) and pyrene-1,3,6,8-tetrasulphonic acid tetrasodium salt (PS4). While PS1 and PS4 have already been demonstrated to be eligible surfactants for graphene liquid phase exfoliation, [16,18,23] and have been extensively discussed in Chapter 3, we include here also the more complex analogues PS2 and PS3 having electron accepting, sulphonic (–SO_3) groups and electron donatinghydroxyl (–OH) groups, whose charge and dipole can be modified with adjusting pH. We

selected these pH sensitive derivatives because they are not only interesting for fundamental research, but also for practical applications due to their high quantum yield and excellent water solubility. [24] PS3 for instance, also known as pyranine or solvent green 7, is commonly used in commercial highlighters and soaps.

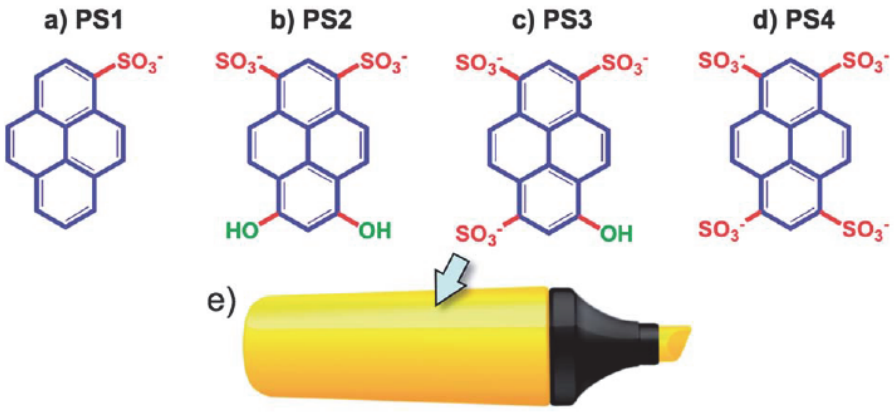

Fig. 1. (a–d) show the chemical formulas of the four pyrene derivatives under study. The moieties which shall be protonated/ deprotonated are indicated in green. (e) Typical highlighter containing pyrene-based sulphonated dyes such as PS3.

The extraordinary optical and chemical properties of these molecules such as their well-defined absorption and emission in the visible spectrum, tuneable absorption, emission and molecular charge, and pH sensitive dipole, make them interesting materials to be combined with graphene. To provide precise, comparable and quantitative insight into the efficiency of these pyrene sulphonic sodium salts for the preparation of graphene, we carefully respected the same procedures for all derivatives including the solvent, sonication and excess dye removal parameters. Such a reliable comparison is not simply achieved by considering previously reported results as processing methods and characterization techniques largely vary and consequently do not allow for direct comparison. [18,19,25]

4.2. Results

4.2.1. Properties of the free dyes

Fig. 2a–d (red curves) show the different absorption spectra of the four molecules. The spectra reported in Fig. 2 reveal that the UV/VIS absorption of pyrene is strongly influenced by the

molecule's side functionalization. The distinct response of pyrene optical absorption is well known, and was also exploited to create a "pyrene scale of solvents", to rank the polarity of solvents. [17]

PS1 and PS4 exhibit a well-defined optical absorption band structure, with three main sharp peaks similar to those of pristine pyrene; [26] conversely, the presence of –OH groups in PS2 and PS3 greatly influences the electronic structure of the molecule, leading to broadened and red shifted peaks. The different absorption is not due to a change in molecular aggregation behaviour in solution, as proven by performing concentration dependent absorption studies (not included here); instead the $–SO_3$ groups act as electron withdrawing units on the polyaromatic scaffold, while the –OH is a weak (mesomeric) electron donor. The push–pull action of the two groups results in a significant reduction of the lowest optical electronic excitation, thus moving the absorption peaks to longer wavelengths,[42] an effect successfully used in the last few years to improve light absorption and efficiency in organic photovoltaic dyes. [11]

A further important consequence of the different core functionalization is a change in the molecular dipole moment, which has been calculated in an implicit water environment using ab initio methods (Calculations performed by University of Mons, Belgium). Regardless of the highly polar functionalization, the dipole moment is zero for PS4 as a consequence of the molecule's highly symmetric geometry. PS1 and PS3, which belong to the same symmetry group, show comparable molecular dipole moments (25.9 Debye for PS1 and 28.0 Debye for PS3). The dipole is instead strongly pronounced in PS2 (46.6 Debye), due to the presence of both electron-withdrawing groups in positions 1 and 3 and the electron pushing –OH groups in positions 6 and 8.

The –OH group also adds another degree of freedom to control molecular properties: while the sulphonic groups are salts of strong acids and can be considered as negatively charged in any relevant pH conditions (pK_a for sulphonic acids is < 0), the –OH groups in PS2 and PS3 are weakly acidic and their protonation state is highly sensitive to pH (for PS3 the pK_a is 7.3, for the two –OH of PS2 the pK_a are 7.33 and 8.53). [24] The dipole of PS2 and PS3 dyes changes significantly with pH from acidic to basic conditions, decreasing from 46.6 to 25.0 Debye for PS2 and from 28.0 to 17.4 Debye for PS3. In both PS2 and PS3, basic conditions give rise to the characteristic, lower energy absorption band that is attributed to the deprotonated species. The absorption of the protonated species, which is blue shifted as compared to the deprotonated one, can be fully recovered by tuning the pH to acidic conditions. Thus, the acid/ base forms of those molecules can easily be

discriminated by considering their different absorption spectra, and have already been used to monitor pyrene interactions with reduced graphene oxide (RGO) sheets in solution. [27]

4.2.2. Dye adsorption on graphite powder

The first stage of any exfoliation process is the interaction of the exfoliating agents with the pristine, bulk graphite powder. Before comparing the ability of the selected molecules to exfoliate graphene sheets from graphite, we estimated their potential to interact with graphitic substrates by monitoring their spontaneous physisorption from solution onto bulk graphite, which typically takes place in few hours. As previously reported, the spontaneous adsorption process of PS1 on carbon nanotubes reaches equilibrium after 12 h exposure time. [28] In our experiment, a fixed amount of graphite powder (Aldrich) was immersed in an aqueous solution of the studied molecules. Gentle stirring was applied to avoid artefacts due to diffusion limits; samples were stirred for four days to ensure efficient adsorption. In the absence of sonication the exfoliation does not take place, although the molecules having a higher affinity for graphite may initiate their adsorption process on the surface of the graphite powder. Therefore, the graphite powder acts as a trap for the molecules in solution, thereby capturing the dyes from the solution. The amount of this "dye capture" process was calculated by simply observing the decrease in optical absorption intensity upon exposure time. Fig. 2 compares the absorption spectrum in water for the four molecules, after stirring in the presence (green lines) or absence (red lines) of graphite. As expected, stirring without graphite does not change the original absorption spectrum of the dyes; conversely, in the presence of graphite spontaneous adsorption from solution to the graphitic surface is observed, with its efficiency being inversely proportional to the number of $–SO_3$ groups present (Fig. 2 f). The fraction of molecules adsorbed on graphite has been calculated by monitoring the change in the main absorption peak for each molecule (at 346 nm, 408 nm, 404 nm and 375 nm for PS1, PS2, PS3, PS4 respectively). For the mono-substituted derivative PS1, most of the molecules are adsorbed on the graphite surface after 4 days. PS4, having four sulphonic groups, did not show a change in free dye concentration after four days, indicating significantly lower affinity for graphite powder than PS1. Both molecules exposing hydroxyl groups show similar behaviour in spontaneous adsorption, with adsorption efficiencies between those of PS1 and PS4.

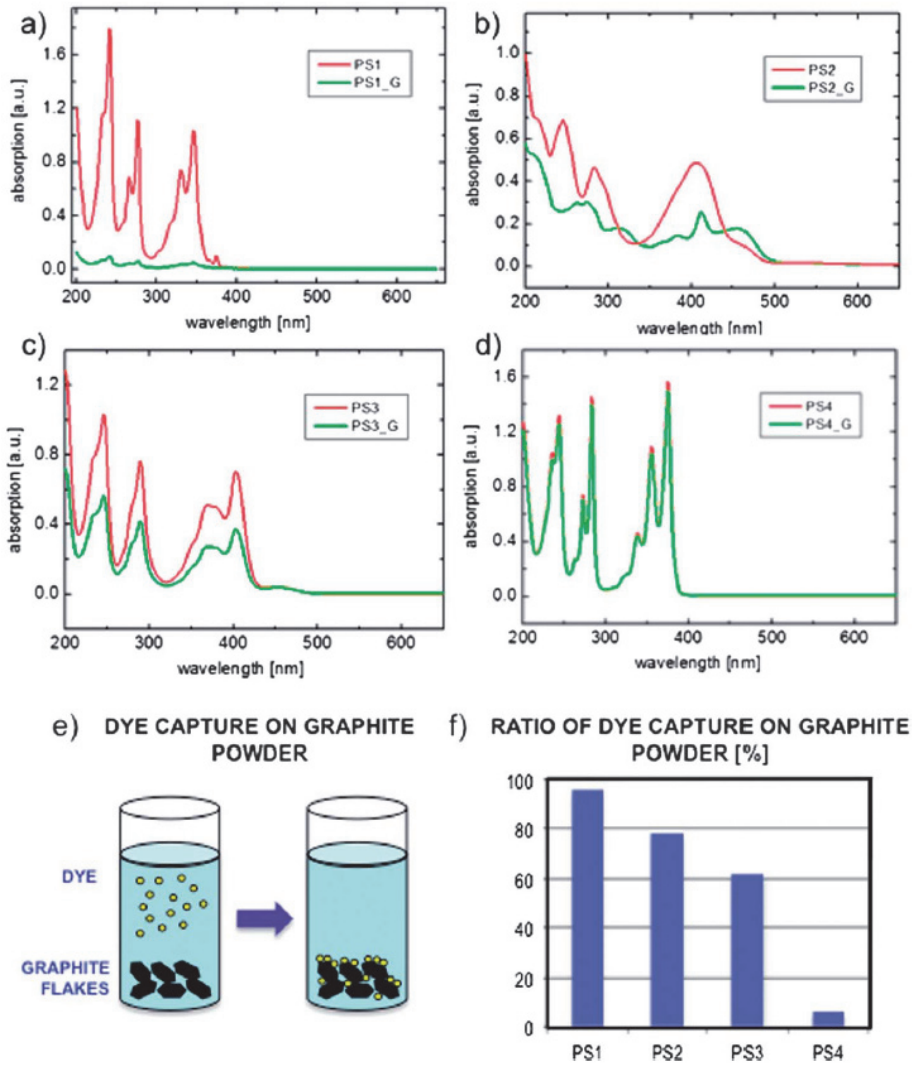

Fig. 2. (a–d) UV/VIS absorption spectra of aqueous solutions of PS1, PS2, PS3, PS4 dyes after stirring for 4 days in pure water (red curves) or in water in the presence of graphite powder (green curves). All samples contain the same initial dye concentration and ratio of molecules and graphite powder. (e) Schematic representation of "dye capture" from solution to the graphite substrate. (f) Ratio of molecules removed from solution upon exposure to graphite powder.

The change is not linear with the number of $-SO_3$ groups on the pyrene core (decrease in absorbance of dye captured is 18% going from one sulphonic group to two, 16% from two to three, and 56% going from three to four). A quantitative correlation between the amount of dye adsorbed and the graphite surface available cannot be derived directly with the drop in dye concentration: the dyes tend to form a multilayer on graphitic substrates rather than adsorbing into homogeneous monolayers, as it will be evident from the results of the following sections. However, this qualitative insight reveals that the more sulphonic groups present on the pyrene core, the less favourable the interaction with graphite powder.

4.2.3. Exfoliation and stabilization of graphene in suspension

Previous works demonstrated that both PS1 and PS4 serve as effective agents in exfoliating graphene by sonication. [16,17,23] To compare the exfoliation efficiencies of the four dyes under study, a concentrated aqueous solution of each molecule was mixed with graphite powder (Aldrich) and sonicated in a water bath. A rough estimation of the amount of suspended graphitic material is obtained by comparing the total light absorption at 650 nm. Given that all dyes used are transparent at $\lambda > 500$ nm (Fig. 2), the increase in absorption can be attributed uniquely to light absorption and scattering of the exfoliated material for any wavelength >500 nm. Optical absorption spectroscopy showed that the exfoliation yield, i.e., the quantity of suspended material, increases with sonication time.

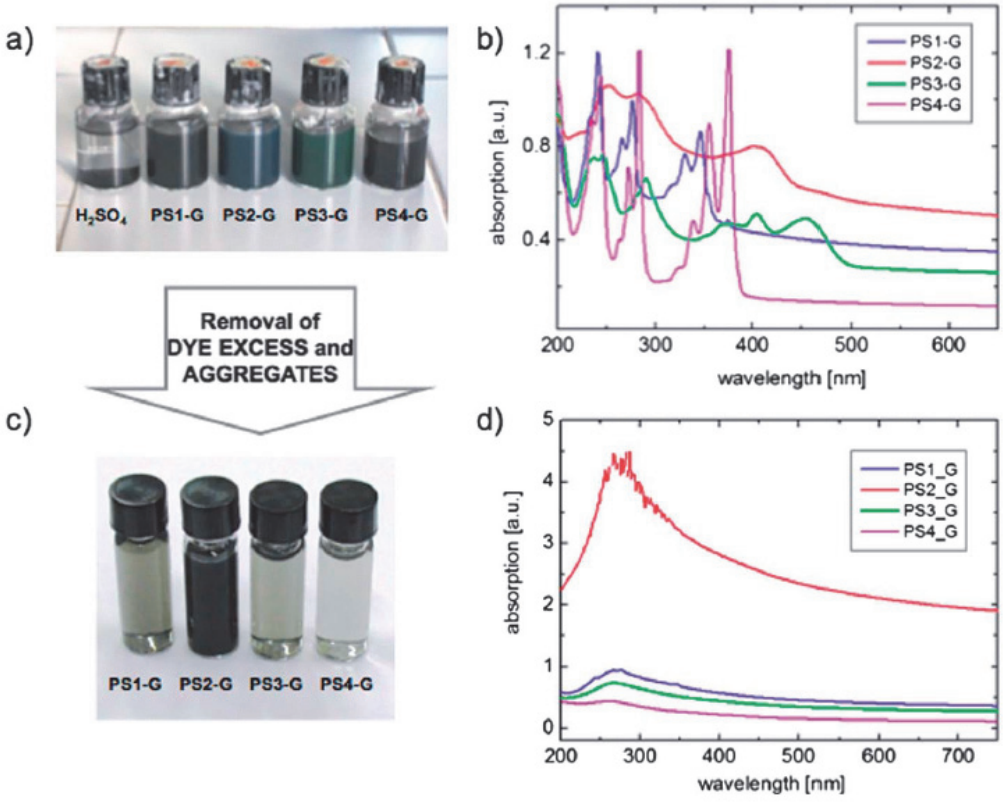

Fig. 3. Picture of the four dye solutions after sonication with graphite and centrifugation. (b) UV/VIS absorption spectra of the suspensions (samples diluted 1 : 20 for measurement). Pyrene concentration $c = 10^{-4}$ mol L^{-1}. (c) Image of the suspensions after dye removal by washing and centrifugation. (d) Optical absorption of the solutions in (c) (no dilution).

Even if relevant exfoliation shall be observed after few hours, extensive sonication was performed to monitor the increase of solubilized material with time. After sonication all four solutions

contained well-suspended and dark graphitic material (showing a light shade of the typical dye colour, Fig. 3a). Exfoliation in H_2SO_4 solutions containing as well $–SO_3$ charged groups but no aromatic moiety (performed as a control experiment) did not yield any suspended material, as evident by the transparent colour of the suspension in Fig. 3a. Fig. 3b clearly reveals that the increase in concentration strongly depends on the type of employed pyrene; for any sonication time tested, without further processing, the final concentration is the highest for PS2, followed by PS1, PS3 and PS4.

Indeed, PS2 features a particular efficient action in dissolving graphite, while for the other derivatives PS1, PS3 and PS4 the graphite dissolution is inversely proportional to the number of sulphonic groups, as observed also in the "dye capture" experiment. The freshly exfoliated suspensions contain a large excess of free dyes, as evident from the absorption spectra (Fig. 3b). The UV spectra show a superposition of the typical, well-defined pyrene band structure with the more uniform, slowly decaying light dispersion of graphene sheets in solution. The graphene was purified using a procedure based on multiple centrifugation steps, to remove excess dye and large graphite fragments, which was previously described in Ref. [29]. After the washing and centrifugation procedure, the amount of material (both dye and graphene) present in suspension was significantly lower for all pyrene derivatives, even if PS2 suspensions were again the ones with the highest amount of solubilized graphene (Fig. 3c). Noteworthy, the typical absorption bands of pyrenes cannot be observed after the washing procedure, suggesting residual or adsorbed dye concentration being below the absorption spectrometer detection limit. All the suspensions obtained in this way were stable for several months, allowing efficient processing and further characterization.

4.2.4. Morphology and composition of graphene–pyrene flakes

The purified suspensions obtained by graphite sonication with the four different dyes were drop-cast on silicon substrates covered with 90 nm SiO_2 and characterized by TEM, AFM and Raman spectroscopy. The distribution in sheet thicknesses and the presence of monolayers were measured with Raman spectroscopy by statistical analysis of the Raman 2D peak performed on several flakes. A significant part of the solubilized material was composed of single graphene sheets (up to 22% for PS3), with most of the remaining material composed of a few-layer graphene (50% to 60% of flakes having less than 7 layers). A table with the statistical distribution

of different layer thicknesses obtained for each molecule is reported in Fig. S3. The presence of a significant D peak at 1350 cm^{-1} and of a small peak at 1505 cm^{-1} was also observed by Raman, and attributed to the presence of the organic dyes (a more detailed study of the effect of PS1 on graphene Raman spectrum is reported in Ref. [23]). The presence of graphene sheets together with adsorbed molecules was also confirmed by TEM analysis. Fig. 4 displays a TEM image of the typical sheets obtained using PS2, having lateral size of some hundreds of nanometers. Electron diffraction showed the typical hexagonal pattern of graphene, with reflections from 0.213 nm and 0.123 nm spaced lattice planes. In some flakes, the presence of a coating on graphene was observed by TEM.

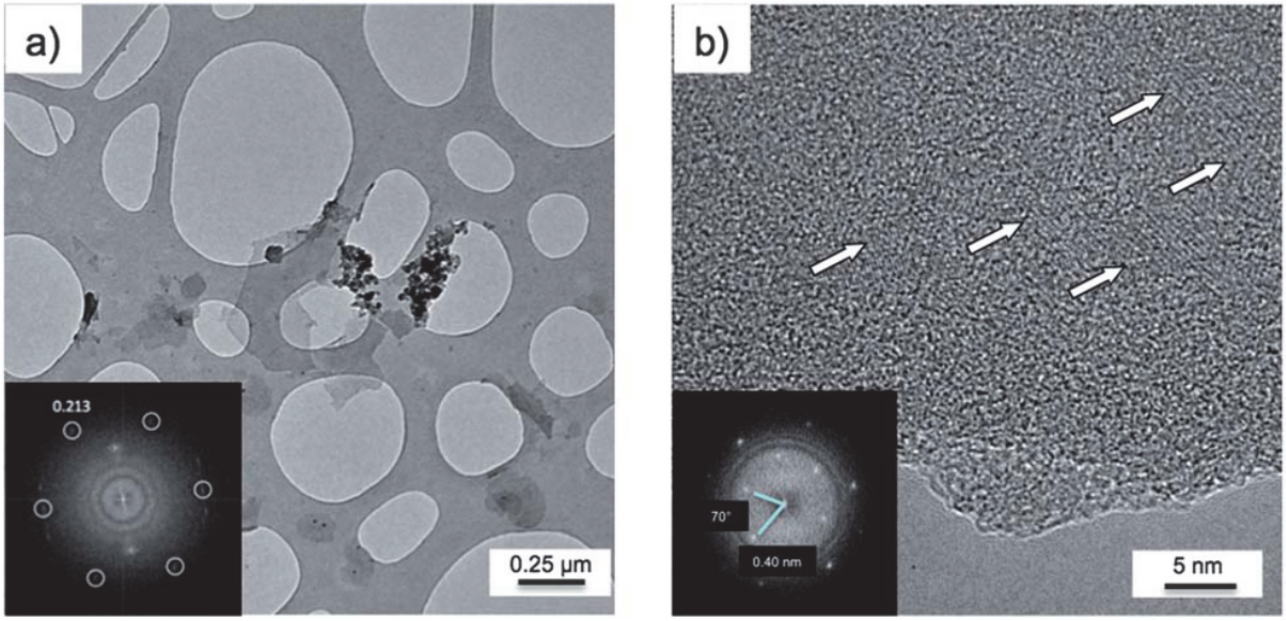

Fig. 4. TEM image of graphene sheets exfoliated with PS2. In the inset, the typical SAED pattern of graphene is shown. (b) Zoom-in on a sheet, showing ordered areas with a packing different from the one observed for graphene (SAED measurements are shown in the inset).

In such regions some superstructure appears in high-resolution images. Some patches of organized material are visible in Fig. 4b as highlighted by the arrows. Selected Area Electron Diffraction (SAED) measurements performed on the sheets showed that the hexagonal motif within the sheets was intact and undamaged by the interaction with the dyes, and that the dye molecules were organized in a crystal-like structure, with hexagonal symmetry and spacing corresponding to 0.44–0.45 nm (inset in Fig. 4b). The coating, though, showed different symmetry in different regions, having sometimes 0.40 nm reflections and cubic symmetry. TEM analysis did

not provide statistical evidence, but this variation in symmetry and spacing could be explained by the presence of residual traces of crystallized solvent molecules. [30]

Fig. 5 shows typical AFM images of the graphene–pyrene composites spin coated on silicon. They display well-defined sheets, with polygonal shapes and sharp edges, having lateral sizes of some hundreds of nm.

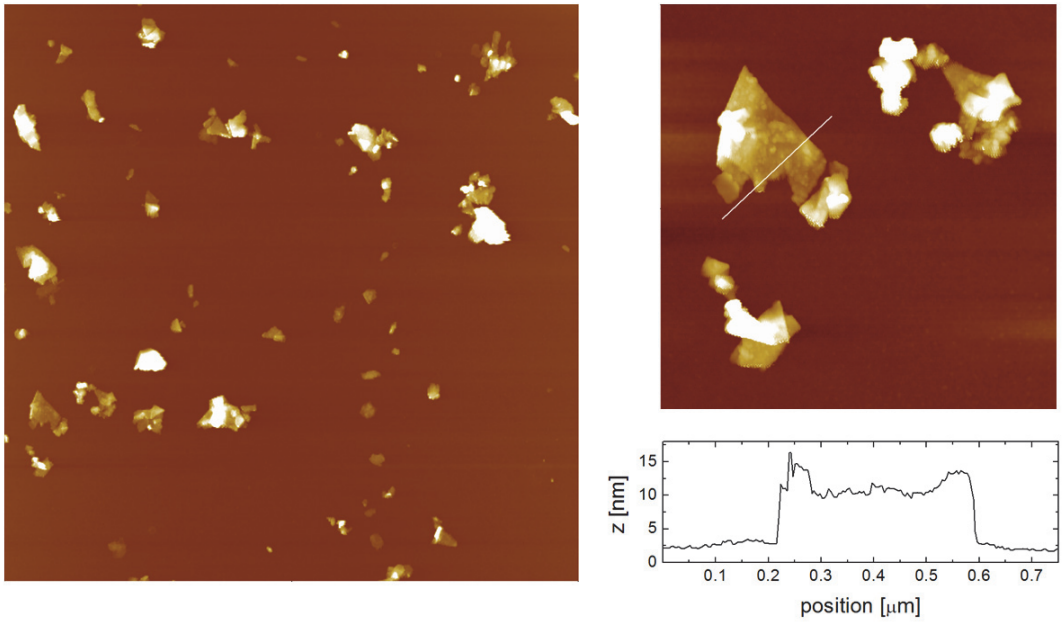

Fig. 5. Topographical AFM image of PS2 suspension deposited by drop-casting on SiO2. Image width 10.0 μm. Z-range, 50 nm. (b) Zoom-in showing the flake surface. Image width 3.3 μm. (c) Height profile taken along the white line in (b). Z-range, 30 nm.

Nevertheless, AFM did not provide evidence for the presence of well-defined thicknesses; in fact, sheets with varying thickness (typically 2–4 nm) were obtained with all four dyes, in agreement with previous studies on PS1. [23] The thickness observed is much higher than the theoretical one for monolayer graphene (0.33 nm); given that, as seen by Raman, the majority of flakes are <7 layers, the high thickness measured by AFM confirms the presence of a layer of adsorbed dye molecules on the graphene sheets, in agreement with Raman and TEM data.

4.2.5. Influence of molecular polarity on graphene–pyrene interactions

The main goal of this chapter is to provide a better understanding on the driving force for graphite exfoliation and stabilization with pH sensitive, water-soluble pyrene derivatives. Although the dye adsorption on graphite is simply correlated to the number of sulphonic groups on the aromatic

core (Fig. 2), the highest concentration of suspended material has been obtained with the dihydroxyl–disulphonic derivative PS2, not the mono-sulphonic derivative PS1, excluding thus a simple effect on exfoliation of the steric demand of the side-groups. As described above, PS2 has the highest dipole moment resulting from its molecular geometry with both bulky electron acceptor –SO3 groups in positions 1 and 3, and two smaller electron-donor –OH groups in positions 6 and 8 (Fig. 1). In Fig. 6 we correlate for each molecule experimental data and calculated molecular properties.

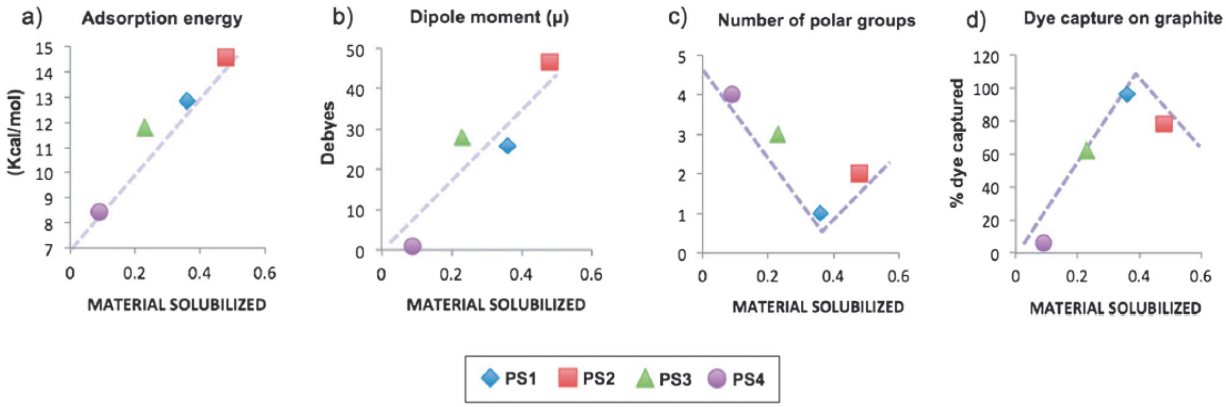

Fig. 6. Correlation between exfoliation efficiency and (a) calculated adsorption energy, (b) calculated molecular dipole, (c) number of charged groups on each molecule, (d) tendency of each molecule to adsorb on bulk graphite. The X axis reports the amount of solubilised material, measured experimentally from UV/VIS absorption. The dashed lines are a reference for the eye.

For all graphs, the X-axis reports the amount of material transferred from graphite into the suspension with sonication (quantified by the optical absorption at 650 nm). The concentration of graphitic material in suspension is then plotted against the adsorption energy calculated by modelling (Fig. 6a, from force field calculations, see below) the molecular dipole (Fig. 6b, from DFT calculations), the number of polar, charged groups (Fig. 6c) and the tendency of each molecule to adsorb on bulk graphite (Fig. 6d, obtained from Fig. 2f). The amount of exfoliated material (X-axis) shows no clear correlation with both the number of polar groups present on the molecule (Fig. 6c), and the tendency of each molecule to adsorb on bulk graphite (Fig. 6d). Instead, a linear correlation with the molecule–graphene adsorption free energy is observed, Fig. 6a. The correlation with the molecular dipole is less clear; in particular, even if PS1 and PS3 dyes share the same group symmetry (Cs) and have a comparable dipole (25.9 D vs. 28.0 D), they do not yield the same concentration of exfoliated material. Experimental evidence in Fig. 3 shows that PS3 (which

has a stronger acceptor–donor character due to the presence of one –OH and 3 sulphonic groups, but also features a large steric hindrance) performs worse than PS1. The lower steric hindrance of PS1, more than the strongest polarization of the PS3 aromatic core, is a factor important (but not sufficient) for successful exfoliation.

The correlations of physical properties with the amount of exfoliated material show that the pyrene derivative with both the highest molecular dipole and largest adsorption energy yields the most exfoliated material in suspension. However, a large molecular dipole moment is not enough for efficient graphene exfoliation, otherwise graphene would simply exfoliate with highly polar solvents; the presence of the pyrene core, strongly interacting with graphene through π-π interactions, plays of course a major role.

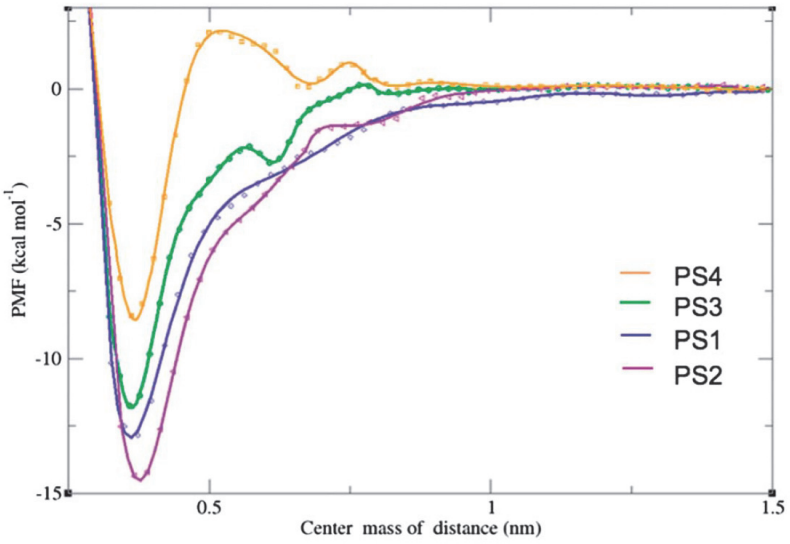

Fig. 7. Potential of mean force (PMF) curve as a function of graphene–dye distance, calculated from umbrella pulling simulation technique.

To better unravel the graphene–pyrene interaction, the adsorption process of each molecule on the surface of graphene in an explicit water medium was simulated using Molecular Dynamics simulations. The respective molecule was placed in a box, at a starting perpendicular distance of 1.8 nm from the basis plane consisting of a graphene sheet, and the box was then filled with water molecules. Periodic boundary conditions were maintained in all cases. An umbrella pulling simulation technique (Simulation were done by University Mons, Belgium details not reported here) was used to calculate the potential of mean force (PMF) of the adsorption process within several sampling windows. The free energy of adsorption of each molecule was determined from the resulting PMF curves. Fig. 7 shows the PMF curves obtained for all four molecules.

4. Nanoscale insight into the exfoliation mechanism

In contrast to PS1 and PS2 that show a single global minimum in free energy, two local minima are identified on the PMF as the PS3 and PS4 molecules approach the graphene surface that could potentially act as kinetic traps. In particular, the calculations indicate that an energy barrier of a few kcal mol^{-1} has to be overpassed to allow for close contact between PS4 and graphene. In order to gain insight into the 'landing on graphene' mechanism, snapshots at different stages of the molecular adsorption of PS2 and PS4 are reported in Fig. 8a) and Fig. 8b), respectively.

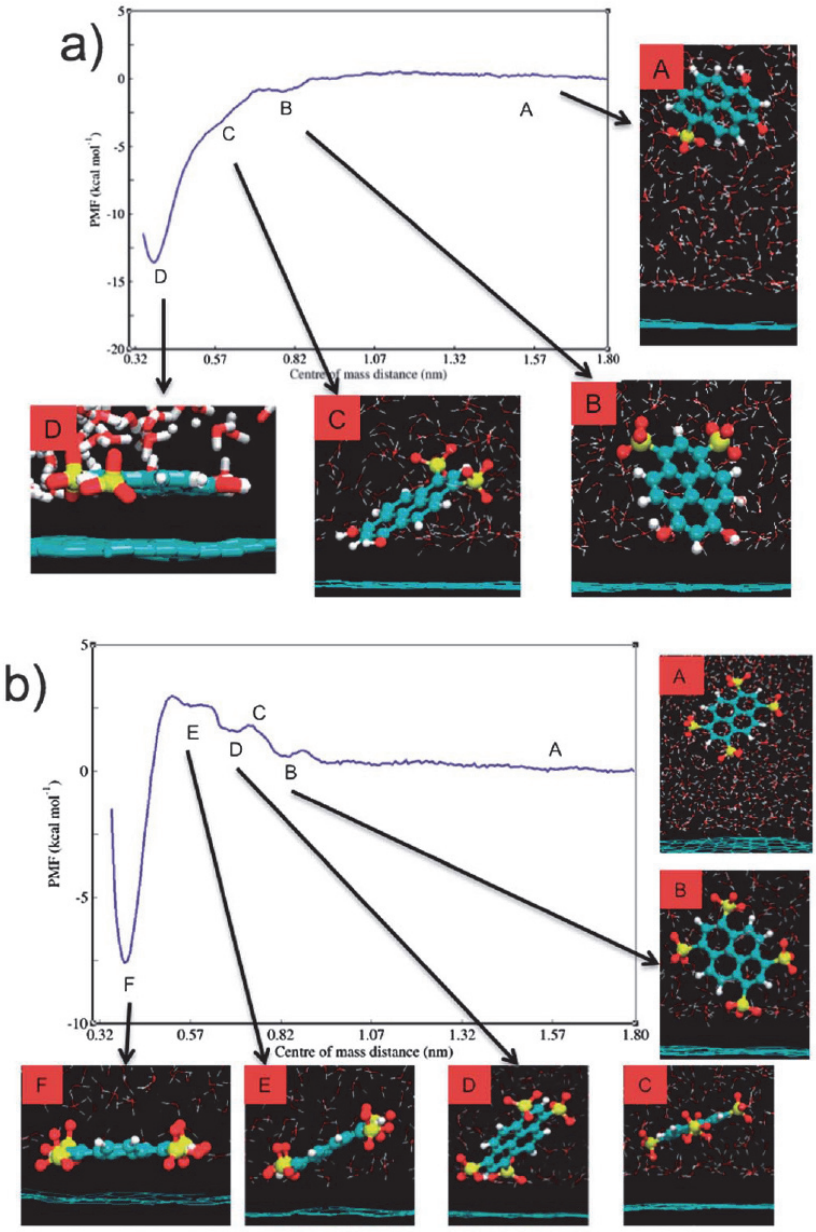

Fig. 8. PMF curve of a) PS2 and b) PS4 approaching a graphene surface. Snapshots of equilibrium structures at different distances are also shown corresponding to the points on the curve indicated by letters.

As the PS2 dye adsorbs onto the surface of graphene, distinct structural features can be observed. While at large distance (position A), the molecule–graphene orientation is not relevant, at closer

distance the molecule tilts, approaching the surface with the –SO3 side group pointing away from the graphene surface, as expected for an amphiphilic surfactant (B). However, once the molecule is at close distance from graphene (C), the molecule slides and orients parallel to the surface, regardless of the presence of the charged sulphonic groups (D), maximizing π-π interactions as already observed for similar molecules in vacuum.[8] In the case of PS4, the adsorption mechanism is even more complex, with the molecule approaching the surface first with one sulphonic group (position B), then two (position D), and finally arranging flatly on the surface.

In both PS3 and PS4, the structures corresponding to the local minima of the PMF curves represent the molecules at an edge-on (more or less perpendicular) interaction with the surface. Even at this configuration, the edges of the molecules are at the optimum interaction distance with graphene (0.34 nm). But as the molecules tilt to go to the fully adsorbed state they have to pass through energy barriers that appear at tilted configurations. It is important to mention that the presence of energy minima is underestimated by modelling just one molecule, as in the real system it is likely that the perpendicular configurations are further stabilized (namely, we would expect deeper local minima) by face-on van der Waals interaction with neighbouring molecules. Simulations show that the molecular asymmetry plays a central role in favouring the approach of the amphiphilic molecule toward graphene, displacing the water molecules present in between them (the presence of water molecules between the aromatic core of PS4 and the graphene surface is shown as an example in Fig. 8b and S4 with snapshots revealing the process as seen from below the graphene surface).

Due to the asymmetric approach observed in Fig. 8, the water molecules initially present between the aromatic core and graphene at this stage are pushed laterally and removed in the subsequent steps, thus allowing maximal interaction. This “sliding” mechanism is similar, on a smaller scale, to what was recently postulated in simulations of the stacking of large graphene sheets in water, where the removal of an intercalated water layer is the ultimate step of the stacking process. [31]

The adsorption free energies of the four molecules determined from MD simulations correspond to the lowest minima in Fig. 7, and amount for each dye to 12.8 kcal mol^{-1} (PS1), 14.6 kcal mol^{-1} (PS2), 11.8 kcal mol^{-1} (PS3), and 8.4 kcal mol^{-1} (PS4). The adsorption free energy is determined by the interplay of the solvation free energy and the interaction free energy with the graphene surface. With increasing number of hydrophilic sulphonic groups, the solvation free energy of the molecules increases (see Table S3), which in turn results in smaller (in magnitude) adsorption free energy.

4. Nanoscale insight into the exfoliation mechanism

The sulphonic groups do not only interact with the solvent, but also screen the hydrophobic pyrene core in aqueous solution. Yet, instead of a regular decrease in adsorption free energy with increasing number of sulphonic groups, the MD simulations yield the largest adsorption energy for PS2, followed by PS1, PS3 and PS4. To unravel the different factors influencing adsorption, the two-body interaction energies at the global minima on the PMF were analyzed further.

Fig. 9a displays the contributions to the interaction energy with the graphene substrate involving the aromatic core, the –SO3 and the –OH groups. The corresponding energy values together with the associated standard deviations are reported in Table S1. We find that the interaction energy of the pyrene core with graphene as well as the contribution from each –SO3 unit to the overall interaction energy is about the same in all the dyes. (Table S1 reports also the total graphene–SO3 interaction normalized by the number of –SO3 groups for each dye.) Instead, it is the interaction of the pyrene core with the solvent (Fig. 9b) that varies in a less linear way, correlating well with the observed experimental exfoliation efficiency. As the –OH groups are grafted on the pyrene core (in going from PS1 to PS2), its interaction with water is less favoured. Subsequently replacing the –OH by –SO3 moieties (in PS4) yields an increase in the interaction energy with water. The decomposition of this interaction energy into van der Waals and electrostatic interactions shows that the differences are mostly due to long-ranged electrostatic interactions that make PS4 too water-soluble to favour adsorption on graphene, while the pyrene moiety of PS2 shows the worst interaction with the solvent relative to the other dyes, making it more prone to stick to graphene sheets. The interaction of the functional groups (–SO3 and –OH) with the solvent is overwhelmingly high, as detailed in Tables S2 and S3, suggesting that a major obstacle to the adsorption is due to solvent restructuring, in agreement with the PMF results.

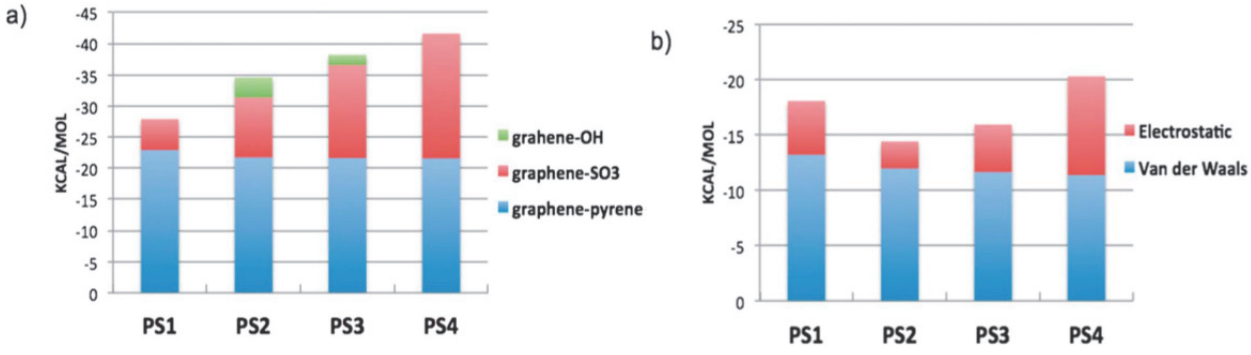

Fig. 9. Contribution of the different components of the PSx dyes to the interaction energy of the molecules with graphene. (b) Electrostatic and van der Waals contributions of the pyrene core of adsorbed PSx molecules with the surrounding aqueous medium.

4.2.6. pH response: influence of molecular charges on graphene stability in suspensions

As aforementioned, the dipole of PS2 and PS3 dyes changes significantly with pH, influencing the optical and chemical properties of the dye. It is reasonable to assume that the large pH response will influence the exfoliation efficiency as well. We explored the effect of eventual charges present in correspondence of –OH groups by sonicating graphite with the respective dyes at different pH.
A systematic effect of pH could be observed on the total amount of suspended graphene. The pH effect on the absorption of dyes is portrayed in Fig. 10a.
We used absorption spectroscopy to monitor

(i) the amount of graphene material suspended at 650 nm (Fig. 10b) and
(ii) changes in pyrene protonation and charging at wavelengths between 200 and 500 nm

For comparison, Fig. S1 shows the pH dependent UV spectra of pristine dye solutions.
A significant change in the amount of dissolved material was observed by varying the pH: the exfoliation efficiency is highest at neutral pH and decreases in strongly basic or acidic conditions (Fig. 10b). Acidic conditions induce a significantly more pronounced destabilization effect than basic conditions, for all four derivatives.

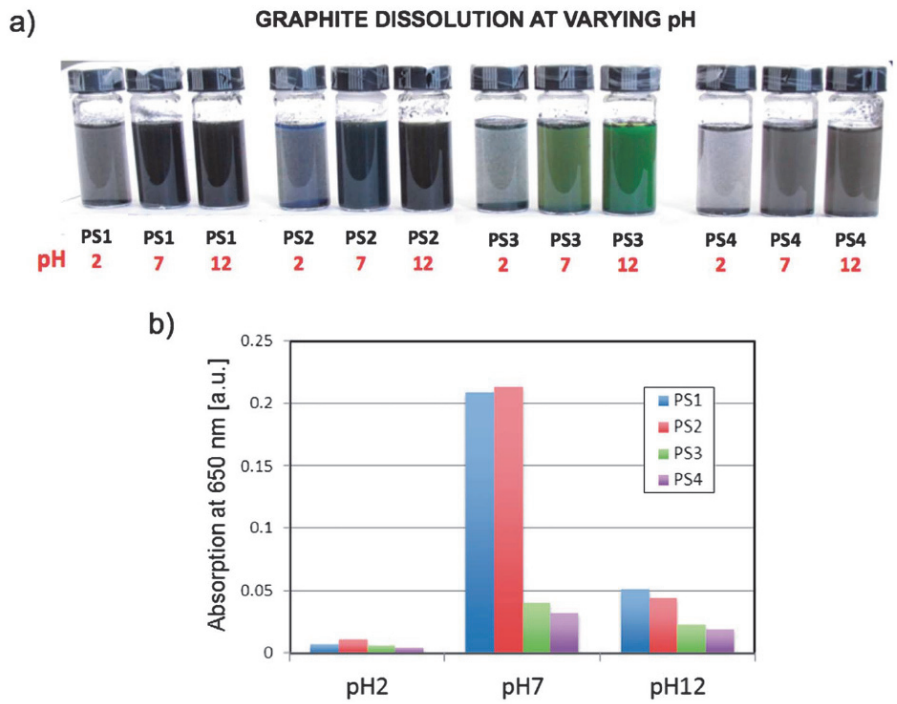

Fig. 10. a) Image of the solutions obtained on sonicating graphite with the different dyes at pH 2, 7 and 10. pH was adjusted to pH 2 and pH 12 by adding HCl and NaOH. Initial dye concentration 3 $*10^{-4}$ mol L^{-1}, sonicated for 4 hours. b) Absorbance at 650 nm for all the solutions at different pH; (solutions diluted 1 : 20 for measurement).

Interestingly, this trend is also observed for pyrenes exposing only $–SO_3$ moieties in the periphery such as PS1 and PS4, in which neither dye conformation nor light absorption is sensitive to pH. Given that the addition of salt induces precipitation as well (as shown as an example by adding Na_2SO_4 to PS3, blue curve in Fig. 11), these results indicate an overall effect of ionic strength inducing destabilization, similarly to previous observations on reduced graphene oxide and graphene sheets stabilized by surfactants containing carbonyl groups.[47] As expected for the pH indicators PS2 and PS3, the absorption band changes, because acidic conditions give rise to a blue shifted absorption band for the deprotonated species. [32]

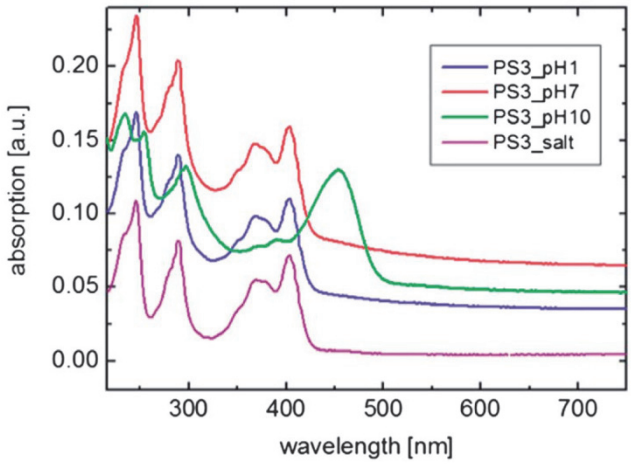

Fig. 11. Typical changes in the visible light absorption spectra for exfoliation at different pH values, in this case for PS3 dye at c=7*10_5 mol L_1, and for addition of salt (solutions diluted 1 : 20 for measurement).

Although the change in the protonation state can be clearly observed in the presence of graphene, the protonation state is found to be not relevant for the ability of molecules to stabilize graphene sheets in suspension: the same trend in pH dependent suspension efficiency is observed for all the common pyrene sulphonic acid derivatives with and without hydroxyl functionalization, with the highest efficiency in neutral, decreased graphene concentration in basic and heavy precipitation in acidic conditions (Fig. 10 and 11).

4.3. Discussion

The screening effect of molecules on graphene–graphene stacking interactions has been previously studied at the molecular scale, showing that the main factor hindering aggregation is the presence of a layer of molecules adsorbed on the graphene sheets; atomic scale modelling has been used to reproduce the stabilizing effect of solvents and surfactants on graphene sheets. [33] Empirical, mean field approaches have been developed to correlate exfoliation efficiency to solubility parameters quantifying the dispersive, polar, and hydrogen bonding properties of the solvent, or more simply to the surface tension or the refractive index of solvents (for an extensive review, see ref. 50). In case of graphite exfoliation into solutions of aliphatic or aromatic surfactants, complex processes may take place, which involve the formation of charged graphene–molecule complexes, and even charge or energy transfer between the molecules and graphene. [34,35]

4. Nanoscale insight into the exfoliation mechanism

The results obtained here show that the true picture is more complex than those reported in previous works, with a relevant interaction of both the aromatic and polar moieties with the graphene surface. UV/VIS absorption data reveal that PS2 yielded the highest amount of exfoliated material in suspension, before and after purification, with PS2 being the derivative with the largest adsorption energy on graphene and the highest molecular dipole in water, as demonstrated by MD simulations. For effective interaction, the aromatic cores of pyrene and graphene have to overcome the steric repulsions originating from a confined single layer of solvent, similarly to what was observed for the re-aggregation process of large, parallel graphene sheets. [33]

The molecular dipole of PS2 is thus not important per se; instead, an asymmetry in polarity can facilitate the "sliding" of the molecule into the solvent layer, and the lateral displacement of the water molecules confined between the aromatic core and the graphene surface, removing the energy barrier to be overcome for dye adsorption. A similar mechanism takes place for the mono-substituted derivative PS1, where, however, the lower polarity of the molecule decreases the graphene solubilization effect. With PS3 and PS4, the presence of polar groups on both sides of the pyrene moiety hinders the release of the confined water, thus hindering the molecular approach to graphene. As highly functionalized PS3 and PS4 derivatives are expected to exhibit stronger solvent interaction, the solvent layer may also be strongly localized, rendering non-covalent functionalization of graphene less favourable. The combination of molecular polarity, molecular dipole and adsorption mechanism thus reveals PS2 being the most effective molecule for graphene solubilization among the four dyes studied. Noteworthy, a different ranking was observed for "dye capture" and exfoliation experiments, suggesting that the adsorption on bulk graphite is governed to a less extent by the interaction between the dye and graphene than the exfoliation process. The adsorption on graphite surfaces is simply inversely proportional to the number of sulphonic groups present on the pyrene core and thus to molecule solvation energy. Instead, exfoliation relies more on an efficient interaction of the dye with the graphene surface.

The exfoliation efficiency changes significantly with pH, yielding lower graphene concentrations in acidic and basic conditions. The pH dependent exfoliation efficiency is not related to the protonation or deprotonation of the pH sensitive molecules, as could be expected. All suspensions, even the ones based on molecules without pH sensitive hydroxyl groups, show a loss in stability in both high and low pH conditions. Destabilization was also observed in the presence of salts. A similar pH dependence is well documented with common aliphatic surfactants such as

SDBS. The suspended graphene–pyrene composite studied here, once exfoliated, can be considered in a good approximation as suspensions stabilized by electrostatic repulsion, comparable to micelle stabilized particles, even if the mechanism of colloidal stabilization is not based on micelle formation, but on the interaction of the aromatic molecule with the graphene lattice. Even if the functionalization of the pyrene core plays a major role in the graphene yield obtained with the respective molecule, an additional effect of protonation state with the pH sensitive derivatives PS2 and PS3 was not observed.

4.4. Conclusion

We compared four pyrene derivatives with varying number of polar functionalization for their efficiency as exfoliation agents in the preparation of stable, aqueous graphene suspensions with liquid phase exfoliation. We found that the four studied derivatives exfoliate graphite, yielding stable suspensions in water. A relevant fraction of monolayer graphene was obtained in all samples, but AFM and TEM show that a layer of molecules covers the sheets. The total concentration of suspended graphene depends significantly on the polar functionalization present on the pyrene core.

The concentration of graphene exfoliated and dissolved from bulk graphite to suspension is highest for the PS2 derivative, the latter having the largest dipole and most asymmetric functionalization. The adsorption of the molecules from solution to bulk graphite is simply inversely proportional to the number of highly polar sulphonic groups present. Molecular dynamic calculation revealed that a critical factor in the interaction of pyrene derivatives with graphene involves a thin solvent layer confined between the dye and the graphene surface; the amphiphilic molecule changes its orientation when approaching the surface to slide into this layer, and the asymmetric shape of PS2 molecule facilitates this step. Simulations indicate that the molecular dipole is thus not important per se, but because it facilitates the “sliding” of the molecule into the solvent layer, and therefore the lateral displacement of the water molecules collocated between the aromatic cores of the dye and the graphene substrate.

Once the molecules are adsorbed on graphene, these graphene – organic hybrids yield stable suspensions in water. The stability of the suspensions is highly pH responsive for all four derivatives, and the solubility trend observed with varying pH is the same for the different

functionalization of the pyrene core: in these graphene organic hybrid systems, colloidal stabilization is achieved through electrostatic repulsion between charges introduced by the surfactant and can be overcome by changing pH or adding salts. The prepared graphene can be considered in a good approximation as suspensions stabilized by electrostatic repulsion.

4.5. Experimental Details

Experimental part. Pyrene derivatives and graphite powder were obtained from Aldrich, and dissolved in ultrapure water using high power sonication in a water bath (Hielscher UP 50H). Pyrene concentration was $3.3*10^{-4}$ mol/L in all cases. Different previous works show the advantages of long sonication time (until 400 h) for exfoliation of graphene in water[53] or in other solvents.[54] The highest concentration of dispersed graphene can be achieved by increasing the sonication time, and this can facilitate the comparison of different derivatives especially for molecules with different kinetics of exfoliation. The suspensions of four derivatives were processed in the same way at the same time to reduce the variables related to the method like temperature, time, power etc. Absorption spectra were recorded using a Perkin-Elmer Lambda 20 spectrometer.

AFM measurements were carried out using a Digital Instruments AFM (NT-MDT), using Nanoprobe cantilevers (model: RTESP, material: 1–10 Ohm cm phosphorus (n) doped Si, f0: 27–309 kHz, k: 20–80 N m_{-1}; from Veeco) operating in tapping mode. The Scanning Electron Microscopy (SEM) images were obtained with a ZEISS 1530 instrument. Transmission Electron Microscopy (TEM) observations were carried out with a Fei Tecnai F20 TEM equipped with a Schottky emitter and operating at 80 keV. Raman measurements were performed using a Witec alpha300 Raman spectrometer, equipped with 488, 514.5 and 633 nm excitation lines and a piezoelectric stage for Raman mapping.

Author contributions.

Raman data were provided by School of Chemistry and Photon Science Institute, Manchester University, UK. TEM analysis was performed at IMM – National Research Council, Bologna, Italy. Simulation data were provided by the Laboratory for Chemistry of Novel Materials, University of Mons, Mons, Belgium. Details on simulations, with the data presented here, are available in Schlierf et al., Nanoscale, 2013,5, 4205-4216.

3.5 Supporting information

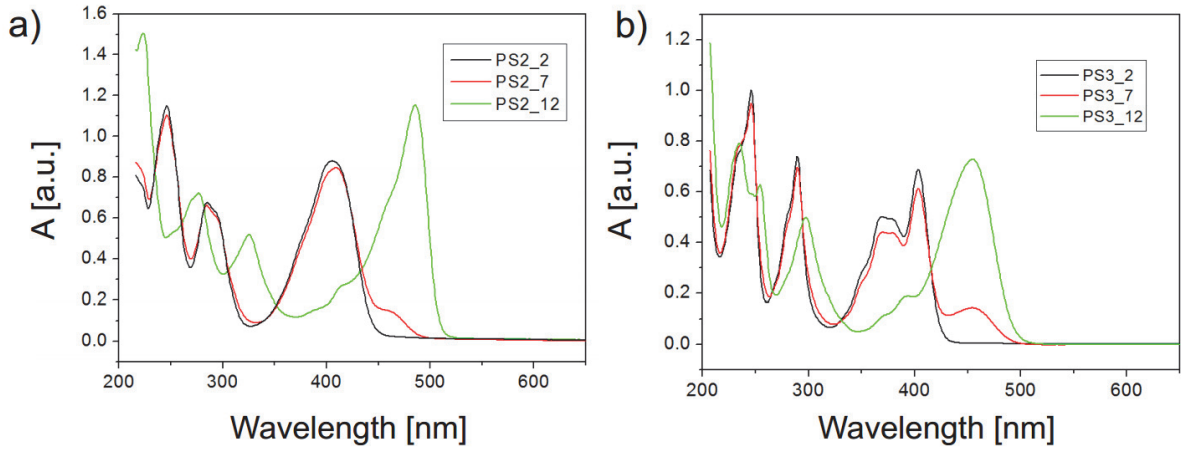

Fig. S1 Absorption spectra of a) PS2, and b) PS3 dyes at different pH.

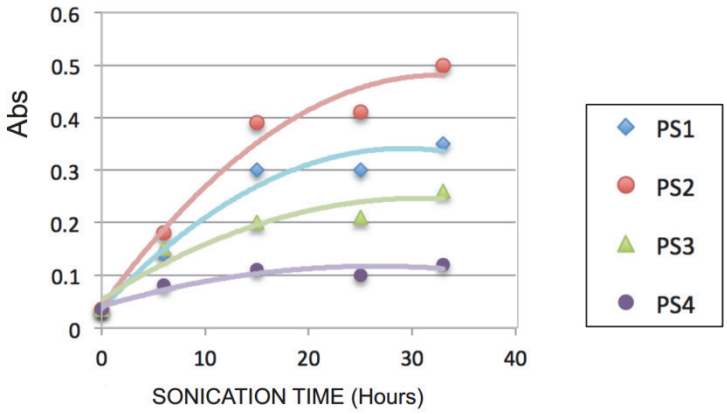

Fig. S2 Estimation of dissolved material by measuring optical absorption of the different solutions at 650 nm for different sonication times. The lines are a reference for the eye.

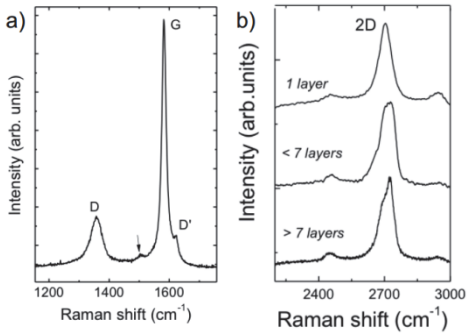

c)

Molecule	% single layers	% thin sheets (2-7 layers)	% thick sheets (>7 layers)	Total
PS1	18	68	14	100
PS2	15	55	31	100
PS3	22	65	13	100
PS4	9	55	36	100

Fig. S3 Raman analysis of graphene-pyrene composites, obtained by spin coating the sonicated solutions on silicon. a) typical first order peaks, the peak at 1505 cm-1 (black arrow) is related to the molecules residual. b) Typical shapes of 2D peaks obtained for monolayers, thin sheets, less than 7 layers and thick flakes. c) Raman statistical analysis of sheet thickness. Suspensions drop cast on SiO2, statistic on 60 to 70 flakes for each dye.

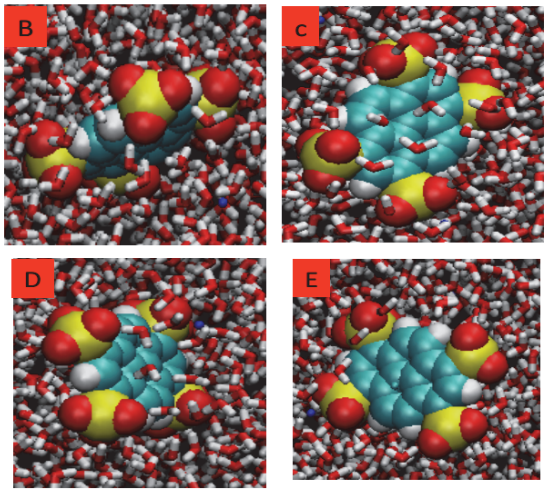

Fig. S4 Snapshots PS4 molecules at different distances from graphene, as seen from below the graphene layer. The letters correspond to selected points in the PMF curve shown in Fig. 8 in main text.

	graph-pyrene	graph-SO_3	graph-OH	Total	graph-SO_3 normalized	graph-OH normalized
PS1	-22.93 ± 0.09	-4.94 ± 0.04	-	-27.87	-4.94	-
PS2	-21.75 ± 0.06	-9.63 ± 0.06	-3.22 ± 0.02	-34.60	-4.82	-1.61
PS3	-21.63 ± 0.09	-14.91 ± 0.19	-1.63 ± 0.05	-38.19	-4.97	-1.64
PS4	-21.59 ± 0.05	-19.99 ± 0.08	-	-41.59	-4.99	-

* The term "normalized" refers to the interaction energy between graphene and all the functional groups of a given type (graph-pyrene, graph-SO3, or graph-OH) divided by the number of the functional groups of that type within the molecule.
* "Total" refers to the interaction energy between graphene and the whole molecule.

Table S1. The interaction energies (kcal/mol) of the component functional groups (pyrene core, SO3, OH) of adsorbed PSx molecules with graphene.

	solv-pyrene			solv-SO_3	solv-OH	Total	solv-SO3 normalized	solv-OH normalized
	Van der Waals	Electrostatic	Total					
PS1	-13.22 ± 0.02	-4.83 ± 0.03	-18.05	-69.01 ± 0.36	-	-87.06	-69.01	-
PS2	-11.98 ± 0.05	-2.40 ± 0.17	-14.38	-138.82 ± 0.71	-21.75 ± 0.31	-174.95	-69.41	-10.87
PS3	-11.65 ± 0.04	-4.25 ± 0.11	-15.90	-205.29 ± 3.7	-11.46 ± 0.24	-232.66	-68.43	-11.46
PS4	-11.37 ± 0.03	-8.91 ± 0.20	-20.28	-259.07 ± 7.61	-	-279.35	-64.77	-

* The term “normalized” refers to the interaction energy between the aqueous medium and all the functional groups of a given type (solv-pyrene, solv-SO3, or solv-OH) divided by the number of the functional groups of that type within the molecule.
* “Total” refers to the interaction energy between the aqueous medium and the whole molecule.

Table S2. The interaction energies (kcal/mol) of the component functional groups (pyrene core, SO3, OH) of adsorbed PSx molecules with surrounding aqueous medium.

	Hydration energy (kcal/mol)
PS1	-91.96
PS2	-299.77
PS3	-379.24
PS4	-574.26

Table S3. Hydration free energy of PSx ions.

References

(1) Hernandez, Y.; Nicolosi, V.; Lotya, M.; Blighe, F. M.; Sun, Z. Y.; De, S.; McGovern, I. T.; Holland, B.; Byrne, M.; Gun'ko, Y. K.; Boland, J. J.; Niraj, P.; Duesberg, G.; Krishnamurthy, S.; Goodhue, R.; Hutchison, J.; Scardaci, V.; Ferrari, A. C.; Coleman, J. N. *Nature Nanotechnology* 2008, *3*, 563.

(2) Lotya, M.; Hernandez, Y.; King, P. J.; Smith, R. J.; Nicolosi, V.; Karlsson, L. S.; Blighe, F. M.; De, S.; Wang, Z.; McGovern, I. T.; Duesberg, G. S.; Coleman, J. N. *Journal of the American Chemical Society* 2009, *131*, 3611.

(3) Guardia, L.; Fernandez-Merino, M. J.; Paredes, J. I.; Solis-Fernandez, P.; Villar-Rodil, S.; Martinez-Alonso, A.; Tascon, J. M. D. *Carbon* 2011, *49*, 1653.

(4) Seo, J. W. T.; Green, A. A.; Antaris, A. L.; Hersam, M. C. *Journal of Physical Chemistry Letters* 2011, *2*, 1004.

(5) Behabtu, N.; Lomeda, J. R.; Green, M. J.; Higginbotham, A. L.; Sinitskii, A.; Kosynkin, D. V.; Tsentalovich, D.; Parra-Vasquez, A. N. G.; Schmidt, J.; Kesselman, E.; Cohen, Y.; Talmon, Y.; Tour, J. M.; Pasquali, M. *Nature Nanotechnology* 2010, *5*, 406.

(6) Valles, C.; Drummond, C.; Saadaoui, H.; Furtado, C. A.; He, M.; Roubeau, O.; Ortolani, L.; Monthioux, M.; Penicaud, A. *Journal of the American Chemical Society* 2008, *130*, 15802.

(7) Wang, Q. H.; Hersam, M. C. *Nature Chemistry* 2009, *1*, 206.

(8) Sirringhaus, H.; Brown, P. J.; Friend, R. H.; Nielsen, M. M.; Bechgaard, K.; Langeveld-Voss, B. M. W.; Spiering, A. J. H.; Janssen, R. A. J.; Meijer, E. W.; Herwig, P.; de Leeuw, D. M. *Nature* 1999, *401*, 685.

(9) Schmidt-Mende, L.; Fechtenkotter, A.; Mullen, K.; Moons, E.; Friend, R. H.; MacKenzie, J. D. *Science* 2001, *293*, 1119.

(10) Nelson, J. *Curr. Op. Sol. St. Mat. Sci.* 2002, *6*, 87.

(11) Kim, J. Y.; Lee, K.; Coates, N. E.; Moses, D.; Nguyen, T. Q.; Dante, M.; Heeger, A. J. *Science* 2007, *317*, 222.

(12) Jones, B. A.; Ahrens, M. J.; Yoon, M.-H.; Facchetti, A.; Marks, T. J.; Wasielewski, M. R. *Angewandte Chemie International Edition* 2004, *43*, 6363.

(13) Arias, A. C.; MacKenzie, J. D.; McCulloch, I.; Rivnay, J.; Salleo, A. *Chem Rev* 2010, *110*, 3.

(14) Hamilton, C. E.; Lomeda, J. R.; Sun, Z.; Tour, J. M.; Barron, A. R. *Nano Letters* 2009, *9*, 3460.

(15) Schmidt, R.; Ling, M. M.; Oh, J. H.; Winkler, M.; Könemann, M.; Bao, Z.; Würthner, F. *Advanced Materials* 2007, *19*, 3692.

(16) Jang, J. H.; Rangappa, D.; Kwon, Y. U.; Honma, I. *Journal of Materials Chemistry* 2011, *21*, 3462.

(17) Dong, X. C.; Fu, D. L.; Fang, W. J.; Shi, Y. M.; Chen, P.; Li, L. J. *Small* 2009, *5*, 1422.

(18) Zhang, M.; Parajuli, R. R.; Mastrogiovanni, D.; Dai, B.; Lo, P.; Cheung, W.; Brukh, R.; Chiu, P. L.; Zhou, T.; Liu, Z.; Garfunkel, E.; He, H. *Small* 2010, *6*, 1100.

(19) An, X. H.; Simmons, T. J.; Shah, R.; Wolfe, C.; Lewis, K. M.; Washington, M.; Nayak, S. K.; Talapatra, S.; Kar, S. *Nano Letters* 2010, *10*, 4295.
(20) Xu, Y. X.; Bai, H.; Lu, G. W.; Li, C.; Shi, G. Q. *J. Am. Chem. Soc.* 2008, *130*, 5856.
(21) Parviz, D.; Das, S.; Ahmed, H. S. T.; Irin, F.; Bhattacharia, S.; Green, M. J. *Acs Nano* 2012, *6*, 8857.
(22) Palermo, V.; Samori, P. *Angewandte Chemie-International Edition* 2007, *46*, 4428.
(23) Yang, H.; Hernandez, Y.; Schlierf, A.; Felten, A.; Eckmann, A.; Johal, S.; Louette, P.; Pireaux, J. J.; Feng, X.; Mullen, K.; Palermo, V.; Casiraghi, C. *Carbon* 2013, *53*, 357.
(24) Hakonen, A.; Hulth, S. *Talanta* 2010, *80*, 1964.
(25) Saswata, B.; Tapas, K.; Ananta Kumar, M.; Nam Hoon, K.; Joong Hee, L. *Nanotechnology* 2011, *22*, 405603.
(26) Ottonelli, M.; Piccardo, M.; Duce, D.; Thea, S.; Dellepiane, G. *Journal of Physical Chemistry A* 2012, *116*, 611.
(27) Pan, X. Y.; Li, H.; Nguyen, K. T.; Gruner, G.; Zhao, Y. L. *Journal of Physical Chemistry C* 2012, *116*, 4175.
(28) Detriche, S.; Devillers, S.; Seffer, J. F.; Nagy, J. B.; Mekhalif, Z.; Delhalle, J. *Carbon* 2011, *49*, 2935.
(29) He, Q. Y.; Sudibya, H. G.; Yin, Z. Y.; Wu, S. X.; Li, H.; Boey, F.; Huang, W.; Chen, P.; Zhang, H. *ACS Nano* 2010, *4*, 3201.
(30) Colle, R.; Grosso, G.; Ronzani, A.; Gazzano, M.; Palermo, V. *Carbon* 2012, *50*, 1332.
(31) Smith, R. J.; Lotya, M.; Coleman, J. N. *New J. Phys.* 2010, *12*.
(32) Velasquez, G.; Ureta-Zanartu, M. S.; Lopez-Alarcon, C.; Aspee, A. *Journal of Physical Chemistry B* 2011, *115*, 6661.
(33) Shih, C. J.; Lin, S. C.; Strano, M. S.; Blankschtein, D. *Journal of the American Chemical Society* 2010, *132*, 14638.
(34) Kozhemyakina, N. V.; Englert, J. M.; Yang, G. A.; Spiecker, E.; Schmidt, C. D.; Hauke, F.; Hirsch, A. *Advanced Materials* 2010, *22*, 5483.
(35) Swathi, R. S.; Sebastian, K. L. *J. Chem. Phys.* 2008, *129*, 054703.

Chapter 5

Water soluble perylene diimide derivatives for graphene exfoliation in polar solvents and fundamental graphene-dye interactions

5. Water soluble perylene diimide derivatives for graphene exfoliation

5.1. Introduction

Small poly-aromatic dyes and pigments such as pyrene and anthracene derivatives functionalized with charged moieties were found being effective in exfoliating and stabilizing graphene sheets in suspension, similar effects have been observed with perylene based chromophores. [1-4] While graphene is a very recent and emerging topic in organic electronic research, the chemistry and photo-physical properties of perylene-diimide derivatives have been extensively studied for their potential as dye or pigment in polymer composite or even as colouring additive for food. PDI derivatives are particularly interesting for organic electronics due to their outstanding chemical and physical properties including high electron mobility and high molar absorption coefficients. They represent one of the most promising class of electron accepting materials, and their rigid fused aromatic core favours π–π intermolecular interactions.[5-8]

For the present study, based on the concepts we developed for pyrene assisted LPE, we have chosen polar functionalized perylene diimide cores as agents for graphene liquid phase exfoliation. The molecules are based on a perylene core featuring an extended π-system which can be expected to favour non-covalent functionalization of the graphene lattice through π-π interaction, and contain polar moieties similar to the amphiphilic structure of sulphonated pyrene derivatives discussed before. In addition, perylene diimide (PDI) is a valuable model compound in investigations on the interaction of polyaromatic molecular compounds with surfaces: In particular, vibrational spectra such as Raman spectroscopy provide indispensable information on graphene-organic chromophore hybrids. This chapter discusses Raman spectroscopy on in-situ exfoliated graphene organic hybrids and steady state optical spectroscopy on a dye-graphene system, obtaining information on graphene quality, graphene-perylene diimide interaction and the fingerprint of the dye itself.

5.2. Results

5.2.1. Dyes under study

We selected the commercial, water soluble perylene diimide derivatives TA1 (N',N'-bis(2-methy, 6-ethyl-sulphonic acid) perylene-3,4,9,10-tetracarboxylic diimide) and TA2 (N',N'-bis(2,6 dimethy) disulphonic perylene-3,4,9,10-tetracarboxylic diimide) for this study. These PDIs bearing sulphonic groups were chosen not only for PDI being an ideal model compound for probing chromophore-

surface interactions, but also for their demonstrated ideal properties in processing: The water soluble PDI derivatives TA1 and TA2 are commercial molecules that already find application on an industrial scale in ink formulation, paints and colouring additives for many consumer products. [9] Introducing polar sulphonic acid functionalization to the perylene-diimide core - in bay position for TA2 and with an aliphatic spacer for TA1 – can be expected to increase solubility of the molecule in polar protic solvents. Fig. 1a, b shows the structure of the molecules selected.

The bay functionalized derivative TA2 is well dissolved in water, ethanol and isopropanol at concentrations as high as 1mg/mL, whereas the derivative TA1 forms stable, pigment-like dispersions over a wide range of concentrations at room temperature. Such aqueous self-dispersion behaviour is commonly exploited industrially for formulation of surfactant-free aqueous pigment dispersions that find application in various fields, reaching from paints, coatings to application in food industries and cosmetics. [9] The self-dispersion behaviour of TA1 is observed with other polar-protic solvents such as EtOH and IPA. However, even both perylene diimide derivatives are commercial and commonly applied, no in depth study on TA1 and TA2 photophysical properties is available to our best knowledge.

5.2.2. Exfoliation in polar solvents

To study the effectiveness of TA1 and TA2 for dispersing graphene in polar solvents, we employed graphite liquid phase exfoliation in solutions of the respective dye with water, EtOH and isopropanol. The actual graphene suspensions were prepared by sonicating 3mg/mL graphite flakes in 0.1mg/mL solutions of each of the perylene diimides for 4.5hrs, and using as well blank solvent for comparison. After sonication, the suspensions were centrifuged at 1500 rpm for 20 minutes to remove large unexfoliated graphite particles. The same procedure was employed for all three solvents, and no further processing was applied at this stage to maintain comparability.

5. Water soluble perylene diimide derivatives for graphene exfoliation

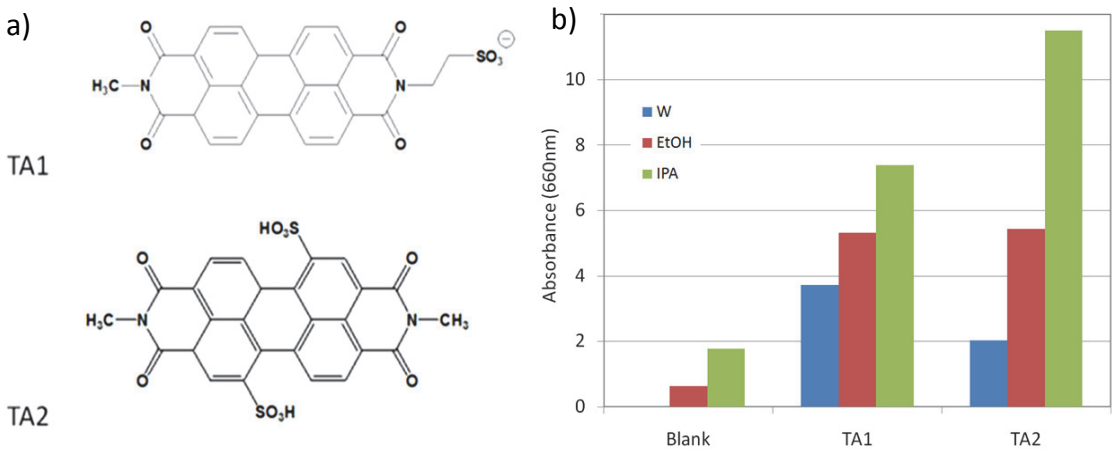

Fig. 1. a) Structures of perylene diimide chromophores; b) Yield in suspended graphene, exfoliation in respective solvents for blank solvent, TA1 or TA2 solutions respectively.

The post-centrifugtion concentration in dispersed material is an important indicator for the effectiveness of a surfactant and this concentration is in direct correlation with the extinction at a selected wavelength. We have chosen to compare the absorption values at 660nm (α(660nm) =2460 L/(g*m) as suggested in Ref. [10]) and correct for the contribution of blank dye to avoid any artifact originating at 660 nm from strong dye absorption bands or scattering on dispersed pigments. In literature, the correlation value α is applied to estimate graphene concentrations in various solvent systems, see for example Ref. [4,10], therefore we assume α(660nm) =2460 L/(g*m) being valid and unchanged for graphene in water, EtOH and isopropanol. The mass concentrations of graphene obtained in the different solvents or dye solutions is reported in Tab. 1. As expected for surfactant-free exfoliation in polar solvents (similar exeriments are reported in Ref. [11]), isopropanol yields 0.07 mg/mL of graphene stabilized in suspension, while the efficiency of EtOH is as low as 0.03 mg/mL and water does not yield any suspended material. In presence of both PDI derivatives TA1 and TA2, the same trend in graphene concentration is observed as in the blank solvent exfoliation experiment, with a significant increase in graphene concentration when the respective dye was employed as exfoliation agent. In isopropanol, the yield in exfoliation increased for a factor of 4 for TA1 (reaching 0.32mg/mL) in respect to exfoliation in blank solvent, and a factor of 7 with TA2 yielding 0.5mg/mL of suspended matter.

c(Graphene) [mg/mL]	blank	TA1	TA2
Water	0.00	0.16	0.09
EtOH	0.03	0.23	0.24
IPA	0.07	0.32	0.50

Fig. 2. Graphene yield in mg/mL obtained with liquid phase exfoliation in water, EtOH and IPA, blank solvent, TA1 or TA2 solution respectively. Concentrations measured spectroscopically, mass concentrations calculated from UV/VIS absorption using α(660nm) =2460 L/(g*m) [10].

Visible absorption specta of TA2-graphene suspensions exhibit a convolution of the typical, slowly decaying graphene background and bands that are attributed to dye (Fig. (left)). Comparing with the maximum absorption wavelengths of the free dye in solution (486nm for water, 499nm for EtOH and 495nm for isopropanol) with the spectra of TA2-graphene suspensions, new bands with lower energy transitions appear with TA2-graphene hybrid suspension for the same solvent (the maxima of free dye are indicated left, the normalized spectra of free dye are shown on the right for better comparison). In water, the effect is less pronounced, while a new, broadened absorption band appears at 570nm in ethanol or isopropanol.

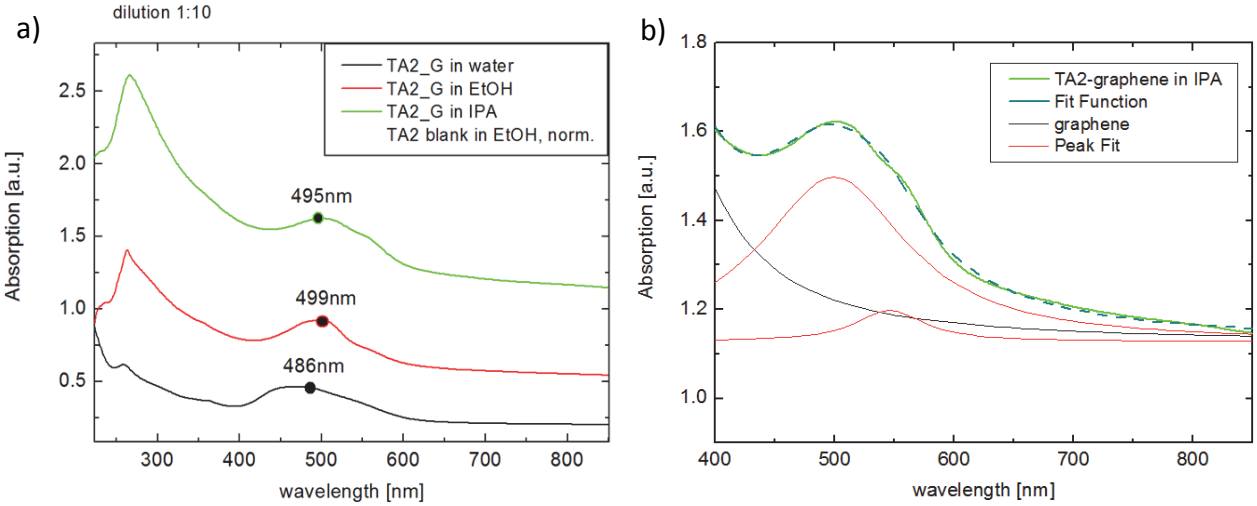

Fig. 3. a) UV/Vis absorption spectra of graphene-TA2 hybrid suspensions in water, EtOH and isopropanol, dilution 1:10. Interaction graphene-TA2 induces rise of an additional red shifted absorption band, numbers indicate peak position of blank dye solutions in respective solvent. b) Demonstration of peak fit for TA2_G in isopropanol with graphene contribution, original blank peak position and new re-shifted band.

For both PDI derivatives, no change in solvation behaviour is observed when changing from water to EtOH or isopropanol (TA1 forms dispersions while TA2 is dissolved), suggesting that dye solubility is less important to the exfoliation result than the solvent medium chosen. Still, the

trend of better stabilization with decreasing solvent polarity and the increase in concentration in presence of a PDI exfoliation agent suggests that both selection of solvent and exfoliation agent is critical for efficient small molecules assisted graphene exfoliation. A new, red shifted ground state absorption band appears with graphene, being a first indication for electronic interaction between graphene and TA2 in solution.

5.2.3. Flake morphology

The presence of few layer graphene has been unambiguously demonstrated with Raman spectroscopy. First, the quality of graphene flakes exfoliated with the perylene diimide TA2 is studied. The non-resonant experiment allows the study of characteristic graphene bands without the dye bands in the lower energetic range. With excitation at 633 nm, the absorption cross section of the dye in solid state is low and graphene vibrational bands are accessible. Graphene samples typically contain two main features (as already discussed in Chapter 2): the G peak, corresponding to the E2g phonon mode at the Brillouin zone center, at 1580 cm^{-1} and the 2D peak, which is activated by two-phonons intervalley assisted Raman scattering, at 2700 cm^{-1}. The 2D peak can be used to identify graphene layers [12]: the 2D peak is a single and sharp peak in the case of monolayer graphene, while in AB-stacked bilayer the 2D peak is composed by four bands. Multilayer graphene shows a broad and up-shifted 2D peak, which in first approximation can be fitted with two peaks. The 2D peak shape quickly evolves with the number of layers, so that the 2D band of a sample containing more than 8–10 layers is hardly distinguishable from that of bulk graphite (see Fig. 4 reprint from Ref [12] and previous chapters).

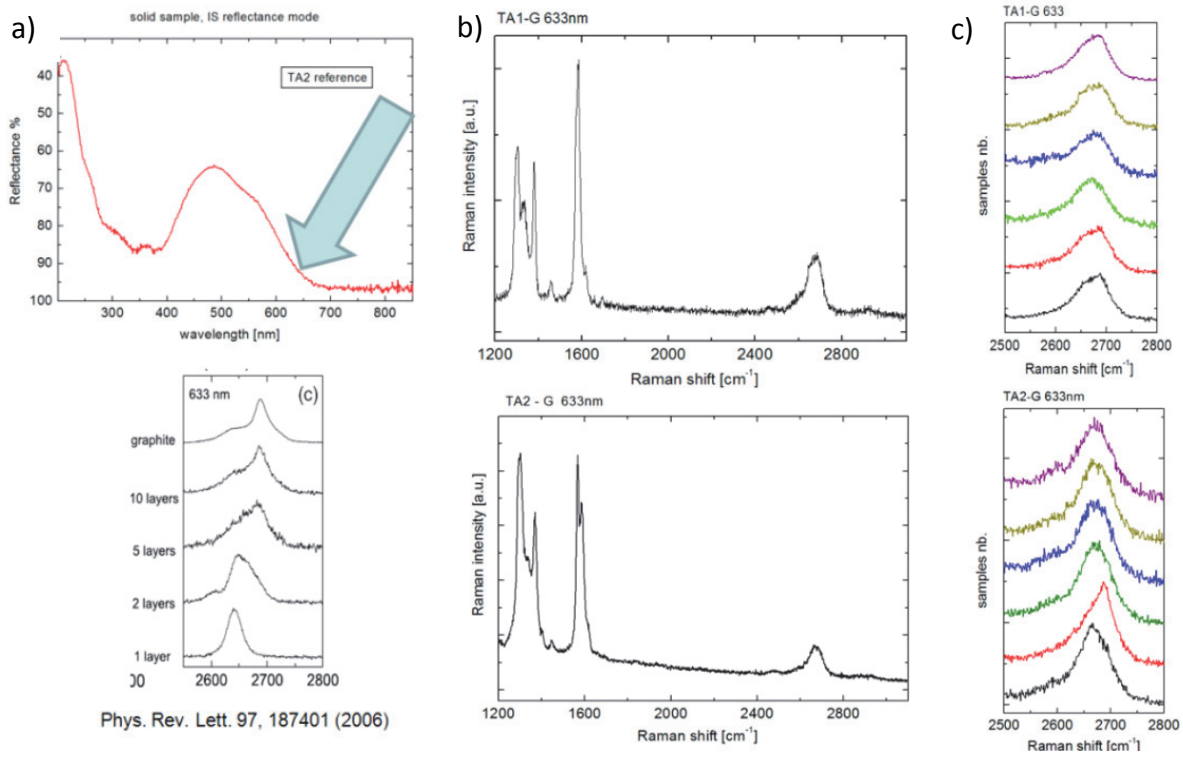

Fig. 4. a) Representative solid state reflectance spectrum of perylene diimide dye deposited by dropcasting on quartz glass, here TA2. b) Typical high resolution Raman spectra of graphene flakes (spectra of 6 different flakes for each dye are reported here), dropcast from graphene-TA1 (top) or graphene-TA2 (bottom) suspensions exfoliated in EtOH. Excitation wavelength is 633nm, the excitation power 300µW. c) Zoom on 2D region (2500cm^-1 to 2800cm^-1) of 6 different graphene flakes exfoliated in TA1 (top) and TA2 (bottom).

With Raman analysis, we found mainly few layer graphene: The analysis of the 2D peak, reported in Fig. 4, reveals the presence of graphene, with a flake composition of mainly few layer graphene, but also the presence of thinner material. However, it should be mentioned that rotationally stacked few-layers graphene layers can result electronically decoupled and behave as a collection of monolayers, both for what concerns the electronic properties and the Raman spectrum.

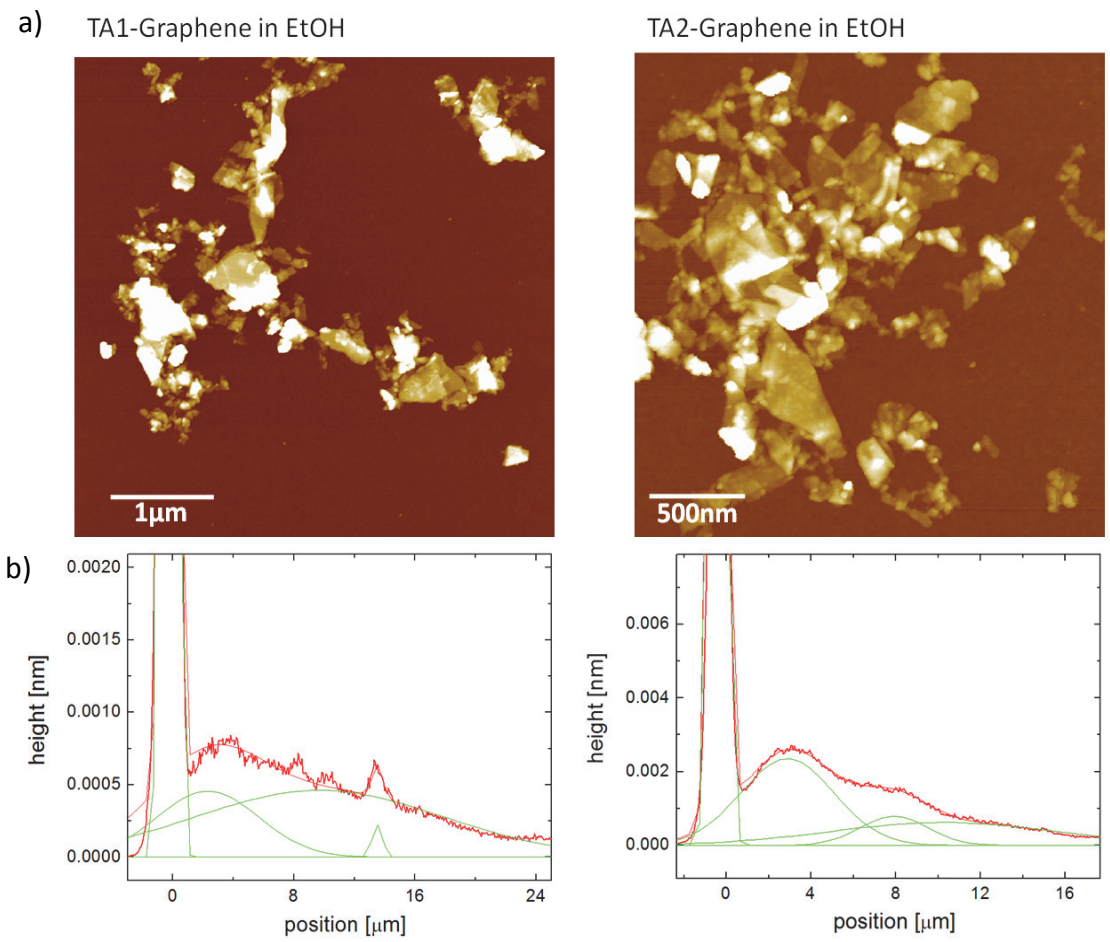

Fig. 5. a) AFM topography analysis (z=30nm) on drop-cast suspensions reveals that well defined flakes with lateral dimensions up to 1micron were obtained. b) Height histograms indicating an ensemble of flakes with varying thicknesses; the height distribution (red line) is roughly approximated with fitting 4 Gaussian peaks, representing 3 predominant flake thicknesses and the background peak (green lines).

The presence of few layer graphene is in agreement with AFM results shown in Fig. 5, revealing that well defined flakes with lateral dimensions up to 1 micron were obtained. Histogram analysis shows that the flakes are of varying thickness and mainly few layer graphene platelets as typically obtained from graphite flakes with sonication based liquid phase exfoliation. Thicker, few layer platelets of 8.3nm +/-0.1 nm up to 13.7 nm +/- 0.1 nm are present in with both dyes, and the minimum flake thickness was 2.6 nm +/- 0.4 nm for TA1, 3.25 nm +/- 0.1 nm for TA2 exfoliated graphene. The flakes contain a surface modification which can be attributed to a thicker coating with the dye used for exfoliation. This observation confirms the previous studies on graphene liquid phase exfoliation in polar solvents when sulphonated chromophores such as pyrene sulphonic acid sodium salt were used as exfoliation agents, such as exfoliation with pyrenes sulphonic acid sodium salt discussed in chapter 3 and 4.

5.2.4. Emission quenching in mixtures of graphene and dye

Former studies on $\pi-\pi$ interaction, e.g. of dyes with carbon nanotubes (CNTs), report the formation of a ground state association complex (observable in a UV band shift) [13-16]. With direct exfoliation of graphene in TA2 solutions, a new red-shifted band appears, giving a first indication for electronic communication through the formation of a ground state complex between graphene and the dye. As a proof of principle and to shine light on the effect observed in direct exfoliation, further studies on mixtures of graphene exfoliated in isopropanol and TA2 solutions where performed. First, an inverse titration experiment was done, in which the chromophore (TA2) concentration was increased while keeping the quencher (graphene) concentration constant. With this setup, we aim to observe emission quenching while ruling artefacts resulting from graphene scattering out. Then, we performed time resolved emission measurements on graphene/TA2 mixtures.

Experimental restrictions prevented from working directly on in situ exfoliated graphene-dye hybrids in suspension: In order to maintain linearity of the instrumental response, absorption and emission measurements had to be performed on a system that differs from in situ exfoliated graphene-hybrids in terms of concentration. Both graphene and dye were diluted for the following photo-spectrometric experiment.

Dye titration into constant graphene concentration. A linear setup in transmission mode was chosen for absorption measurements. The dye TA2 was titrated stepwise into a blank sample R of pure isopropanol and a graphene sample G (graphene exfoliated in isopropanol, concentration 0.2 mg/mL, see Fig. 6); this approach was chosen in order to keep the scattering/reabsorption background resulting from suspended graphene constant while changing the dye to graphene ratios. The low concentrations in dye (c= 3*10^-8 mol/L to 3.6*10^-7 mol/L) was selected to keep dye absorbance in the linear range for all concentrations.

In contrast to our findings with direct exfoliation of graphene in TA2 solutions discussed before, no peak shift appears in absorption nor emission bands when exposed to graphene. For excitation, 263nm was selected to circumvent artefacts resulting from reabsorption, a consequence of TA2's very small Stokes shift. Other than could be expected for a ground state association, no isosbestic point appeared with titration. The unchanged band structure in the steady state spectra indicates

that titration - in contrary to direct exfoliation - results in a less favourable, weak interaction between graphene and TA2 in isopropanol.

a)

	0	1	2	3	4	5	6	7	8
Conc (TA2)	0	3.3 *10^-8	6.4*10^-8	9.5 *10^-8	1.3 *10^-7	1.5 *10^-7	1.8*10^-7	2.1 *10^-7	3.6 *10^-7

b)

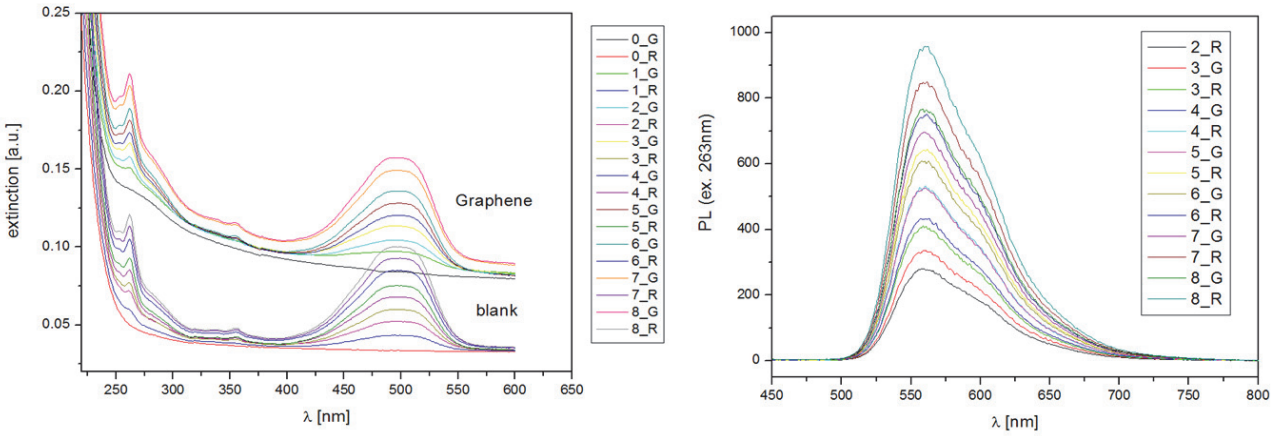

Fig. 6. Titration experiment. a) Table of TA2 concentrations in mg/mL. b) Absorption spectra of TA2 with increasing concentrations in isopropanol, with blank solvent (R) or graphene (G) background respectively. Right: Emission spectra recorded with constant experimental settings, irradiation into 263nm band.

However, we observe an effect on the emission intensity when comparing the dye in blank solvent with dye in presence of a graphene background. Unexpectedly, the loss in emission intensity seems to be independent of the quencher/dye ratio when irradiating with UV light. When irradiated into 263nm, the graphene sample emissions are reduced for about 19% in respect to the blank samples (see Fig. 7a).

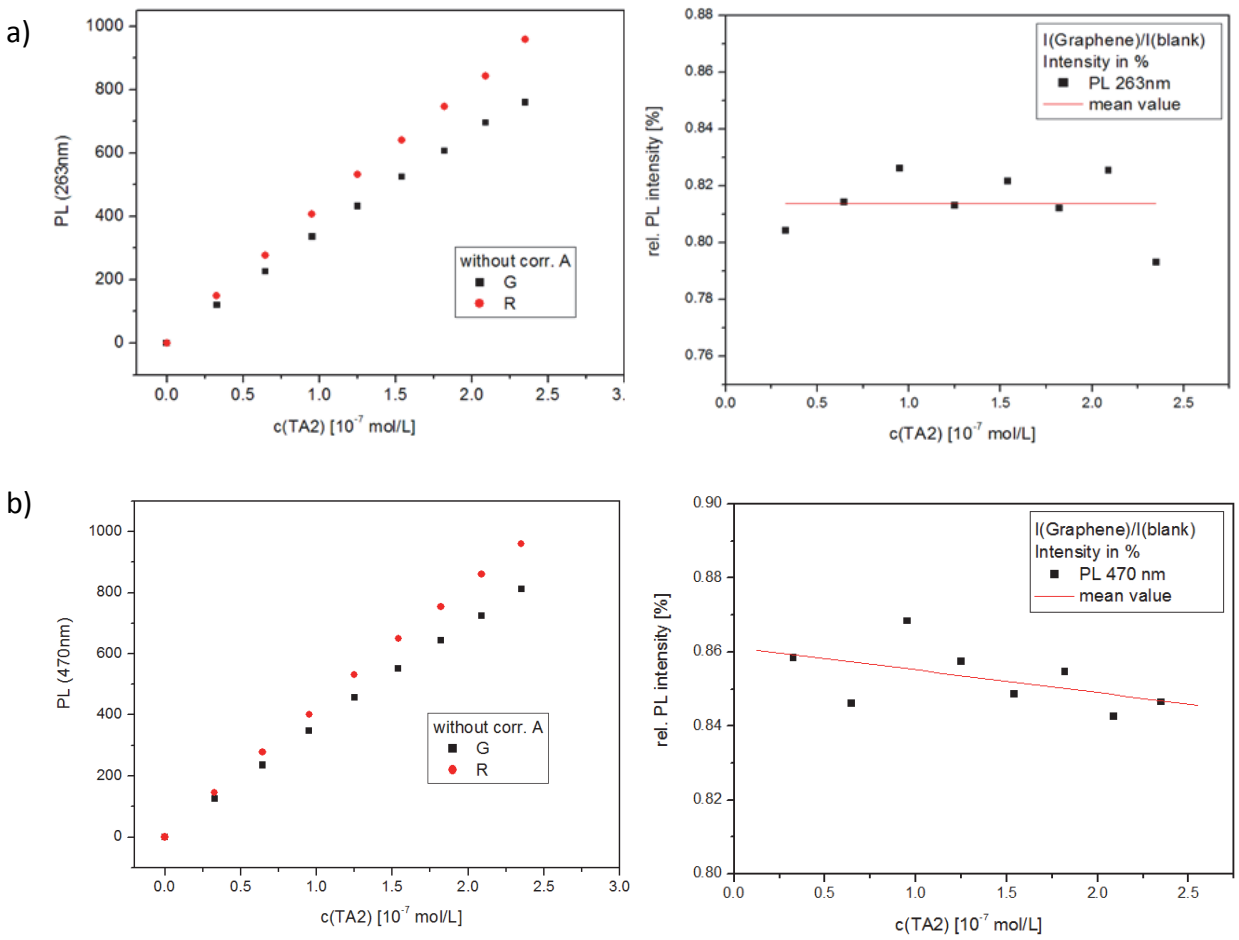

Fig. 7. TA2 concentrations versus emission intensity for solvent blank and graphene background; relative emission intensity obtained with graphene background versus blank solvent background with increasing dye concentration, excitation into a) 263 nm and b) 470 nm.

The data are not conclusive and likely indicating the limitations of this experimental setup: The constant drop of emission intensity for about 19% may be caused by saturation of the quencher, or even result from artefacts such as an inner filter effect caused by graphene (e.g. a scattering effect in the emission path, reabsorption by graphene).

5.2.5. Time resolved photoluminescence study on purified graphene-hybrid suspensions

We then investigate the photophysical characterization of graphene-TA2 interactions on in situ exfoliated graphene-TA2 hybrids and compare with graphene and dye in blank solvent.

5. Water soluble perylene diimide derivatives for graphene exfoliation

Time resolved photoluminescence measurements were performed on freshly prepared samples in isopropanol, namely Graphene (G, c=7 µg/mL), TA2 (c(TA2) = 2*10^-5 mol/L) and Graphene+TA2 (G+TA2, c=7.5 µg/mL). Isopropanol was chosen as a solvent because it stabilizes a reasonable amount of graphene even without surfactant and makes a graphene blank sample without dye accessible for measurement.

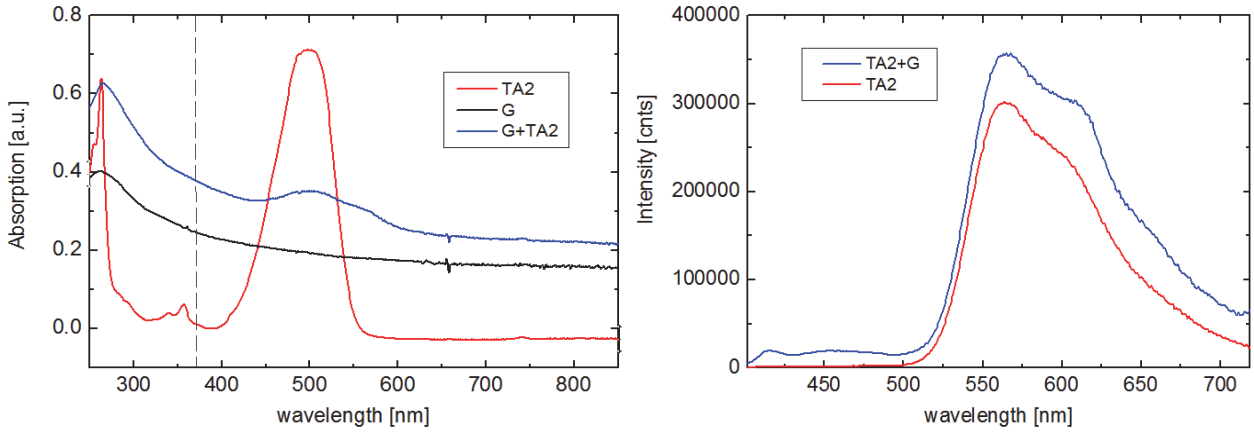

Fig. 8. Absorption and emission measurements on samples prepared for time resolved photoluminescence measurements. Excitation wavelength for emission measurements was 371nm.

A mixture of graphene and TA2 in isopropanol was prepared (G+TA2), showing absorption features of both graphene and TA2 as could be expected. As shown in Fig. 8, excitation with 371nm results in photoluminescence of G+TA2, characterized by emission of TA2: The emission band does not show a shift in respect with the dye reference without graphene, but there is a small broadening of the emission band.

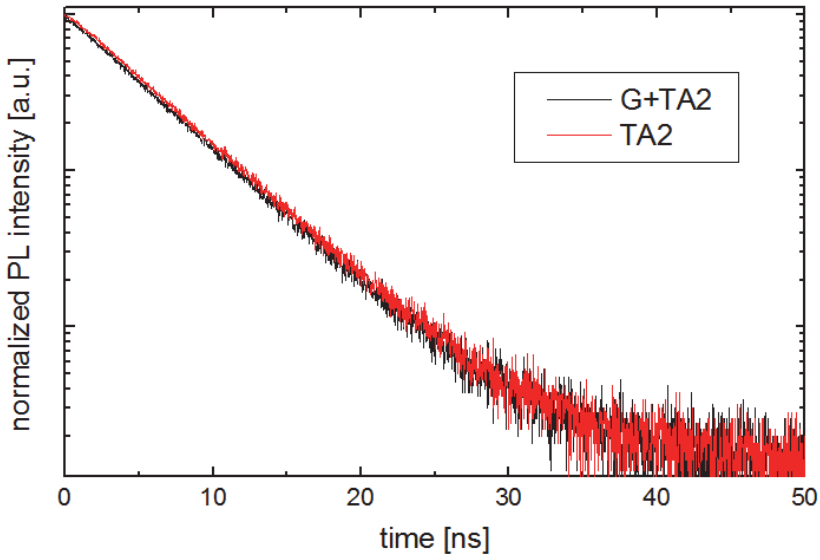

Fig. 9. Normalized emission lifetime spectra of TA2 (red line) and TA2/graphene (black line).

The lifetime of TA2 is not affected by the presence of graphene, suggesting that there is no interaction between graphene and TA2 upon titration: TA2 exhibits a very short lifetime of 5.2ns (at 565nm) upon irradiation; to perturb this fast decay process through interaction with graphene, the molecule needs to be very close to the graphene surface, which may be not the case in the experimental conditions that were necessary to perform this measurement.

We found the following PL lifetimes:

- TA2 = 5.1 ns
- G/TA2 = 5.1 ns

The PL quantum yield (PLQY) was determined with a relative single-point method using as reference the quantum yield of quinine sulphate dehydrate in 0.5 M sulphuric acid, PLQY ref=(54.6±5)%. The excitation wavelength was 371 nm. The PLQY can be calculated using:

$$\mathrm{PLQY} = \mathrm{PLQY}_{\mathrm{ref}} \frac{\mathrm{PL}}{\mathrm{PL_{ref}}} \frac{\mathrm{abs_{ref}}}{\mathrm{abs}} \frac{\mathrm{n}^2}{\mathrm{n}^2_{\mathrm{ref}}}$$

However, we observe a loss on emission intensity of TA2 in presence of graphene. Where PL is the total number of emitted photons, abs the absorbance at the excitation wavelength and n the refractive index of the solvent. We assume an error of 10% on the photoluminescence quantum yield (PLQY) measured.
We found the following PLQY:

- TA2 = 21%
- G/TA2 = 1.4%

Such drop in intensity may result from an inner filter effect rather than a real quenching, namely a primary inner filtering (Graphene absorbs at 371 nm ($\lambda_{excitation}$)) and/or a secondary inner filtering (Graphene absorbs at the $\lambda_{emission}$ of TA2). On the other hand, as we irradiate at 371nm and not in the newly formed, red-shifted dye band, we may observe emission only from free molecules in solution that do not interact with graphene. Ground state complexation may lead to a reduced

concentration of free dye in presence of graphene and could explain the lower quantum yield in presence of graphene being a consequence of a change in free, emitting TA2 concentration.
Overall, our spectroscopic investigations show no clear evidence for electronic communication between TA2 and graphene in isopropanol, suggesting a rather weak interaction in these experimental conditions; however, our experimental setup may not be sufficient to finally explain the nature of the interaction that may occur for graphene and TA2 in solution.

5.2.6. Exploiting graphene-dye interaction for Raman characterization of perylene diimide

Interestingly, a dichromatic Raman study (633nm or 514nm excitation) revealed signals attributed to the perylene diimide TA2 itself and the typical signature of few layer graphene. Solid state reflectance spectra are reported in Fig. 10, which roughly correspond to the inverse of UV/VIS absorbance; due to a scattering contribution resulting from an inhomogeneous morphology on quartz glass and the strong absorption of TA2 in the visible range, recording solid state spectra in the visible range is more informative when working in reflectance mode than in transmission.

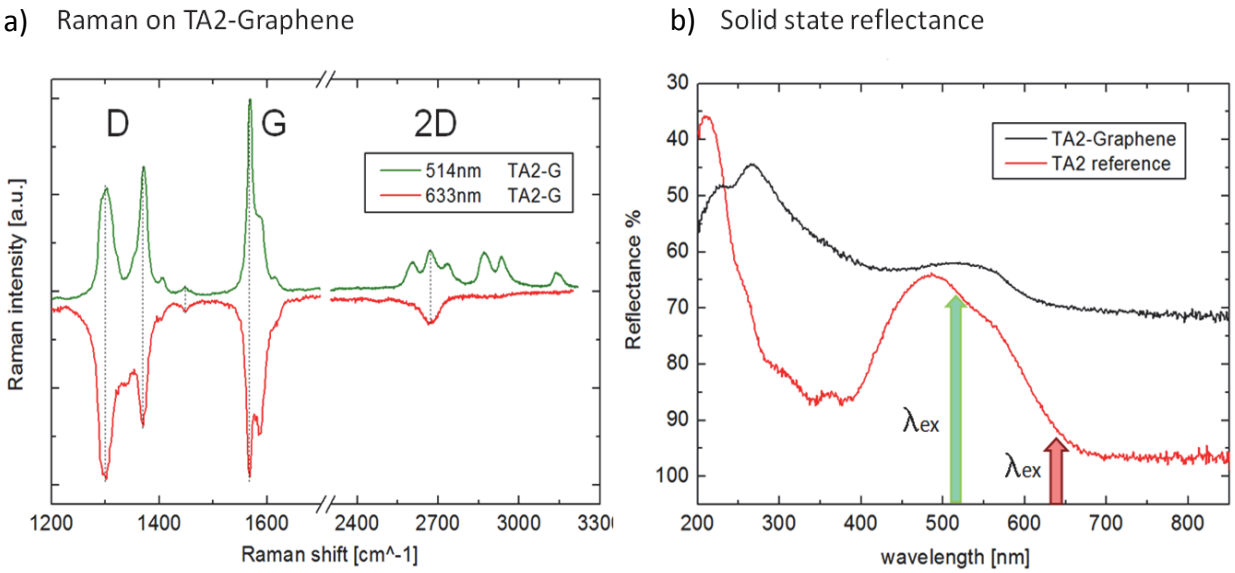

Fig. 10. a) Raman spectra of graphene/TA2 suspensions dropcast on SiO2. For excitation, the wavelengths 514nm (green) and 633nm (red) were used respectively. The red curve has been flipped vertically to allow for a better comparison. b) Solid state reflectance spectra of graphene/TA2 suspension (black) and a TA2 blank film on quartz glass (red), arrows indicating excitation wavelength selected for Raman experiments.

PDIs show strong photoluminescence in the visible range; even when excess dye was removed from graphene-dye suspensions with filtration and redispersion, the residual perylene diimide traces serving for graphene stabilization in polar solvents result in a strong emission background when resonantly excited in the visible range (see Fig. 11).

In the case of graphene, the absence of a bandgap makes all wavelengths of incident radiation resonant thus the Raman spectrum contains information about both vibrational and electronic properties (dichromatic Raman spectra of TA2/graphene hybrids are reported in Fig. 10). Differently from graphene, perylene diimide derivatives exhibit a bandgap, resulting in absorption in the visible range and inducing the typical red colour of the dyes studied here (see Fig. 10 b). Raman techniques are particularly useful to study order and structure of chromophores; however the strong emission background upon resonant excitation makes resolving resonant Raman bands resulting from the pure dye films difficult.

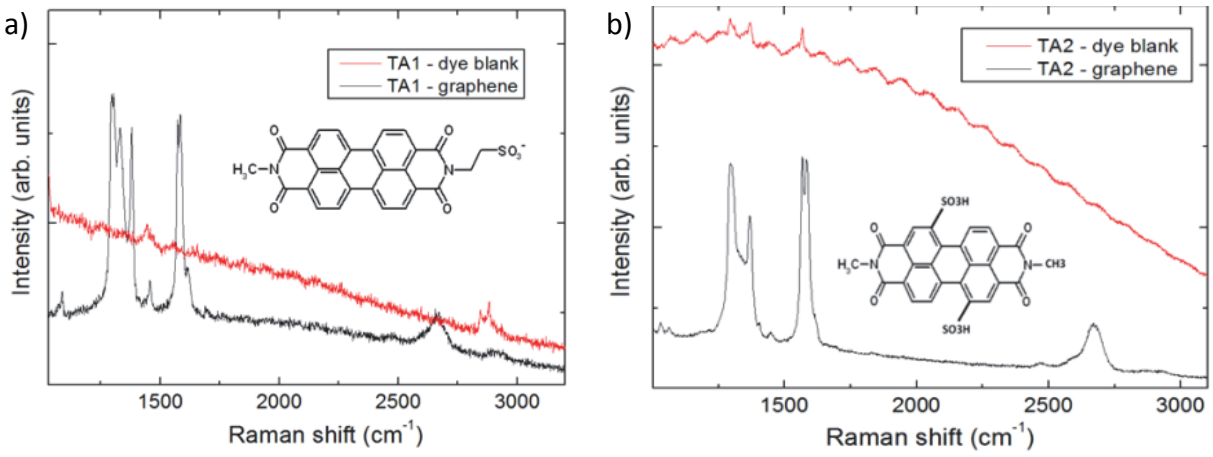

Fig. 11. a) Raman spectra of respective dye without graphene (red spectra) and purified graphene/dye suspensions (black spectra) spin coated on SiO2; note that the TA1 solid state spectra are only indicative as quantitative measurements were not possible due to a microscopically inhomogeneous sample morphology caused by dye particles.

In presence of graphene this background can be quenched and allows to use Raman spectroscopy on strongly emitting molecules (see Fig. 11 and Ref. [4,17]). Excitation into the perylene diimides absorption bands – thus a resonant Raman experiment - leads to a dramatic increase in intensity of the PDI's Raman bands. However, observation of these Raman bands requires the elimination of emission resulting from the dye: Perylene diimide films undergo radiative dissipation of excitation energy, resulting in a strong emission background when excited into 514nm.

Interacting with graphene, this emission background is eliminated through a transfer of charge and/or excitation energy from the dye to graphene [18]. In the Raman experiment, that effect may be exploited to study Raman transitions of strong emitters.

Solid state emission quenching further allows for excitation into the perylene diimides absorption bands – thus a resonant Raman experiment – which leads to a dramatic increase in intensity of the PDI's Raman bands. As reported in Fig. 5, the derivative TA1 exhibits a microscopically inhomogeneous morphology when spin coated on SiO2. This is a consequence of the molecule's limited solubility in polar solvents, leading to uncontrolled aggregation and a pigment-like dispersion of fine particles. For Raman analysis, the well-dissolved derivative TA2 was chosen ensure a controlled sample preparation.

Excitation into the resonant dye regimes results in a composition of band characteristic for graphene and TA2 (see Fig. 12). In symmetric in plane ring breathing modes of the TA2 molecule appear at 1304 cm^-1 and 1373 cm^-1; the corresponding peaks, slightly shifted modes are found in simulations in PTCDA at 1300cm^-1 and 1376cm^-1. Ring deformation within the perylene diimide core results in a mode at 1457.9 cm^-1for TA2, which correspond well to the value reported for other PDI derivatives (see Ref. [18], PDI ring deformation band in 1458 cm^-1).

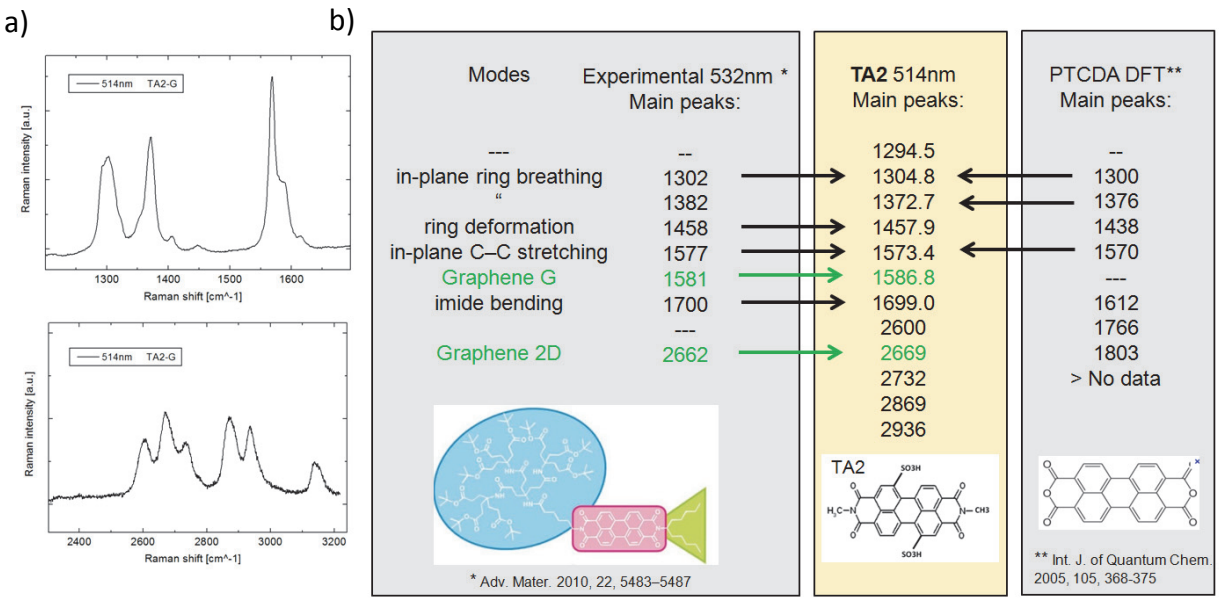

Fig. 12. a) Raman features of graphene-TA2 hybrids, deposition from aqueous suspension on SiO2. b) TA2-graphene hybrids, obtained Raman signature in comparison with a NMP soluble perylene diimide on graphene [18] and the simulated Raman modes for perylene tetra carboxylic acid anhydride (PTCDA) [19].

The in-plane C-C stretching mode with 1573.4 cm^-1 is up-shifted for TA2 on graphene with respect to the theoretical PTCDA value of 1570cm^-1, and down-shifted compared to the asymmetrically functionalized PDI on graphene reported by Hirsch and co-workers. Typical imide bending -naturally being absent in PTCDA - appears at 1699cm^-1 with 514nm excitation of TA2. Additional modes at 1586.8 cm^-1 and 2669 cm^-1 are attributed to the typical bands, namely G band and 2D band resulting from graphene.

5.3. Discussion

Exfoliation of graphite into few layer graphene was performed in three different solvents: water, ethanol and isopropanol. We find that the obtained concentration in suspended material increases with decreasing solvent polarity, in agreement with previous studies. Then, we studied the beneficial effect of two sulphonated perylene diimide derivatives when used as exfoliation agent in the same solvents. Both derivatives carry -SO3 functional groups, resulting in good solubility (TA2) or self-dispersion (TA1) in all three solvents. For a given solvent, the presence of either PDI derivative is found beneficial in terms of graphene concentration. Overall, the highest concentration of 0.5 mg/mL is obtained with the soluble PDI derivative TA2 and the most promising solvent, isopropanol. While the concentration of graphene obtained is lower than what is obtained with different, non-aromatic surfactants or solvents[20,21] the use of aromatic perylene diimides allows monitoring more quantitatively the exfoliation process using optical spectroscopy. Furthermore, the quenching of molecule's fluorescence due to the presence of graphene allows for studying the molecule optoelectronic properties by Raman, something not possible with the pure molecule.

However, while comparing different solvents, the selected solvent used for exfoliation are polar and protic, and they differ significantly in their viscosity and density. As we employ the post-centrifugation concentration as measure for the achieved graphene concentration and therefore the effectiveness of a solvent/dye system, intrinsic solvent parameters have to be taken into consideration: in centrifugation, the sedimentation rate of graphene and graphitic particles in suspension is a function of both the mediums' density and viscosity: The sedimentation rate v decreases as the medium viscosity increases, and it is proportional to the difference in density between the particle and the medium [22].

$$v = \frac{d^2 (p–L) \times g}{18\, n}$$

v = sedimentation rate or velocity of the sphere
d = diameter of the sphere
p = particle density
L = medium density
n = viscosity of medium
g = gravitational force

		water	EtOH	IPA
density	L[g/mL]	1.00	0.79	0.78
Viscosity(20°C)	n [cP]	0.89	1.07	1.26
	(p-L)/n =	1.35	1.32	1.12

Fig. 13. Sedimentation rate of dispersed graphene, dependance of sedimentation rate on particle/solvent parameters[23] calculated term for water, EtOH and IPA [24].

we shall approximate that, in all solvents, a similar, highly dispersed distribution of sheet sizes is obtained, typically following a lognormal distribution, as we have demonstrated recently with sonication of BN in IPA [25]. This ensemble consists of macroscopic, unexfoliated graphite particles as well as graphene flakes with lateral sizes of some hundreds of nm. Before centrifugation, applying same exfoliation parameters, we find a wide distribution in particle sizes resulting from the exfoliation process; it is reasonable to assume that the distribution of graphitic material is comparable at this stage, given that even after purification and a varying surfactant effectiveness with functionlization, we observe no change in flake dimensions, even four different -SO3 functionalized pyrenes derivatives are used for exfoliation (see chapter 4). Therefore, for a given graphene suspensions, particle density, diameter of the spheres and the gravitational force are approximated as constant for all 3 solvents and can be grouped in a constant factor K = (d^2 x g)/18 for comparison.

The sedimentation rate is then defined as follows:

v = K (p-L)/n with p = 2.2 g/cm3 (for graphite powder)
v(water) = K*1.35 units: K * [(g/cm3)/(10^-3Pas]
v(EtOH) = K*1.32
v(IPA) = K* 1.12

While we cannot use this formula to obtain quantitative values of sedimentation velocity (the particles are not spherical, but rather 2-dimensional), we shall apply it to qualitatively compare the

results obtained with different solvents. The sedimentation speed in centrifugation is reduced to roughly 80% in isopropanol in respect to EtOH and water, suggesting better stabilization of graphitic material in isopropanol.

In conclusion, these data suggest that the solvent itself plays a role in liquid phase exfoliation with the sulphonated PDIs under study; however, in water, EtOH and IPA the presence of a aromatic core is beneficial for graphene stabilization. A new, red shifted ground state absorption band appears with graphene, being a first indication for electronic interaction between graphene and TA2 in solution. Steady state and time resolved spectroscopy was applied to further investigate the interaction of graphene and TA2 in solution: We found that found state complexation may lead to a reduced concentration of that free dye in presence of graphene and could explain the lower quantum yield in presence of graphene being a consequence of a change in free, emitting TA2 concentration. Overall, our results show no evidence for electronic communication between TA2 and graphene in isopropanol. However it is to mention, that our experimental setup may not have been not sufficient to finally explain the interaction of graphene and TA2 in solution.

Wavelength dependent Raman response of graphene blends with perylene diimide (exfoliation of graphene without dye in organic solvents) has been reported by Hirsch and co-workers [18]. We perform Raman on directly exfoliated graphene-perylene diimide hybrids in polar solvents, with excitation in two wavelength regimes. Excitation into the non-resonant regime of the dye allows for probing the graphene sheet quality in terms of numbers of layers. We find mainly few layer graphene, but observed also some thinner material likely resulting from electronically decoupled, rotationally stacked few-layers graphene. Few layer graphene is confirmed additionally by probing the sheet morphology with AFM. In addition, AFM reveals that the graphene flakes are not pristine, but coated with dye. This finding, as is the distribution in flake thickness, is in agreement with previous studies on aromatic chromophore assisted exfoliation of graphene in water (see, for example, previous chapters on pyrenes sulphonic acid sodium salt derivatives).

Excitation into the resonant dye regime (514 nm) and the quenching of background fluorescence with graphene allows for observing modes corresponding to the perylene diimide core that have not been reported before to our best knowledge. The vibrational transitions could be correlated and interpreted with simulation data and Raman data of a perylene diimide derivative and PTCDA, reported in previous studies.

5.4. Experimental

Materials.

The chromophores TA1 (N',N'-bis(2-methy, 6-ethyl-sulphonic acid) perylene-3,4,9,10-tetracarboxylic diimide) and TA2 (N',N'-bis(2,6 dimethy) disulphonic perylene-3,4,9,10-tetracarboxylic diimide) were provided by BASF, Ludwigshafen, Germany, and used as received. Natural graphite flakes were purchased from Aldrich.

Material Preparation.

Graphene suspensions were prepared by sonication of 3mg/mL graphite flakes in 0.1mg/mL solutions of each of the perylene diimides for 4.5hrs, and using as well blank solvent with no dye for comparison. A bath sonicator was used (Elmasonic, ultrasonic frequency 37kHz, effective power 30% corresponding to ~70W), an ice bath was used to ensure the temperature was kept below 40°C during sonication. After sonication, the suspensions were centrifuged at 1500 rpm for 20 minutes to remove large unexfoliated graphite particles for all three solvents.

Purification procedure.

A purification process based on filtration was used in this study using solvent exchange through filtration and redispersion of the residual carbon material in a defined volume of solvent. This physical separation technique has several advantages over centrifugation: The process allows for nearly complete removal of the liquid phase, which increases the purification efficiency in respect procedures based on centrifugation/dilution.

AFM analysis.

AFM measurements were carried out using a Digital Instruments AFM (NT-MDT), using Nanoprobe cantilevers (model: RTESP, material: 1–10 Ohm cm phosphorus (n) doped Si, f0: 27–309 kHz, k: 20–80 N m_1; from Veeco) operating in tapping mode.

Raman studies.

Raman spectra were collected with a Renishaw InVia spectrometer using laser excitation wavelengths of 633nm. The excitation power was kept well below 1mW to avoid effects of local heating. The scattered light was collected with a 100x objective.

Time resolved photoluminescence measurements.

A time-correlated single photon counting (TCSPC) spectrometer was used for time-resolved photoluminescence (PL) measurements. The sample were excited at 317 nm with a using a pulsed diode laser (Edinburg Instruments-EPL-375) and the light emission was detected with a cooled photomultiplier (Becker & Hickl PMC-100-1) coupled to a monochromator and finally the signal was elaborated by the TCSPC electronics (Edinburg Instrument Lifespec-ps TCC-900 PC card) with a temporal resolution of 100 ps.

References

(1) Parviz, D.; Das, S.; Ahmed, H. S. T.; Irin, F.; Bhattacharia, S.; Green, M. J. *Acs Nano* 2012, *6*, 8857.

(2) Schlierf, A.; Yang, H.; Gebremedhn, E.; Treossi, E.; Ortolani, L.; Chen, L.; Minoia, A.; Morandi, V.; Samori, P.; Casiraghi, C.; Beljonne, D.; Palermo, V. *Nanoscale* 2013, *5*, 4205.

(3) Schlierf, A.; Samori, P.; Palermo, V. *Journal of Materials Chemistry C* 2014.

(4) Yang, H.; Hernandez, Y.; Schlierf, A.; Felten, A.; Eckmann, A.; Johal, S.; Louette, P.; Pireaux, J. J.; Feng, X.; Mullen, K.; Palermo, V.; Casiraghi, C. *Carbon* 2013, *53*, 357.

(5) Schmidt, R.; Oh, J. H.; Sun, Y.-S.; Deppisch, M.; Krause, A.-M.; Radacki, K.; Braunschweig, H.; Könemann, M.; Erk, P.; Bao, Z.; Würthner, F. *Journal of the American Chemical Society* 2009, *131*, 6215.

(6) Schmidt-Mende, L.; Fechtenkotter, A.; Mullen, K.; Moons, E.; Friend, R. H.; MacKenzie, J. D. *Science* 2001, *293*, 1119.

(7) Kozma, E.; Catellani, M. *Dyes and Pigments* 2013, *98*, 160.

(8) Facchetti, A. *Materials Today* 2013, *16*, 123.

(9) Uemura, T.; Iguchi, T.; Kato, M.; Mochizuki, A.; Google Patents: 2002.

(10) Khan, U.; O'Neill, A.; Lotya, M.; De, S.; Coleman, J. N. *Small* 2010, *6*, 864.

(11) Coleman, J. N. *Advanced Functional Materials* 2009, *19*, 3680.

(12) Ferrari, A. C.; Meyer, J. C.; Scardaci, V.; Casiraghi, C.; Lazzeri, M.; Mauri, F.; Piscanec, S.; Jiang, D.; Novoselov, K. S.; Roth, S.; Geim, A. K. *Physical Review Letters* 2006, *97*, 187401.

(13) Chitta, R.; Sandanayaka, A. S. D.; Schumacher, A. L.; D'Souza, L.; Araki, Y.; Ito, O.; D'Souza, F. *The Journal of Physical Chemistry C* 2007, *111*, 6947.

(14) Rahman, G. M. A.; Guldi, D. M.; Campidelli, S.; Prato, M. *Journal of Materials Chemistry* 2006, *16*, 62.

(15) Álvaro, M.; Atienzar, P.; Bourdelande, J. L.; García, H. *Chemical Physics Letters* 2004, *384*, 119.
(16) Rahman, G. M. A.; Guldi, D. M.; Cagnoli, R.; Mucci, A.; Schenetti, L.; Vaccari, L.; Prato, M. *Journal of the American Chemical Society* 2005, *127*, 10051.
(17) Backes, C.; Schmidt, C. D.; Rosenlehner, K.; Hauke, F.; Coleman, J. N.; Hirsch, A. *Advanced Materials* 2010, *22*, 788.
(18) Kozhemyakina, N. V.; Englert, J. M.; Yang, G. A.; Spiecker, E.; Schmidt, C. D.; Hauke, F.; Hirsch, A. *Advanced Materials* 2010, *22*, 5483.
(19) Zhanpeisov, N. U.; Nishio, S.; Fukumura, H. *International Journal of Quantum Chemistry* 2005, *105*, 368.
(20) Hernandez, Y.; Nicolosi, V.; Lotya, M.; Blighe, F. M.; Sun, Z. Y.; De, S.; McGovern, I. T.; Holland, B.; Byrne, M.; Gun'ko, Y. K.; Boland, J. J.; Niraj, P.; Duesberg, G.; Krishnamurthy, S.; Goodhue, R.; Hutchison, J.; Scardaci, V.; Ferrari, A. C.; Coleman, J. N. *Nature Nanotechnology* 2008, *3*, 563.
(21) Guardia, L.; Fernandez-Merino, M. J.; Paredes, J. I.; Solis-Fernandez, P.; Villar-Rodil, S.; Martinez-Alonso, A.; Tascon, J. M. D. *Carbon* 2011, *49*, 1653.
(22) Wood, E. J. *Biochem. Educ.* 1991, *19*, 156.
(23) Rickwood, D. *Centrifugation: a practical approach*; IRL Press, 1984.
(24) http://www.dynesonline.com/
(25) Kouroupis-Agalou, K.; Liscio, A.; Treossi, E.; Ortolani, L.; Morandi, V.; Pugno, N. M.; Palermo, V. *Nanoscale* 2014, *6*, 5926.

Chapter 6

High performance perylene diimides for graphene exfoliation in organic solvents

6. High performance perylene diimides

6.1 Introduction

It has been demonstrated that graphene LPE with small aromatic dyes is a complex interplay between graphene-dye interactions and solvent interaction of both species. For instance, water does not allow for direct suspension of pristine graphene due to hydrophobic interactions, provoking aggregation. Such aggregation can be overcome through non-covalent functionalization of graphene with water soluble dyes carrying polar moieties, as already detailed in the previous chapters: Small chromophores such as the pyrene sulphonic acid derivatives discussed before, and other chromophores, for instance perylene diimide derivatives with polar moieties, have been demonstrated efficient exfoliation agents in graphite liquid phase exfoliation [1-3]. Exfoliation with chromophore-based surfactants allows for suspending graphene even in polar protic solvents such as water, EtOH or isopropanol. The interaction of the aromatic core with graphene – reflected in the physical-chemical properties of such a system, for example in the molecules' adsorption free energy[2] - plays a key role in the effectiveness of a chromophore as an agent in graphite liquid phase exfoliation.

However, when aiming for application of graphene organic hybrid materials in organic electronics, water contamination can dramatically impact the device performance, therefore deposition procedures are optimized for device processing with (dry) organic solvents. Some selected solvents matching the graphene's surface energy allow for direct, surfactant-free liquid exfoliation of graphite, yielding stable graphene suspensions of concentrations in the range of 10^-1 mg/mL depending on exfoliation parameters and purification procedure (for example, NMP, DMF and oDCB have been found effective [4]). NMP and oDCB are readily applied in semiconductor liquid phase processing, but they suffer from drawbacks originating from their high boiling point (204°C for NMP, 180° for oDCB) that urges for additional processing to remove solvent residues from organic semiconductor layers upon deposition. In many other low boiling point solvent systems, such as chloroform, yields in graphene obtained with direct, surfactant –free exfoliation are significantly lower (See Ref. [5]) to what has been achieved with NMP or oDCB; a mismatch in surface energy between graphene and solvent is assumed being reason for the lower graphene yield in CHCl3. In this chapter, we demonstrate the use of perylene-based chromophores as exfoliating agents to overcome constraints faced with exfoliation in organic solvents. From our studies, discussed in previous chapters, we expect that these exfoliation agents may have beneficial effects for liquid phase exfoliation in low boiling point solvents such as CHCl3, similar to

what has been found for dye-assisted graphite exfoliation in water. A one-step process to access processable graphene-OSC hybrids in organic suspensions is particularly of interest for prospective application as electronic inks for organic field effect transistor, and we address this question in the present chapter. Two conventional solvents, oDCB and $CHCl_3$, are compared for their performance in dye assisted graphite LPE with high performance n-type semiconductors. Graphene-solvent, OSC-solvent and graphene-OSC-solvent interactions are addressed. In particular, we aim answering to the following key questions:

a. Is the dye assisted LPE approach, which is established for water, extendable to all-organic OSC-graphene systems?
b. Is there indication for a specific, electronic interaction between OSC and graphene in organics?
c. Overall, which effects are governing OSC assisted LPE in organics?

6.2 Results

6.2.1 Organic small molecules semiconductors under study - OSC-solvent interactions

Aim of combining graphene with N-type organic semiconductor materials is to create a highly performing electron acceptor material with good carrier transport properties. N-type core-cyanated perylene diimide derivatives are used to directly exfoliate graphene in organics and to generate in-situ graphene-hybrids. The perylene diimide (PDI) derivatives under study bear alkyl chains (butyl dicyano-perylenecarboxydiimide, PDI-CN2) or fluoroalkyl chains, (N,N'-1H,1H-perfluorobutyl dicyanoperylenecarboxydiimide, PDIF-CN2), as shown in Fig. 1, to ensure solubility in oDCB and CHCl3. Additionally, fluorination and bay functionalization with cyano groups has been demonstrated a successful route to lower the lowest unoccupied molecular orbital (LUMO) of aromatic compounds and to improve the molecule's air stability [6-8]: The inductive effect of σ-acceptors (electron-withdrawing groups such are Cl, F, Br and CN) stabilize the LUMO slightly more than the HOMO, therefore narrowing the molecule's energy gap. This band gap narrowing likely occurs as a consequence of a more pronounced electron coupling between the PDI LUMO and the attached electron accepting moiety[9-11], which in our case are cyano groups in bay positions.

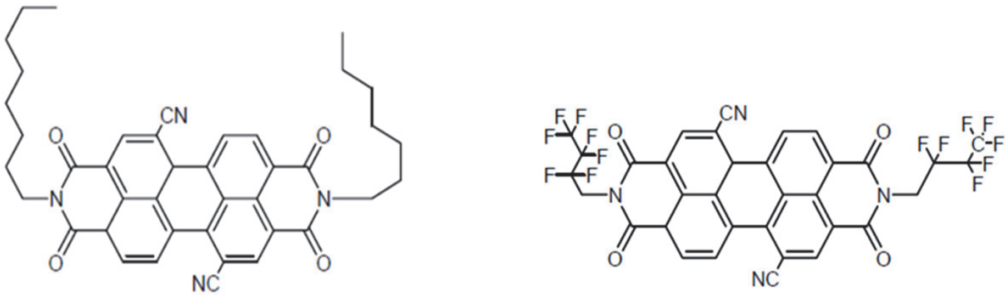

PDI-CN2 PDIF-CN2

Fig. 1. Molecular structures of the high performance semiconductor derivatives PDI-CN2 and PDIF-CN2. The PDI derivatives under study bear alkyl chains (butyl dicyano- perylenecarboxydiimide, PDI-CN2) or fluoroalkyl chains, (N,N'-1H,1H-perfluorobutyl dicyanoperylenecarboxydiimide, PDIF-CN2).

The optical properties of many PDI-based dyes are known to depend on solution concentration and its environmental conditions, such as solvent polarity and temperature [9]. This physic-chemical

behaviour of perylene diimide derivatives is often originating from intermolecular interactions, from dimer formation up to growth of mesoscopic aggregates or crystals.

PDI-CN2 and PDIF-CN2 are stable and soluble in chloroform (CHCl3) and ortho-dichlorobenzene (oDCB), both being solvents commonly used in organic semiconductor liquid phase device processing. A small bathochromic shift of 6 nm appears for the main peak of PDI-CN2, and 8 nm for the main peak of PDIF-CN2, when moving from CHCl3 to oDCB. For PDIF-CN2 and PDI-CN2 in both oDCB and CHCl3, the overall band structure is conserved, with the typical PDI electronic S0-0 transition characterized by vibronic progression (S0-1 and S0-2) [12]. Such solvatochromism is a well-known effect with chromophores such are perylene diimide derivatives, in which the light absorption of a chromophore depends on the choice of solvent; the effect is caused by electrostatic interactions with the surrounding solvent molecules, causing the absorption bands moving continuously to lower (or in some cases as well to higher) photon energies as a function of the solvent's polarity [13].

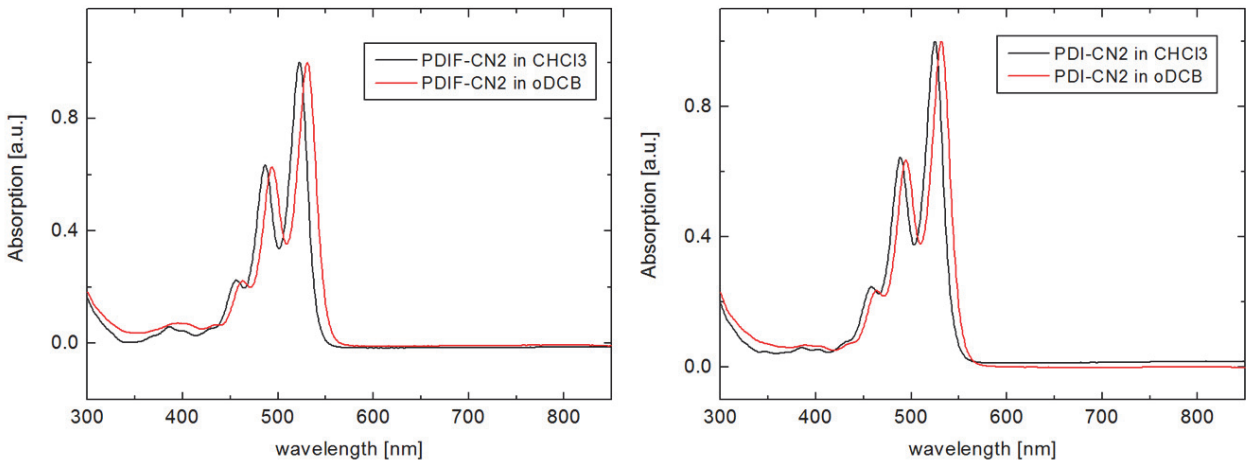

Fig. 2. Normalized UV spectra of PDIF-CN2 and PDI-CN2 respectively, in CHCl3 or oDCB. Measurements were done on c= 2*10^-5 mol/L solutions. Both molecules exhibit a slight solvatochromic effect, characterized by a small red shift in oDCB compared to the spectra in CHCl3.

Stronger distortion of the ground state transitions – resulting in a significant change in UV/VIS absorption such are peak broadening or shifted bands - may be originating not only from a solvent effect, but also from a change of the molecules' aggregation state in solution. Perylene diimide derivatives are known to form supramolecular assemblies in both solid and liquid phase through π-π interaction. In liquid phase, such supramolecular assemblies are reflected by the modified

ground state absorption depending on the specific molecular stacking (particularly into J- or H-aggregates, for more details see for example Ref. [14]). The aggregation behaviour can be controlled by structural features e.g. symmetric or asymmetric side functionalization with sterically demanding groups, or by modification of the chemical environment (see Ref. [9], [13]).

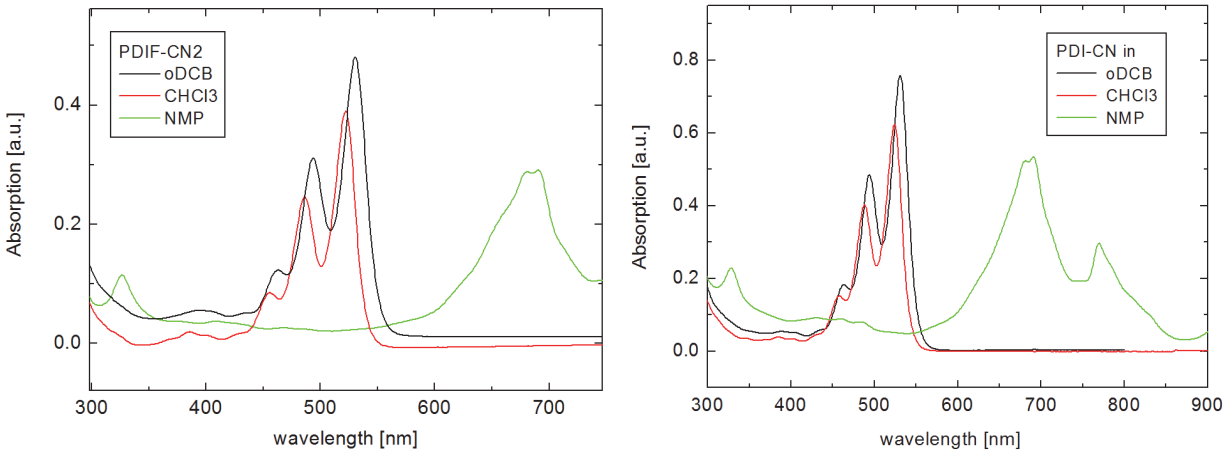

Fig. 3. Absorption spectra of PDIF-CN2 in a mixed solvent. PDIF-CN2 (left) and PDI-CN2 (right) in NMP, CHCl3 and oDCB; concentration in respective solvent or solvent mixture was c=1.2*10^-5 mol/L.

For example, aggregation between the aromatic cores occurring in higher concentrated (c > 10-4 mol/L) solutions results in a broadened absorption and a large bathochromic shift, with a low energy absorption that can even extend to the near infrared range for some selected PDI derivatives[9].

In the case of PDIF-CN2 and PDI-CN2, both molecules are well dissolved with NMP and CHCl3 at concentrations of 1.2*10^-5 mol/L. While CHCl3 solutions show the typical three band absorption fingerprint of perylene, the absorption bands are broadened and red-shifted in NMP (see Fig. 3).

It should be mentioned here that pronounced spectral changes occur as well upon covalent substitution of the perylene aromatic core with an electron donors such is a pyrrolidino groups, which yields PDI derivatives with a dark-green colour as a result of the bathochromic shift over 150 nm. Such a large spectral shift is associated with the internal charge-transfer (ICT) from amino to PDI moiety.[9]

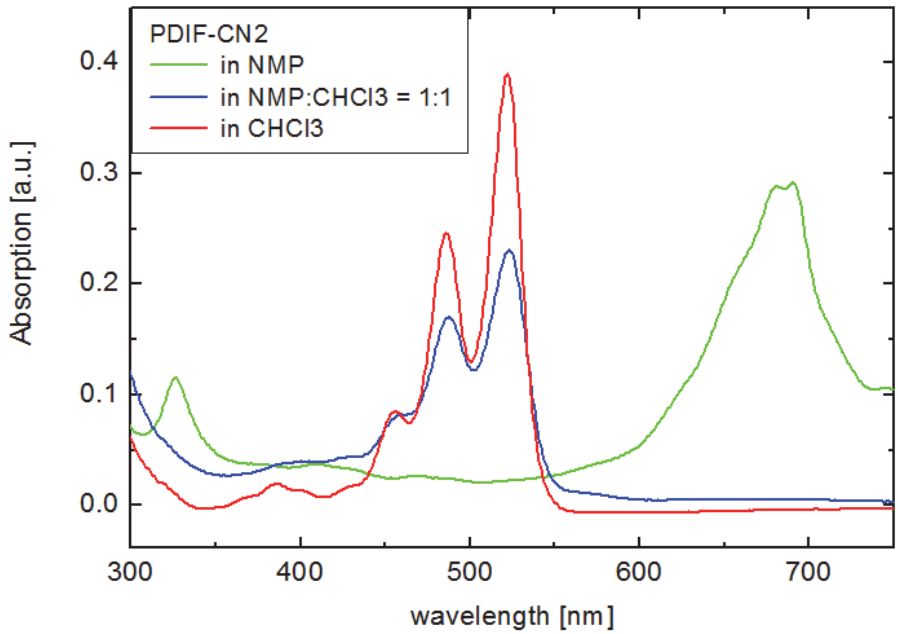

Fig. 4. Absorption spectra of PDIF-CN2 in NMP, CHCl3 and a mixture of NMP and CHCl3 (1:1), the concentration is kept constant for all solvent systems at c=1.2*10^-5 mol/L.

Dissolving PDIF-CN2 in a solvent mixture (1:1 CHCl3 and NMP, Fig. 4) gives rise to a broadened aggregation band at 570nm, an effect that has been observed and exploited already in different solvent systems, for example with hydroxyl functionalized PDIs. This characteristic shift in electronic properties and the broadened band can be fingerprint for non-covalent interactions through π-π stacking, and indication that similar functionalization can be expected with PDI and graphene.

6.2.2 Solvent dependence of OSC assisted LPE

Solvent–graphene interactions in bulk suspensions can be addressed indirectly through the stabilization of exfoliated graphene in suspension. The effectiveness of a solvent to stabilize graphene in suspension is estimated with the remaining graphene concentration upon exposure to a field of gravity through centrifugation. For exfoliation, 3mg/mL of graphite is sonicated in oDCB or CHCl3 respectively for 4.5hrs at 40% power. The samples are then centrifuged with 500 rpm, 2000 rpm or 5000 rpm respectively. The concentration in remaining dispersed material is then measured with UV/VIS absorption as already described in previous chapters (comparing the absorption value at 660nm, see Ref. [5]).

In a first step, blank solvents are used for exfoliation. Here, higher concentrations after centrifugation are obtained with oDCB in respect to CHCl3 (see Fig. 5). Upon centrifugation with 500 rpm, 2000 rpm or 5000 rpm respectively for 30min, the overall concentration of suspended graphene particles doubles when moving from chloroform to oDCB, suggesting that an overall better stabilization of suspended graphene-like material is achieved in oDCB than in CHCl3.

a)

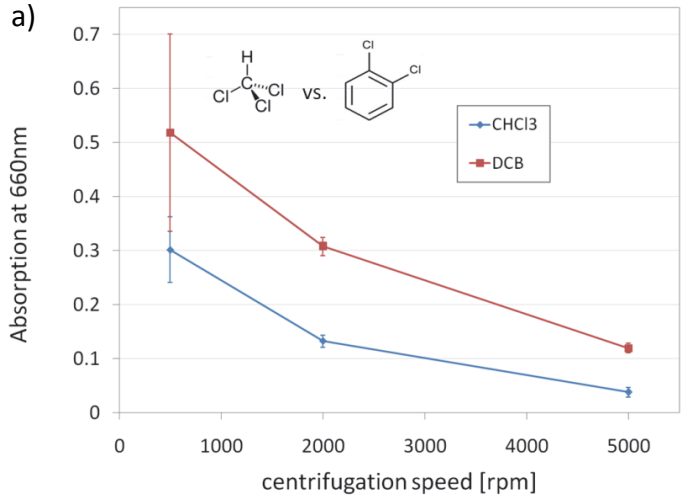

b)

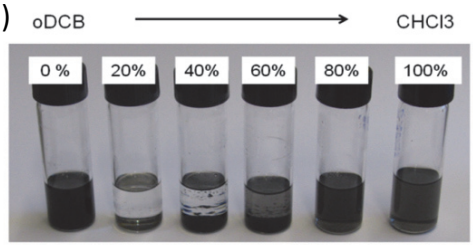

c) Concentration of graphitic material in mg/mL

Centrifugation speed	CHCl3	DCB
500 rpm	0.12	0.21
2000 rpm	0.05	0.13
5000 rpm	0.02	0.05

Fig. 5. Chromophore-free exfoliation in oDCB and CHCl3. a) The graph reports the absorption values at 660nm (directly proportional to the concentration of suspended material) in CHCl3 and oDCB respectively. The deviation at low centrifugation speeds is large as at this stage; the suspensions are metastable systems of graphitic particles dispersed in the respective solvent. b) Picture of suspensions, obtained by surfactant free exfoliation in solvent mixtures of oDCB and CHCl3 with increasing CHCl3 content from 0% to 100% (from left). Quantitative measurement of graphene concentration was not informative due to heavy aggregation in solvent mixtures. c) The table on the right reports the mass concentration of graphitic material in suspensions in [mg/mL] determined from the absorption at 660nm (α = 2460 L/(g*m) [15]).

In more detail, we observed that the graphite exfoliation in oDCB in respect to CHCl3 is more effective; this finding is in agreement with previous studies that found oDCB being an eligible solvent for direct LPE of graphite and stabilizing graphene in suspension [4,16]. Already in 2009, Hamilton et al. obtained a graphene concentration of 0.03 mg/mL in oDCB with direct, surfactant - free exfoliation of graphite. The picture reported in Fig. 5b shows graphene suspensions exfoliated in solvent mixtures without a surfactant. The stabilization is not systematically decreasing with increasing content of CHCl3 in oDCB from 0% to 100%, as could be expected from exfoliation in the respective pure solvent, but solvent mixtures of CHCl3 and oDCB did yield less suspended material with a tendency to aggregation and precipitation. This unexpected aggregation behaviour likely results from inhomogeneous mixing and solvent interactions of these two dissimilar organic solvents, with CHCl3 exhibiting low and oDCB showing high boiling point and viscosity; for instance, mixtures of oDCB and CHCl3 have even been used for controlled self-assembly of other colloidal systems such as single wall carbon nanotube in suspension [17].

Then, the experiment was repeated using solutions of the perylene diimides PDI-CN2 or PDIF-CN2 as exfoliation agents, probing those OSC molecules for their effectiveness as surfactant in graphite liquid phase exfoliation in oDCB and CHCl3.

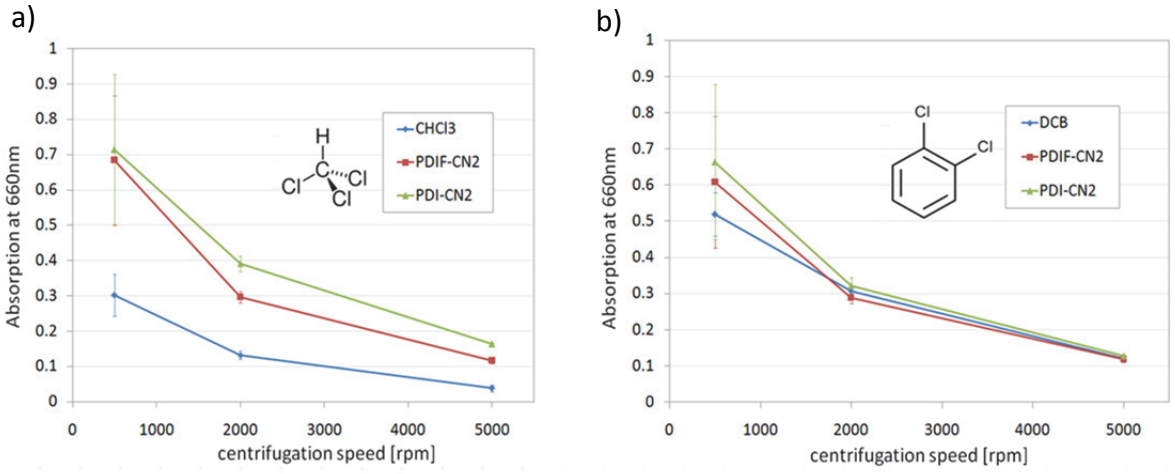

Fig. 6. UV/VIS absorption at 660nm reflecting the yield of suspended graphene as a function of centrifugation speed. Liquid phase exfoliation of graphite with solutions of PDI-CN2, PDIF-CN2 or blank solvent are reported for a) CHCl3 and b) oDCB

6. High performance perylene diimides

The same exfoliation parameters were applied for graphene/OSC hybrid suspensions to maintain comparability with the blank solvent graphene suspensions, namely sonication of 3mg/mL graphite for 4.5hrs, in solutions containing 0.1mg/mL of each molecule. Fig. 6 concludes the results of the exfoliation with the perylene diimide derivatives in CHCl3 (left) and oDCB (right): Again, three different centrifugation speeds, 500rpm, 2000rpm or 5000rpm are applied to fresh suspensions (centrifugation time 30min) to estimate the stability of dispersed graphite fragments in each solution. Naturally, the values at 500rpm centrifugation speed exhibit a large deviation, originating likely from turbidity induced by poorly stabilized larger particles still present in very gently centrifuged suspensions.

With oDCB, no beneficial effect in terms of concentration (as an indication for stabilization in solution) is observed, with an average graphene concentration of 0.1 mg/mL for blank solvent, PDI-CN2 or PDIF-CN2 solutions (calculated from A(660nm), α = 2460 L g_1 m_1). Also comparing graphene concentrations of dispersions centrifuged with 2000 rpm, the results was not affected by the presence of an OSC in the case of oDCB.

In chloroform, overall higher yields of suspended graphene are obtained when exfoliating with OSC solutions instead of pure solvent: Comparing the obtained graphene concentrations after centrifugation with 2000rpm for 30min, exfoliation in chloroform results in an increase of concentration for a factor of 3 for PDIF-CN2 and a factor of 4 for PDI-CN2, suggesting a stabilizing effect on graphene in suspension originating from the OSC molecule in solution.

In presence of a well-dissolved aromatic exfoliation agent, a surfactant effect can be expected, causing better stabilization and higher yields in suspended graphene. With centrifugation at increasing speeds, we found indeed a better stabilization in a gravity field (reflected in a higher concentration) for graphene suspensions in CHCl3 if OSC was used.

These findings suggest that the PDI chromophores have an effect on exfoliation yield for CHCl3, which is a poor solvent for LPE, but not for oDCB, which shows good performance for graphite LPE even without applying a stabilization agent. We speculate that this additional effect on the stabilization of graphene platelets in CHCl3, which was not observed in oDCB, is due to a competition between OSC - graphene and solvent -graphene interaction.

6.2.3 Photo-spectrometric characterization of graphene- PDI-CN hybrids

UV/Visible light absorption. Steady state UV/VIS absorption spectroscopy provides valuable information on the interaction of chromophores with graphene through their π-system (see Chapter 2 for pyrene-graphene interaction). As mentioned before, perylene diimide derivatives undergo self-assembly in solution phase through π-π interactions under certain conditions, resulting in a characteristically modified ground state UV/VIS absorption spectrum. To probe the interaction with graphene, two experimental approaches were applied.

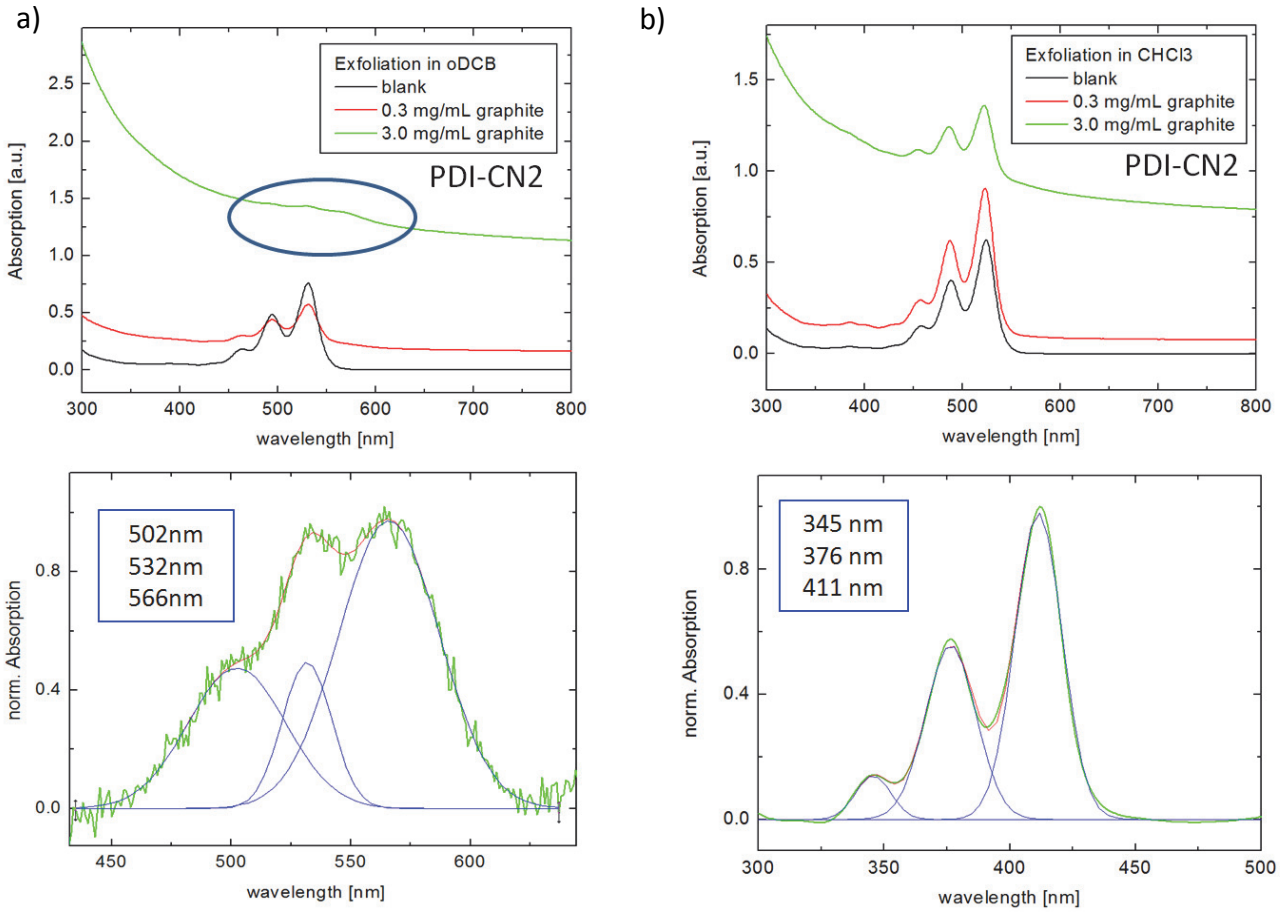

Fig. 7. Graphene-dye interaction in liquid phase for derivative PDI-CN2, absorption and emission spectra in oDCB (a) and chloroform (b), respectively. UV spectra shown here are without dilution. Below: Zoom on normalized main absorption bands appearing with highest graphene concentrations (green line), fitted with tree Gaussian peaks (blue), positions of the peak fits are reported.

Firstly, graphite liquid phase exfoliation was performed in CHCl3 and oDCB, this time with a lower concentration of PDI-CN2 and two concentrations of graphite (see experimental section); the OSC concentration was reduced to 0.01 mg/mL in order to achieve a higher OSC to graphene ratio with exfoliation, which is expected to allow observation of graphene-dye ground state complexation without bands from excess in free OSC being predominant.

As a further approach in investigating ground state interaction between PDI-CN2 and graphene, visible absorption spectra were also taken from graphene exfoliated in blank CHCl3 or oDCB, mixed with PDI-CN2 solution in the respective solvents. In this case, no sonication is applied. Fig. 8 shows the spectra corrected for the blank graphene background.

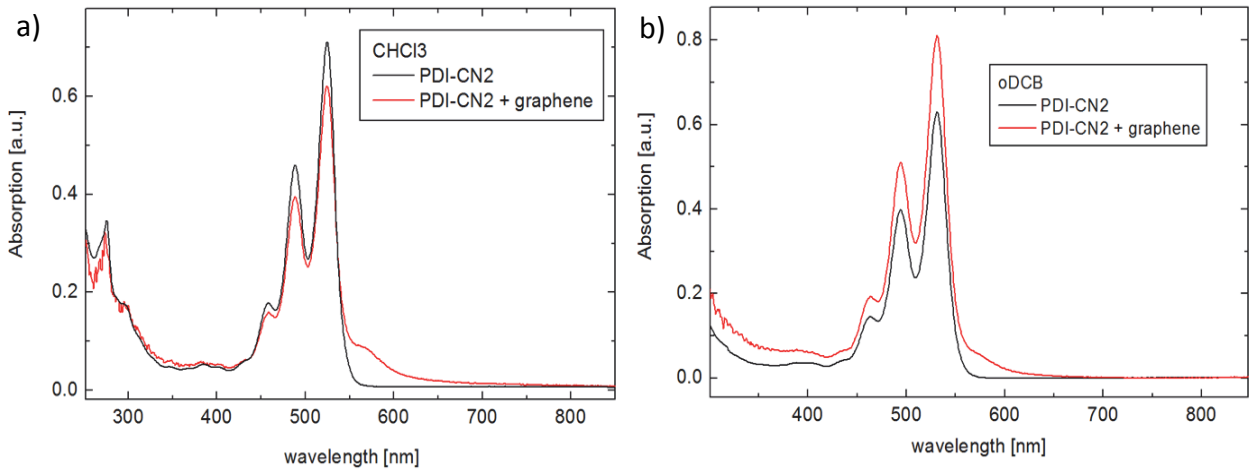

Fig. 8. Absorption spectra of mixtures of graphene exfoliated in a) CHCl3 or b) oDCB and PDI-CN dissolved in the same solvent. The spectra of graphene-PDI-CN2 mixtures are corrected for the graphene background of blank graphene for better comparison.

In both oDCB and CHCl3 mixtures, the presence of graphene gives rise to an additional lower energy band at 567nm, in good agreement with the band observed with directly exfoliated graphene-PDI hybrids. This indicates that the effect is not an artefact resulting from, as example, decomposition of the PDI due to temperature or sonication, but rather spontaneous adsorption behaviour of PDI-CN2 on graphene. Interestingly, the red shifted band is observed with both CHCl3 and oDCB, suggesting that spontaneous adsorption is favourable despite of solvent-graphene interactions.

6.2.4 Graphene-PDI-CN excited state interaction – steady state emission

Electronic communication between chromophores can be studied through the dissipation pathway of light-induced excited states. Emission quenching is commonly used as a measure to observe electronic interactions between an emissive dye and a quencher. However, in case of graphene-chromophore hybrid materials in liquid phase, quantitative emission measurements remain challenging from an experimental point of view, for different reasons: First of all, it is very important to stress that we deal not with actual solutions of graphene, but with dispersions of graphene and particle-like graphene nano-platelets. As typically found with direct liquid phase exfoliation of graphite, the dispersed graphene flakes exhibit different lateral sizes, thicknesses and possibly different aggregated states, which are likely to induce strong light scattering when measuring both absorption and fluorescence. The scheme below indicates possible dissipation pathways of excited energy and additional loss channels that may induce a drop in emission intensity in graphene-perylene diimide liquid phase systems:

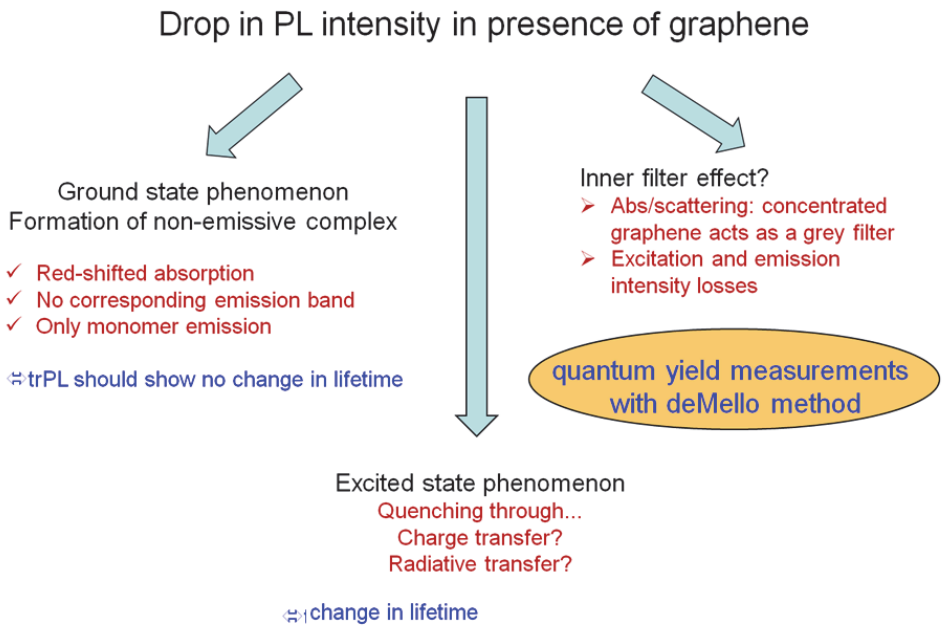

Fig. 9. Scheme suggesting possible excitation energy dissipation pathways for graphene-dye excited state interaction in liquid phase. Ground state phenomena, exited state phenomena and artefacts may contribute and have to be taken into consideration when dealing with loss in emission intensity in such graphene-organic hybrid systems.

Loss in emission intensity may originate from ground state phenomena, such is the formation of a non-emissive charge transfer complex; this kind of ground state interaction is often coupled to a distortion of the dyes' ground state light absorption, resulting in peak broadening and/or generation of new absorption bands, often at lower energies. Emission intensity also depends on excited state phenomena; upon light irradiation, emission quenching - for instance through graphene - may occur through charge or energy transfer from the dye to graphene.

Other phenomena causing a drop in emission intensity do not originate from an interaction between graphene and the perylene diimide, such is an inner filter effect: Part of the excitation energy may be lost through absorption or scattering on graphene, reducing the intensity of incident light available for excitation. Furthermore, the concentration of perylene diimide and graphene in oDCB has to be balanced carefully to observe an effect of quenching experimentally: The graphene dispersion has to be relatively concentrated as the quenching effect is barely detectable, but on the other hand, this increases the contribution of light scattering altering the true values of absorption. In addition, as we investigate non-covalent functionalization in a liquid phase, the adsorption and therefore likely interaction processes are in equilibrium and the equilibrium may shift to different sides depending on the actual conditions of the system under study.

As graphene-dye hybrid dispersions are a complex systems to be studied relying on steady-state optical spectroscopy, quantitative emission measurements particularly on concentrated graphene samples need a tailored experimental setup to circumvent artefacts resulting from scattering and reabsorption on graphene flakes over a wide wavelengths range. In order to record emission of a dye in presence of such predominant scattering and absorption background, we suggest and investigate an approach proposed by John de Mello: Here, absorption or emission is collected simultaneously in a 3D volume (integrating sphere) [18].

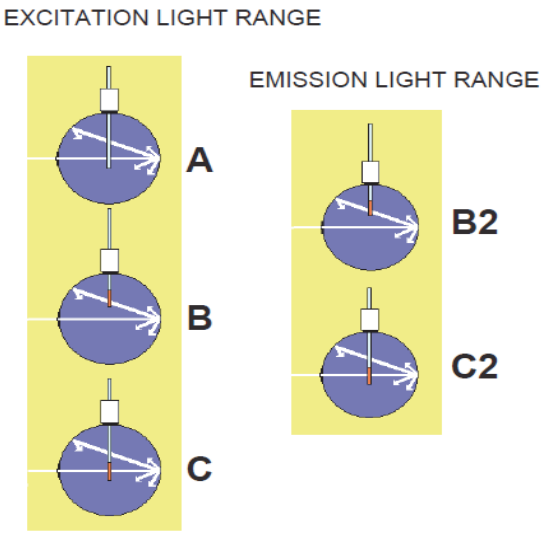

Fig. 10. Schematic representation of the de Mello method using an integrating sphere for the determination of the absolute emission quantum yield, proposed by J.C. de Mello, H. R. Wittmann and R. H. Friend, Advanced Materials, 1997, 9. A detailed description of the de Mello method is available in the method sections of this thesis.

We have selected graphene that was directly exfoliated into solutions of CN-PDI in oDCB to apply this method for direct measurements of absolute quantum yields for the following reasons: First, we observe a change (red-shift) in the absorption spectra which may be indicative of electronic interactions between PDI-CN2 and graphene in oDCB (see Fig. 7). Secondly, differently from CHCl3, oDCB stabilizes graphene in reasonably high concentrations without surfactant, allowing to have a graphene “blank” (i.e. without PDI-CN2) sample solution.

Graphene was exfoliated as described above, namely sonication of 3 mg/mL graphite flakes in blank oDCB or in a solution of PDI-CN2 in oDCB (c=0.01 mg/mL). The graphene dispersions were then centrifuged at 10 krpm for 30min to remove larger graphitic aggregates from dispersion, resulting in 0.3 mg/mL dispersed graphene flakes for both blank sample and PDI-CN2 solution (concentration calculated from UV/VIS absorption at 660nm, see Fig. 7a). In addition, a PDI-CN2 blank sample (c=0.01 mg/mL) was prepared.

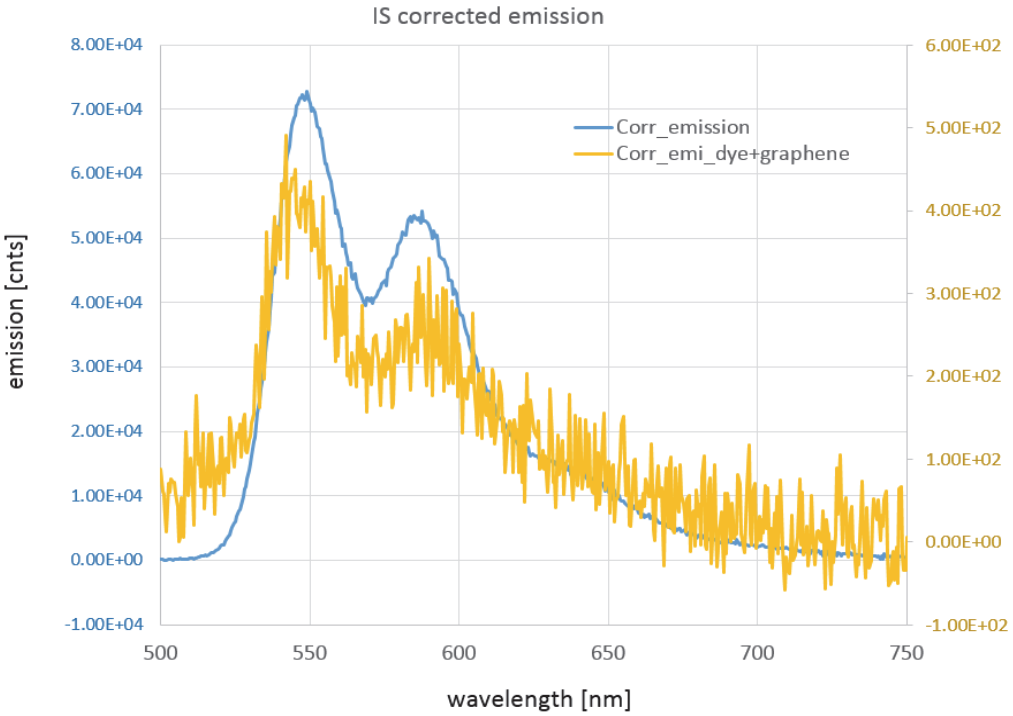

Fig. 11. Absolute emission spectra of graphene PDI-CN2 recorded with de Mello setup. Scale of emission intensity was adapted to the spectra for better comparison and clarity.

Fig. 11 reports the emission spectra of graphene-PDI-CN2 hybrid suspension (yellow line) and a PDI-CN2 blank solution in oDCB (blue line). The emission spectra are corrected for the instrumental response function and the reabsorption term. We observe a significant drop in emission of PDI-CN2 emission intensity in presence of graphene. To quantify the effect, we estimated the absolute quantum yield applying the following relations introduced by De Mello et al.

The fraction of light absorbed by the sample is defined as

$$\mathrm{Abs\%} = 1 - \frac{\mathrm{C}}{\mathrm{B}}$$

The emission quantum yield η is then calculated using the following relation:

$$\eta = \frac{\mathrm{C2} - (1 - \mathrm{Abs\%}) * \mathrm{B2}}{\mathrm{Abs\%} * \mathrm{A0}}$$

Spectra A0, B and C address the intensity of the excitation light, while the emission range is probed with spectra B2 and C2. Spectra A records the background, namely the instrumental response of the IS to the excitation beam. Then, the excitation beam is monitored in presence of the sample. The sample is placed once inside the sample beam (spectrum C) to monitor the absorption of collimated light (direct excitation), once placed outside the incident beam (spectra B) to consider the secondary excitation by absorption of diffuse excitation light scattered on the IS's wall. A more detailed description of this method is reported in the methods' section of this thesis.

Applying the de Mello method, we evaluated the absolute quantum yields of the dye to be η = 53% approximately for free dye (dye blank sample) and η = 0.2% approximately for graphene-PDI-CN2 hybrid dispersions. Such a significant drop in quantum yields suggest an excited state interaction between PDI-CN2 and graphene in oDCB through a quenching mechanism such is charge or energy transfer.

6.3 Discussion

a. Is the dye assisted LPE approach, which is established for water, extendable to all-organic OSC-graphene systems in organic solvents?

Exfoliation in blank solvent yields higher concentration of graphene in suspension in oDCB than it does in chloroform. This is not new, physical-chemical parameters – for instance viscosity or surface energy – plays a crucial role in the effectiveness of centrifugation in a separation technique. Exfoliation in different solvent systems has been extensively addressed, experimentally and theoretically, and correlated to intrinsic solvent properties, including Hildebrandt parameter, surface energy and boiling point [5].

Solvent molecules may undergo physisorption on graphitic surfaces; chloroform adsorption energies on graphitic templates have been reported in previous work. Trihalomethanes (THM) adsorption energies are in the 350–360 meV range depending on the precise position on graphene, with the differences in adsorption energies in the various positions on graphene being

small. Chloroform physisorbs with its H atom pointing away from graphene, yielding adsorption energies of ≈357 meV (34.4 kJ/mol). This suggests that THMs such as CHCl3 bind sufficiently strongly to graphene for graphene; an application for filtering of chlorinated water to remove the THM byproducts has been also recently suggested [19].

We find exfoliation in OSC solutions beneficial in graphite liquid phase exfoliation in CHCl3. CHCl3 is a less favourable solvent for surfactant-free exfoliation, comparable to the situation of surfactant free exfoliation in water. In both aqueous and CHCl3 based system employing an eligible chromophore-based exfoliation agent promotes stabilization of graphene in the respective solvent; this finding suggests that the dye assisted LPE approach, which is established for water, is extendable to all-organic OSC-graphene systems in organic solvents.

However, a beneficial effect in terms of graphene concentration in presence of an OSC was not observed when oDCB was selected as a solvent, suggesting that the situation is more complex with this system:In the case of oDCB, being it an aromatic solvent, π-π interactions come into play; oDCB is a common reaction solvent for fullerenes and is known to form stable SWNT dispersions presumably as a result of efficient interactions via π-π interaction.[20] Further strong evidence for π-system based solvent interaction was found recently, when the formation of a charge transfer complex between oDCB and graphene was demonstrated theoretically. [Balamurugan 21217]

Our results, in agreement with literature, give indication that solvent-graphene interaction play a pronounced role in graphite LPE in oDCB. Such π-π based solvent-graphene interactions can be assumed being predominant over graphene-OSC interactions, suggesting that this system is even more complex than dye-assisted LPE in water with a relevant contribution of both graphene-solvent and graphene-OSC interactions.

b. Is there indication for a specific, electronic interaction between dye and graphene in organics?

Mixing of OSC (PDI-CN2 or PDIF-CN2 respectively) with separately exfoliated graphene gives new absorption bands, not visible in pure OSC solutions, suggesting formation of a ground state complex with graphene and the chromophore. In both oDCB and CHCl3, the presence of graphene gives rise to an additional lower energy band at 567nm. This in agreement with the band observed with directly exfoliated graphene-PDI hybrids indicating that the effect is not an artefact resulting

from sonication, but rather spontaneous adsorption behaviour of PDI-CN2 on graphene. Interestingly, the red shifted band is observed with both $CHCl_3$ and oDCB, suggesting that spontaneous adsorption is favourable despite of solvent-graphene interactions. However, it has to be mentioned that observation of such ground state phenomenon need a relatively high ratio of graphene in respect with the dye. This kind of graphene-dye interaction can be observed by optical spectroscopy only for a suitable graphene-dye ratio, and tuning all the experimental measurements conditions (linear detector response, sufficient absorption intensity for resolution…).

We attempted to address such instrumental limitations in emission measurements applying the de Mello method. With this setup, we evaluated the absolute quantum yields of the dye to be η = 53% approximately for free dye (dye blank sample) and η = 0.2% approximately for graphene-PDI-CN2 hybrid dispersions. Such a significant drop in quantum yields suggest an excited state interaction between PDI-CN2 and graphene in oDCB through a quenching mechanism such is charge or energy transfer.

c. Concluding, which are the parameters governing dye assisted LPE in organics?

Generally, the observations of this study are of a qualitative nature, however indications are found that both solvent-graphene and dye-graphene interaction is key to high yield graphite liquid phase exfoliation and stabilization of graphene in solutions. A too favourable solvent interaction seems to hinder from an additional surfactant effect with chromophores. For a detailed understanding of the processes involved, MD simulation of dye adsorption in chloroform or oDCB and further experimental studies on charge-transfer complex formation would be of great interest. We further found indication for electronic communication between the high performance n-type organic semiconductor and liquid phase exfoliated graphene.

6.4 Experimental

Materials. The PDI derivatives butyl-dicyano-perylenecarboxydiimide (PDI-CN2) N,N'-1H,1H-perfluorobutyl-dicyano-perylenecarboxydiimide (PDIF-CN2) were purchased from Polyera and used as received.

Exfoliation. 3 mg/mL and 0.3 mg/mL of graphite were sonicated for 4.5 hrs in dye solutions of 0.1 mg/mL and subsequently diluted for a factor of 10 for UV/VIS absorption measurements after sonication.

Absorption and emission measurements.

Absorption spectra were recorded with a Perkin-Elmer Lambda 950 spectrophotometer. The emission spectra were obtained using an Edinburgh FLS 920 spectrometer equipped with a Peltier-cooled Hamamatsu R928 photomultiplier tube (sensitive from 185nm to 850nm) and a Hamamatsu R5509-72 supercooled photomultiplier tube. An Edinburgh Xe 900 450W xenon arc lamp was used for excitation. Details on quantum yield measurements and deMello method are reported in the methods chapter.

References.

(1) Yang, H.; Hernandez, Y.; Schlierf, A.; Felten, A.; Eckmann, A.; Johal, S.; Louette, P.; Pireaux, J. J.; Feng, X.; Mullen, K.; Palermo, V.; Casiraghi, C. Carbon 2013, 53, 357.
(2) Schlierf, A.; Yang, H.; Gebremedhn, E.; Treossi, E.; Ortolani, L.; Chen, L.; Minoia, A.; Morandi, V.; Samori, P.; Casiraghi, C.; Beljonne, D.; Palermo, V. Nanoscale 2013, 5, 4205.
(3) Backes, C.; Schmidt, C. D.; Rosenlehner, K.; Hauke, F.; Coleman, J. N.; Hirsch, A. Advanced Materials 2010, 22, 788.
(4) Hernandez, Y.; Nicolosi, V.; Lotya, M.; Blighe, F. M.; Sun, Z. Y.; De, S.; McGovern, I. T.; Holland, B.; Byrne, M.; Gun'ko, Y. K.; Boland, J. J.; Niraj, P.; Duesberg, G.; Krishnamurthy, S.; Goodhue, R.; Hutchison, J.; Scardaci, V.; Ferrari, A. C.; Coleman, J. N. Nature Nanotechnology 2008, 3, 563.
(5) Khan, U.; O'Neill, A.; Lotya, M.; De, S.; Coleman, J. N. Small 2010, 6, 864.
(6) Jones, B. A.; Ahrens, M. J.; Yoon, M.-H.; Facchetti, A.; Marks, T. J.; Wasielewski, M. R. Angewandte Chemie International Edition 2004, 43, 6363.
(7) Weitz, R. T.; Amsharov, K.; Zschieschang, U.; Villas, E. B.; Goswami, D. K.; Burghard, M.; Dosch, H.; Jansen, M.; Kern, K.; Klauk, H. Journal of the American Chemical Society 2008, 130, 4637.
(8) Schmidt, R.; Oh, J. H.; Sun, Y.-S.; Deppisch, M.; Krause, A.-M.; Radacki, K.; Braunschweig, H.; Könemann, M.; Erk, P.; Bao, Z.; Würthner, F. Journal of the American Chemical Society 2009, 131, 6215.
(9) Würthner, F. Chem. Commun. 2004, 1564.
(10) Schmidt, R.; Ling, M. M.; Oh, J. H.; Winkler, M.; Könemann, M.; Bao, Z.; Würthner, F. Advanced Materials 2007, 19, 3692.
(11) Ahrens, M. J.; Fuller, M. J.; Wasielewski, M. R. Chemistry of Materials 2003, 15, 2684.
(12) Kistler, K. A.; Pochas, C. M.; Yamagata, H.; Matsika, S.; Spano, F. C. Journal of Physical Chemistry B 2012, 116, 77.
(13) Steyrleuthner, R.; Schubert, M.; Howard, I.; Klaumünzer, B.; Schilling, K.; Chen, Z.; Saalfrank, P.; Laquai, F.; Facchetti, A.; Neher, D. Journal of the American Chemical Society 2012, 134, 18303.
(14) Ghosh, A.; Rao, K. V.; George, S. J.; Rao, C. N. R. Chemistry – A European Journal 2010, 16, 2700.
(15) Khan, U.; Porwal, H.; O'Neill, A.; Nawaz, K.; May, P.; Coleman, J. N. Langmuir 2011, 27, 9077.
(16) Hamilton, C. E.; Lomeda, J. R.; Sun, Z.; Tour, J. M.; Barron, A. R. Nano Letters 2009, 9, 3460.
(17) Diehl, M. R.; Yaliraki, S. N.; Beckman, R. A.; Barahona, M.; Heath, J. R. Angewandte Chemie International Edition 2002, 41, 353.
(18) de Mello, J. C.; Wittmann, H. F.; Friend, R. H. Advanced Materials 1997, 9, 230.
(19) Åkesson, J.; Sundborg, O.; Wahlström, O.; Schröder, E. The Journal of Chemical Physics 2012, 137.
(20) Bahr, J. L.; Mickelson, E. T.; Bronikowski, M. J.; Smalley, R. E.; Tour, J. M. Chemical Communications 2001, 193.

Chapter 7

Processing graphene-organic hybrid suspensions into polymer composites

7. Processing of graphene suspensions into polymer composites

7.1 Introduction

Conductive fillers are key in engineering functional plastics, providing solutions in electromagnetic interference (EMI) shielding and anti-static applications in various industries such as aerospace, automotive electronics, computers, data communications, medical equipment etc..

Graphitic nanostructures attract increasing attention as filler in polymer composites, owing to their unique electrical, optical and mechanical properties. In particular, the properties of graphene, such as its large specific surface area, high electrical conductivity, well-defined thermal conductivity and thermal stability make it an ideal choice as nanofiller for the preparation polymer composites [1]. Polymer composites of graphene precursors such as reduced graphene oxide have been found interesting conductive nano-size fillers, as they can create a percolation network within a polymer matrix [2]

The field of graphene-based composites is bursting, with more than 3900 papers published in 2013,[3] and intense activity from major industrial companies. Graphene has been demonstrated interesting for engineering properties of a great variety of polymeric systems, but it is still not clear how and to which extent graphene will benefit large-scale industrial applications. Improvement of composite performance has been demonstrated on lab scale for a great variety of systems, but industrial scale exploitation requires a significant improvement of performance at a cost competitive with already established additives such, as example, carbon black, graphite powder, etc.

Large scale exfoliation of graphene at low cost has been recently demonstrated by Coleman and co-workers.[4] Applications of graphene in composites will require processing steps compatible with the actual technology, finding ways to process graphene effectively in polymer granules and liquid master batches. As already discussed in chapter 1, the best solvents used at the moment are high-boiling and toxic solvents such as DMF and NMP, which are difficult to remove from the polymer composite and are in this way affecting its properties. Exfoliation in water may be more feasible for water-based polymer systems, but in this way the surfactants necessary for the exfoliation and stabilization of graphene in water will remain as well, at least in traces and possibly adsorbed on graphene sheets. Particularly common surfactants for aqueous systems, such as SDBS, can reduce

the graphene sheets' interaction with the polymer matrix and the beneficial effect, mechanical, thermal or electric, of graphene additives.

An ideal solution to issues arising from solvent or surfactant contamination would be graphene production using industrial dyes or pigments for exfoliation, that are commercially available and already well-established in industrial compounding of polymers. The advantages of this approach are manyfold:

1) industrial dyes are already produced on large scale and have low cost as compared to any of the organic surfactants used for fundamental research
2) the effect of such dyes on the properties of the polymer matrix are well known, and are normally controlled or minimized using optimized procedures
3) the processing of these dyes in different polymers is routinely done and, last but not least,
4) these dyes, to be used in commercial products, have already been screened and approved for toxicity or environment protection issues, depending on their main applications.

In the previous chapters, we discussed graphite liquid phase exfoliation with pyrene and perylene diimide derivatives in different solvent systems. Following this approach, we take advantage of the extensive expertise on dye processing and commercialization broadly established in industry to select the ones most suitable for graphene exfoliation AND successive use in polymers blends. Some of these dyes find application for more than fifty years, and have thus the advantage of being well known at industrial level. Such dyes and pigments are commonly used as colorants, stabilizers, plasticizers, etc.

This chapter describes the direct exfoliation of graphite with an industrial commercial dye that is largely used in industry. We selected the molecule indanthrone sulphonic acid sodium salt (IBS), a commercial liquid crystal precursor and colorant additive, to achieve water-soluble pristine graphene nanoplatelets, readily dispersible in a polyvinylalcohol matrix. Indanthrone based derivatives are versatile pigments that can be used in different media, for example to dye unmordanted cotton, as a pigment in quality paints and enamels and as a food colorant (is found as E number E130). Towards application in organic electronics, IBS in particular known as intermediate for liquid crystal preparation and for its optical properties. [5,6]

7. Processing of graphene suspensions into polymer composites

Here, we demonstrate the application of IBS as agent to successfully exfoliate few-layers graphene into stable and processable aqueous dispersions. The graphene dispersions obtained in this way are characterized by spectroscopic and microscopic methods; then, to demonstrate that the exfoliation method suggested in this chapter is suitable for applications in composites, the graphene-organic hybrids are processed into a commercial commodity polymer (poly-vinyl alcohol, PVA) enhancing its electrical bulk conductivity by several orders of magnitude.

7.2 Results

7.2.1 Dye properties and self-assembly

IBS exhibits excellent water solubility and it is known to improve rheology parameters in pigment composites, being an interesting candidate in developing water soluble graphene based fillers towards application in commercial polymer composites. The liquid crystalline nature of indanthrone dyes has been previously used to align sheets at the nanoscale, forming vertically aligned graphene layer arrays on substrates. [7]

From a molecular structure point of view, IBS (structure reported in Fig. 1) is amphiphilic, a property found beneficial for graphite exfoliation with perylene diimide and pyrene derivatives before; [8-10] in these systems, core functionalization with a sulphonic group improves the molecules' solubility, and an extended aromatic core allows for hydrophobic interactions between graphene and the molecule. [8,10,11]

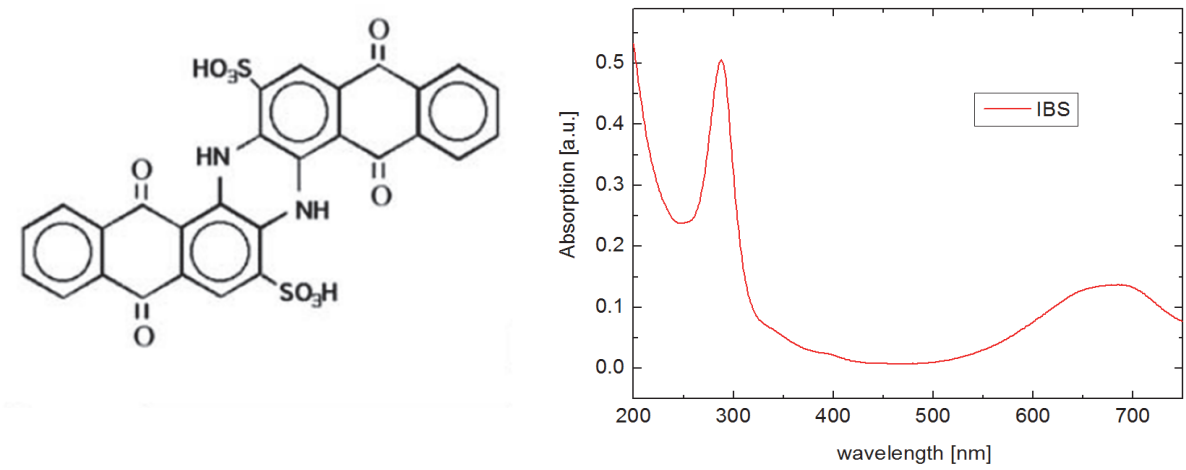

Fig. 1. Molecular structure of indanthrone disulphonic acid and visible absorption spectrum of the free dye without graphene in aqueous solution, c=1.8*10^-5 mol/L.

We first studied the self-assembling behaviour and structure of indanthrone disulphonate at the nanoscale, to be compared with the graphene-IBS dispersions obtained afterwards. Indanthrone disulphonate (structure shown in Fig. 1) is a lyotropic dye, forming self-assembled structures when dissolved in higher concentrations in water.

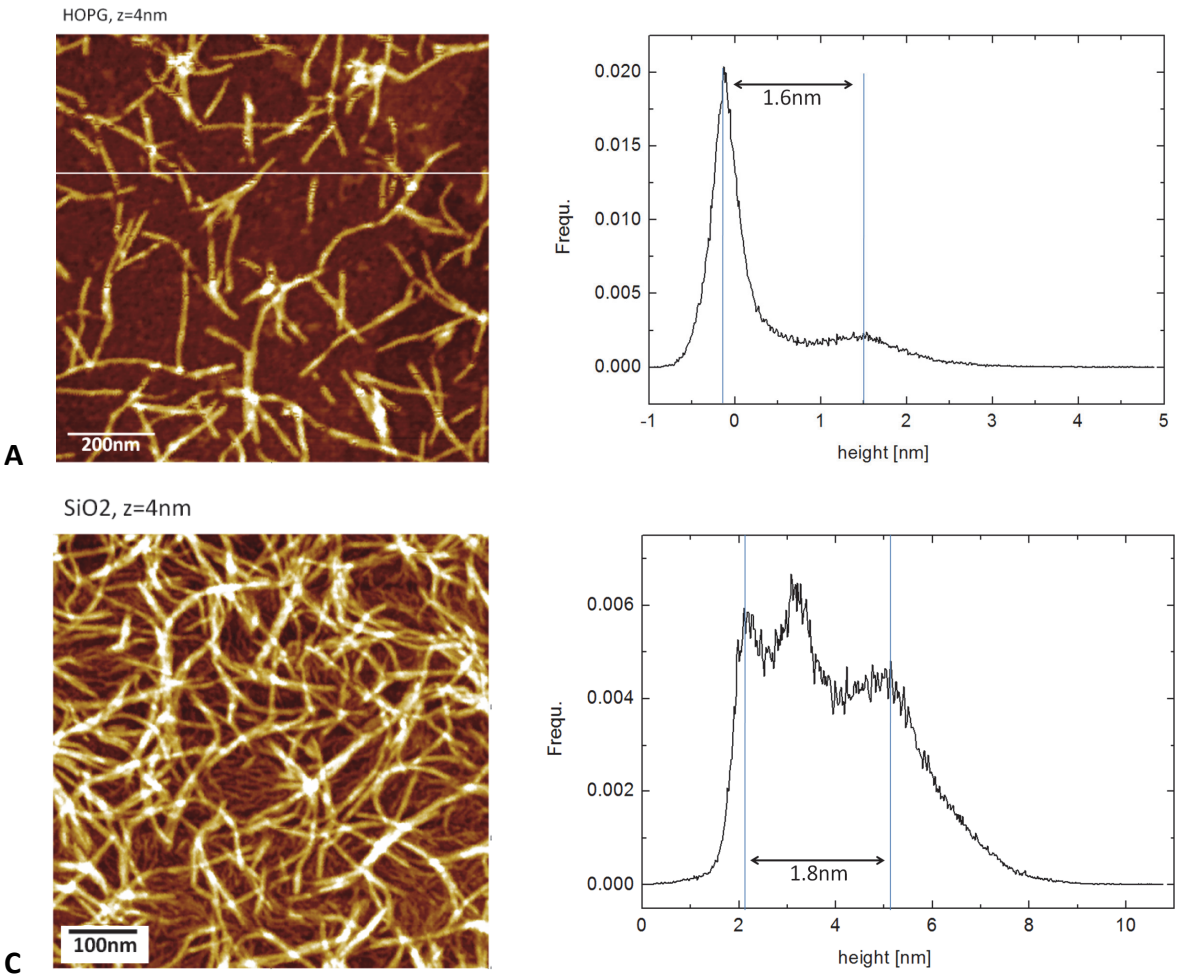

Fig. 2. Morphology of IBS deposited on hydrophobic and hydrophilic surface. 1mg/mL aqueous IBS solution are spuncoat on HOPG (A) and SiO2 (C); Left: AFM images, z range 4 nm. Right: Corresponding height histogram of AFM images.

Spin coating 1 mg/mL aqueous solutions of IBS on SiO2 results in a complex binary structure featuring an uppermost network of large fibers with widths *w*=19 ± 5 nm, and thickness 1.8 ± 0.2 nm, roughly comparable to IBS long axis (≈1.57 nm), thus indicating a vertical arrangement of the molecules; beneath this, another network of smaller fibers is visible on SiO2 (see Fig. 2) having widths *w*=10±2 nm, and heights 1.0 +/- 0.2 nm, roughly comparable to IBS short axis (≈0.8 nm, depending if sulphonic and CO groups are considered or not).

Spin coating on highly oriented pyrolytic graphite (HOPG) yields a similar upper layer of large smooth belt-like structure with average widths *w*= 22 ±5 nm, and heights 1.6 +/- 0.2 nm. Below this, there are no smaller fibers, but a disordered coating of molecules. Details on image analysis are reported in the methods chapter.

From AFM results, we extract that the upper network of larger fibres exhibit similar morphology on both substrates with comparable fibre height and width. This finding suggests that the fibres form in solution during solvent evaporation rather than on the substrate.

Hydrophilic-hydrophobic interactions are key to properties of such amphiphilic molecules:

IBS undergoes solution phase self-assembly into π-stacks, typically resulting from the amphiphilic nature of such dyes: Indanthrone bisulphonate shall form in solution a liquid crystal phase by a self-assembly process driven by the hydrophobic effect: this supramolecular assembly results in large solution-assembled stacks and, in higher dye concentrations, to hydrogel formation (see following sections).

Conversely, the layer in direct contact with the substrate depends on the substrate, showing highly ordered fibres on SiOx and no self-assembling on HOPG. The weaker self-assembly on HOPG is an indication for a stronger interaction with the hydrophobic graphite surface (as compared to the SiO2 substrate)[12] that allow IBS molecules to interact and self-assemble on the surface.

7.2.2 Dye adsorption on bulk graphite

We first estimated the interaction of the molecule with pristine, bulk graphite. To this aim, we used an approach we described in previous work; [8] for the spontaneous adsorption experiment, aqueous IBS solutions with concentration of c= 1.8*10^-5 mol/L and constant volume of 15 mL were exposed to an increasing amount of graphite flakes having a surface of 6.5 m^2/g (as measured from the producer, Aldrich graphite nano-powder, particle size below 20μm). The dye solutions were exposed to graphite powder for 5 days, applying gentle stirring in order to prevent from artefacts originating from diffusion limits.

The results of the spontaneous sorption experiment is reported in Fig. 3; we found that most of the dye remains in solution when exposed to lower amounts of graphite (<< 4 nm^2/mol). In case of an excess in graphitic substrate (>4 nm^2/mol) in respect with the dye we expect most of the dye adsorbing on a pristine graphite surface.

The adsorption process saturates at up to 80% of the molecules removed from solution with increasing graphitic surface area present. The adsorption process of IBS on graphite powder does not reach 100%, in agreement with what we previously observed with pyrene disulphonate moieties discussed before. [8]

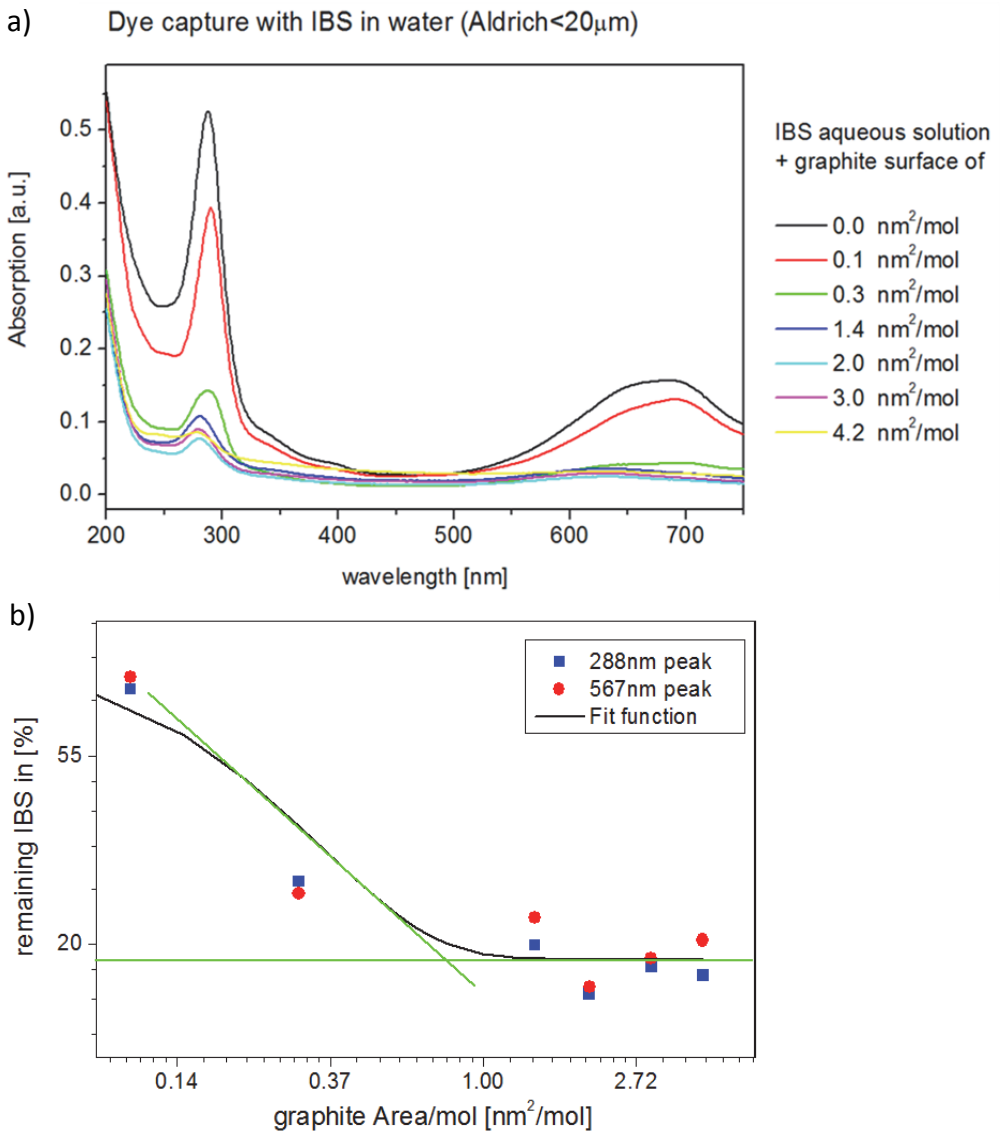

Fig. 3. Spontaneous dye sorption on graphite micro-powder, aqueous IBS solutions with c= 1.8*10^-5 mol/L and constant volume of 15 mL were exposed to an increasing graphite surface and stirred gently for 5 days. a) The absorption spectra show the remaining dye in solution after exposure to graphite. b) Remaining IBS concentration as a function of surface/molecule ratio, black line indicates first order exponential decay as fit function, green line indicate asymptotic values for sorption regime and saturation regime.

7. Processing of graphene suspensions into polymer composites

In principle it is not possible to directly correlate the quantity of molecules adsorbed on a substrate with the molecular packing on the substrate, because of the likely presence of multilayers and preferential adsorption at defects of the graphite substrate. Here, however, we assume that most of the surface of the graphite flakes used is flat, high quality graphite; with minor contribution from edges and defects, and that the great excess of graphite surface available going from monolayer to sub-monolayer coverage will favour adsorption of single molecules on graphite rather than formation of multilayers.

By increasing the amount of graphite surface available/molecule, it is thus possible to estimate the transition from monolayer to sub-monolayer coverage.
The adsorption reaches saturation at graphite surface to molecules ratio of ca. 0.8 nm^2/mol (see Fig. 3). Relating this value to a molecular footprint of ≈1.3 nm^2/mol for IBS (assuming roughly a length of 1.6 nm and a width of 0.8 nm), we speculate that our results rather points towards a tilted adsorption of the molecule on graphite than for a flat surface arrangement.

7.2.3 Exfoliation of graphene with indanthrone bisulphonate

When sonication is applied to the solution, graphite exfoliation takes place, yielding dark solutions (Fig. 4). At typical high concentration of IBS (5 mg/mL) hydrogel formation through supramolecular interaction is observed as well after exfoliation. Therefore, a concentration study was necessary to estimate the most promising dye concentration for polymer composites, in terms of suspension processability, graphene yield and purity of graphene suspension. Bulk graphite flakes with a constant concentration of 50 mg/mL were sonicated for 4.5 hours with 0.1 mg/mL, 0.5 mg/mL, 1.0 mg/mL, 2.5 mg/mL and 5.0 mg/mL IBS dye respectively. All dye contents yield dark dispersions after sonication and centrifugation (1500 rpm for 15 minutes), with a strong blue colour being predominant in the suspensions with highest dye content. After one week, slight precipitation of black aggregates is observed with 0.1, 0.5 and 1.0 mg/mL IBS suspensions. With an IBS concentration of 2.5 mg/mL, dye and possibly graphene precipitates. In all cases, a possible precipitate is redispersed homogeneously with agitation.

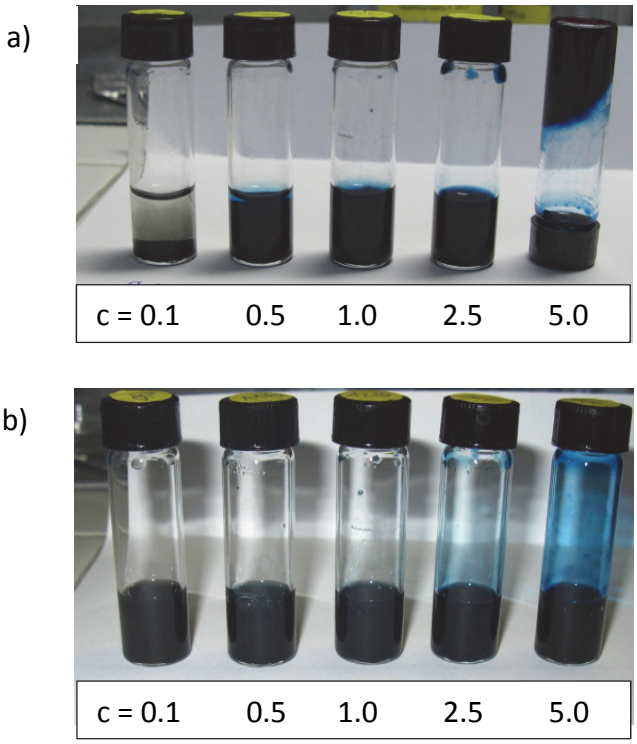

Fig. 4. Graphene suspensions obtained with exfoliation in different IBS concentrations. 0.1, 0.5, 1.0, 2.5 and 5.0 mg/mL IBS were tested. a) Suspensions after settling for one week; b) redispersed suspensions upon agitation.

7. Processing of graphene suspensions into polymer composites

The graphene suspension with highest dye content (5mg/mL) forms a metastable gel that is easily solubilized with agitation. UV/VIS absorption spectra were taken after sonication and centrifugation. In the case of 0.1mg/mL IBS, the graphene light absorption is nearly featureless with a slowly decaying slope over the visible range, reflecting absorption and a maybe of scattering caused by the dispersed flakes.

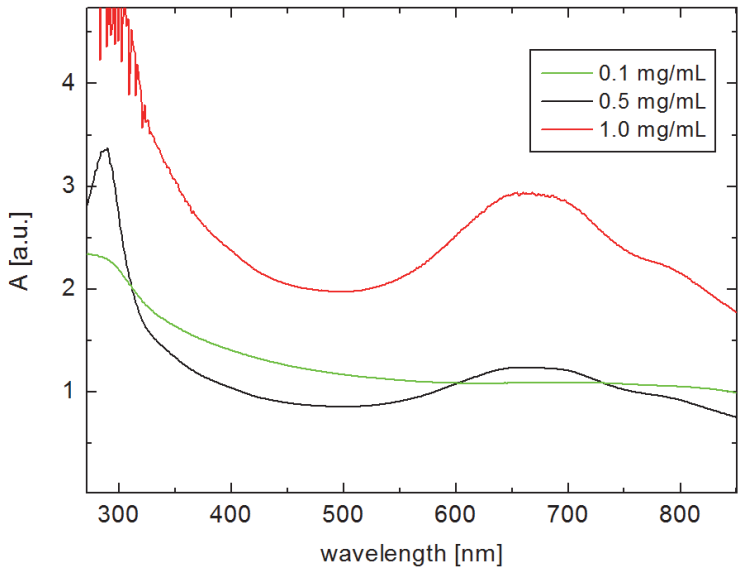

Fig. 5. UV/VIS absorption of graphene/IBS blends obtained with different IBS concentrations in water. The samples were diluted 1:10 for measurement and are reproduced dilution corrected, absorption spectra at higher concentrations than 1.0 mg/mL are not reproduced here because gel formation is observed.

With exfoliation in 0.1 mg/mL IBS solution (green spectrum, Fig. 5), no peaks due to IBS are visible, indicating that such low concentration of dye is sufficient to stabilize the nanosheets in solution, in agreement with what observed for pyrene dyes. [8] Dye concentrations of 0.5 and 1.0 mg/mL show a clear contribution of IBS peaks to the UV/Vis absorption, an indication for a significant amount of excess dye as reported [13]. Higher dye concentrations (2.5mg/mL and 5mg/mL) do not allow for quantitative absorption measurements due to high viscosity, gel formation and saturated light absorbance.

The nearly featureless graphene light dispersion in the case of 0.1 mg/mL IBS suggests a clean graphene-organic hybrid system, with minimum amount of excess in IBS. Therefore a concentration of 0.1 mg/mL IBS was chosen for further characterization and experiments.

7. Processing of graphene suspensions into polymer composites

We then analyse the obtained graphene flaked with microscopy:

The flake morphology in pristine graphene/IBS hybrid suspensions is shown for exfoliation in 0.1mg/mL aqueous IBS solutions. SEM images confirm the typical mixture of graphene nanoplatelets with rather graphitic character as suggested from the contrast observed with SEM, typically having lateral size of some hundreds nm.

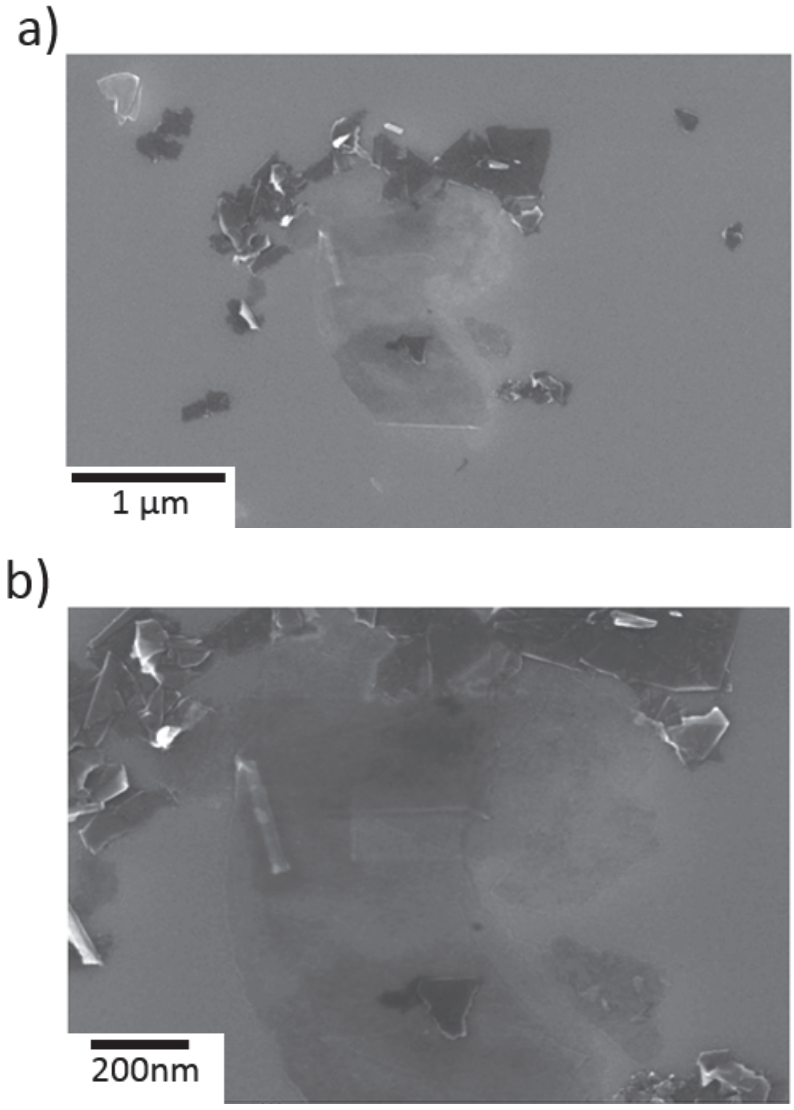

Fig. 6. Morphology of IBS exfoliated graphene flakes. a) SEM image of IBS exfoliated graphene, b) zoom on graphene flake. The samples were prepared from dropcasting as-prepared suspensions on Si substrates.

Some large, thin graphene sheets with up to 2 µm lateral dimension are observed. These flakes are folded and almost transparent to the electron beam, indicating a low number of layers.

7.2.4 Bulk composite processing

The as-prepared GNP suspensions were subsequently filtrated over a 0.2 µm acetate filter. We assume that the functionalization of graphene with IBS, which leads to stabilization in water, allows as well for filtration and re-dispersion of the material without major re-aggregation of the exfoliated graphene nanoplatelets. Once deposited on a filter, the black graphene film is redispersed easily and nearly quantitatively with slight sonication for one minute.

For final formulation of polymer/graphene suspensions of a given graphene filler content, the respective amount of GNP powder was redispersed in polymer solution (4% Poly(vinyl alcohol) Mw 9,000-10,000, 80%hydrolyzed (PVA10)) to obtain suspensions with varying PVA/GNP dry mass ratio. UV/VIS spectra confirms that PVA suspensions with relative graphene-hybrid filler loadings of 0.1 w%, 0.5 w%, 1.0 w%, 1.5 w% and 3.0 w% were achieved. Absorption spectra were taken of diluted suspensions (factor 1:10) to ensure linearity in spectrometer's detector response.

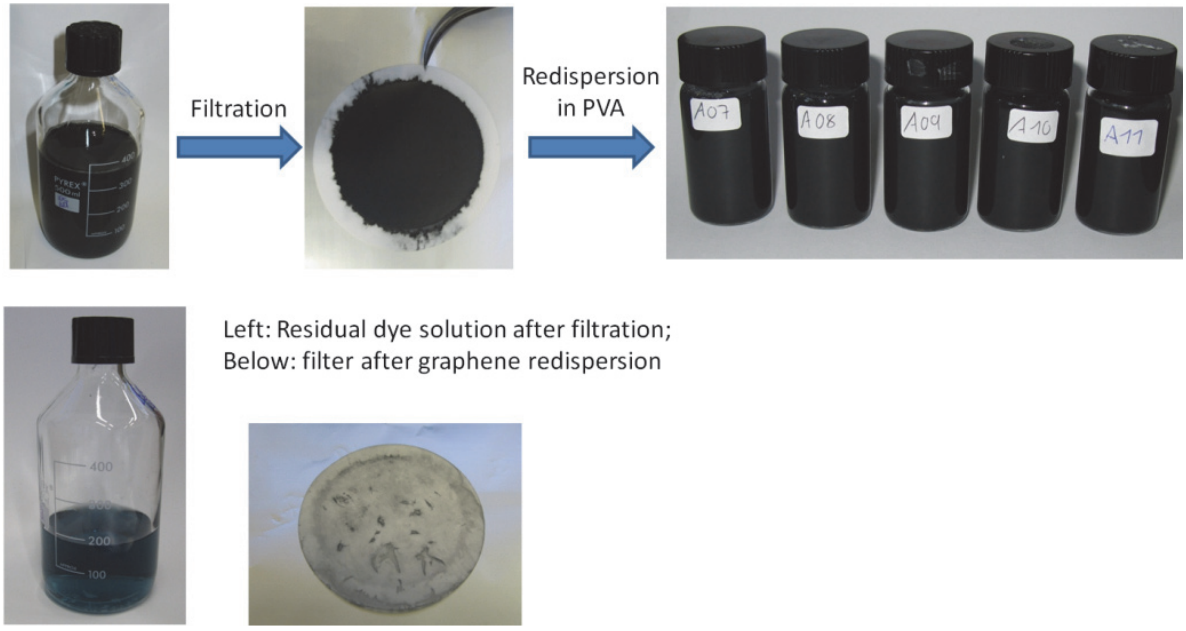

Fig. 7. Process for preparation of graphene/IBS in polymer dispersion with filtration and redispersion in a 4% aqueous Poly(vinyl alcohol) Mw 9,000-10,000, 80%hydrolyzed (PVA10) solution. Below: Aqueous residual containing excess indanthrone. Filter after redispersion.

7. Processing of graphene suspensions into polymer composites

PVA membranes are produced easily with drying polymer/graphene suspensions in a suitable mould. For this, 4 mL of suspension were transferred into plastic moulds and dried slowly at room temperature within 2-3 days. The dried composites form self-standing PVA membranes, blended with increasing filler content. These composites are then tested in electrical conductivity measurements (Fig. 8).

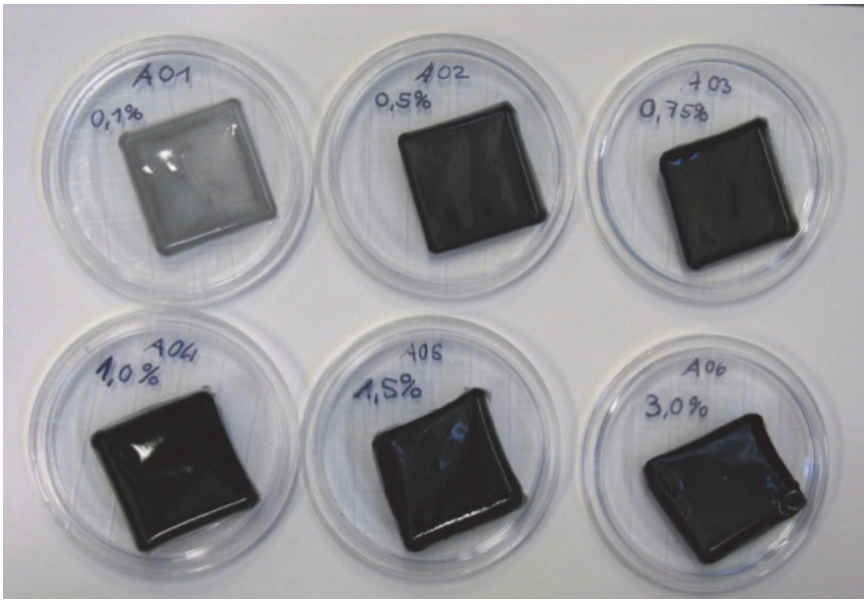

Fig. 8. Self-standing PVA membranes with increasing graphene filler content. The membranes were produced in a mould; upon drying free-standing PVA membranes are obtained with filler weight content of 0.1 %, 0.5 %, 0.75%, 1.0 %, 1.5 % and 3.0 %.

7.2.5 Characterization of polymer composites

Conductivity measurements of these bulk composites are reported in Fig. 9. The conductivity ranges from 10^{-12} S/cm for pure PVA to 10^{-2} S/cm in composites containing 3% GNP. The significant decrease in the specific volume resistivity indicates that the percolation threshold is attained with about 1 wt% GNP content. This filler level is significantly lower than the one typically observed for carbon black additives and can be attributed to the highly anisotropic morphology of GNPs.

In terms of applications this resistance level does not reach the conductivity which is required electromagnetic interference shielding (that is about 1 S/cm), but it does satisfy requirements for electrostatic discharge which requires specific volume resistivity values of 10^{-10} S/cm and below). Besides bulk characterization, we also measured the surface conductivity of the composite, to detect the eventual presence inhomogeneous dispersion of the nanosheets in the composite.

Surface conductivity of the lower side of the mould shows a trend similar to what observed for bulk conductivity, with ≈6 orders of magnitude increase (Fig. 9). However, conductivity of the top surface (i.e. the one exposed to air during the solvent evaporation) showed erratic results, with no clear correlation with GNP content, likely due to an uneven distribution of the material in the composite.

a)

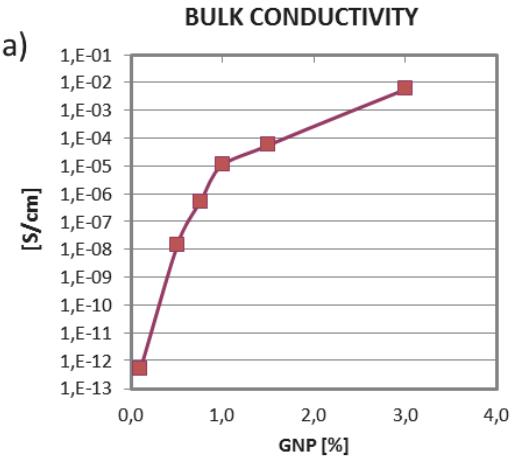

b)

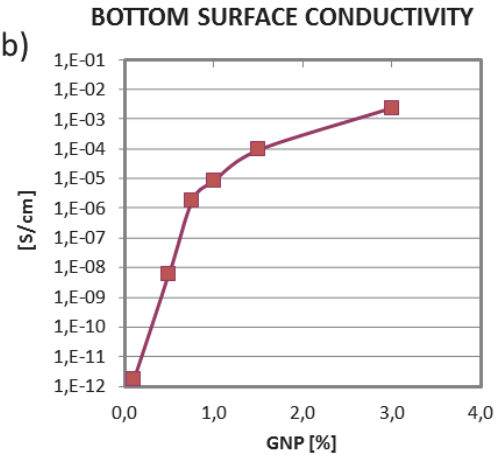

c)

GNP %	Thickness [mm]	Top spec. R (ohm)	Bottom spec. R (ohm)	Top spec. Cond. (S/cm)	Bottom spec. Cond. (S/cm)
0.1	0.0240	-	-		
0.5	0.0380	1.8E+04	4.2E+10	1.5E-02	6.3E-09
0.75	0.0470	3.8E+04	1.1E+08	5.5E-03	1.9E-06
1	0.0520	1.2E+08	2.1E+07	1.6E-06	9.0E-06
1.5	0.0560	1.4E+08	1.7E+06	1.3E-06	1.0E-04
3	0.0680	6.4E+08	6.0E+04	2.3E-07	2.5E-03

Fig. 9. Electrical conductivity as a function of filler load, a) bulk conductivity and b) bottom surface conductance. Table c) reports measurement data for membranes with different GNP filler contents.

To better unravel the origin of this non-conclusive conductivity behaviour, SEM was used to image the flake distribution and alignments along the membranes cross-section, top and back side respectively. Fig. 10 reports a typical SEM image of the cross section (black arrow) or surface

(white arrow). The image confirms the presence densely packed small polymer particles with some cracks with lateral dimension of several tens of nanometres. Note that these defects may be created with fracturing the freeze dried samples.

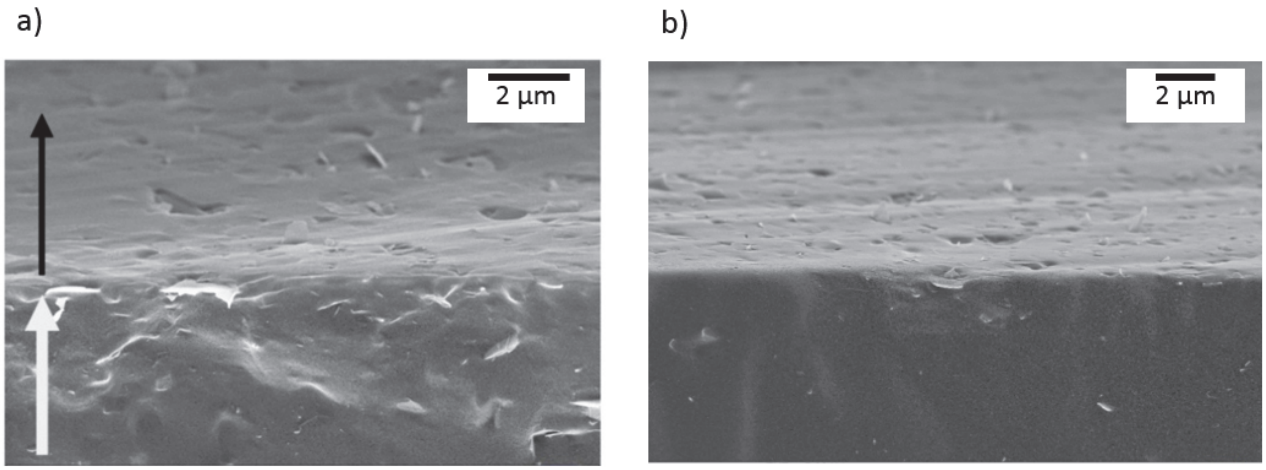

Fig. 10. Typical morphology of bulk membrane cross-sections obtained with SEM. The membrane shown here contains 3.0% graphene filler, sample was prepared on an alumina support. The cross-sectional sample was obtained by fracture of freeze dried membranes, sputtered 35s with Au. a) reverse side; b) top side.

In all graphite concentrations, the flakes are coated with polymer indicating that the polymer sticks well on graphene. However, GNPs are arranged with random orientation and not aligned horizontally as could be expected in this slow drying process. For the PVA membrane containing 3.0 % GNP filler shown in Fig. 10, graphene flakes are both on the surface and in the bulk, however the bulk concentration shows a significant gradient in flake distribution, with higher flake concentrations on the alumina support and lower concentrations on the top of the samples. This gradient is likely resulting from the flakes settling during the slow drying process, explaining the significant difference observed with surface conductivity measurements on top and reverse side.

7.3 Discussion

In the previous sections we described the complete process of exfoliating, processing and embedding in composites of graphene nanoplatelets functionalized with IBS, an industrial dye. The whole process, even if performed on lab scale, can be easily up-scaled, and adapted for other

graphene production techniques, such as ball milling [14] or shear mixing. [4] We did not use for this process any complex purification step (such, as example, density gradient ultracentrifugation), [15] which could be effective in purifying the GNP and increase the fraction of monolayer graphene.
While mono- or bi-layers are fundamental for electronic applications such as transparent conductive layers, in composites application cost is a much stronger issue, and the use of GNP instead of pure graphene is for this intensively studied. [16]

We attribute the eligibility of IBS in dispersing GNP into aqueous solutions to its amphiphilic nature and the tendency to self-assemble through π-π interaction:
The amphiphilic nature of indanthrone bisulphonate makes it a lyotropic dye, forming liquid crystal phases upon the addition of a solvent. Lyotropic liquid crystal phases in those materials are formed by a process of self-assembly that is driven by the hydrophobic effect. The reversible gel formation can be attributed to self-assembly of IBS in solutions of higher concentrations (>2.5 mg/mL) into massive π-stacked rod-like aggregates in agreement with literature (see Fig. 11 and Ref. [13]).

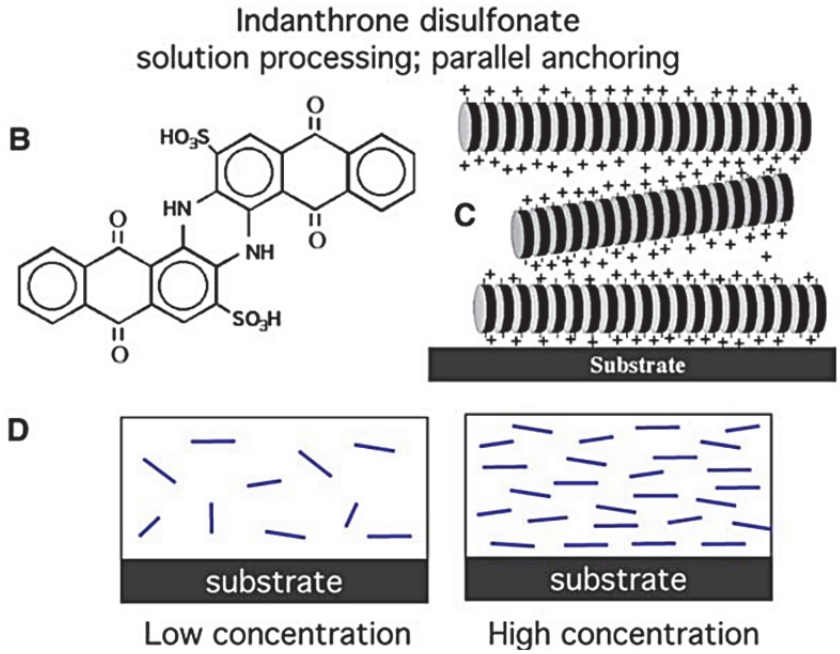

Fig. 11. Liquid crystalline precursors used in this study and their self-assembly in liquid phase. Panel B: indanthrone disulphonate, a lyotropic liquid crystal whose rod-like aggregates in aqueous solution anchor parallel to substrates (Panel C), and align as concentration increases (Panel D). Reproduced with permission from Ref. [13].

As graphene has been demonstrated to be a good template for π-π driven self-assembly (for review, see Chapter 1 and Ref. [10]), non-covalent functionalization of graphene in IBS solution allows direct exfoliation in water, even with dye concentration as low as 0.1 mg/mL, yields up to 0.2 mg/mL of suspended GNP. The graphene/IBS hybrid can be readily redispersed in a polyvinyl alcohol matrix with different loadings of graphene filler.

Bulk PVA-based composite membranes were successfully formed with the exfoliated graphene/IBS hybrid. The percolation threshold was reached with only a 0.8 wt% loading in PVA; a non-uniform distribution of the GNP in the polymer was demonstrated by comparing surface and bulk conductivity measurements. This non-even distribution is a common issue in processing nano-materials such as GNP or carbon nanotubes, and was mainly due to the technique used (moulding). We expect that using most suitable techniques, commonly used at industrial scale, a much better distribution shall be obtained.

While it is quite straightforward to compare the different efficiency of surfactants to exfoliate graphene,[17] it is much more difficult to estimate the industrial economic viability of a given technique to produce graphene on large scale. The approach described here, that does not use a normal soap to stabilize graphene, but a dye highly compatible with industrial application, could be a feasible way to translate the graphene technology from a scientific breakthrough to a true scientific revolution.

7.4 Experimental

Materials. IBS was provided by BASF, Ludwigshafen, Poly(vinyl alcohol) Mw 9,000-10,000, 80%hydrolyzed (PVA 10) from Aldrich. All molecules were used as received. Spontaneous dye adsorption experiments were done with Aldrich synthetic graphite powder, <20 μm.

Preparation of GNP-hybrid – PVA dispersions. GNP-IBS hybrid dispersions were prepared by direct LPE of graphite. Natural graphite flakes (3 mg/mL, Aldrich) were sonicated in aqueous solutions of IBS of 0.1 mg/mL for 4.5 hrs. Graphene/IBS was extracted from liquid phase with filtration. Polymer dispersion were prepared with redispersion in a 4% aqueous Poly(vinyl alcohol) Mw 9,000-10,000, 80%hydrolyzed (PVA10).

Characterization. AFM measurements were carried out using a Digital Instruments AFM (NT-MDT), using Nanoprobe cantilevers (model: RTESP, material: 1–10 Ohm cm phosphorus (n) doped Si, f0: 27–309 kHz, k: 20–80 N m^{-1}; from Veeco) operating in tapping mode. The Scanning Electron Microscopy (SEM) images were obtained with a ZEISS 1530 instrument. Absorption spectra were recorded using a Perkin-Elmer Lambda 20 spectrometer.

References

(1) Stankovich, S.; Piner, R. D.; Nguyen, S. T.; Ruoff, R. S. *Carbon* 2006, *44*, 3342.
(2) Tantis, I.; Psarras, G. C.; Tasis, D. *Express Polymer Letters* 2012, *6*, 283.
(3) Reuters, T.; Thompson Reuters: 2013.
(4) Paton, K. R.; Varrla, E.; Backes, C.; Smith, R. J.; Khan, U.; O,ÄôNeill, A.; Boland, C.; Lotya, M.; Istrate, O. M.; King, P.; Higgins, T.; Barwich, S.; May, P.; Puczkarski, P.; Ahmed, I.; Moebius, M.; Pettersson, H.; Long, E.; Coelho, J. o.; O,ÄôBrien, S. E.; McGuire, E. K.; Sanchez, B. M.; Duesberg, G. S.; McEvoy, N.; Pennycook, T. J.; Downing, C.; Crossley, A.; Nicolosi, V.; Coleman, J. N. *Nat Mater* 2014, *13*, 624.
(5) Hoffman, R. C.; Stetyick, K. A.; Potember, R. S.; McLean, D. G. *J. Opt. Soc. Am. B* 1989, *6*, 772.
(6) Nazarov, V. V.; Sidorenko, E. N.; Google Patents: 2005.
(7) Guo, F.; Mukhopadhyay, A.; Sheldon, B. W.; Hurt, R. H. *Advanced Materials* 2011, *23*, 508.
(8) Schlierf, A.; Yang, H.; Gebremedhn, E.; Treossi, E.; Ortolani, L.; Chen, L.; Minoia, A.; Morandi, V.; Samori, P.; Casiraghi, C.; Beljonne, D.; Palermo, V. *Nanoscale* 2013, *5*, 4205.
(9) Backes, C.; Schmidt, C. D.; Rosenlehner, K.; Hauke, F.; Coleman, J. N.; Hirsch, A. *Advanced Materials* 2010, *22*, 788.
(10) Yang, H.; Hernandez, Y.; Schlierf, A.; Felten, A.; Eckmann, A.; Johal, S.; Louette, P.; Pireaux, J. J.; Feng, X.; Mullen, K.; Palermo, V.; Casiraghi, C. *Carbon* 2013, *53*, 357.
(11) An, X. H.; Simmons, T. J.; Shah, R.; Wolfe, C.; Lewis, K. M.; Washington, M.; Nayak, S. K.; Talapatra, S.; Kar, S. *Nano Letters* 2010, *10*, 4295.
(12) Palermo, V.; Samori, P. *Angewandte Chemie-International Edition* 2007, *46*, 4428.
(13) Chan, C.; Crawford, G.; Gao, Y.; Hurt, R.; Jian, K.; Li, H.; Sheldon, B.; Sousa, M.; Yang, N. *Carbon* 2005, *43*, 2431.
(14) Kouroupis-Agalou, K.; Liscio, A.; Treossi, E.; Ortolani, L.; Morandi, V.; Pugno, N. M.; Palermo, V. *Nanoscale* 2014, *6*, 5926.
(15) Bonaccorso, F.; Sun, Z.; Hasan, T.; Ferrari, A. C. *Nat. Photonics* 2010, *4*, 611.
(16) Gong, L.; Kinloch, I. A.; Young, R. J.; Riaz, I.; Jalil, R.; Novoselov, K. S. *Advanced Materials* 2010, *22*, 2694.
(17) Guardia, L.; Fernandez-Merino, M. J.; Paredes, J. I.; Solis-Fernandez, P.; Villar-Rodil, S.; Martinez-Alonso, A.; Tascon, J. M. D. *Carbon* 2011, *49*, 1653.

Chapter 8

Methods for production, characterization and processing of graphene suspensions

8.1. Graphene in suspension

8.1.1. Liquid phase exfoliation and centrifugation

Graphene flakes can be produced by exfoliation of graphite via wet chemical dispersion, followed by ultra-sonication. This process is commonly referred to as graphite liquid phase exfoliation of graphene. In sonication, activation is based on the physical phenomenon of acoustic cavitation: Cavitation is a mechanical process in which activation destroys the attractive forces, in our case interlayer forces within the graphite crystal in the liquid phase. Applying ultrasound, compression of the liquid is followed by rapid expansion; the sudden pressure drop created forms small, oscillating bubbles of gaseous substances in the liquid medium. These bubbles expand with each compression/expansion cycle of the applied ultrasonic energy. When the bubbles reach an unstable size; they can collide and/or violently collapse. [1] Such sono-chemically applying shear forces and cavitation on the bulk graphite material induces exfoliation of the crystal into thinner fragments and graphene flakes. [2]

In this work, a bath sonicator with adjustable sonication power and a sonication frequency of 37 kHZ was applied (Elmasonic). As ultrasonic energy is a mean to effectively apply mechanical force on graphite, this energy must be transmitted through a liquid medium to the bulk surfaces to be exfoliated; the selection of an eligible liquid medium is not only key in the exfoliation step, but particularly to the final stabilization of graphene in suspension.

Following the exfoliation step, solvent–graphene interactions need to be balanced in order to avoid attractive forces between the sheets that could cause destabilization of the sheets in suspension. Solvents being ideal to disperse graphene are those that minimize the interfacial tension between the liquid and graphene flakes, i.e. the force that minimizes the area of the surfaces in contact. In selected organic solvents such as NMP, DMF or oDCB, graphene can be dispersed into surfactant-free pure solvents.[3-6] In other solvent systems, using a surfactant can help to overcome inter-sheet attractive forces that destabilize the dispersion and induce re-aggregation and even precipitation of graphene from the liquid phase.

Liquid phase exfoliation of graphite typically results in an ensemble of mono- and multilayer graphene and thicker, graphitic particles. Thicker aggregates and graphitic particles are commonly removed through centrifugation of the freshly prepared dispersions and subsequent decanting of the supernatant.

Different approaches are reported in literature: Density gradient ultracentrifugation (DGU) [7] which is performed in a density gradient medium, sedimentation based-separation centrifugation or centrifugation in a uniform medium [8]. DGU is an emerging approach for production on mono-disperse graphene suspensions; however DGU efforts significantly longer centrifugation times since even the slowest moving species must be afforded enough time to reach their isopycnic points. [9]

Further, the suspension's liquid medium needs to be exchanged with a density gradient medium which prevents from application of this method for in-situ processed graphene-organic hybrid materials. In this thesis, sedimentation based separation is applied; this process separates suspended particles on the basis of their sedimentation rate [8], caused by centrifugal force acting to the particles. Sedimentation based separation is the most common separation strategy, of which suspensions of graphene or derivatized graphene flakes with dimensions ranging from few nanometers to a few microns have been obtained.[3,5,10,11]

8.1.2. Quantifying concentrations of graphene in suspension

Gravimetric analysis is commonly applied for concentration measurements; in this case, a distinct volume of graphene suspension is deposited on a filter and the residue is weighted. The method is less eligible for our system: the filtered material is made up not only of graphitic flakes, but contains surfactants or solvents and residual from the filter [3,12] which may cause artefacts and problems in reproducibility to the concentration measurement. Thermo-gravimetric (TGA) analysis can be used in addition to determine the weight percentage of graphitic material in the filtrate, allowing the measurement of the actual graphene concentration c, but this method is time consuming and needs careful sample preparation for reproducible results. To quantify and compare liquid phase exfoliation

procedures, it is key having a fast and reliable method accessible to measure the concentration of dispersed graphitic material.

The most convenient and reproducible way to calculate the concentration c [g L−1] of dispersed graphene organic hybrid materials is to apply UV/VIS absorption. Here, c is usually determined exploiting the Beer-Lambert Law:

$$A = \alpha c l$$

Where A is the absorbance, α [L g^{-1} m^{-1}] is the absorption coefficient and l[13] the length of the optical path. α can be determined experimentally, for example by filtering a known volume of dispersion onto a filter of known mass [3,5,12,14], and subsequently measuring the resulting mass using a microbalance after careful drying of the sample. Another way for measuring α of an unknown graphene organic hybrid suspension is to re-disperse a distinct mass of graphene nano-powder in the respective solvent system.

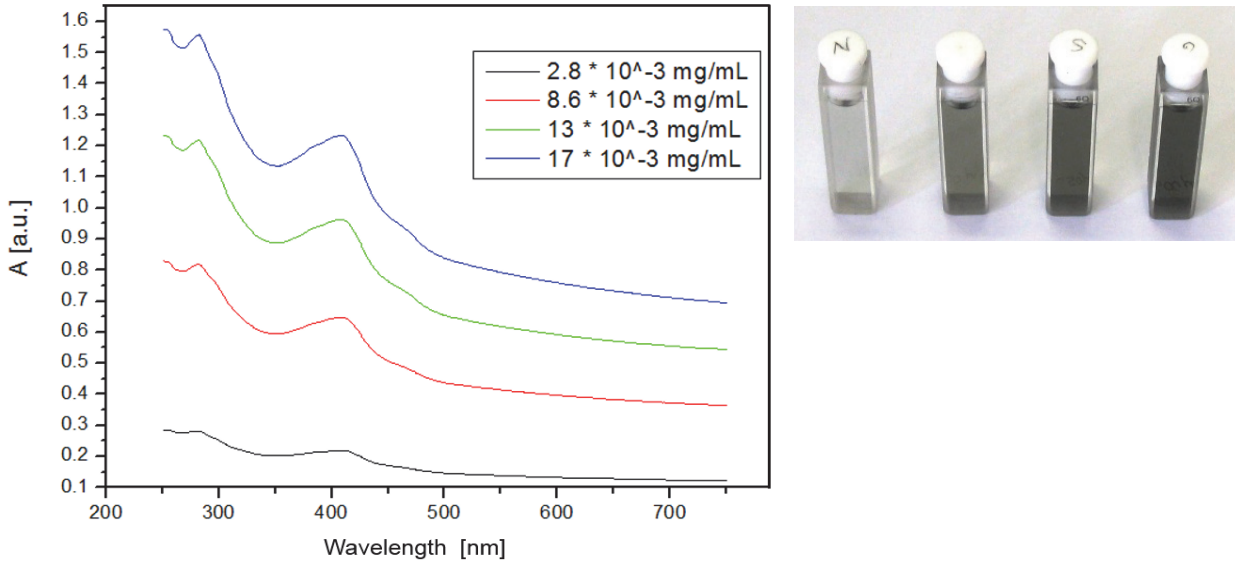

Fig. 1. Measuring α for a new graphene organic hybrid system. As an example, the absorption spectra of graphite nano-powder re-dispersed in 1.8 * 10`-4 mol/L PS2 solution and the corresponding picture is shown, at four selected graphite concentrations (increasing concentration from left to right).

In recording absorption spectra of several dilutions, α can be extracted graphically from the Lambert-Beer plot (Fig. 2).

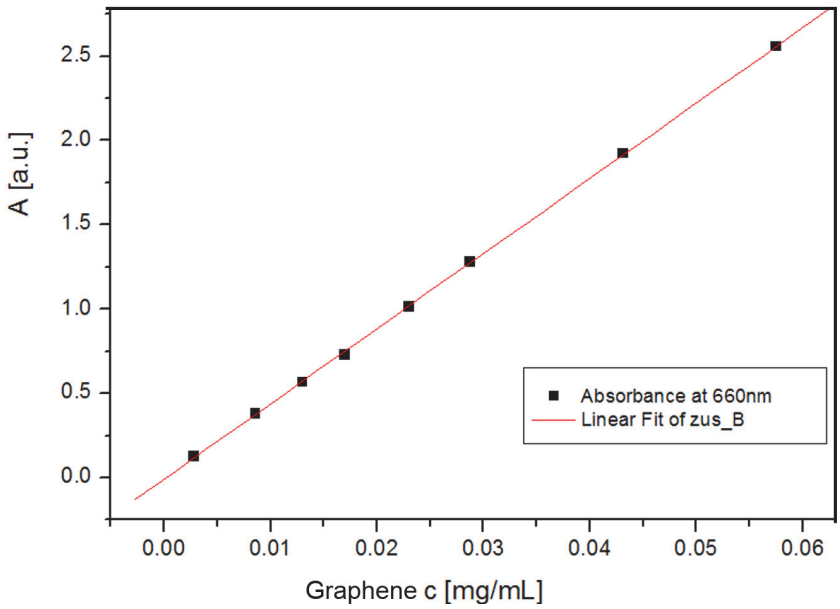

Fig. 2. Lambert-Beer plot. This example shows graphite nano-powder re-dispersed in PS2 aqueous solution, absorption values at 660 nm are related to the concentration of nano-powder.

Different values of α have been reported both for aqueous and non-aqueous-based graphene dispersions: Reference [3] reports α~2460 L $g^{-1}m^{-1}$ for a variety of solvents such are N-Methyl Pyrolidone (NMP), Dimethyl-formamyde (DMF), etc., while later, Ref. [5] found α ~3620 L g^{-1}m−1 for NMP. The value applied in this thesis for mass concentration calculations is indicated in the respective chapters.

8.2. Strategies for excess dye management

Excess dye management is often key when it comes to application of graphene-organic hybrid materials; most strategies are based on separation of dissolved species (such are dyes) and suspended particle matter (graphene or functionalized graphene in liquid phase). Here, we investigate separation techniques based on mechanical or thermo-dynamical separation, respectively.

Separation techniques	
Mechanical	Thermodynamical
Centrifugation	Adsorption
Filtration	Dialysis

Fig. 3. Table suggesting physico-chemical separation techniques based on a mechanical or thermodynamically driven separation.

Mechanical separation is based to different response of dispersed matter and dissolved species towards mechanical force; such is gravity in the case of centrifugation. With filtration, interposition of a porous medium allows for separation of liquid and solid applying pressure.

8.2.1. Dialysis

Dialysis has been tested for excess dye management of aqueous graphene suspensions.

The physico-chemical principal of this separation technique is differential diffusion: A dialysis tube (purchased from Visking tube) was used, namely a semi-permeable membrane with cut-off at 12 000 Dalton, to separate small, well dissolved molecules from graphene in solution.

a)  b) 

Fig. 4. Excess dye management with dialysis. Pictures show PS4 exfoliated graphene in aqueous suspension a) before and b) following extensive dialysis.

The graphene-hybrid suspensions are transferred into a Visking tube and sealed (see Fig. 4). The sealed samples are then transferred into a large volume of water (2.5 L) which was exchange on a daily basis.

Dialysis provides separation without loss in graphene particles; however, for our systems, we found this method less effective: As the separation relies on a physico-chemical diffusion process, the method is very time consuming and – as large amount of solvent are necessary with our setup -not transferable for application in non-aqueous systems. In addition, direct monitoring and therefore controlling of the diffusion process is not accessible and may result in issues in reproducibility and suspension stability, for example through precipitation of graphene if the dye concentration becomes too low (see Fig. 4b).

8.2.2. Centrifugation based solvent exchange

The mixture of dispersed graphene hybrid material and excess dye is centrifuged to force the denser solid to the bottom, while the dissolved species, namely the dye, remains in solution. The supernatant containing dissolved dye can then be carefully decanted and replaced with clean solvent. This procedure needs to be repeated for three times to achieve good results.

In more details, we applied the following procedure (a schematic presentation of the process is shown in below):

First, the larger particles of non-exfoliated graphite are removed by mild centrifugation at 1000 rpm for 20 min. The dispersion was then refilled with water, keeping the volume constant in order to maintain information on graphene concentration. The mixture is then slightly sonicated for one minute at low sonication power to re-disperse the graphene. The dispersion is then centrifuged at 12,000 rpm for 20 min, the supernatant carefully decanted and refilled with pure solvent. The procedure is repeated for three times in order to wash the excess exfoliation agent. In a last step, the sample is centrifuged again 20 min at 1000 rpm in order to remove larger aggregates that may not have been ideally re-dispersed upon deposition.

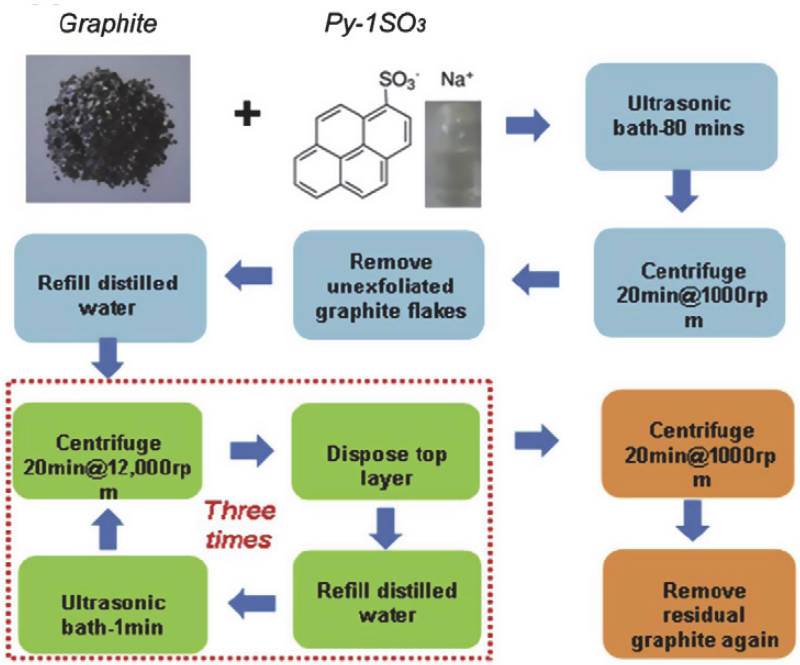

Fig. 5. Schematic of the exfoliation of graphite flakes using 1-pyrenesulfonic acid sodium salt (Py–1SO3). The process includes different steps (mixing, exfoliation, and washing). The washing step is repeated for three times in order to remove the excess Py–1SO3. Image reprinted with permission from Ref. [11].

The centrifugation based solvent exchange procedure yields few and thin layer graphene, however, due to a concentration gradient large loss in graphene concentration. It is a useful

technique for well dissolved dyes and working on laboratory scale, however the procedure needs several steps and is therefore too time consuming and costly for upscaling.

8.2.3. Filtration based solvent exchange

The second separation techniques applied in this thesis is filtration based. The mother suspension is filtrated over a 0.2 µm filter membrane and washed with solvent (Fig. 6). The filtrate, namely the dye solution, is discarded. The graphene hybrids are collected on the filter paper and then easily re-dispersed in the same solvent or a solvent of choice with slight sonication.

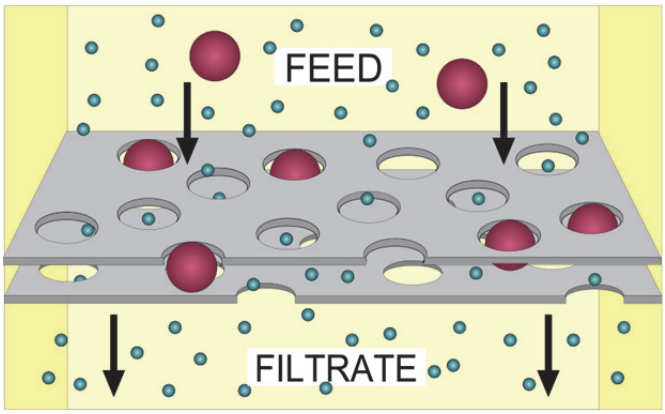

Fig. 6. Scheme demonstrating the filtration principle. The suspensions containing graphene-organic hybrids and excess in exfoliation agent is fed onto the filter membrane, for aqueous systems ususally a cellulose acetate filter paper with pore sizes around 0.2 µm. Reprinted from www.wikicommons.com

We found this method yielding few and thin layer graphene with high yields. It is a simple, fast and up-scalable process, versatile in selection of solvents. However the actual amount of dissolved species removed can be monitored with UV/VIS absorption spectroscopy for not volatile solvent systems, and – depending on the pore size selected for filtration – sheets with lateral dimensions significantly below the pore size are lost.

8.3. Spontaneous dye adsorption experiments

Physical-chemical adsorption on such a high surface area graphitic substrates was used as a model to probe different chromophores for their potential of interacting non-covalently with graphene. Here, we monitor the morphology of the substrate.

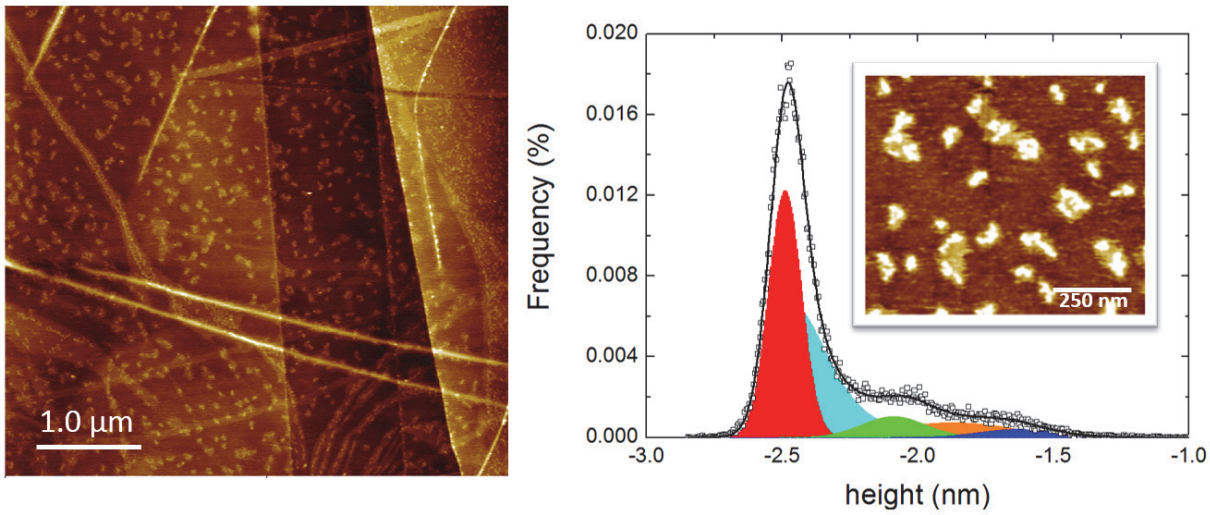

Fig. 7. AFM images of HOPG upon exposure to aqueous solution of PS3. Inset: Zoom (z= 2.2 nm) on main image and corresponding height histogram. Clusters of 0.85 nm and 0.4 nm (+/- 0.15nm) are observed.

Adsorption of dye from solution on HOPG was done as a preliminary experiment since the well-defined clean surface of HOPG allows for monitoring the morphology upon spontaneous sorption of dye. For that, freshly cleaved HOPG was immersed in pure water or a solution of dye, in the images shown below the pyrene derivative PS3. Upon exposure for several day, the HOPG samples were rinsed carefully with water and dried with nitrogen. Fig. 7 shows a typical AFM of HOPG upon exposure to a dye solution and corresponding height histogram. Clusters are found on the surface, particularly on surface defects such as cracks, suggesting that dye was non-covalently adsorbed on HOPG.

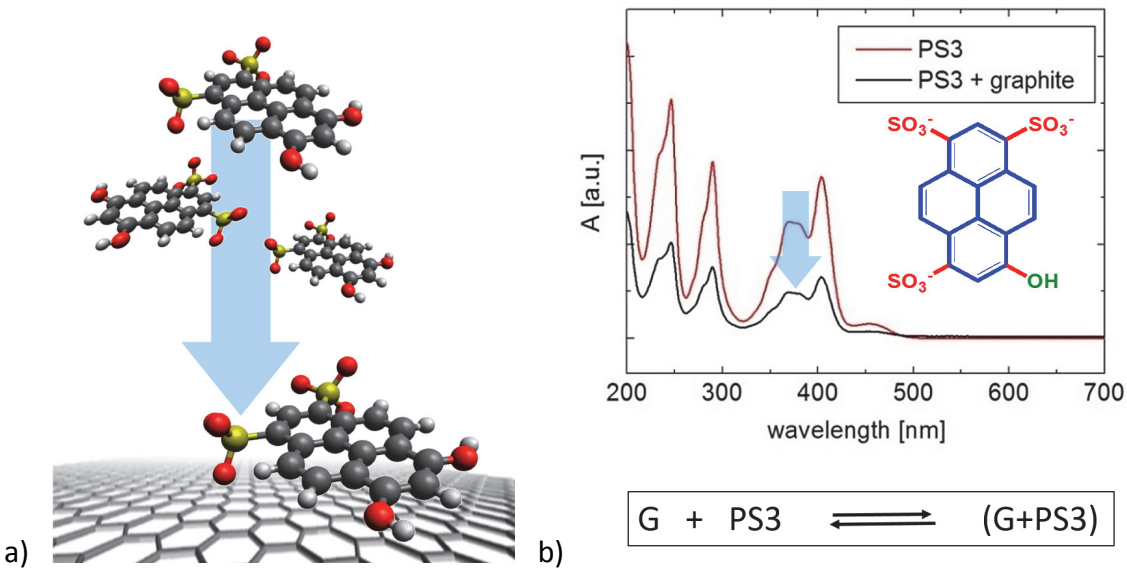

Fig. 8. Spontaneous dye adsorption on graphite powder. a) Schematic presentation of the sorption process, b) Drop in free dye absorption intensity of a PS3 solution upon exposure to graphite.

In order to quantify the spontaneous sorption process, we changed perspective on the experiment, monitoring the residual concentration of dye in solution upon exposure to a graphitic surface (see Fig. 8, a) scheme and b) absorption spectra). Here, we used graphite powder instead of HOPG, allowing for exposure to larger and adjustable graphite surface areas. The adsorption process is an equilibrium balancing the free dye in solution with the associated species (G+PS3). This process may be limited by diffusion; therefore gently continuous stirring was applied.

8.4. Spectroscopic characterization

8.4.1. Steady state absorption, emission and reflectance spectra

All spectroscopic measurements in solution were carried out in cleaned 1cm or 0.1cm quartz cuvettes respectively. Absorption spectra in solution were recorded with a Perkin Elmer Lambda 950 spectrophotometer, using double baseline correction (both 100% and 0% of transmittance). Reflectance spectra of solid films were recorded using an integrating sphere instead of the linear detection system, as the graphene films show high optical density and a rather rough, scattering surface (see 8.4.2 for instrumental details on integrating sphere).

Solid state measurements are performed in reflectance mode to account for the samples' high optical density and diffuse scattering typically found with bulk graphene and nano-platelet films. Surfaces reflect light differently depending on texture, rough or matte surfaces exhibit diffuse reflection, in which the rays of the incident beam are scattered in all directions. Typically, surfaces such as graphene films are in between these two cases, having contribution of both specular and diffuse scattering. In this work, reflectance spectra were used to study the absorption of samples with high optical density, that exhibit a significant contribution of absorption in addition to the scattering components.

8.4.2. Steady state emission – measurement and calculation of quantum yields

deMello et al. (Cavendish Lab, Cambridge, UK) suggested in 1997 a new approach measuring absolute quantum yields in samples of high refractive index samples such as films of conjugated polymers, to circumvent experimental problems arising from an angular distribution of emission, reflectivity and absorbance. As we are facing similar experimental constraints using a linear spectro-photometrical setup with concentrated graphene dispersions, we employ their approach for measuring external quantum yields to our graphene-chromophore hybrid systems in solution phase.

The external radiative quantum yield η is defined as

$$\eta = \frac{\text{number of photons emitted}}{\text{number of photons absorbed}}$$

The experimental setup is based on a commercial spectrophotometer equipped with an integrating sphere. An integrating sphere (IS) is a hollow sphere coated with barium sulfate or another diffusely reflecting material. When placing a light emitting source into the IS, the light is redistributed isotropically over the sphere, eliminating a possible angular dependence of the emission.

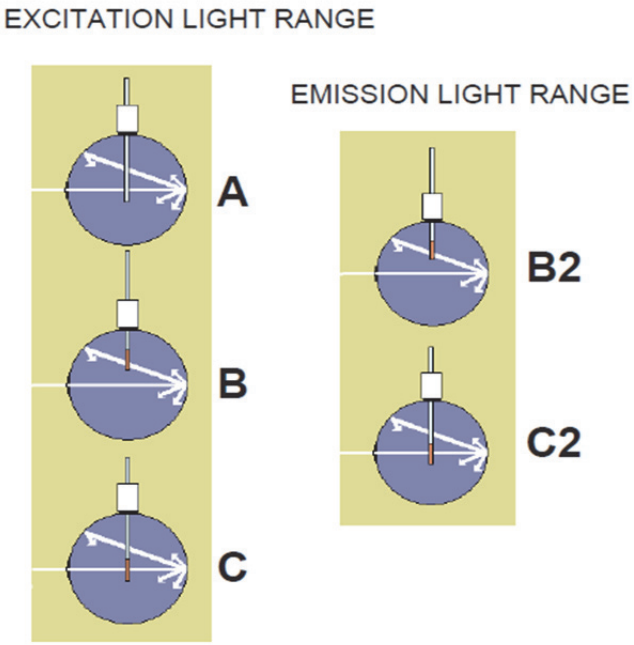

Fig. 9. Description of the de Mello method for the determination of the absolute emission quantum yield, proposed by de Mello et al. Adapted from J.C. de Mello, H. R. Wittmann and R. H. Friend, Advanced Materials, 1997, 9.

With the sphere, the measurement is performed in the following steps:

Spectra A, B and C address the intensity of the excitation light, while the emission range is probed with spectra B2 and C2. Spectra A records the background, namely the instrumental response of the IS to the excitation beam. Then, the excitation beam is monitored in presence of the sample. The sample is placed once inside the sample beam (spectrum C) to monitor the absorption of collimated light (direct excitation), once placed outside the

incident beam (spectra B) to consider the secondary excitation by absorption of diffuse excitation light scattered on the IS's wall.

The fraction of light absorbed by the sample is defined as

$$\mathrm{Abs\%} = 1 - \frac{\mathrm{C}}{\mathrm{B}}$$

The number of number of photons emitted is defined as

$$\mathrm{N(Em)} = \mathrm{C2} - \mathrm{B2} * (1 - \mathrm{Abs\%})$$

The number of number of photons emitted is defined as

$$\mathrm{N(Abs)} = \mathrm{A} * \mathrm{Abs\%}$$

The emission quantum yield is then calculated using the following relation:

$$\eta = \frac{\mathrm{C2} - (1 - \mathrm{Abs\%}) * \mathrm{B2}}{\mathrm{Abs\%} * \mathrm{A}}$$

8.4.3. Raman spectroscopy

Raman spectroscopy is a surface sensitive method that probes the inelastic scattering of monochromatic light on a sample. When light hits a sample, the beam can be scattered elastically (Rayleigh scattering), without a change in energy, or inelastically: As the incident laser light is not only scattered in this case, but interacts with molecular vibrations, phonons or other excitations of the sample, the energy of the laser photons being shifted up or down. This shift in energy in respect to the incident light gives information about the vibrational modes in the system. A Raman vibration is active and can be detected only if the polarizability of the system under study is changed during the normal vibration; in general, molecular vibrations that are symmetric with respect to the center of symmetry are allowd in Raman, resulting in an active Raman band. [15] This selection rule makes Raman a particularly informative method in characterizing sp2 carbon backbones as are found in chromophores, nano-graphenes, graphene-organic hybrid materials or polymers.

Raman spectra of graphene samples typically contain two main features (Fig. 10): the G peak, corresponding to the E2g phonon mode at the Brillouin zone center, at 1580 cm_1 and the 2D peak, which is activated by two-phonons intervalley assisted Raman scattering, at 2700 cm_1. Since this thesis deals with liquid phase exfoliated graphene, typically resulting in a mixture of mono- and few layer flakes, we expect the appearance of a D peak in our Raman spectra. The D peak is caused by breathing-like modes corresponding to the transverse optical phonons near the K point. [16]

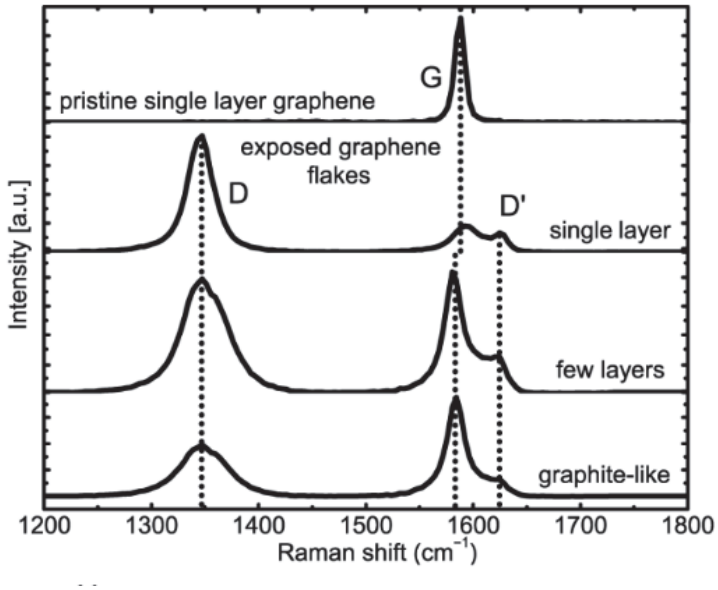

Fig. 10. Typical Raman features observed with pristine single layer graphene, defective graphene exposed to plasma, few layer graphene and graphite-like structures. 633 nm excitation, reprinted with permission from Ref. [16]

The 2D peak can be used to identify graphene layers [17]:

The 2D peak is a single and sharp peak in the case of monolayer graphene, while in AB-stacked bilayer the 2D peak is composed by four bands. Multilayer graphene shows a broad and up-shifted 2D peak, which in first approximation can be fitted with two peaks. The 2D peak shape quickly evolves with the number of layers, so that the 2D band of a sample containing more than 8–10 layers is hardly distinguishable from that of bulk graphite [17]. However, it should be mentioned that rotationally stacked few-layers graphene layers can result electronically decoupled and behave as a collection of monolayers, both for what concerns the electronic properties and the Raman spectrum.

Raman spectroscopy on chromophore allows for resonant excitation into a real electronic state instead of a virtual level (Fig. 11):

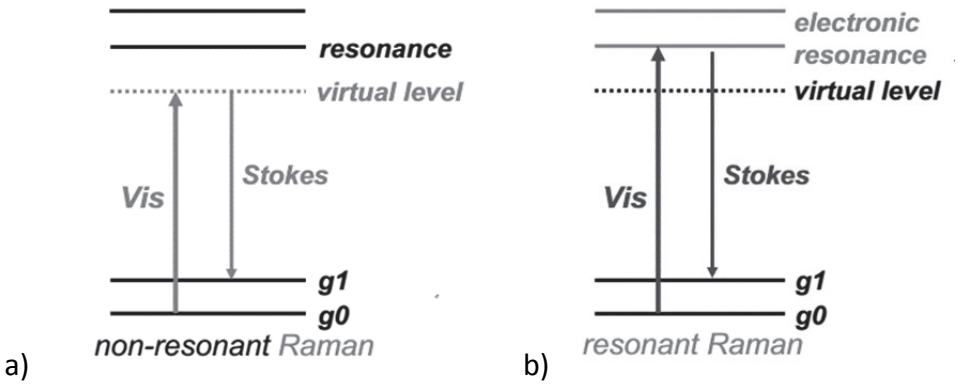

Fig. 11. Schematic presentation of energy diagrams, corresponding to a) non-resonant excitation and b) resonant excitation into an electronically resonant state, localized for example on a chromphore.

The resonance Raman Effect results in an enhancement of Raman intensities by a factor of 10^2 to 10^6 compared to the band intensities of the same vibration observed with non-resonant excitation. [18]

8.5. Microscopic characterization

8.5.1. Atomic Force microscopy.

Basic setup. Topographical images are recorded with scanning a cantilever across the sample surface. The cantilever contains a sharp tip interacting with the surface in the area of interest. The cantilever is excited mechanically with a piezo element, resulting in an oscillation of a known frequency that is monitored through a lock-in amplifier.

Sample-surface interactions induce a perturbation of the cantilever oscillation, which is detected with a laser system (deflection mode detection): The laser beam is reflected off the back of the cantilever, and small changes in cantilever deflection are observed with a position-sensitive four quadrant photodiode. This deflection is processed by the system electronics to determine topological height changes on the sample surface. The detection technique based on deflection of a laser beam has been first reported by Meyer et al. in 1988. [13]

In our system, the exact position of the laser beam on the cantilever is controlled and optimized manually using an optical microscope.

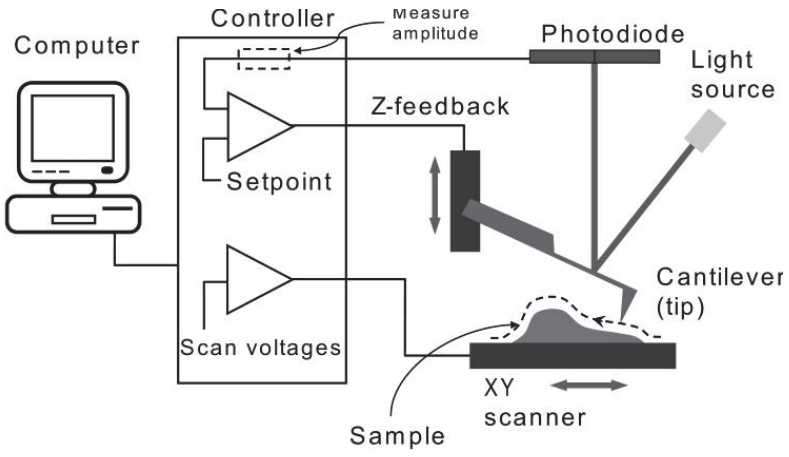

Fig. 12. Schematic of the operation of an AFM. For image recording, a cantilever is scanned over the sample surface. A laser beam is deflected off the back of this cantilever; then, changes in deflection are monitored with a photodiode detector. Reprinted with permission from Asylum Research (Santa Barbara, CA).

Scanning probe techniques do not use lenses, unlike traditional optical microscopes; the resolution in scanning probe systems is limited by the size of the probe rather than by diffraction effects. With this approach, the lateral image resolution of features depends on the tip geometry, but it can reach sub-nanometer levels, whereas the height resolution is sub-angstrom.

The imaging can be performed with either contact mode or tapping mode: The tip is in constant contact with the sample surface in contact mode, whereas in tapping mode the cantilever is oscillated as it is scanned across the sample surface. We usually work in tapping mode to reduce the lateral forces on the sample and consequently reducing sample damage, which may cause artefacts to the recorded morphology. Generally, the tapping mode is more commonly used when imaging very soft materials such are the small semiconductor self-assemblies, thin films and non-covalently functionalized graphene sheets discussed in this thesis.

8.5.2. Image metrology – characterization of self-assembled nanostructures

The commercial image metrology program SPIP was applied for image analysis. Plane correction of the images is applied any further step of image metrology. Then, the distribution in fiber heights is analyzed using the topographical image‘s height histogram. A histogram is a graphical representation of the frequency in which occur within certain ranges or intervals, so-called bins; the height histogram of a topographical image shows the statistical distribution of z-values (heights) within the image.

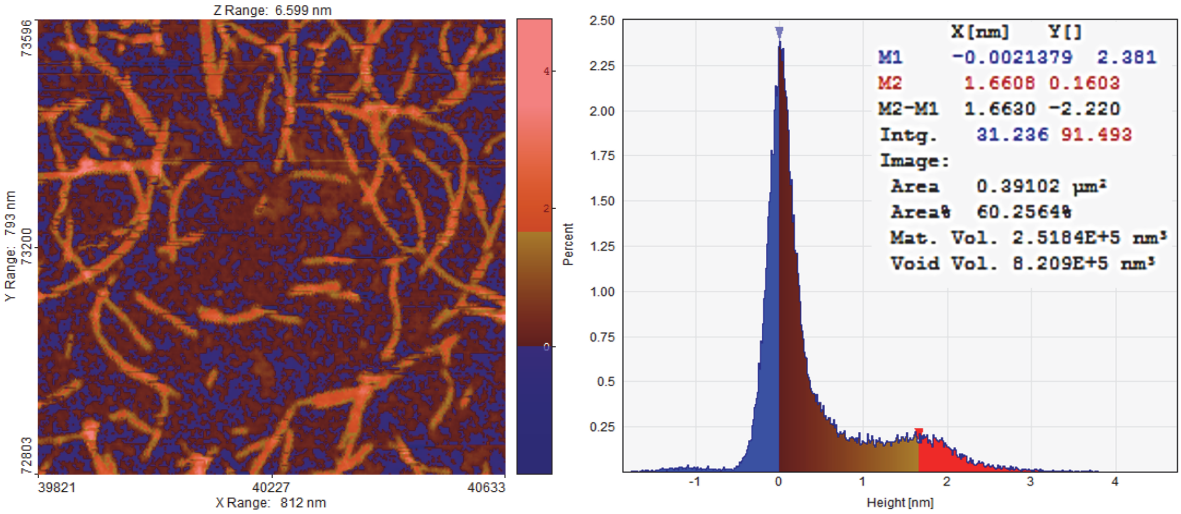

Fig. 13. Height histogram analysis on a typical topographical image showing a well-defined fiber structure on a flat substrate. The graph reports the corresponding height histogram. M1 and M2 indicate the main (most frequent) height contributions derived for this image.

If the surface is random, the histogram will be bell shaped with the bell top at the mean height in the image. The histogram of an image showing predominantly a tilt surface will be flat with all z-values contributing approximately equal in height.

If the surface has two rather distinct levels as for example the fiber structure reported below, the histogram will have two distinct peaks each centered on the respective height levels. The two distinct levels detect in the image below are attributed to background (substrate) and a fiber structure being mono-disperse in fiber thickness.

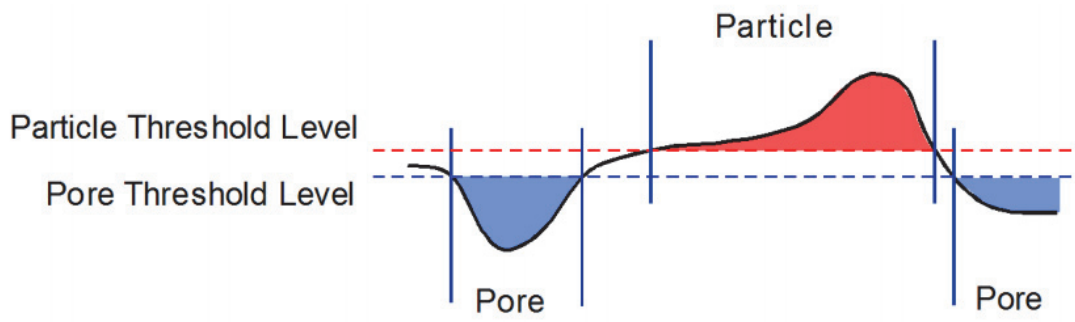

Fig. 14. Schematic presentation of the definition of key parameters describing a fiber based skeleton. Reprinted and adapted from SPIP Image metrology online tutorial.

Typical features in topographical analysis are pores or particles, in our samples the analysis of particles is of interest. In detection of such particles or fibers, which are defined as a shape in the image higher than its surroundings, we apply a threshold for detection: The threshold level defines above which z-level a point or region in the image is counted as a particle (or fiber).

More complex structures, for example in images dominated by more than one height contribution, a threshold split can be applied using the SPIP software. This advanced threshold detection mode is used as well for detection and quantitative description of fiber structures, for example fiber length and width. The skeleton of a polygon shape is the result of thinning the feature into a one pixel wide branched line, as is shown schematically in 0. The length of an as-defined skeleton is calculated as sum of the length of all branches detected for a skeleton.

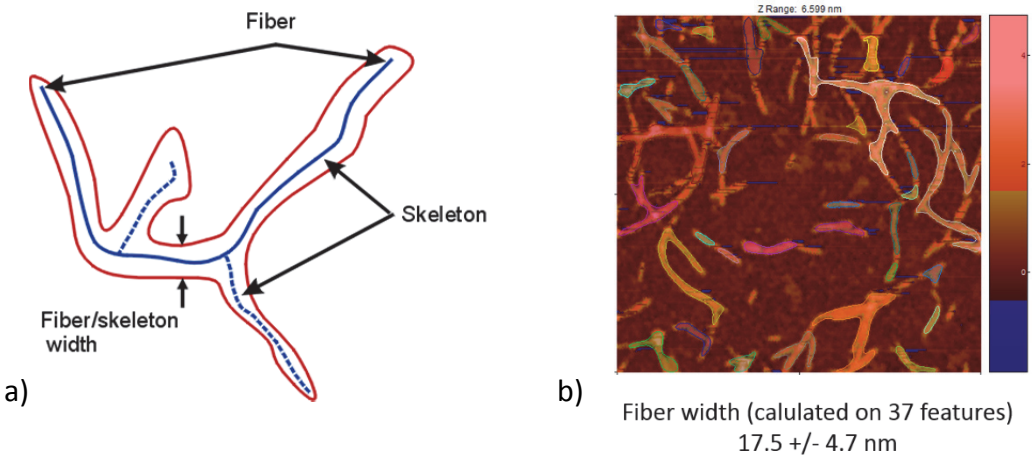

Fig. 15. Schematic presentation of the definition of key parameters describing a fiber based skeleton. Reprinted from SPIP Image metrology online tutorial. b) Typical AFM image of a fiber structure obtained with indanthrone di sulphonate. Color highlights skeletons automatically detected with particle analysis for quantitative description.

The fiber width, or more accurately skeleton width, is derived from the area of the detected skeleton divided by its length. For a worm-like feature, the fiber width equals the mean width perpendicular to its fiber. Fiber dimensions are then calculated with statistics on all detected skeletons in an image, typically on 20 to 80 features.

References

(1) Sanderson, B. *Journal of Chemical Technology & Biotechnology* 2004, *79*, 207.

(2) Mason, T. J.; Lorimer, J. P. In *Applied Sonochemistry*; Wiley-VCH Verlag GmbH & Co. KGaA: 2003, p 25.

(3) Hernandez, Y.; Nicolosi, V.; Lotya, M.; Blighe, F. M.; Sun, Z. Y.; De, S.; McGovern, I. T.; Holland, B.; Byrne, M.; Gun'ko, Y. K.; Boland, J. J.; Niraj, P.; Duesberg, G.; Krishnamurthy, S.; Goodhue, R.; Hutchison, J.; Scardaci, V.; Ferrari, A. C.; Coleman, J. N. *Nature Nanotechnology* 2008, *3*, 563.

(4) Hamilton, C. E.; Lomeda, J. R.; Sun, Z.; Tour, J. M.; Barron, A. R. *Nano Letters* 2009, *9*, 3460.

(5) Khan, U.; O'Neill, A.; Lotya, M.; De, S.; Coleman, J. N. *Small* 2010, *6*, 864.

(6) Israelachvili, J. N. *Intermolecular and Surface Forces, 3rd Edition*; Elsevier Academic Press Inc: San Diego, 2011.

(7) Green, A. A.; Hersam, M. C. *Nano Letters* 2009, *9*, 4031.

(8) Svedberg, T., Pedersen, K. O *The Ultracentrifuge*; Oxford, 1940.

(9) Green, A. A.; Hersam, M. C. *The Journal of Physical Chemistry Letters* 2009, *1*, 544.

(10) Schlierf, A.; Yang, H.; Gebremedhn, E.; Treossi, E.; Ortolani, L.; Chen, L.; Minoia, A.; Morandi, V.; Samori, P.; Casiraghi, C.; Beljonne, D.; Palermo, V. *Nanoscale* 2013.

(11) Yang, H.; Hernandez, Y.; Schlierf, A.; Felten, A.; Eckmann, A.; Johal, S.; Louette, P.; Pireaux, J. J.; Feng, X.; Mullen, K.; Palermo, V.; Casiraghi, C. *Carbon* 2013, *53*, 357.

(12) Lotya, M.; Hernandez, Y.; King, P. J.; Smith, R. J.; Nicolosi, V.; Karlsson, L. S.; Blighe, F. M.; De, S.; Wang, Z.; McGovern, I. T.; Duesberg, G. S.; Coleman, J. N. *Journal of the American Chemical Society* 2009, *131*, 3611.

(13) Meyer, G.; Amer, N. M. *Applied Physics Letters* 1988, *53*, 1045.

(14) Lotya, M.; King, P. J.; Khan, U.; De, S.; Coleman, J. N. *Acs Nano* 2010, *4*, 3155.

(15) Fateley, W. G.; McDevitt, N. T.; Bentley, F. F. *Appl. Spectrosc.* 1971, *25*, 155.

(16) Eren, B.; Hug, D.; Marot, L.; Pawlak, R.; Kisiel, M.; Steiner, R.; Zumbühl, D. M.; Meyer, E. *Beilstein Journal of Nanotechnology* 2012, *3*, 852.

(17) Ferrari, A. C.; Meyer, J. C.; Scardaci, V.; Casiraghi, C.; Lazzeri, M.; Mauri, F.; Piscanec, S.; Jiang, D.; Novoselov, K. S.; Roth, S.; Geim, A. K. *Physical Review Letters* 2006, *97*, #187401.

(18) Strommen, D. P.; Nakamoto, K. *Journal of Chemical Education* 1977, *54*, 474.

V. Conclusions and Perspectives

In this thesis we describe design, production and investigation all-organic graphene hybrid materials based on small aromatic dyes and organic semiconductor molecules. In more detail, we investigated properties of such novel graphene-based hybrid materials starting from fundamental physico-chemical aspects towards an application oriented point of view, suggesting new approaches in both characterization and processing.

We have demonstrated a simple and innovative method for production of aqueous graphene suspensions, using pyrene sulphonic acid sodium salt (PS1) as agent in graphite liquid phase exfoliation. We found that by using our method, based on ultra-sonication with PS1, it was possible to achieve stable graphene suspensions directly in water. With a washing procedure based on centrifugation and solvent exchange, the suspensions could be purified, yielding hydrophobic graphene flakes stabilized with PS1 in aqueous solution. Motivated by these results, we took a closer look at the mechanism of chromophore-assisted graphite exfoliation in water, comparing four pyrene derivatives with systematically varying, polar core functionalization. We unravelled the mechanism of surface adsorption of such dyes on graphene, and successive exfoliation of these dye-functionalized graphene sheets in water. By combining experimental and modelling investigations, we have proven an unambiguous correlation between the graphene–dye interaction energy, the molecular structure and the amount of graphene flakes solubilized. Our results were showing that the molecular dipole of the exfoliation agent was not important per se, but because it facilitated adsorption on graphene: by a “sliding” mechanism of the molecule into the solvent layer during the adsorption process, the lateral displacement of the water molecules collocated between the aromatic cores of the dye and graphene was facilitated with derivatives of larger dipole and asymmetric functionalization. While a large dipole and molecular asymmetry clearly promote the adsorption of the molecule on graphene, the overall stability and pH response of the suspensions obtained depend on colloidal stabilization, with no significant influence of molecular charging and dipole.

We then extend our approach to perylene diimide (PDI) derivatives with polar moieties, as a model system for perylene diimide based organic semiconductor materials commonly applied in

organic electronics. Graphene-PDI hybrids are directly exfoliated in polar solvents such as water, EtOH or isopropanol. Raman, steady state and time resolved spectroscopy was applied on in-situ exfoliated graphene organic hybrids, obtaining information on graphene quality, graphene-perylene diimide interaction and the fingerprint of the dye itself.
In a next step towards application of graphene-organic hybrids in organic electronics, we studied the direct exfoliation with high performance n-type semiconductors in organic solvents. N-type PDI derivatives (butyl dicyano- perylenecarboxydiimide PDI-CN2 and fluoroalkyl chains, N,N'-1H,1H-perfluorobutyl dicyanoperylenecarboxydiimide PDIF-CN2), have been employed as exfoliation agents and studied for their steady state optical properties in liquid phase.

We then exploit the non-covalent chemistry of graphene to develop graphene-organic hybrids as nanofiller for the preparation polymer composites. The dye studied here is indanthrone sulphonic acid sodium salt (IBS), a commercial chromophore applied on large scale in industrial pigment formulations. In collaboration with BASF, Germany, direct exfoliation of graphite with IBS was used to achieve aqueous suspensions of graphene hybrids, readily dispersible in a polyvinylalcohol matrix for prospective application in anti-statics.

Overall, we investigate and exploit non-covalent chemistry of graphene to design, produce, and process and characterize novel graphene organic hybrid materials. We unravel mechanistic aspects of graphene liquid phase exfoliation with dyes, fundamental aspects of graphene-chromophore interactions in liquid and solid phase and exploit our findings for the formulation of graphene hybrid suspensions towards application in organic electronics and functional polymer composite materials.

The graphene-organic hybrid materials developed here are not only valuable model systems to investigate the non-covalent chemistry of graphene, but they have great potential for application particularly related to nanotechnologies and organic electronics. With our approach, we focus on a new and versatile route of graphene production which allows accessing graphene's outstanding properties, namely the implementation of graphene into all-organic graphene hybrid materials based on small aromatic dyes or organic semiconductor molecules:[1]

V. Conclusions and Perspectives

Through careful design and manipulation of small, aromatic carbon-based molecules, hybrid structures with graphene are accessible through non-covalent interactions. The controlled interaction of graphene with, for instance, organic semiconductors (OSC) can offer an in-situ solution to improve graphene's processibility [1-3] and to tailor graphene properties for application, enabling an optimal control over the molecular self-assembly process with graphene to form low-dimensional graphene-organic architectures. [4-6]

With recent developments in large-scale production techniques, one of which is liquid-phase exfoliation, new layered materials beyond graphene such as BN, $NbSe_2$, TaS_2, MoS_2 based nanosheets holding great potential in both fundamental and applied research become more and more available (see [7,8]). If the electronic interaction of organic molecules with graphene (a semi-metal) was rather complex and rising great research interest, their interaction with semiconducting 2D nanosheets will give systems even more challenging and versatile for application as novel 2D hybrid materials,[9,10] as alternative gate insulators, photo-responsive components, active materials for field-effect transistors or electrode materials.

A polymer nanocomposite of liquid phase exfoliated MoS_2 and polyethylene oxide (PEO) has been recently already demonstrated as an anode material for lithium ion batteries. MoS_2/PEO electrodes exhibit high charge storage capacities and long-term reversibility. [11] Hybrid materials from organic semiconductors and other non-carbon based 2D materials, such as tin sulphite or tin selenide, are particularly promising. For instance, it has been found that the presence of 1,10-phenanthroline shall govern the morphology of SnSe giving 2D nanosheets, instead of 3D SnSe nanoflowers obtained in the absence of the molecule. Single-crystalline nanosheets are obtained from the coalescence of the SnSe nucleus in an orientated attachment mechanism. Bandgap determination and optoelectronic test based on hybrid films of SnSe and poly(3-hexylthiophene) indicate the great potential of the ultrathin SnSe nanosheets in photodection and photovoltaics[12].

(1) Schlierf, A.; Samori, P.; Palermo, V. *Journal of Materials Chemistry C* 2014.
(2) Ciesielski, A.; Samori, P. *Chemical Society Reviews* 2013.
(3) Yang, J.; Bai, L.; Feng, G.; Yang, X.; Lv, M.; Zhang, C. a.; Hu, H.; Wang, X. *Industrial & Engineering Chemistry Research* 2013, *52*, 16745.
(4) Pathipati, S. R.; Pavlica, E.; Treossi, E.; Rizzoli, R.; Veronese, G. P.; Palermo, V.; Chen, L.; Beljonne, D.; Cai, J.; Fasel, R.; Ruffieux, P.; Bratina, G. *Organic Electronics* 2013, *14*, 1787.
(5) Xiao, K.; Deng, W.; Keum, J. K.; Yoon, M.; Vlassiouk, I. V.; Clark, K. W.; Li, A.-P.; Kravchenko, I. I.; Gu, G.; Payzant, E. A.; Sumpter, B. G.; Smith, S. C.; Browning, J. F.; Geohegan, D. B. *Journal of the American Chemical Society* 2013, *135*, 3680.
(6) Järvinen, P.; Hämäläinen, S. K.; Banerjee, K.; Häkkinen, P.; Ijäs, M.; Harju, A.; Liljeroth, P. *Nano Letters* 2013, *13*, 3199.
(7) Nicolosi, V.; Chhowalla, M.; Kanatzidis, M. G.; Strano, M. S.; Coleman, J. N. *Science* 2013, *340*.
(8) Geim, A. K.; Grigorieva, I. V. *Nature* 2013, *499*, 419.
(9) Britnell, L.; Gorbachev, R. V.; Jalil, R.; Belle, B. D.; Schedin, F.; Mishchenko, A.; Georgiou, T.; Katsnelson, M. I.; Eaves, L.; Morozov, S. V.; Peres, N. M. R.; Leist, J.; Geim, A. K.; Novoselov, K. S.; Ponomarenko, L. A. *Science* 2012, *335*, 947.
(10) Britnell, L.; Ribeiro, R. M.; Eckmann, A.; Jalil, R.; Belle, B. D.; Mishchenko, A.; Kim, Y. J.; Gorbachev, R. V.; Georgiou, T.; Morozov, S. V.; Grigorenko, A. N.; Geim, A. K.; Casiraghi, C.; Neto, A. H. C.; Novoselov, K. S. *Science* 2013, *340*, 1311.
(11) Xiao, J.; Choi, D.; Cosimbescu, L.; Koech, P.; Liu, J.; Lemmon, J. P. *Chemistry of Materials* 2010, *22*, 4522.
(12) Li, L.; Chen, Z.; Hu, Y.; Wang, X.; Zhang, T.; Chen, W.; Wang, Q. *Journal of the American Chemical Society* 2013, *135*, 1213.

V. Acknowledgement

I would like to thank my colleagues from the nanochemistry lab at ISIS in Strasbourg, for their great professionalism, continuous knowledgeable feedback and support. Thanks to my supervisor Prof. Paolo Samori for your open-minded approach, your creativity and support on my way to achieving my goals and following my own ideas. Thanks to my group and great colleagues from university of Strasbourg, in particular Maria de Rosso and Mirella Gemayel, for your open welcome and support.

Thanks for collaboration and countless formal and informal discussion on photochemistry and spectroscopic techniques to my colleagues Barbara Ventura, Andrea Barbieri, Francesco Manoli and Praveen Vakayil Karthikeyan; to Nicola Armaroli and Filippo Monti for their support and curiosity in applying spectroscopic techniques to new systems. Thanks to Vincenzo Palermo, Vittorio Morandi, Luca Ortolani and Franco Corticelli for their training and support in scanning probe and electron microscopy, and Prof. Massimo Gazzano from University Bologna for his support with XRD measurements. Thanks to Zhenyuan Xia and Prof. Müllen at Max Planck Institute in Mainz for supporting with broad knowledge on synthesis.

This thesis was financially supported by Marie Curie Actions, opening great training opportunities and enabling rewarding collaborations within the GENIUS project. In this, I would like to acknowledge Prof. David Beljonne and his students from the Laboratory of Novel Materials, University Mons, Belgium, for their help with simulations and the valuable contribution to our collaborative work. Thanks to Prof. Franco Cacialli, Giulia Tregnago and Francesco Bausi from University College of London for their work on time resolved emission and on transparent electrodes. Thanks to Prof. Andrea Ferrari's group at NMS in Cambridge, in particular to Felice Torrisi and Matteo Bruna, for your support with Raman spectroscopy and inkjet printing and for welcoming me to a great secondment in UK. Thanks to Matthias G. Schwab, Yanfei Xu and Kitty Cha from the BASF Graphene research center in Germany, for our rewarding collaboration on developing GOHs towards industrial application. Thanks to Prof. Cinzia Casiraghi and Huafeng Yang from University of Manchester, UK for your input, feedback and support with Raman spectroscopy.

Thanks for their encouraging smile and optimism to my colleagues, all coffee and chocolate treats and for fun discussions far beyond science. Many thanks to my loving family and friends all over Europe, for their trust, support and encouragement throughout my years living and working abroad and for being great company travelling the world.

VI. PUBLICATIONS

11/2014 *Exfoliation of graphene with an industrial dye: Teaching an old dog new tricks.*
Andrea Schlierf, Kitty Cha, Matthias Georg Schwab, Paolo Samorì, Vincenzo Palermo, 2D Materials, 2014, 1, 035006.

09/2014 *Graphene-induced enhancement of n-type mobility in perylenediimide thin films*.
Srinivasa Rao Pathipati, Egon Pavlica, Andrea Schlierf, Mirella El Gemayel, Paolo Samorì, Vincenzo Palermo, and Gvido Bratina
J. Phys. Chem. C., 2014, 118, 24819.

04/2014 *Leveraging the ambipolar transport in polymeric field-effect transistors via blending with liquid-phase exfoliated graphene.*
Mirella El Gemayel, Sébastien Haar, Fabiola Liscio, Andrea Schlierf, Georgian Melinte, Silvia Milita, Ovidiu Ersen, Artur Ciesielski, Vincenzo Palermo, Paolo Samorì
Adv. Mater., 2014, 26, 4814–4819.

10/2013 *Graphene-organic composites for electronics; optical and electronic interactions in vacuum, liquids and thin solid films.*
Feature article for special issue on Emerging Investigators
Andrea Schlierf, Paolo Samori and Vincenzo Palermo
J. Mater. Chem. C, 2014, 2 (17), 3129 – 3143.

05/2013 *Nanoscale insight into the exfoliation mechanism of graphene with organic dyes: Effect of charge, dipole and molecular structure.*
Andrea Schlierf, Huafeng Yang, Elias Gebremedhn, Emanuele Treossi, Luca Ortolani, Liping Chen, Vittorio Morandi, David Beljonne, Paolo Samorì, Cinzia Casiraghi, Vincenzo Palermo
Nanoscale, 2013, 5, 4205-4216.

03/2013 *A simple method for graphene production based on exfoliation of graphite in water using 1-pyrenesulfonic acid salt.*
Huafeng Yang, Yenny Hernandez, Andrea Schlierf, Alexandre Felten, Axel Eckmann, S. Johal, P. Louette, J.-J. Pireaux, Xinglang Feng, Klaus Mullen, Vincenzo Palermo, Cinzia Casiraghi
Carbon 2013, 3, 53:357–365.

11/2014 *Thermal Treatment and Chemical Doping of Semi Transparent Graphene Films.*
Francesco Bausi, Andrea Schlierf, Matthias Georg Schwab, Emanuele Treossi, Vincenzo Palermo, Franco Cacialli
Submitted.

ORAL CONTRIBUTIONS

05/2014 Conference talk
Work function modulation via p-doping of graphene and reduced graphene oxide transparent conductive films.
Francesco Bausi, Andrea Schlierf, Emanuele Treossi, Vincenzo Palermo, Franco Cacialli
E-MRS 2014 SPRING MEETING, Lille, France

11/2013 Seminar talk
Graphene organic hybrid materials.
Andrea Schlierf, ISOF - CNR Area della Ricerca di Bologna, Bologna, Italy

09/2013 Conference talk
Nanoscale insight into the exfoliation mechanism of graphene with organic dyes: Effect of charge, dipole and molecular structure.
Andrea Schlierf
Conference on advanced materials and processes (EUROMAT)
Sevilla, Spain

06/2013 Conference talk
Insight into the exfoliation mechanism of graphene with organic dyes: Effect of charge, dipole and molecular structure.
Andrea Schlierf
Symposium on Functional pi- systems (Fπ11), Arcachon, France

03/2013 Talk
Graphene exfoliation with industrial dyes and pigments.
Andrea Schlierf
GENIUS project meeting
University College of London (UCL), London, UK

12/2012 Invited talk
Graphene organic hybrid materials.
Andrea Schlierf
NMS group Engineering Department, Cambridge University
Cambridge, UK

10/2012 Talk
Graphene exfoliation with organic dyes.
Andrea Schlierf
GENIUS project meeting, Université de Strasbourg, France

04/2012 Talk
The interaction of pyrene derivatives with graphene nanoplatelets.
Andrea Schlierf
GENIUS meeting, Université de Mons, Mons, Belgium

POSTER CONTRIBUTIONS

05/2014 *Nanoscale insight into the exfoliation mechanism of graphene with organic dyes.*
Andrea Schlierf, Huafeng Yang, Elias Gebremedhn, Emanuele Treossi, Luca Ortolani, Liping Chen, Vittorio Morandi, David Beljonne, Paolo Samorì, Cinzia Casiraghi, Vincenzo Palermo
E-MRS 2014 SPRING MEETING, Lille, France

06/2013 *Nanoscale insight into the exfoliation mechanism of graphene with organic dyes: Effect of charge, dipole and molecular structure.*
Andrea Schlierf, Huafeng Yang, Elias Gebremedhn, Emanuele Treossi, Luca Ortolani, Liping Chen, Vittorio Morandi, David Beljonne, Paolo Samorì, Cinzia Casiraghi, Vincenzo Palermo

Honored with the RCS Publishing POSTER AWARD
Supramolecular functional systems for organic electronics conference (SUPERIOR), Strasbourg, France

04/2012 *The interaction of pyrene derivatives with graphene nanoplatelets.*
Andrea Schlierf, Huafeng Yang, Emanuele Treossi, Cinzia Casiraghi, Vincenzo Palermo
Graphene 2012
Brussels, Belgium

SCHOLARSHIPS AND AWARDS

06/2013 Best Poster Award
RCS Publishing
Supramolecular functional systems for organic electronics conference (SUPERIOR)
Strasbourg, France

05/2011-05/2014 Marie Curie Fellowship for Early Stage researcher
Graphene-organic hybrid architectures for organic electronics (GENIUS project)

ACCEPTED PROPOSALS

09/2013	Travel Grant EUROMAT conference, Sevilla, Spain ESF (European Science Foundation)
04/2013	Travel Grant Graphene School in Nova Gorica, Slovenia ESF (European Science Foundation)
08/2004	Academic exchange funding and travel grant 2 months internship, Yokohama, Japan DAAD German Academic Exchange Service IAESTE (International Association for the Exchange of Students for Technical Experience)